# Environmental and Economic Assessment of Microalgae-derived Jet Fuel

by

2LT Nicholas Aaron Carter, USAF

B.Sc. Aeronautical Engineering, 2010
United States Air Force Academy

Submitted to the Department of Aeronautics and Astronautics in Partial Fulfillment of the Requirements for the Degree of

Master of Science in Aeronautics and Astronautics

at the

MASSACHUSETTS INSTITUTE OF TECHNOLOGY

June 2012



The views expressed in this article are those of the author and do not reflect the official policy or position of the United States Air Force, Department of Defense, or the U.S. Government.

Signature of Author……
Department of Aeronautics and Astronautics
May 24, 2012

Certified by……
Steven R.H. Barrett
Charles Stark Draper Assistant Professor of Aeronautics and Astronautics
Thesis Supervisor

Accepted by……...
Eytan H. Modiano
Professor of Aeronautics and Astronautics
Chair, Graduate Program Committee

*[Page Intentionally Left Blank]*

Environmental and Economic Assessment of Microalgae-derived Jet Fuel

by

2LT Nicholas Aaron Carter, USAF

Submitted to the Department of Aeronautics and Astronautics on
May 24, 2012 in Partial Fulfillment of the Requirements for the Degree of
Master of Science in Aeronautics and Astronautics

## Abstract

Significant efforts must be undertaken to quantitatively assess various alternative jet fuel pathways when working towards achieving environmental and economic United States commercial and military alternative aviation fuel goals within the next decade. This thesis provides lifecycle assessments (LCAs) of the environmental and economic impacts of cultivating and harvesting phototrophic microalgae; extracting, transporting, and processing algal oils to hydrocarbon fuels; and distributing and combusting the processed renewable jet fuel for a pilot scale facility. Specifically, lifecycle greenhouse gas (GHG) emissions, production costs, freshwater consumption, and land use were quantified for four cultivation and two extraction technology sets. For each cultivation and extraction type, low, baseline, and high scenarios were used to assess the variability of each performance metric. Furthermore, sensitivity analyses were used to gain insights as to where efforts towards improving certain technologies could have the largest impact on improving the lifecycle metrics.

The four cultivation technologies include open raceway ponds, horizontal serpentine tubular photobioreactors (PBRs), vertical serpentine tubular PBRs, and vertical flat panel PBRs. Open raceway ponds were modeled from previous literature, while the PBRs were modeled, validated and optimized for specific constraints and growth inputs. The algal oil extraction techniques include conventional dewatering, drying, and extraction using hexane in a similar process to seed oil extraction (termed dry extraction in this study) as well as algal cell lysing with steam and potassium hydroxide as well as fluid separation and washing processes (termed wet extraction).

Overall, open raceway pond cultivation with wet extraction performed most favorably when compared with the other scenarios for GHG emissions, production costs, freshwater consumption, and areal productivity (including the entire cultivation and extraction facility), yielding 31.3 g-$CO_2$e/$MJ_{HEFA-J}$, 0.078 \$/$MJ_{HEFA-J}$ (9.86 \$/$gal_{HEFA-J}$), 0.38 $L_{freshwater}$/$MJ_{HEFA-J}$ and 17,600 $L_{TAG}$/ha/yr for the baseline cases with brackish water makeup. The lifecycle GHG emissions and production cost metrics for the open raceway pond with wet extraction low scenario were both lower than that of conventional jet fuel baselines. For all cases, the inputs most sensitive to the lifecycle metrics were the cultivation system biomass areal productivity, algal extractable lipid weight fraction, and downstream harvesting system choices.

**Thesis Supervisor:** Prof. Steven R.H. Barrett
**Title:** Charles Stark Draper Assistant Professor of Aeronautics and Astronautics

*[Page Intentionally Left Blank]*

## Acknowledgements

I would like to thank my advisors Dr. James Hileman and Prof. Steven Barrett for providing their knowledge and advice for both this thesis as well as other areas in my life. Their insights and perspectives helped shape how I conducted my research throughout this thesis. Lifecycle GHG emissions and photobioreactor modeling and simulation was also greatly improved with initial help with derivations and review from Mr. Russell Stratton of MIT (currently at Bombardier Inc.).

My appreciation additionally goes out to the following people who helped shape all or parts of this thesis into a higher quality product: Dr. Kristen Lewis (Volpe National Transportation Systems Center), Mr. Warren Gillette (FAA), Dr. Tim Edwards (AFRL), Mr. Bill Harrison (AFRL), Dr. Prem Lobo (MS&T), Dr. Mike Timko (Aerodyne Research Inc.), Mr. Daniel Baniszewski (DLA-Energy), Mr. John Heimlich (A4A) as well as Dr. Hakan Olcay, Dr. Robert Malina, Dr. Christoph Wollersheim, Mr. Matthew Pearlson, Mr. Dominic McConnachie, Mr. Michael Bredehoeft, Mr. Christopher Gilmore and Ms. Kristina Bishop (all from MIT).

This work was conducted with funding from the Federal Aviation Administration Office of Energy and Environment and Air Force Research Labs as a part of PARTNER Project 28 with project management provided by Mr. Warren Gillette, Mr. Bill Harrison, and Dr. Tim Edwards.

Lastly, I would like to thank my father, mother, and sister as well as my friends for their encouragement and support. Moreover, I'd like to thank my wife for her patience, understanding, and guidance while living in Cambridge. Her love has helped me immensely throughout this process.

*[Page Intentionally Left Blank]*

## Table of Contents

## List of Figures

*[Page Intentionally Left Blank]*

## List of Tables

## Nomenclature, Units, Abbreviations and Acronyms

Nomenclature

$A_{sc}$ Tubular solar collector cross-sectional area, $m^2$

$A_{np}$ Tubular non-productive cross-sectional area, $m^2$

$A_r$ Degasser riser gross-sectional area, $m^2$

$A_{PBR}$ Photobioreactor 2-D total areal footprint (including spacing), $m^2$

$a_1$ Specific energy optimization weighting coefficient, -

$a_2$ Areal productivity optimization weighting coefficient, -

$C$ Downstream pump capital cost, $

$C_{capex}$ Annualized facility capital expenses, $/yr

$C_f$ Fanning friction factor, -

$C_{fopex}$ Annual fixed operating expenses, $/yr

$C_L$ Oxygen concentration, $kg/m^3$

$C_p$ Specific heat of air at constant pressure, J/kg/K

$C_{p_{evap}}$ Specific heat of water evaporation at constant pressure, kJ/kg/K

$C_s$ Culture solids content, $kg/m^3$

$C_{sat}$ Saturation concentration of $O_2$ in water at standard atmospheric pressure, $kg/m^3$

$C_{vopex}$ Annual variable operating expenses, $/yr

$c_{water}$ molar concentration of water, $mol/m^3$

$D$ Dilution rate, $m^3$/day

$D_L$ Diffusivity of oxygen in water at standard atmospheric pressure, $m^2/s$

$d$ Distance between solar collector tubes, m

$d_{\text{algae}}$ Algal cell diameter, m

$d_{cluster}$ Distance between skid columns, m

$d_{np}$ Non-productive tube diameter, m

$d_{pond}$ Open pond depth, m

$d_r$ Degasser riser outer diameter, m

$d_d$ Degasser downcommer outer diameter, m

$d_{sc}$ Solar collector tube inner diameter, m

$d_{sc_{initial}}$ Initial solar collector tube diameter (when varying volumetric productivity), m

$d_{sc_{norm}}$ Normalized solar collector tube diameter (when varying volumetric productivity), -

$d_{skid}$ Distance between photobioreactor rows, m

$E_s$ Single photobioreactor cultivation specific energy, excluding cooling, $MJ/kg_{\text{algae}}$

$\dot{E}_{airlift}$ Photobioreactor airlift power input, W

$\dot{E}_{pump}$ Photobioreactor pump power input, W

$\dot{E}_{friction}$ Photobioreactor power required to overcome friction losses, W

$\dot{E}_{head}$ Photobioreactor power required to overcome head losses, W

$\dot{E}_{potential}$ Photobioreactor power required to overcome potential energy, W

$E_b$ Specific energy of dry biomass, MJ/kg

$E_{in}$ Specific energy input into the photobioreactor system not undergoing photosynthesis, $MJ/kg_{\text{algae}}$

$f$ Darcy friction factor, -

$g$ Acceleration due to gravity, $m/s^2$

$H$ Total daily direct solar radiation on a horizontal surface, $MJ/m^2$/day

$H_0$ Daily global extraterrestrial solar radiation (MJ/m$^2$/day)

$H_b$ Daily direct radiation on a horizontal surface (MJ/m$^2$/day)

$H_d$ Daily diffuse radiation impinging on a horizontal surface (MJ/m$^2$/day)

$H_y$ Annual average direct solar radiation on a horizontal surface (MJ/m$^2$/day)

$h$ Height between solar collector tubes or pump head, m

$h_L$ Liquid height in degasser, m

$h_{L_{pond}}$ Open pond head loss, m

$h_s$ Height of vertical tubular photobioreactor solar collector tube stack, m

$h_{v_{sc}}$ Solar collector tube head loss factor, -

$h_{v_{np}}$ Non-productive tube head loss factor, -

$k$ Number of sensitivity input parameters, -

$k_{B_{np}}$ Nonproductive tube Haaland friction coefficient, -

$k_{B_{sc}}$ Solar collector tube Haaland friction coefficient, -

$k_L a$ Liquid-air mass transfer coefficient, 1/s

$L$ Flat panel length, m

$L_1$ Photobioreactor areal length, m

$L_{1_{cluster}}$ Cluster areal length, m

$L_{1_{skid}}$ Skid areal length, m

$L_{1_{system}}$ System boundary areal length, m

$L_2$ Photobioreactor areal width, m

$L_{2_{cluster}}$ Cluster areal width, m

$L_{2_{skid}}$ Skid areal width, m

$L_{2_{system}}$ System boundary areal width, m

$L_{sc}$ Single solar collector tube length, m

$L_{np}$ Single non-productive arm tube length, m

$L_{PBR}$ Single photobioreactor cooling pipe length, m

$L_{pond}$ Open pond channel length, m

$M_{air}$ Molar mass of air, g/mol

$m$ Number of arms per degasser, -

$\dot{m}_{air}$ Air mass flow rate in degasser, kg/s

$\dot{m}_w$ Photobioreactor specific water flow, $kg_{water}/kg_{algae}$

$\dot{m}_{loss}$ Photobioreactor specific cooling water loss, $kg_{water}/kg_{algae}$

$N$ Number of sensitivity iterations or day of the year, -

$N_b$ Number of solar collector tube U-bends, -

$n$ Number of solar collectors per arm, -

$n_{pond}$ Open pond Manning's roughness s/m$^{1/3}$

$n_{years}$ Facility lifetime, years

$[O_2]_{in}$ $C_{sat}$ Normalized oxygen concentration into the solar collector, -

$[O_2]_{out}$ $C_{sat}$ normalized oxygen concentration into the degasser, -

$O_{2_{mm}}$ Molar mass of oxygen, g/mol

$O_{2_{mf}}$ Molar fraction of oxygen in air, -

$P$ Algae volumetric productivity, g/L/day

$P_a$ Ambient air pressure, Pa

$P_{airh}$ Air pressure at a specific height in the degasser, Pa

$P_{\text{algae}}$ Photobioreactor or facility algae productivity, kg/s or kg/yr

$P_{norm}$ Normalized algae volumetric productivity (when varying volumetric productivity), -

$P_{areal}$ Photobioreactor areal productivity, g/m$^2$/day

$P_{input}$ Single photobioreactor power required for cultivation, excluding cooling, W

$P_L$ Component tube friction loss, Pa/m

$P_r$ $P_a$ normalized pressure rise over pump, -

$PE$ Algae photosynthetic efficiency, -

$Q$ Pump volumetric flow rate, $m^3/s$

$R_{\substack{capex \\ upgrading}}$ Upgrading capital expenses, $/kg$_{algae}$

Re Reynolds number, -

$R_{\substack{fopex \\ upgrading}}$ Upgrading fixed operating expenses, $/kg$_{algae}$

$R_{O_2}$ Algae oxygen production ($g_{O2}/L/day)

$R_{prod}$ Total production expenses, $/kg$_{algae}$, $/gal$_{TAG}$, $/MJ$_{HEFA-J}$, or $/gal$_{HEFA-J}$

$R_{\substack{vopex \\ upgrading}}$ Upgrading variable operating expenses, $/kg$_{algae}$

$r_{evap}$ Cooling evaporation rate, m/day

$r_i$ Internal rate of return, -

$S$ Salinity of culture medium, ppt

$S_i$ Main sensitivity index array, -

$S_{pond}$ Open pond hydraulic slope, -

$S_{T_i}$ Global sensitivity index array, -

$T_{op}$ Operating air temperature, K

TPI Total Project Investment, $/ha

$t$ Flat panel thickness, m

$t_w$ Solar collector tube wall thickness, m

$U_b$ Degasser bubble velocity, m/s

$U_G$ Superficial gas velocity in degasser, m/s

$U_{L_{np}}$ Non-productive tube superficial liquid velocity, m/s

$U_L$ Superficial (liquid only equivalent) velocity, m/s

$V_p$ Photobioreactor productive volume, $m^3$

$\dot{V}_w$ Cooling water specific volume, $m^3$_{water}$/kg$_{algae}$

$V_{pond}$ Pond flow velocity, m/s

$w_{cluster}$ Cluster center artery width, m

$w_p$ Width between central processing fields, m

$w_{system}$ Width between system quadrants, m

$X$ Photobioreactor solar collector spacing, m

$Y$ Optimization objective function, -

$y_{A/B/C}$ Sensitivity matrix model output arrays, -

$\Delta H_{evap}$ Heat of vaporization for water, kJ/kg

$\Delta h$ Height between photobioreactor solar collector tubes, m

$\Delta P$ Component pressure loss, Pa

$\alpha$ Oxygen production per unit algae, g-$O_2$/g-algae

$\beta$ Ratio of superficial gas velocity to total superficial velocity, -

$\gamma$ Ratio of specific heats for air, -

$\gamma_i$ Maximum oxygen concentration in culture as a multiple of $C_{sat}$, -

$\delta$ Declination of the angular position of the Sun at solar noon with respect to the plane of the equator, rad

$\varepsilon$ Flat panel gas holdup, $m^3$_{air}$/m^3$_{air+liquid}$

$\varepsilon_m$ Pipe roughness height, m

$\varepsilon_r$ Degasser riser gas holdup, $m^3$_{air}$/m^3$_{air+liquid}$

$\zeta$ Universal solar constant, $W/m^2$

$\eta_c$ Compressor efficiency, -

$\eta_p$ Pump efficiency, -

$\eta_{pond}$ Paddle wheel and drive train efficiency, -

$\theta$ Degasser diffuser angle from vertical, deg

$\lambda$ Degasser riser characteristic velocity profile parameter, -

$\phi$ Culture flow microeddy length, m

$\mu_L$ Liquid culture viscosity, Pa-s

$\xi$ Specific energy dissipation due to turbulence, J/kg

$\rho_{air}$ Air density, $kg/m^3$

$\rho_{airh}$ Air density at a specific height in the degasser, kg/m$^3$

$\rho_L$ Liquid culture density, kg/m$^3$

$\rho_w$ Water density, kg/m$^3$

$\sigma$ Interfacial tension, J/m$^2$

$\phi$ Geographic latitude, rad

$\omega_s$ Hour angle at sunrise, deg

א Atmospheric clarity index, -

Units, Abbreviations and Acronyms

| | |
|---|---|
| A4A | Airlines for America |
| AEDT | Aviation Environmental Design Tool |
| AQ | Air Quality |
| bpd | Barrels per day |
| BTL | Biomass-to-liquid |
| BFW | Boiler Feed Water |
| CAP | Calorically Perfect Gas |
| CBTL | Coal and biomass-to-liquid |
| CHP | Combined Heat and Power (Cogeneration) |
| $C_nH_{2n+2}$ | Noncyclic saturated hydrocarbons |
| CONUS | Contiguous United States |
| CO | Carbon monoxide |
| $CO_2$ | Carbon dioxide |
| $CO_2e$ | Carbon dioxide equivalent |
| $CH_4$ | Methane gas |
| CTL | Coal-to-liquid |
| DAF | Dissolved Air Flotation |
| DLA | Defense Logistics Agency |
| DOD | Department of Defense |
| DOE | Department of Energy |
| EISA | Energy Independence and Security Act of 2007 |
| $FeSO_4$ | Iron(II) Sulfate |
| FPDE | Flat Panel Dry Extraction |
| FPWE | Flat Panel Wet Extraction |
| F-T | Fischer-Tropsch |
| GHG | Greenhouse gas |
| GREET | Greenhouse Gasses, Regulated Emissions, and Energy Use in Transportation |
| GTL | Gas-to-liquid |
| $H_2$ | Hydrogen gas |
| HCl | Hydrochloric acid |
| HDPE | High Density Polyethylene |
| HEFA-J | Hydroprocessed Esters and Fatty Acids Jet Fuel |
| HRJ | Hydroprocessed Renewable Jet |
| HTDE | Horizontal Tubular Dry Extraction |
| HTWE | Horizontal Tubular Wet Extraction |
| ICC | Installed Capital Cost |
| ISBL | Inside Battery Limits |
| IRR | Internal Rate of Return |
| JP-X | Jet Propellant Classification Number X |
| KOH | Potassium hydroxide |
| LCA | Lifecycle Assessment |
| LDPE | Low Density Polyethylene |
| LPG | Liquid Petroleum Gas |
| LHV | Lower Heating Value |
| LTO | Landing and Takeoff |
| LUC | Land Use Change |
| MATLAB | Matrix Laboratory |
| MEA | Mono-Ethanol Amine |
| MIT | Massachusetts Institute of Technology |
| $N_2O$ | Nitrous oxide |
| NETL | National Energy Technology Laboratory |
| NGCC | Natural Gas Combined Cycle |
| NO | Nitrogen oxide |
| $NO_2$ | Nitrogen dioxide |
| $NO_X$ | Nitrogen oxides |
| NREL | National Renewable Energy Laboratory |
| OPDE | Open Pond Dry Extraction |
| OPWE | Open Pond Wet Extraction |
| OSBL | Outside Battery Limits |
| $P_2O_5$ | Phosphorous pentoxide |
| PARTNER | Partnership for AiR Transportation Noise and Emissions Reduction |
| PBR | Photobioreactor |
| PTW | Pump-to-wake |
| $PM_{2.5}$ | Primary and secondary volatile and nonvolatile particulate matter smaller than 2.5 microns |
| $PM_{10}$ | Primary and secondary volatile and nonvolatile particulate matter smaller than 10 microns |
| $PM_{NV}$ | Primary nonvolatile particulate matter |
| ppt | Parts per thousand |

| | |
|---|---|
| ppm | Parts per million |
| RFS2 | Renewable Fuel Standard 2 |
| SCC | Social Cost of Carbon (Dioxide) |
| SCCe | Social Cost of Carbon Dioxide Equivalent |
| $SO_X$ | Sulfur oxides |
| SPK | Synthetic Paraffinic Kerosene |
| SQP | Sequential Quadratic Programming |
| TAG | Triglyceride (or triacylglyceride) |
| TDS | Total Dissolved Solids |
| TPI | Total Project Investment |
| UHC | Unburned Hydrocarbons |
| U.S. | The United States of America |
| USA | United States Army |
| USAF | United States Air Force |
| USN | United States Navy |
| VOC | Volatile Organic Compounds |
| VTDE | Vertical Tubular Dry Extraction |
| VTWE | Vertical Tubular Wet Extraction |
| WTP | Well-to-pump |
| WTW | Well-to-wake |

# Chapter 1: Introduction and Background

The current interest from the United States (U.S.) commercial and military aviation sectors in alternative jet fuel stems from multiple factors including increasing conventional fuel prices, price volatility, current reliance on a small variety of energy sources like conventional crude, global climate impacts, and potential air quality (AQ) benefits [1,2,3,4]. To avoid expenses associated with infrastructure changes, civil and military jet aircraft will require a near-term fuel replacement for conventional petroleum based jet fuel that is a "drop-in" hydrocarbon substitute. This substitute will need to function with the existing aircraft infrastructure while meeting rigorous safety and quality standards [5]. The following sections provide the background necessary for understanding alternative aviation fuels' role over the next decade.

## 1.1 Conventional and Alternative Jet Fuels

As previously mentioned, aviation fuels must adhere to high safety and quality standards. Conventional jet fuels vary by user, but can be generally categorized as Jet A or Jet A-1 and Jet Propellant 5 or 8 (JP-5 or JP-8) for the civil and military fleets, respectively. Jet A has a higher freeze point than JP-8 and Jet A-1 while JP-5 has higher flash points. Other jet fuels such as Jet B, JP-4, JP-6, and JP-7 were used for specific applications or climates and are either rarely used or no longer available. Jet A, Jet A-1, and JP-8 are the baseline fuels used for the alternative jet fuel comparisons in this analysis. This thesis assumes that these fuel compositions are identical as the fuels are similar in composition as the primary difference is that JP-8 uses an additive package.

Alternative "drop-in" jet fuels can be broken into five broad categories: jet fuel from unconventional sources of petroleum such as oil sands, very heavy oils, and oil shale; synthetic jet fuel from thermochemical processes involving natural gas-to-liquid (GTL), coal-to-liquid (CTL), lignocellulosic biomass-to-liquid (BTL), and/or coal-biomass-to-liquid (CBTL) such as Fischer-Tropsch (F-T) synthesis and pyrolysis; advanced fermentation, catalytic, and other means of converting sugar, including those in lignocellulosic materials, and starches to jet fuel; hydroprocessing of renewable oils to synthetic jet fuel known as hydroprocessed renewable jet (HRJ), also known as hydroprocessed esters and fatty acids jet (HEFA-J) fuels; and conversion of calorific liquids from micro-organisms to synthetic jet fuel [5]. Fuels derived from F-T and HEFA-J processes are generally known as Synthetic Paraffinic Kerosene (SPK) fuels as their composition is mainly normal and iso-paraffin chains [6]. This thesis will focus on SPK fuel derived from algal oils via HEFA processes.

Alternative jet fuels from non-petroleum sources exhibit different compositions than that of their conventional and alternative petroleum counterparts. Figure 1.1 illustrates the various compositions of Jet A-1, JP-8, and HEFA or F-T SPK derived from beef tallow and coal or natural gas, respectively. The left three bars represent samples of conventional commercial and military grade jet fuels while the right six illustrate SPK fuels derived from HEFA, F-T GTL, and F-T CTL processes. As SPK implies, the majority (88-95+%) of the non-petroleum derived alternative jet fuels consist of n- and iso-paraffins while the conventional fuels contain larger amounts of cyclo-paraffins, benzenes, naphthalenes, indanes and tetralins.[*] The differences in

[*]Mono- di- and tri-cycloparaffins are classified generally as naphthenes. Benzene is classified as a monocyclic aromatic hydrocarbon while naphthalenes, indanes, and tetralins are classified as

SPK's composition from conventional jet fuels – particularly the lack of aromatics and sulfur – account for variation in the composition of combustion products (see Appendix E) as well as compatibility issues concerning fuel tank O-ring seal swell and lubricity [3,7]. Note that the jet fuel compositions were referenced from samples provided and used in various emissions tests [8,9,10].

The military and civil specifications for JP-5, JP-8, Jet A, and Jet A-1 are described in the MIL-DTL-5624U, MIL-DTL-83133H, and ASTM D1655 regulatory documents [11,12,13]. Alternative synthesized hydrocarbon fuel blends have been approved in specification regulations MIL-DTL-83133H and ASTM D7566-11a [14]. Through both ground and flight tests, the Department of Defense (DOD) and civilian aviation have certified up to a 50% blend of F-T and HEFA derived SPK fuels with conventional jet fuels provided that they meet all fuel property specifications.

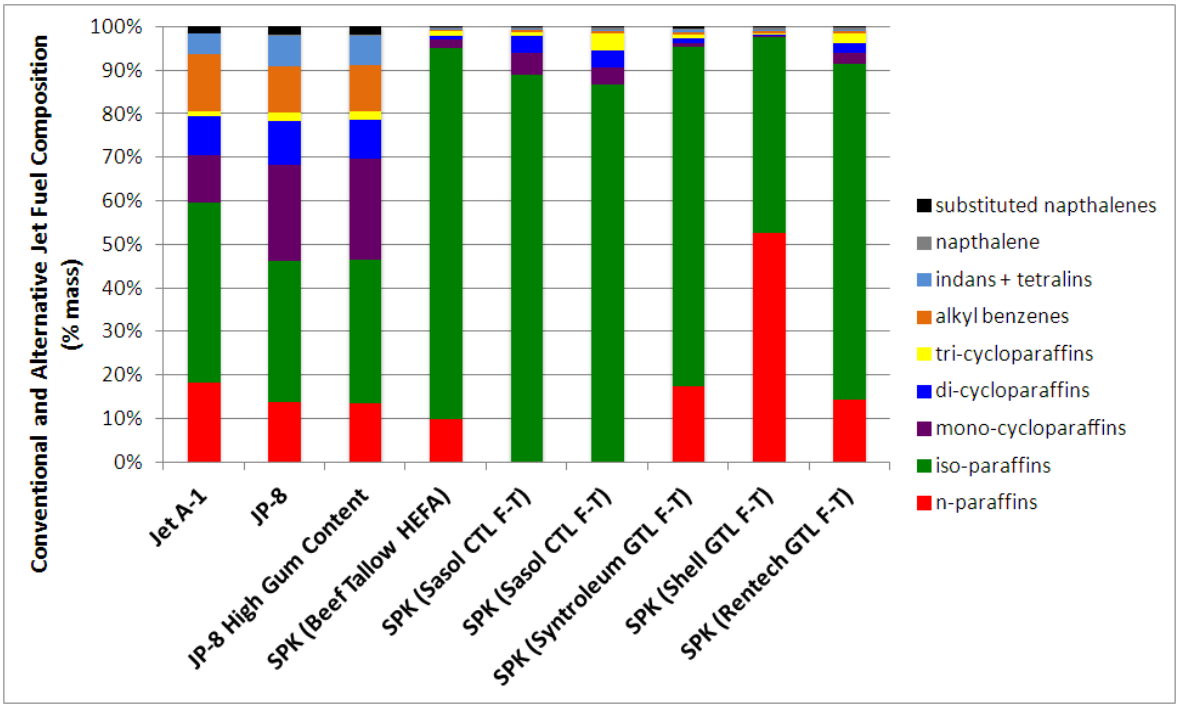


Figure 1.1. Conventional and Neat Alternative Jet Fuel Compositions [8,9,10]

### 1.2 Current United States Military and Civil Conventional Aviation Fuel Sectors

Knowledge of various conventional aviation fuel demands is necessary when determining the production sustainability aspects of alternative jet fuels. U.S. aviation fuel procurement and use can be divided into military and civil sectors. To remain consistent, the conventional aviation fuels considered will consist of either JP-8, Jet A or Jet A-1.

The average relative U.S. refinery yields from 1993 to 2011 are depicted in Figure 1.2. Jet fuel remains steady at nearly 9% throughout this timeframe. Of this percentage, the majority of Contiguous United States (CONUS) jet fuels are produced for civil aviation in the form of Jet A.

---

polycyclic aromatic hydrocarbons. The naphthenes and aromatics each represent nearly 20% of conventional jet fuel on a mass basis.

Table 1.1 illustrates the 2009 CONUS civil and military jet fuel use by type. The 1.16 of the 1.35 million bpd of all jet fuel bought in 2008 were used at CONUS airports in the form of Jet A [15]. Within military aviation fuel, the United States Air Force (USAF), United States Navy (USN), and the United States Army (USA) used 51%, 20%, and 29% of U.S. military aviation fuel in 2009, respectively [16]. These absolute amounts of jet fuel are used as a reference when providing a framework for meeting alternative fuel goals in the following sections.

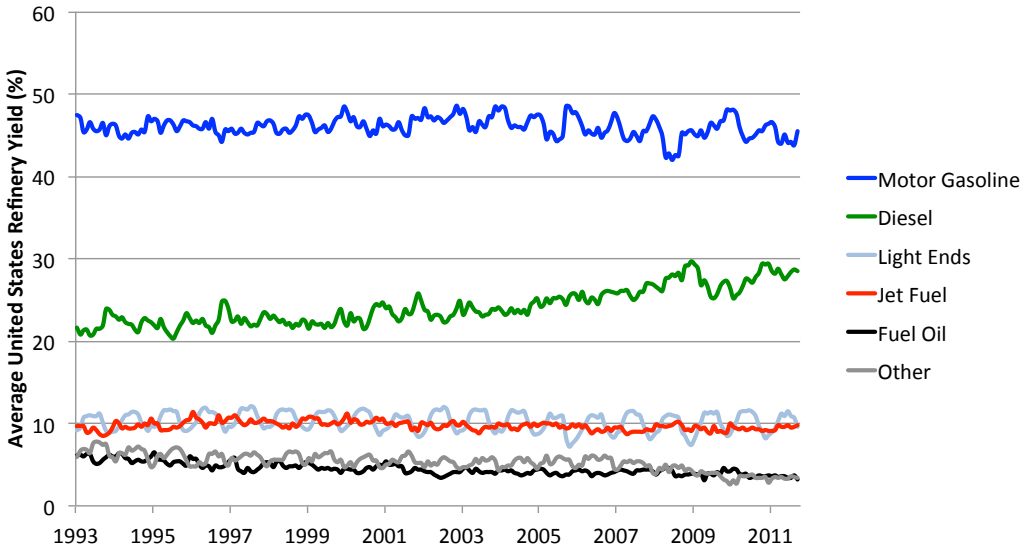


Figure 1.2: 1993-2011 U.S. Average Crude Oil Refinery Yield Distributions [17]

Table 1.1: Military 2010 and Civil 2009 CONUS Jet Fuel Use [15,16]

| | Fuel Use in Barrels per Day (bpd) | | | | |
|---|---|---|---|---|---|
| | Jet-A | JP-8 | JP-5 | Other | Total |
| Civil | 1,160,000 | - | - | - | 1,160,000 |
| USAF | - | 91,600 | - | 3,460 | 95,100 |
| USN | 316 | 11,800 | 25,000 | - | 37,500 |
| USA | - | 52,400 | - | 938 | 53,300 |
| Total | 1,160,000 | 156,000 | 25,000 | 4,700 | 1,350,000 |

## 1.3 Alternative Jet Fuel Goals

Commercial and military aviation have set alternative fuel and environmental targets for the next half century. Airlines for America (A4A) – an industry association representing U.S. airlines – has set goals for alternative fuel providers to produce fuels with lower lifecycle emissions than that of conventional jet fuel [18]. Table 1.2 provides a summary of U.S. civil and military goals and regulations regarding both alternative fuel production and lifecycle greenhouse gas (GHG) emissions. Each entity in Table 1.2 holds an interest in both alternative fuels as an energy source and as a potential means of reducing the environmental impacts of aviation.

Table 1.2: U.S. Alternative Fuel and GHG Goals

| Arena | Entity | Document Date | Alternative Fuel Use | Life Cycle GHG | Alternative Fuel Goal (bpd) |
|---|---|---|---|---|---|
| Civil | A4A | 2011 | --- | Encourage fuel providers to provide a fuel that will have lower GHG than conventional jet fuel [18] | --- |
| | FAA | 2011 | 1 billion gallons of jet fuel per year (65,200 bpd) by 2018 [19] | --- | 32,600 [19] |
| | EPA† | 2007 | 36 billion gallons of per year (2.3 million bpd) of ground and air transportation fuels by 2022 | Reductions from 2005: corn ethanol (20%), advanced biofuel (50%), Biomass-based diesel (50%), Cellulosic biofuel (60%) | --- |
| Military | USAF | 2010 | 50% of USAF domestic aviation via alternative jet fuel blend; cost competitive acquisition from domestic sources by 2016 [20] | Alternative fuels produced in a manner that is "greener" than fuels produced from conventional petroleum | 23,800‡ |
| | USN | 2010 | By 2020, half of the Navy's total energy consumption afloat will come from alternative sources [21] | | 18,700‡ |

## 1.4 Analysis Framework and Scenarios

This thesis provides a holistic assessment of microalgae derived HEFA-J SPK fuels that includes environmental and economic implications. Table 1.3 depicts the areas that were quantified for various scenarios. The air quality and technical feasibility sectors rely on fuel composition and engine characteristics (see Appendix E) that are separate from the other categories. For the purposes of this investigation, the other sections include low, baseline, and high scenarios that have been analyzed in order to capture a variability range. Local sensitivity analyses have also been conducted for each of the inputs to these scenarios to assess prioritization of future research and development efforts.

Table 1.3: Alternative Fuel Feasibility and Sustainability Metrics

| Area | Metric(s) | Quantification methodology |
|---|---|---|
| Technical feasibility | Fuel properties§ | Fuel composition and gas turbine engine characteristics |
| Air quality emissions | g-emission/$MJ_{HEFA-J}$ | |
| Production cost | $/$MJ_{HEFA-J}$ | Lifecycle assessment |
| Land footprint | $L_{TAG}$/ha/yr | |
| GHG emissions | g-$CO_2$e/$MJ_{HEFA-J}$ | |
| Freshwater consumption | L/$MJ_{HEFA-J}$ | |

† EPA provides GHG thresholds for both aviation and traditional ground transportation alternative fuel feedstocks based on the Renewable Fuel Standard (RFS2) as a part of the Energy Independence and Security Act (EISA) of 2007 [134]

‡ Based on CONUS 2009 Defense Logistics Agency (DLA) jet fuel sales [16]

§ Some of these properties are freeze point, flash point, thermal stability, specific energy, and

A "cradle-to-grave" or lifecycle assessment (LCA) was conducted for various cultivation pathways as seen in Figure 1.3. In this analysis, the paths in the microalgae to jet fuel lifecycle involve many different processes and steps linked by black arrows: fossil fuel electricity generation; cultivation, recovery, and extraction of algal oils; movement and upgrading of the algal oil; transportation and blending; and jet fuel combustion. Emissions, freshwater consumption, production cost, and land use quantifications were delineated by their corresponding brown, blue, green and red rectangles, respectively. The LCA process in this thesis was constructed to recycle as much mass and energy as possible [22]. These methods are an expansion of studies presented in previous lifecycle analyses [4,22].

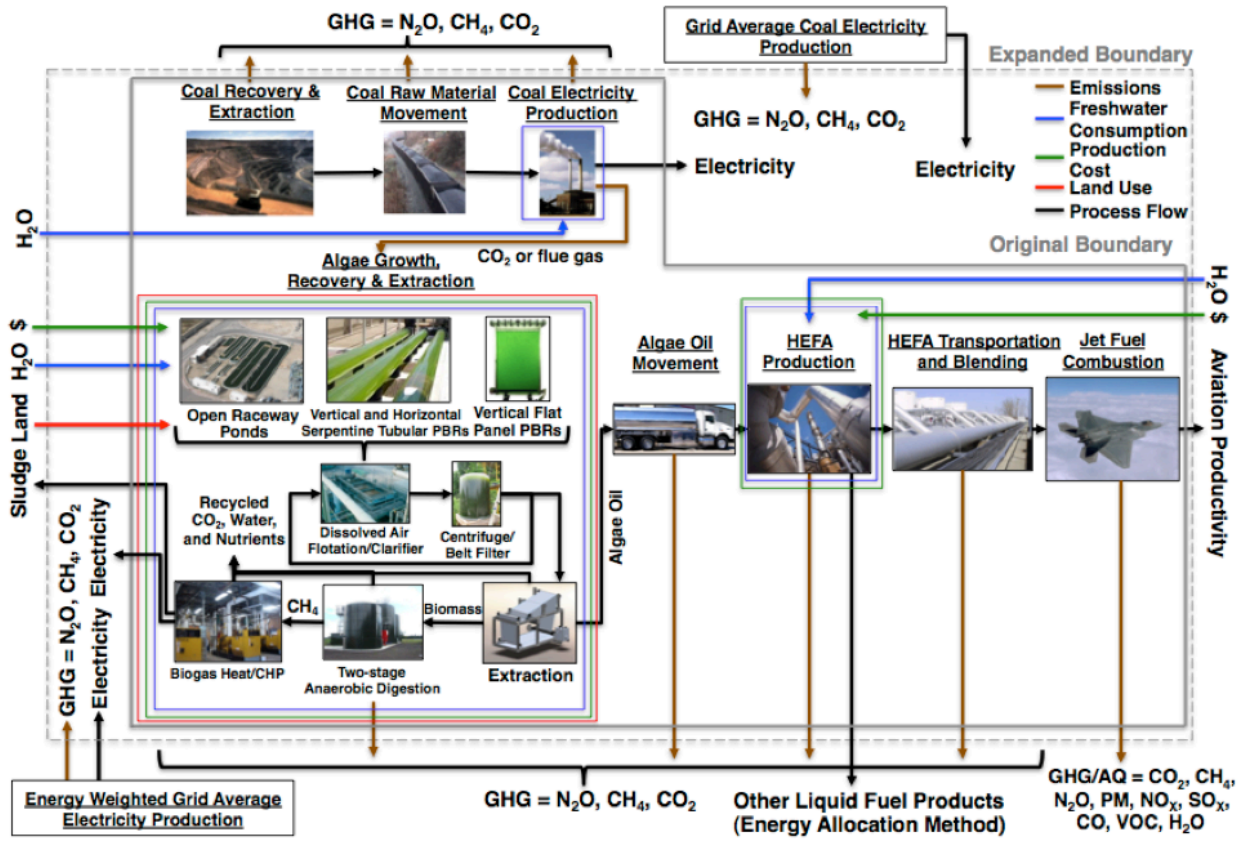


Figure 1.3: CONUS Algae-derived HEFA Environmental Lifecycle Analysis; Emissions (Brown) Cover All Lifecycle Steps; Freshwater Consumption (Blue) Covers Coal Electricity Production, Algae Cultivation, Recovery, Growth, Extraction, and Upgrading; Production Cost (Green) Covers Algae Cultivation, Recovery, Growth, Extraction, and Upgrading; And Land Use Covers The Facility Footprint Used for Algae Cultivation, Recovery, Growth, and Extraction; Displacement Allocation is Used for Electricity Offsets While Energy Allocation is Used for Liquid Fuel Coproducts

Both GHG and AQ Emissions (brown arrows) were delimited by the solid grey boundary. However, the need to feed $CO_2$ to the algae to sustain large growth rates requires an expanded system boundary denoted by dashed grey boundary. The extended boundary represents a displacement method to credit for the emissions from a process that is independent from the algae cultivation. In the upper right of Figure 1.3, the same amount of electricity was assumed to enter the expanded system boundary as the amount leaving the original system boundary. The

emissions balance assumed subcritical pulverized coal power plant emissions as a $CO_2$ source while the external displaced emissions were estimated to be an average coal power plant as well. This combination of system boundary and allocation method results in the $CO_2$ emissions from the electricity generation being unchanged because the emissions from the algae HEFA combustion are attributed to the electricity generation.

In scenarios with minimal thermal loads, surplus electricity generated from a biogas combined heat and power plant (CHP) is exported to the grid. In these cases, energy weighted average U.S. electricity production emissions were displaced by the emissions generated and recycled by the CHP (lower left of Figure 1.3). In addition, an energy allocation method was used to account for other liquid fuel byproducts associated with upgrading. This hybrid allocation methodology was used in previous algae lifecycle analyses where end fuel is not the main upgrading product [2,4]. The units for GHG LCA and AQ emissions are g-$CO_2$e/MJ and g-emission/MJ, respectively. Further information on co-product allocation and GHG LCA emissions are found in Table 4.1 and Chapter 2: Microalgae Derived Fuel Methodologies, respectively.

The water consumption metric in Table 1.3 is defined as freshwater that is taken from a location and not returned directly to the original source [23,24]. Freshwater consumption was accounted for offsite electricity production, cultivation, harvesting, extraction, and upgrading in units of $L_{water}/MJ_{HEFA\text{-}J}$. The allocation methods from the GHG LCA calculations were also employed for freshwater consumption. Similarly, production costs – which include capital, fixed operating, and variable operating costs – were quantified for the cultivation, harvesting, extraction, and upgrading LCA steps in units of $\$/MJ_{HEFA\text{-}J}$. Market allocation was used for determining production cost between HEFA-J and additional liquid coproducts. Lastly, facility land usage ($L_{TAG}$/ha/yr) as well as water and carbon flows were provided for cultivation, harvesting, and extraction steps. Further information on LCA quantification for each step and metric can be found in Section 2.2.

Each of these sustainability metrics were analyzed quantitatively for the various cultivation systems and extraction technologies seen in Table 1.4. The four main cultivation systems in question are open raceway pond, horizontal and vertical serpentine tubular photobioreactors (PBRs) and vertical flat panel PBRs. For all cultivation systems, dry hexane solvent and wet steam lysing technology sets were explored. Each of the 24 scenarios was compared for an output of 137 bpd of oil in the form triglycerides (TAGs) from a pilot facility to a 2000, 4000, or 6500 bpd TAG hydroprocessing facility. Further information on the cultivation system models and extraction technologies, as well as scenario inputs and assumptions can be found in Chapter 2: Microalgae Derived Fuel Methodologies.

Table 1.4: Cultivation and Extraction Scenario Matrix

| Cultivation System | Extraction Technology | GHG Emissions | Water Consumption | Land Use | Production Cost |
|---|---|---|---|---|---|
| Open Raceway Pond | Drying with Hexane Solvent | | Low | | |
| | | | Baseline | | |
| | | | High | | |
| | Wet Steam with KOH Lysing | | Low | | |
| | | | Baseline | | |
| | | | High | | |
| Horizontal Serpentine Tubular PBR | Drying with Hexane Solvent | | Low | | |
| | | | Baseline | | |
| | | | High | | |
| | Wet Steam with KOH Lysing | | Low | | |
| | | | Baseline | | |
| | | | High | | |
| Vertical Serpentine Tubular PBR | Drying with Hexane Solvent | | Low | | |
| | | | Baseline | | |
| | | | High | | |
| | Wet Steam with KOH Lysing | | Low | | |
| | | | Baseline | | |
| | | | High | | |
| Vertical Flat Panel PBR | Drying with Hexane Solvent | | Low | | |
| | | | Baseline | | |
| | | | High | | |
| | Wet Steam with KOH Lysing | | Low | | |
| | | | Baseline | | |
| | | | High | | |

*[Page Intentionally Left Blank]*

# Chapter 2: Microalgae Derived Fuel Methodologies

## 2.1 Microalgae Background

Microalgae are one of the oldest forms of life and are classified generally as thallophytes, i.e., simple plants that lack roots, stems, or any form of well-differentiated body design. The majority of their relatively simple structure and development are for energy conversion, which allows for the rapid reproduction and adaptation of a wide variety of species [25,26]. Algae have eukaryotic cells with organelles that control cell functions in contrast to prokaryotic cells, also known as cyanobacteria, which lack membrane-bound organelles [27]. The thousands of different species and strains of microalgae can be broken into the three main categories based on pigmentation, lifecycle, and cellular structure: chlorophyta (green algae), rhodophyta (red algae), and bacillariophyta (diatoms). Algae can also be classified by cultivation conditions: photoautotrophic, heterotrophic, mixotrophic, and photoheterotrophic. Photoautotrophic (or phototrophic) cultivation involves energy absorbed from light, assimilation of inorganic carbon and uptake of nutrients from an aquatic medium to form chemical energy via photosynthesis. Heterotrophic microalgae grow under dark conditions where both energy and carbon sources come from organic carbon (e.g., sugars such as glucose or xylose). Microalgae under mixotrophic conditions undergo photosynthesis and use both organic and inorganic carbon sources. Lastly, photoheterotrophic cultivation requires light and an organic carbon source for growth [28,29,30]. The microalgae under consideration in this thesis are a range of marine and freshwater photoautotrophs. Compared to other cultivation methods, autotrophic microalgae have less contamination issues which favors scaled outdoor cultivation in open raceway ponds [28,30].

### 2.1.1 Species Suitable for Fuel Production

One of the major benefits of using a diverse and relatively simple feedstock like microalgae is the ability to breed, engineer and select species with characteristics that favor particular environments, cultivation technologies, and extraction techniques. Additional advantages of using certain algae species are that they can: synthesize and accumulate large quantities of neutral lipids/oil; grow at high rates (1-3 doublings per day); thrive in saline, brackish or coastal seawater for which there are few competing demands; tolerate marginal (arid or desert) lands; utilize growth nutrients from a variety of wastewater sources; sequester large amounts carbon dioxide from flue gases; produce value-added coproducts like biopolymers, proteins, polysaccharides, pigments, animal feed, fertilizer, and hydrogen; and can grow year round in suitable vessels and locations [31]. As will be seen in the following sections, performance in the first two categories, biomass growth and lipid content, impact all of the major lifecycle sustainability metrics in Table 1.3.

### 2.1.2 Biomass Yield and Lipid Content

Of the various oil producing feedstocks, microalgae provide the largest oil productivities [32]. Figure 2.1 illustrates the fuel yields of various HEFA and F-T feedstocks and product slates. Note that these yields assume only the cultivation system areal footprint where the algae are growing. The results section in Chapter 4 depicts fuel yields outlined by the entire facility area. Nominal photoautotrophic microalgae to fuel growth rates from open ponds and closed PBRs are estimated at between 15,000-25,000 L/ha/yr; larger than the nearest analyzed biomass feedstock (Palm HEFA) by a factor of six [2,5,22,33]. Lipid content of microalgae depends highly upon growing conditions and strain selection. Certain microalgal species under favorable conditions

can consist of up to 50-70% lipids dry weight and produce up to 58,700 $L_{oil}$/ha, which is two orders of magnitudes higher than the nearest oil producing energy crop [32]. Nutrient-limiting conditions are used to increase the microalgae lipid content, which means that achieving higher lipid content for a given species usually lowers the biomass productivity [30].

A review of phototrophic microalgae production from air and direct $CO_2$ injection in laboratory scale systems ranged biomass volumetric productivities of 0.004-0.47 g/L/day, dry weight lipid contents of 4.10-67.8%, and lipid productivities of 0.85-150 mg/L/day [28]. Figure 2.2 provides a graphical representation of the phototrophic, mixotrophic, and heterotrophic microalgae species. The $CO_2$ and air fed phototrophic species represent the majority of the survey while a few mixotrophs and heterotroph performances were captured. The heterotrophs consisting of species chlorella protothecoides had the highest cell and lipid densities due to their ability to convert large amounts sugars like glucose, acetate, corn powder hydrolysate, and Jerusalem artichoke hydrolysate into chemical energy. Of the phototrophs, $CO_2$ fed Chlorella sp., Nanochloropsis, and Nanochloris Oleoabundans species performed most favorably in ideal laboratory conditions [34,35]. For the purposes of this thesis, a range of productivities were used that represent phototrophic growth rates spanning the $CO_2$ fed spectrum in open pond and closed PBR systems outlined in Figure 2.1.

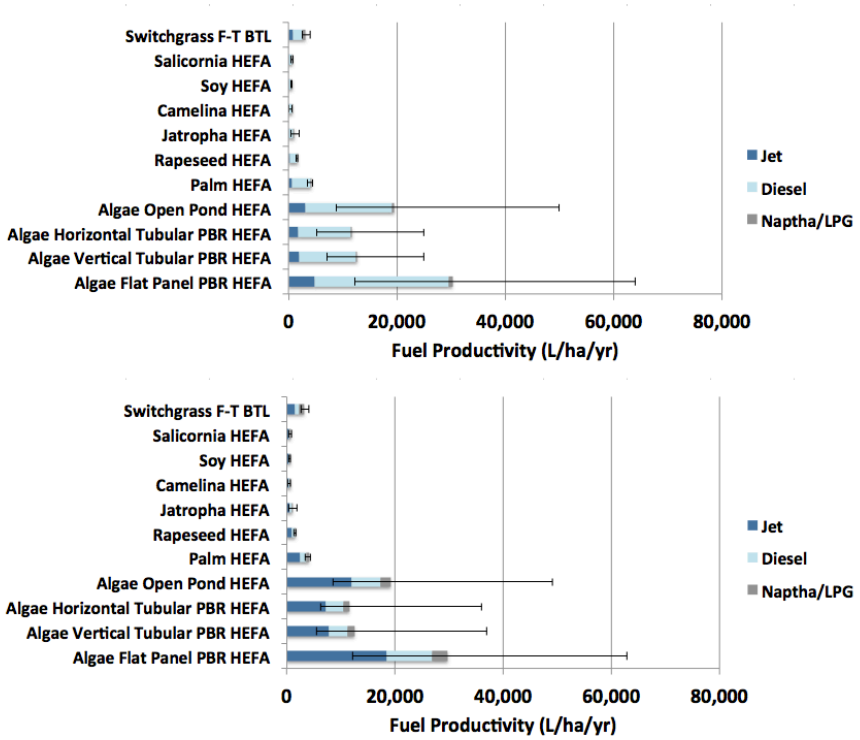


Figure 2.1: Biomass Feedstock-to-Fuel Productivities: Maximum Distillate Product Slate (Top) and Maximum Jet Fuel Product Slate (Bottom) [2,5,33]. Algae Fuel Yields Based on Entire Facility Area Are Derived in Chapter 4.

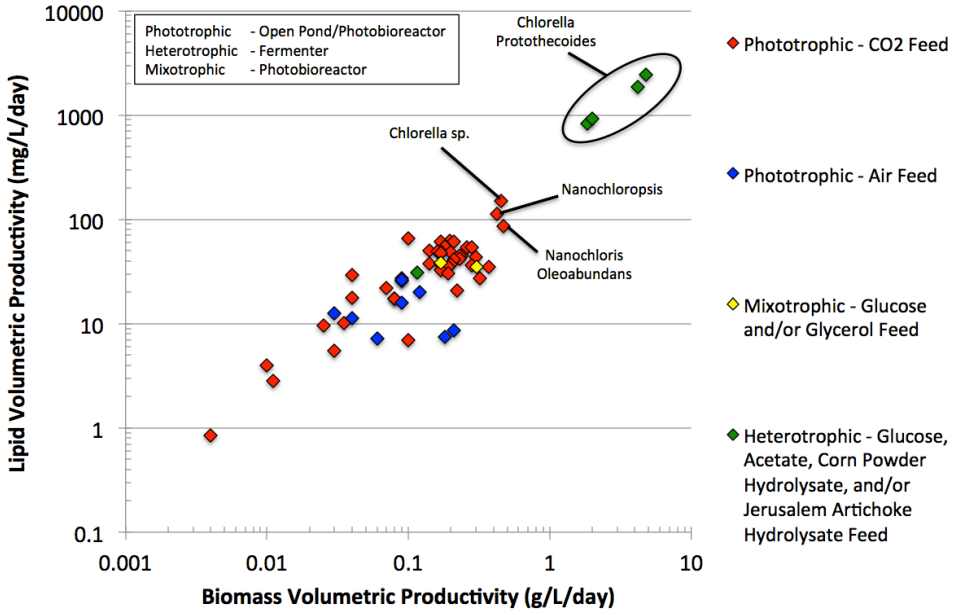


Figure 2.2: Various Algae Cultivation and Species Biomass and Lipid Volumetric Productivities [28,36]

## 2.2 Lifecycle Analysis Methods and Assumptions

### 2.2.1 LCA and Associated Models

The LCA methodology illustrated in Figure 1.3 provides a framework for various scenarios involving different technologies and assumptions outlined in this chapter. The three main tools employed for the various scenarios examined are illustrated in Figure 2.3. The first model consists of three PBR growth simulators that have been validated and optimized for multiple performance metrics. The second tool is the LCA model, which acts as the central model where all information is gathered. The final tool is the Greenhouse Gases, Regulated Emissions, and Energy Use in Transportation Model (GREET1_2011) which takes information from the LCA model and computes LCA GHG emissions for each scenario [37]. The LCA GHG emissions in g-$CO_2$e/$MJ_{HEFA-J}$ consist of $CO_2$, $CH_4$, and $N_2O$ and are based on 2010 technologies and encompass a 100-year time window. The $CO_2$e metric is a combination of these GHGs weighted by their global warming potentials. $CO_2$, $CH_4$, and $N_2O$ are assumed to have global warming potentials of 1, 25, and 298, respectively. Other non-$CO_2$ energy balance effects from the production and combustion of aviation fuel (soot, cirrus, contrails, etc.) were not considered in this analysis. Direct and indirect land use change GHG emissions, as well as emissions associated with site construction, were also not considered. The following sections describe the technologies and processes involved in these scenarios.

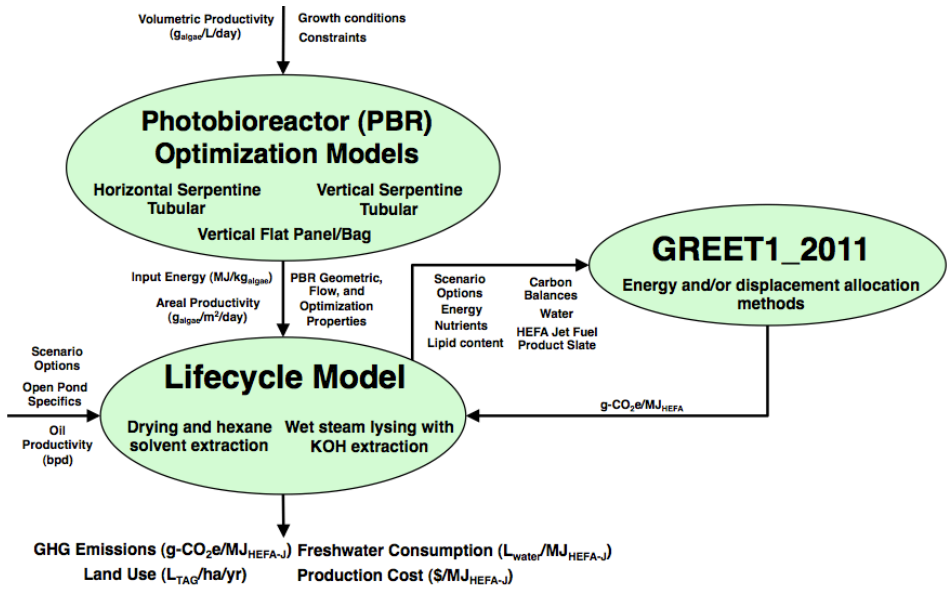


Figure 2.3: Lifecycle Tools and Methods Flowchart

2.2.2 $CO_2$ Capture, Transportation, Distribution, and Recycle from Coal Electricity Production

The first step in the microalgae lifecycle involves the feeding of inorganic carbon in the form of $CO_2$ (either pure, flue gas, or air) to open ponds or closed PBR cultivation units. The carbon source for a microalgae energy crop must be in large enough concentrations for satisfactory growth rates. This analysis focuses on concentrated $CO_2$ and flue gases produced from the combustion of coal at an pulverized coal power plant collocated with the facility. Scenarios requiring concentrated $CO_2$ involve an energy intensive process in which a Mono-Ethanol Amine (MEA) scrubber separates 90% of the $CO_2$ from the flue gas. Table 2.1 provides significant efficiencies, material inputs, and energy inputs for typical MEA separation systems. The direct flue gas and MEA steam and electrical energy requirements for open raceway ponds are depicted in Table 2.2. For the purposes of this thesis, these open raceway pond specific energy inputs were assumed identical for PBRs $CO_2$ distribution. Furthermore, the pressure head associated with piping for $CO_2$ and air distribution were assumed negligible.

Table 2.1: Mono-Ethanol Amine (MEA) Scrubber Parameters and Performances

| MEA Performance Parameters | | Value | Units | Notes/Refs. |
|---|---|---|---|---|
| | $CO_2$ capture efficiency | 90 | % | |
| | $NH_3$ emission | 0.21 | kg/$tonne_{CO2}$ | |
| | MEA | 3.25 | kg/$tonne_{CO2}$ | |
| | NaOH | 0.13 | kg/$tonne_{CO2}$ | [22,38] |
| | Activated C | 0.075 | kg/$tonne_{CO2}$ | |
| Freshwater (subcritical pulverized coal) | | 0.66 | gal/$kg_{CO2}$ | |
| Freshwater (supercritical pulverized coal) | | 0.59 | gal/$kg_{CO2}$ | |
| | Steam | 1110 | kWh/$tonne_{CO2}$ | [22,38] |
| | Electricity | 23.6 | kWh/$tonne_{CO2}$ | |
| | | 1134 | kWh/$tonne_{CO2}$ | [22,38] |
| | Total energy | 1847 | kWh/$tonne_{CO2}$ | [39] |
| | | 1694-2847 | kWh/$tonne_{CO2}$ | [40] |
| GHG emissions from material use | MEA | 3.25 | g-$CO_2$e/$tonne_{CO2}$ | - Wood used as proxy for activated C; Biomass credit from cultivation [41,42] |
| | NaOH | 1.01 | g-$CO_2$e/$tonne_{CO2}$ | |
| | Activated C | -2.30 | g-$CO_2$e/$tonne_{CO2}$ | |

Table 2.2: Direct Injection Flue Gas and Pure $CO_2$ Energy Inputs

| Type of Carbonation | Region | Flue gas/$CO_2$ Transport & Distribution (kWh/tonne) | $CO_2$ Capture (kWh/tonne$_{CO2}$) | Notes/Refs. |
|---|---|---|---|---|
| Flue Gas | Offsite | 0 | - | - Based on 20 wt.% (13 mole%) $CO_2$ in coal flue gas [43]<br>- 8 km transport<br>- 2.32 tonne/km/yr leakage [22] |
| | Onsite | 38.6 | - | - Includes recycle and make-up $CO_2$ streams |
| Pure $CO_2$ | Offsite<br>Onsite | 0<br>38.6 | Steam: 1110,<br>Power: 23.6 | [22,38] |

2.2.3 Microalgae Cultivation

Microalgae cultivation in this analysis has been delineated into two major classes: open raceway pond and closed PBR systems. Table 2.3 presents the major inputs for all cultivation system classes. Lower Heating Values (LHVs) were used for all energy calculations. The low scenarios assume the use of municipal wastewater as the culture makeup source and an increased lipid weight fraction, which lowers the need for the majority of nitrogen and phosphorous inputs. The extractable lipid weight fractions encompass the range of most phototrophic microalgae species investigated by this study [32,44,45,46,47,48,49].

Table 2.3: $CO_2$, Solar Irradiance, Water, Nutrients and Biomass Composition Inputs [22]

| | | Low | Baseline | High | LHV (MJ/kg) | Carbon |
|---|---|---|---|---|---|---|
| $CO_2$ inputs | $CO_2$ required (kg/kg$_{Biomass}$) | 2.43 | 2.05 | 1.93 | | |
| Solar energy | Solar irradiance (MJ/m$^2$/yr) | 7230 | 7230 | 7230 | | |
| Water | Makeup water | Waste | Brackish | Brackish | | |
| | Makeup water mass TDS (ppt) | 1.0 | 20 | 20 | | |
| Nutrient inputs | Nutrient use efficiency | 90% | 90% | 90% | | |
| | N (g/kg$_{Biomass}$) | 36 | 100 | 173 | | |
| | $P_2O_5$ (g/kg$_{Biomass}$) | 4 | 12 | 21 | | |
| | Fe (g/kg$_{Biomass}$) | 2 | 5 | 9 | | |
| | Nitrogenous fertilizer type | Ammonia | GREET Default | Ammonium nitrate/ Ammonium sulfate | | |
| Biomass composition | Lipid (g/kg$_{Biomass}$) | 650 | 350 | 250 | 39 | 78% |
| | Non-extractable lipid (g/kg$_{Biomsas}$) | 600 | 250 | 150 | | |
| | Protein (g/kg$_{Biomass}$) | 250 | 450 | 500 | 23 | 46% |
| | Carbohydrate (g/kg$_{Biomass}$) | 100 | 200 | 250 | 17 | 40% |
| | Extractable lipid mass fraction | 60% | 25% | 15% | | |

2.2.3.1 Open Raceway Pond System

The open raceway ponds considered in this analysis are for a small-scale facility capable of producing 86-315 bpd TAG. This system was initially outlined for TAG upgraded to renewable diesel [22]. The open raceway pond cultivation system in Figure 2.4 consists of a 400 ha area of 40 growth ponds each with ~1 and ~0.1 km lengths and widths, respectively. Additional area includes primary and secondary harvesting, extraction, digestion, and combustion equipment, which increase the total area to ~450 ha. All ponds have 30 cm depths and each pond includes one paddlewheel-mixing unit. Piping tubes include $CO_2$/makeup water feed and recycling, blowdown, and downstream sludge and TAG pipes. Figure 2.5 illustrates the baseline of a single

open raceway pond, which mimics that of similar scaled algae growth ponds [50]. Table 2.4 provides the parameters and inputs specific to open raceway pond cultivation in this analysis. Raceway pond efficiencies are defined as the ratio of the fraction of energy imparted to the water flow to the energy input required to drive the paddlewheel. This ratio is expressed as the product of the paddle wheel and power train efficiencies. The areal and volumetric productivities for the scenarios encompass the majority of open raceway pond values for various microalgae species in recent literature [32,51,52,53,54]. The blowdown ratios are the evaporation-normalized amount of water that must be taken out of the system to prevent solids buildup in the culture. Evaporation rates were estimated based on a location in Southeast Texas. Equation (2.1) through Equation (2.3) provides fundamental equations for calculating hydraulic power required for wide raceway ponds with various scenario inputs [50]. The final power required for the pond $P_{pond}$ is a function of the culture density $\rho_L$, pond depth $d_{pond}$, flow velocity $V_{pond}$ and the Manning roughness coefficient $n_{pond}$. The pond velocity is in turn a function of pond slope, roughness, and hydraulic radius (equates to pond depth for wide channels). The material and economic inputs for open ponds are found in Table B1.

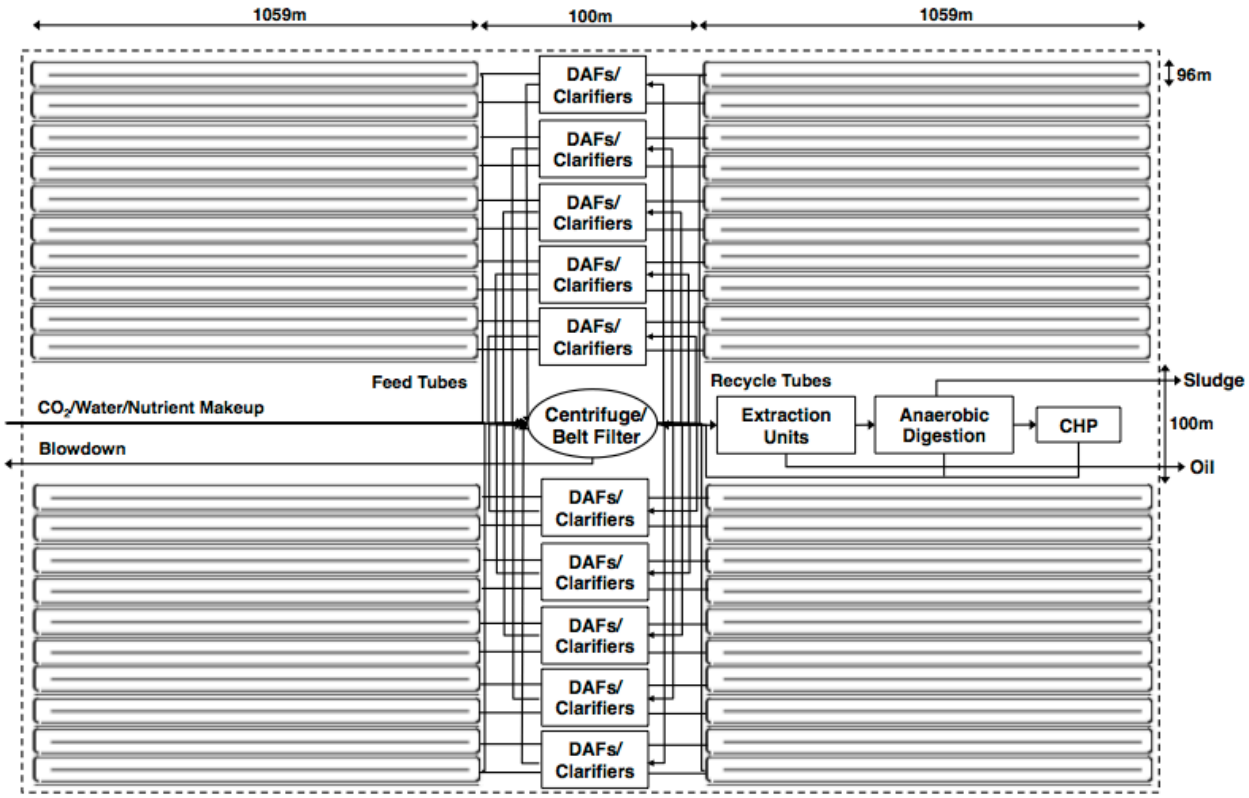


Figure 2.4: Baseline Open Raceway Pond System Schematic

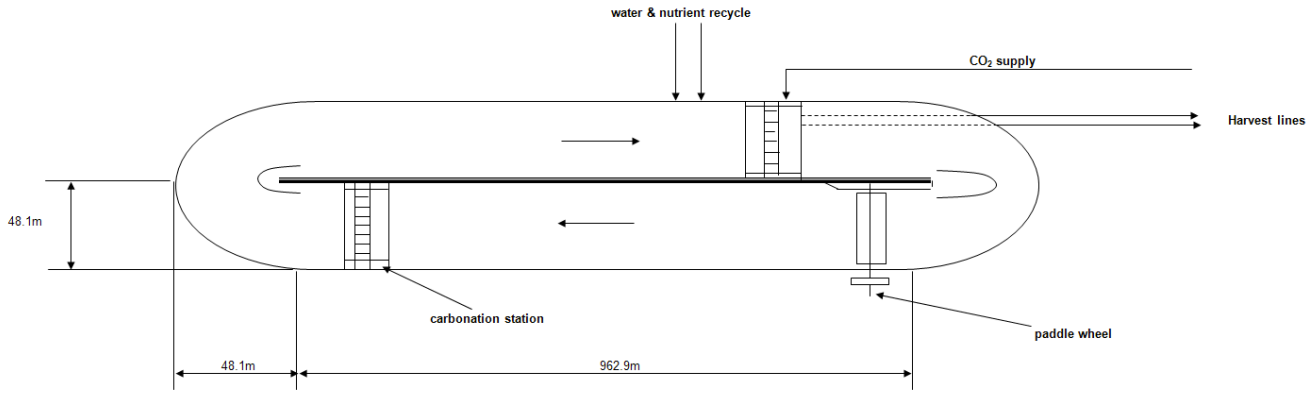


Figure 2.5: Baseline Single Open Raceway Pond

Table 2.4: Open Raceway Pond Cultivation Parameters, Inputs, and Performances

| | Low | Baseline | High | Notes/Refs. |
|---|---|---|---|---|
| Paddle wheel efficiency (%) | 75 | 60 | 60 | [22,50] |
| Power train efficiency (%) | 80 | 70 | 70 | |
| Biomass areal productivity (g/m$^2$/day) | 32 | 20 | 15 | |
| Biomass volumetric productivity (g/L/day) | 1.07 | 0.67 | 0.50 | |
| Biomass pond concentration (ppm) | 475 | 300 | 225 | |
| Evaporation rate (cm/day) | 0.5 | 0.5 | 0.5 | |
| Blowdown ratio | 0.05 | 1.0 | 1.0 | |
| Pond circulation velocity (cm/s) | 20 | 20 | 20 | |
| Manning's roughness coefficient (s/m$^{1/3}$) | 0.02 | 0.02 | 0.02 | |
| Total pond wall height (cm) | 50 | 50 | 50 | |
| Pond depth (cm) | 30 | 30 | 30 | |
| Total surface area of all ponds (ha) | 400 | 400 | 400 | |
| Algae mixing specific energy required (MJ/kg$_{algae}$) | 0.28 | 0.66 | 0.88 | Equation (2.3) [50] |
| Nutrient supply specific energy required (MJ/kg$_{algae}$) | 0.02 | 0.03 | 0.03 | Derived from [50] |
| Makeup water pumping specific energy required (MJ/kg$_{algae}$) | 0.08 | 0.23 | 0.30 | 45.2 Pa/m [22] |
| Initial pumping and filling specific energy (MJ/kg$_{algae}$) | 0.04 | 0.06 | 0.07 | Filled 3 times/year 45.2 Pa/m [22] |
| $CO_2$ capture on-site NG (MJ/kg$_{algae}$) | 0.00 | 0.00 | 7.89 | See Table 2.2 and Table 2.3 |
| $CO_2$ capture on-site electric (MJ/kg$_{algae}$) | 0.00 | 0.00 | 0.14 | |
| Recycle $CO_2$ compressor electric (MJ/kg$_{algae}$) | 0.00 | 0.00 | 0.31 | |
| On-site flue gas distribution electric (MJ/kg$_{algae}$) | 0.38 | 0.32 | 0.00 | |
| Total cultivation specific energy (MJ/kg$_{algae}$) | 0.79 | 1.29 | 9.65 | |

$$V_{pond} = \frac{d_{pond}^{2/3} S_{pond}^{1/2}}{n_{pond}} \tag{2.1}$$

$$S_{pond} = \frac{h_{L_{pond}}}{L_{pond}} = \frac{V_{pond}^2 n_{pond}^2}{d_{pond}^{4/3}} \tag{2.2}$$

$$P_{pond} = \frac{g \rho_L V_{pond}^3 n_{pond}^2}{d_{pond}^{0.3} \eta_{pond}} \tag{2.3}$$

2.2.3.2 Closed Photobioreactor Systems

There are three main types of closed PBR systems considered in this analysis: horizontal serpentine tubular, vertical serpentine tubular, and vertical flat panel. The horizontal and vertical

tubular PBRs are similar in character in that they both consist of solar collector and airlift sections. The solar collector is the portion of tubing where photosynthesis occurs and oxygen is produced. The airlift (or degasser) subsystem consists of two sections: one that inserts air at its base to transport the produced oxygen and harvest from the system (riser) and one that inputs makeup medium, $CO_2$, and nutrients into the solar collector (downcommer). Pumps were added into the tubular systems in cases where the potential energy gained in the airlift was overcome by the energy losses throughout the system. The flat panel system combines the solar collector and airlift degasser into one component. Harvesting and dilution rates for all PBRs were assumed to be continuous at 0.06 $m^3_{culture}$/day [53].

The three PBR designs in Figure 2.6 were modeled, validated against experimental pilot facilities, and optimized for various performance parameters as described in Chapter 3: Algae Photobioreactor Model Development and Optimization [53,54,55,56]. Unlike the fixed geometry open raceway pond cultivation system model, the modular PBRs were modeled to increase in number for a specific algal TAG output. Figure 2.7 illustrates the PBR cultivation facility organization broken into various components. For organization, the facility is compartmentalized into individual PBR modules, skids, and clusters. Skids and clusters were defined to have 100 and 5,000 modular PBR units, respectively. The number of clusters and downstream components are a function of PBR type, scenario inputs, and algal oil demand. The facility grows from the carbon and water sources horizontally outward until the production quota is met. The downstream harvesting and processing units were placed nearest to the middle of the facility. Makeup and recycle tubing to the PBRs were considered, to include all piping turn linkages.

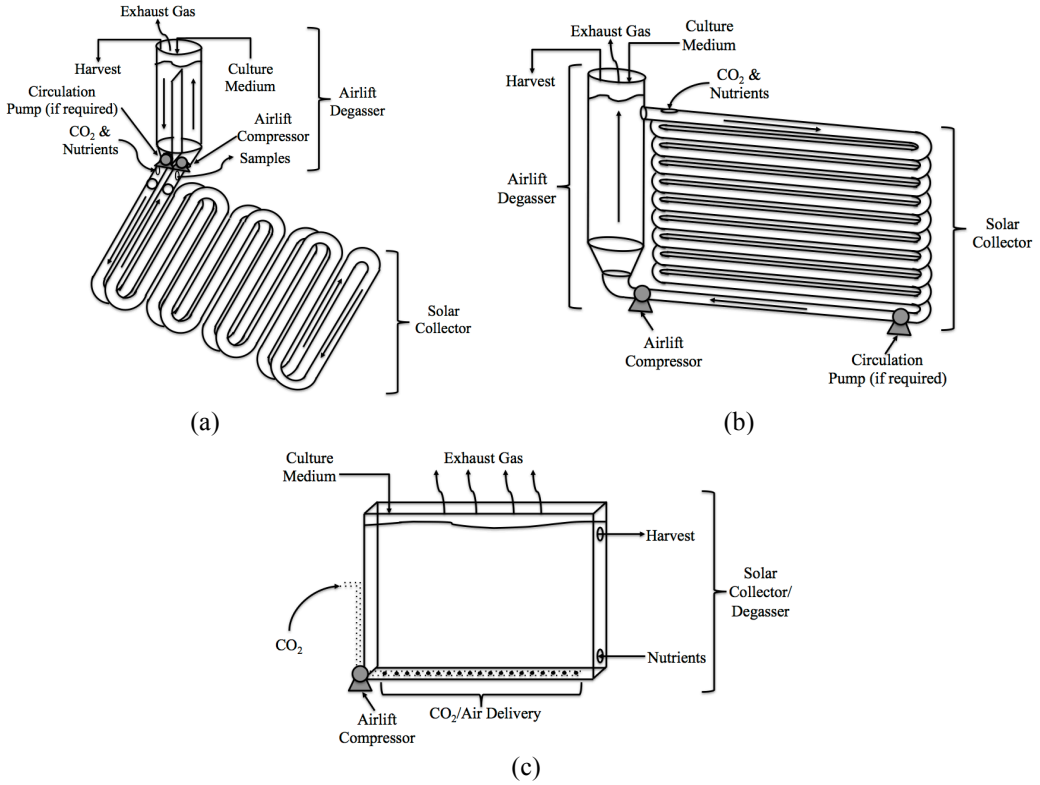


Figure 2.6: Considered Photobioreactor Types: (a) Horizontal Serpentine Tubular, (b) Vertical Serpentine Tubular, and (c) Vertical Flat Panel

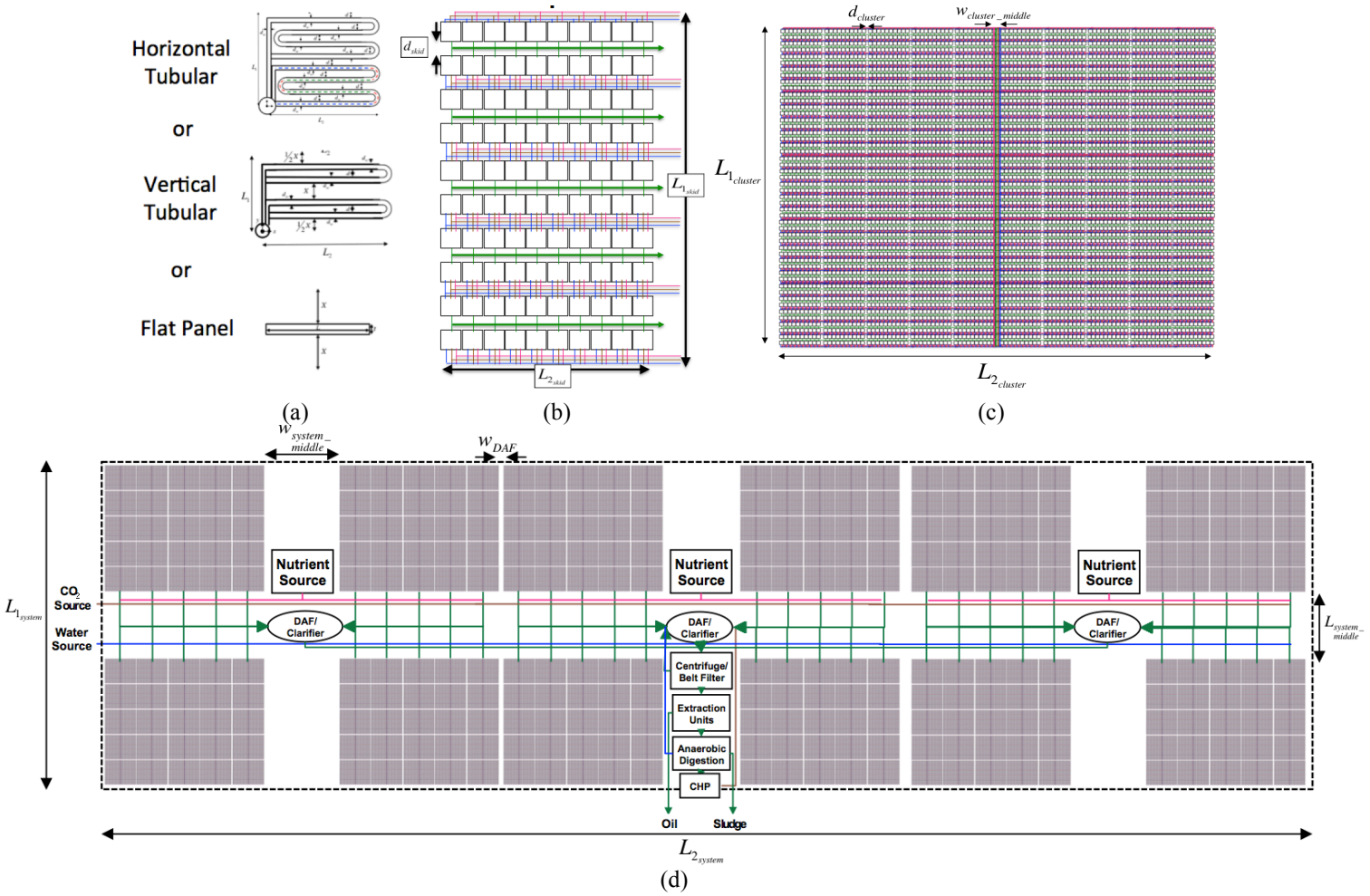


Figure 2.7: Photobioreactor Scaled-to-Demand Facility - (a) PBR Modules, (b) Skid Consisting of 10×10 PBR Modules, (c) Cluster Consisting of 50×10 Skids, and (d) System Consisting of 100 Clusters Per DAF/Clarifier (Number of DAFs/Clarifiers Depends on bpd Algal Oil Demand and PBR Dilution Rates)

Typical volumetric and areal productivities for each of the PBR types are depicted in Table 2.5. The majority of the indoor and outdoor pilot scale PBRs produced 0.25-1.90, 0.5-1.25, and 0.24-2.15 g/L/day for horizontal tubular, vertical tubular, and flat panel PBRs, respectively. The PBR cultivation parameters and inputs for this analysis are shown in Table 2.6 and represent a wide range of productivities. Biomass concentrations and blowdown ratios for these PBRs were also assumed two times higher than their open pond counterparts because although relative evaporation decreases, the larger concentration of TDS can eventually line the solar collector walls, which can inhibit photosynthetic growth over time. This assumption will impact water consumption, steady state TDS and cultivation system energy loads. The variation of biomass concentration and specific energy inputs for cultivation between scenarios is highly nonlinear due to the complex and integrated nature of the optimized PBRs. Each low, baseline, and high scenario represents a different optimized PBR design. To stay consistent with the LCA GHG emission and production cost scenarios, biomass volumetric productivities were chosen to represent PBRs with the highest and lowest areal productivities and specific energies. The biomass concentrations do not vary in a predictable fashion because the PBR geometry varies

with the optimization (See Chapter 3). In some cases, specific energy inputs outside of the PBR electricity requirements for growth make overall cultivation specific energy inputs larger for a low case when compared to the baseline. This is due to the increased flue gas specific energy required for a faster growing microalgae strain scenario.

Table 2.5: Closed Photobioreactor Productivities (Airlift Degasser Unless Otherwise Noted)

| | Biomass Volumetric Productivity (g/L/day) | Biomass Areal Productivity ($g/m^2/day$) | Notes | Refs. |
|---|---|---|---|---|
| Horizontal tubular | 1.2 | - | Outdoor continuous | [57] |
| | 1.9 | - | Outdoor continuous | [55] |
| | 1.5 | - | Outdoor continuous | [58] |
| | 0.25 | - | Outdoor semi-continuous | [59,60] |
| | 1.26 | - | Outdoor continuous | [61] |
| Vertical tubular | 1.25 | 50 | Indoor greenhouse | [54] |
| | 0.5 | - | Indoor laboratory bubble column Continuous | [62] |
| Flat panel | 0.24 | 12.1 | Outdoor continuous | [36] |
| | 0.27 | 18.9 | Outdoor continuous | [36] |
| | 0.58 | 35 | Indoor greenhouse | [54] |
| | 0.56 | 7.25 | Outdoor continuous | [36] |
| | 0.61-1.45 | 59.5 | Outdoor continuous | [63] |
| | 1.0 | 70 | Outdoor continuous | [64] |
| | 1.93 ± 0.03 | - | Indoor laboratory semi-continuous | [61] |
| | 2.15 | - | Outdoor continuous | [65,66] |
| | 2.0 max. | - | Outdoor semi-continuous | [56] |

Table 2.6: Closed Photobioreactor Cultivation Parameters, Inputs, and Performances

| | | Low | Baseline | High | Notes/Refs. |
|---|---|---|---|---|---|
| All PBRs | Airlift efficiency (%) | 43 | 43 | 43 | [53] |
| | Circulation pump efficiency (%) | 80 | 80 | 80 | [67] |
| | Degasser water loss ($g_{water}/m^3_{air}$) | 31.5 | 31.5 | 31.5 | Water saturation at 30°C |
| | Blowdown ratio | 0.1 | 2 | 2 | |
| | Optimization type* | Weighted evenly for specific energy and areal productivity | | | |
| Horizontal tubular | Biomass areal productivity ($g/m^2/day$) | 14.6 | 12.5 | 8.88 | |
| | Biomass volumetric productivity (g/L/day) | 0.8 | 1.0 | 1.5 | |
| | Biomass PBR mass concentration (ppm) | 2230 | 1150 | 328 | |
| | Algae PBR electric ($MJ/kg_{algae}$) | 10.6 | 9.59 | 10.8 | Calculated** |
| | Nutrient supply electric ($MJ/kg_{algae}$) | 0.035 | 0.041 | 0.058 | Derived from [50] |
| | Makeup water pumping electric ($MJ/kg_{algae}$) | 0.004 | 0.013 | 0.017 | Equation (2.4)-(2.9) |
| | Initial pumping and filling electric ($MJ/kg_{algae}$) | 0.006 | 0.003 | 0.004 | Filled 3 times/year [22] |
| | $CO_2$ capture on-site NG ($MJ/kg_{algae}$) | 0.00 | 0.00 | 4.71 | |
| | $CO_2$ capture on-site electric ($MJ/kg_{algae}$) | 0.00 | 0.00 | 0.09 | See Table 2.2 and Table 2.3 |
| | Recycle $CO_2$ compressor electric ($MJ/kg_{algae}$) | 0.00 | 0.00 | 0.18 | |
| | On-site flue gas distribution electric ($MJ/kg_{algae}$) | 0.38 | 0.32 | 0.00 | |
| | Total cultivation specific energy ($MJ/kg_{algae}$) | 11.1 | 9.97 | 15.9 | |
| Vertical tubular | Biomass areal productivity ($g/m^2/day$) | 13.8 | 13.1 | 11.5 | |
| | Biomass volumetric productivity (g/L/day) | 0.8 | 0.85 | 1.0 | |
| | Biomass PBR mass concentration (ppm) | 589 | 587 | 351 | |
| | Algae PBR electric ($MJ/kg_{algae}$) | 10.7 | 10.7 | 10.7 | Calculated** |
| | Nutrient supply electric ($MJ/kg_{algae}$) | 0.037 | 0.039 | 0.045 | Derived from [50] |
| | Makeup water pumping electric ($MJ/kg_{algae}$) | 0.003 | 0.007 | 0.008 | Equation (2.4)-(2.9) |
| | Initial pumping and filling electric ($MJ/kg_{algae}$) | 0.005 | 0.005 | 0.004 | Filled 3 times/year [22] |
| | $CO_2$ capture on-site NG ($MJ/kg_{algae}$) | 0.00 | 0.00 | 4.71 | |
| | $CO_2$ capture on-site electric ($MJ/kg_{algae}$) | 0.00 | 0.00 | 0.09 | See Table 2.2 and Table 2.3 |
| | Recycle $CO_2$ compressor electric ($MJ/kg_{algae}$) | 0.00 | 0.00 | 0.18 | |
| | On-site flue gas distribution electric ($MJ/kg_{algae}$) | 0.38 | 0.32 | 0.00 | |
| | Total cultivation specific energy ($MJ/kg_{algae}$) | 11.1 | 11.1 | 15.8 | |
| Flat panel | Biomass areal productivity ($g/m^2/day$) | 46.0 | 36.0 | 26.0 | |
| | Biomass volumetric productivity (g/L/day) | 0.9 | 0.7 | 0.5 | |
| | Biomass PBR mass concentration (ppm) | 1480 | 1570 | 1326 | |
| | Algae PBR electric ($MJ/kg_{algae}$) | 2.80 | 2.80 | 2.80 | Calculated** |
| | Nutrient supply electric ($MJ/kg_{algae}$) | 0.011 | 0.014 | 0.020 | Derived from [50] |
| | Makeup water pumping electric ($MJ/kg_{algae}$) | 0.003 | 0.006 | 0.005 | Equation (2.4)-(2.9) |
| | Initial pumping and filling electric ($MJ/kg_{algae}$) | 0.004 | 0.005 | 0.007 | Filled 3 times/year [22] |
| | $CO_2$ capture on-site NG ($MJ/kg_{algae}$) | 0.00 | 0.00 | 4.71 | |
| | $CO_2$ capture on-site electric ($MJ/kg_{algae}$) | 0.00 | 0.00 | 0.09 | See Table 2.2 and Table 2.3 |
| | Recycle $CO_2$ compressor electric ($MJ/kg_{algae}$) | 0.00 | 0.00 | 0.18 | |
| | On-site flue gas distribution electric ($MJ/kg_{algae}$) | 0.38 | 0.32 | 0.00 | |
| | Total cultivation specific energy ($MJ/kg_{algae}$) | 3.19 | 3.15 | 7.82 | |

### 2.2.4 Microalgae Harvesting

The harvesting steps consist of primary and secondary stages that progressively dewater the algae in semi-continuous cycles. The primary harvesting stage consists of either Dissolved Air Flotation (DAF) devices that use air to flocculate the microalgae and clarifiers or settling ponds

**Each specific energy inputs and other results based on PBR designs optimized for specific energy and areal productivity at each specified volumetric productivity (See Chapter 3)

that use gravity to partially dewater the microalgae to 2.25 wt.% solids content. The secondary harvesting choices in the analysis scenarios are for either centrifuges, which use centrifugal forces, or belt filter presses, which use mechanical pressure to further dewater the microalgae to 12 wt.% solids content. Table 2.7 depicts all of the various primary and secondary downstream harvesting technologies considered. The performance, sizing, and power parameters for each technology set are also provided. Note that the pumping power between various subsystems is only for the open raceway pond scenarios. The units of 1 kW/m$^3$/hr equate to a pressure of 3.6 MPa. These scenarios assume a pressure drop based on 45.2 Pa/m for the larger pipes for various distances [68]. Table 2.8 provides the harvesting technologies used in the scenarios of this thesis. These technologies were chosen to represent a wide range of specific energy inputs. This assumes that issues involving residence time for batched settling ponds (multiple days) and continuous flow clarifiers (multiple hours), as well as problems with smaller diameter algae in a belt filter press could be overcome through research and development in logistics planning. These harvesting technology choices will affect the overall LCA GHG emissions variability while minimally affecting capital cost variability because the majority of harvesting expenses are associated with pretreatment operating costs [50].

For the varying pipes sizes and flow rates in the scalable PBR facility, power required between units for PBRs accumulated from pressure drops based on friction and minor linkage head losses. Pipe friction losses are based on the Haaland equation in Equation (2.4), which directly solves the Darcy-Weisbach friction factor $f$ for turbulent flow through smooth or rough circular piping by approximating the implicit, empirical Colebrook-White equation. The error (<1%) in this approximation is within the variability of the scenarios in question. The Darcy-Weisbach friction factor depends on the relative pipe roughness $\varepsilon_m$, pipe diameter $d$, and the Reynolds number $\mathrm{Re}$. Each specific case is denoted by the subscript $i$. The Reynolds number in Equation (2.5) depends on the fluid density $\rho_L$, liquid velocity $U_L$, viscosity $\mu_L$, and pipe diameter $d$. Lastly, the pressure drop per unit distance in Equation (2.6) depends on the friction factor, liquid density, liquid velocity, and flow diameter. The head losses at each linkage in the PBR facility are accounted for in Equation (2.7). The non-dimensional linkage loss coefficients used for 90° bends, T-branch, and T-line linkages combine into a single non-dimensional coefficient $hv_i$ for different bends in a subsystem [68]. The total pressure drop and power required are depicted in Equations (2.8) and (2.9). Depending on the fluid, the power equation is a function of culture or water density $\rho_L$ or $\rho_w$, pump efficiency $\eta_p$, specific water flow and loss fractions $\dot{m}_w$ and $\dot{m}_{loss}$ in $kg_{water}/kg_{algae}$, and microalgae cultivation system productivity $P_{algae}$ in $kg_{algae}/s$. The pumping efficiency for all cases was assumed to be 80% [67].

$$\varepsilon_m = 2.5\mu m \text{ (for glass, plastic and perspex)}$$
$$f_i = \left( -1.8 \log\left[ \left( \frac{\varepsilon_m / d_i}{3.7} \right)^{1.11} + \frac{6.9}{\mathrm{Re}_i} \right] \right)^{-2} \tag{2.4}$$

$$\mathrm{Re}_i = \frac{\rho_{L_i} U_{L_i} d_i}{\mu_{L_i}} \tag{2.5}$$

$$P_{L_i} = f_i \frac{\rho_{L_i} U_{L_i}^2}{2 d_i} \tag{2.6}$$

$$h_{v_i} = 0.25 n_{90_i} + 0.75 n_{Tbranch_i} + 0.15 n_{Tline_i} \tag{2.7}$$

$$\Delta P_i = \frac{1}{2} \rho_L U_{L_i}^2 h v_i + L_i P_{L_i} \tag{2.8}$$

$$P_i = \frac{1}{\eta_p \rho_L} \Delta P_i P_{\text{algae}} \text{ or } P_i = \frac{1}{\eta_p \rho_w} \Delta P_i \left( \dot{m}_w + \dot{m}_{loss} \right) P_{\text{algae}} \tag{2.9}$$

Table 2.7: Primary and Secondary Harvesting System Performance, Sizing, and Power Input Parameters (Pumping Power Inputs for Open Pond Cases Only)

| Primary Harvesting | | | | Notes/Refs. |
|---|---|---|---|---|
| DAF | Performance/ Sizing Parameters | Flocculant concentration (ppm) | 5 | Assumes $FeCl_3$ [22] |
| | | Solids content at outlet (wt.%) | 2.25 | [22] |
| | | Recycle solids content (ppm) | 15 | [22] |
| | | Maximum Capacity ($m^3$/hr) | 1,250 | [22] |
| | Power Parameters | DAF recycle pumps (kW) | 120 | Vendor Inputs; max. capacity |
| | | Flocculant mixer (kW/$m^3$/hr) | 19.7 | Vendor Inputs; max. capacity |
| | | Sludge scrapper motor (kW) | 2.98 | Vendor Inputs; max. capacity |
| | | Float transfer pump (kW/$m^3$/hr) | 0.186 | Vendor Inputs; scaled from 2.5 hp for 10 $m^3$/hr at 4% solids |
| | | Coagulant metering pump (kW) | 2.24 | Estimated [22] |
| | | DAF Compressor (kW) | 2.24 | Vendor Inputs; 60 PSIG, 18 SCFM |
| | | Effluent pump to pond (kW/$m^3$/hr) | 45.5 | Vendor Inputs; ~0.8 km at 45.2 Pa/m |
| | | DAF Blowdown Pump (kW/$m^3$/hr) | 455 | Vendor Inputs; ~8 km at 45.2 Pa/m |
| Clarifier | Performance/ Sizing Parameters | Typical effluent concentration (mg/L) | 15 | 5-30 mg/L [22,69] |
| | | Solids content at outlet (wt.%) | 2.25 | Assumed same as DAF [22] |
| | | Typical wall depth (m) | 4 | [70] |
| | | Typical clarifier solids loading rate (kg/$m^2$/day) | 150 | 100-150 kg/$m^2$/day [70] |
| | | Typical overflow rate ($m^3$/$m^2$/day) | 18 | [70,71] |
| | | Volume ($m^3$) | 3,900 | [71] |
| | Power Parameters | Clarifier rake arm driver (kW) | 0.37 | [22] |
| | | Sludge pumps (kW) | 2.98 | [22] |
| | | Growth pond to clarifier (kW/$m^3$/hr) | 45.5 | Vendor Inputs; ~0.8 km at 45.2 Pa/m |
| | | Concentrate to Centrifuge (kW/$m^3$/hr) | 0.186 | Vendor Inputs; same as DAF |
| | | Blowdown Pumps (kW/$m^3$/hr) | 455 | Vendor Inputs; same as DAF |
| Settling Pond | Power Parameters | Total Power (kW/ha) | 0.204 | Batch system [50]; Maximum capacity assumed same as clarifier volume |
| Secondary Harvesting | | | | Notes/Refs. |
| Centrifuge | Performance/ Sizing Parameters | Solids recovery (wt.%) | 95 | [22] |
| | | Maximum Capacity ($m^3$/hr) | 227 decanter<br>90.8 disc | [22] |
| | | Solids content at outlet (%) | 12 | [22] |
| | Power Parameters | Main motor (kW/$m^3$/hr) | 3,500 decanter<br>2,070 disc | Vendor Inputs; Assumes linear scaling of power with inflow rate; 300 hp motor for 1000 gpm decanter centrifuge; 75 kW motor for 400 gpm disc centrifuge (70% rated power) |
| | | Scroll/backdrive motor (kW/$m^3$/hr) | 1,980 decanter<br>0 disc | Vendor Inputs; Assumes linear scaling of power with inflow rate; 125 hp motor for 1000 gpm decanter centrifuge |
| | | Thickened algal pump (kW/$m^3$/hr) | 1,960 | Based on sludge pumps [22] |
| | | Supernatant pump to DAF recycle (kW/$m^3$/hr) | 27.3 | 0.48 km at 45.2 Pa/m |
| Belt Filter Press | Performance/ Sizing Parameters | Cycle time (hours) | 2 | [72] |
| | | Maximum Capacity ($m^3$/hr) | 3.54 | 1000 $ft^3$/cycle/press at two hours/cycle [72] |
| | | Solids content at outlet (%) | 12 | Assumed same as centrifuge [22] |
| | Power Parameters | Total power input (kW) | 103 | [72] |

Table 2.8: Harvesting Technology Sets for Scenarios

| | Low | Baseline | High |
|---|---|---|---|
| Primary harvesting | Settling ponds | Clarifier | Dissolved air flotation |
| Secondary harvesting | Disc centrifuge | Decanter centrifuge | Belt filter press |

### 2.2.5 Microalgae Extraction

Once the microalgae have been harvested and dewatered to ~12 wt.% of the culture, the algal oil is extracted via two main methods, "dry" and "wet" extraction. Dry extraction is the more readily available commercial technology currently used for soybean oil extraction. The process consists of natural gas fed sludge belt dryers that lyse and dry the algae to ~90 wt.% solids. A hexane solvent is then used to recover oil from the dried culture [22,73,74]. Wet extraction is an emerging technology that eliminates the need for post drying of the harvested stream. Several recent patents describe various ways to lyse and extract algal oils from a wet culture. In this analysis, pressurized steam and potassium hydroxide are used to lyse the algal cells, which are then subject to centrifugation and wash cycles to separate the algal oil from the culture [22,75,76,77,78].

#### 2.2.5.1 Dry Extraction

The dry extraction technology set energy and performance parameters used in this analysis are depicted in Table 2.9. The majority of energy used in dry extraction comes from heat produced from combusted from natural gas. In scenarios where a combustor or CHP is used, a fraction of the heat energy required for drying is offset by the combustion of methane from the anaerobic digester.

Table 2.9: Dry Extraction Energy and Performance Inputs

| Process | Inputs | Value | Notes/Refs. |
|---|---|---|---|
| Performance Assumptions | Dryer biomass recovery (%) | 100 | [22] |
| | Influent stream solids (wt.%) | 12 | [22] |
| | Effluent stream solids (wt.%) | 90 | [51,74] |
| Belt Dryer | Dryer heat input (MJ/$kg_{water\text{-}evap}$) | 3.37 | Vendor inputs from commercial sludge dryers [74] |
| | Estimated drying efficiency (%) | 76 | Water heat of vaporization: 2.23 MJ/$kg_{water}$<br>Water specific heat: 4 kJ/$kg_{water}$/K<br>Algae specific heat: 2 kJ/$kg_{biomass}$/K |
| | Power input (kJ/$kg_{biomass}$) | 91.3 | Technology efficiency improvement from 1998 to 2015 from GREET1_2011 (11.1%); Natural gas input calculated from required steam input with 80% thermal efficiency. Soy oil extraction modified for algal feed [73] |
| | Natural gas input (kJ/$kg_{biomass}$) | 965 | |
| | Hexane makeup rate (kg/$kg_{biomass}$) | 0.0021 | |
| | Calorific value of hexane makeup (kJ/$kg_{biomass}$) | 93.0 | |

#### 2.2.5.2 Wet Extraction

The wet extraction technology energy and performance inputs are shown in Table 2.10. The specific energy values and material inputs could not be provided due to the confidential nature of the reference. Nonetheless, an in-house model of the process determined natural gas and electricity specific energy use at 2.68 MJ/$kg_{algae}$ and 0.013 kWh/$kg_{algae}$, respectively. There are three different net oil recovery efficiency values because they are each a function of extractable

lipid content inputs. The majority of the specific energy requirements for wet extraction are for steam generation and for electricity requirements for centrifugation and wash cycles used to separate out the oils. The resulting oil fraction in the biomass effluent stream was assumed negligible.

Table 2.10: Wet Extraction Energy and Performance Inputs

| Process Inputs | Value | Notes/Refs. |
|---|---|---|
| Net algal oil recovery efficiency (%) | 92 (low), 71 (baseline), 60 (high) | Based on extractable lipid wt.% scenario inputs [22] |
| Biomass recovery efficiency (wt.%) | 100 | [22] |
| Oil fraction in effluent (wt.%) | 0 | 0.11 wt.% in reference; assumed negligible [22,76] |
| NG energy input for steam ($kJ/kg_{biomass}$) | Confidential | 85% thermal efficiency and steam enthalpy of 3.37 MJ/kg [76] |
| Electricity ($kJ/kg_{biomass}$) | Confidential | Electricity normalized by biodiesel production and lipid fraction in reference [76] |
| KOH input ($kg/kg_{biomass}$) | Confidential | Used for variable operating cost and GHG calculations: 1.76 kg-$CO_2$e/$kg_{KOH}$ |
| HCl input to neutralize algae ($kg/kg_{biomass}$) | Confidential | Recycled from digester to ponds/PBR; Used for GHG calculations: 0.074 kg-$CO_2$e/$kg_{HCl}$ [79] |

2.2.5.3 Other Emerging Extraction Techniques

Wet extraction technologies are not the only nascent equipment being simulated and tested at a pilot scale. Methods combining ultrasonication with electromagnetic pulse induction to lyse algal cells followed by clarifier settling with $CO_2$ injection to lower pH and further separate have been demonstrated. These processes could provide advantages like lowering variable operating and capital expenses as well as lowering specific energy use, but questions remain regarding extraction efficiency and scalability [80].

2.2.6 Anaerobic Digestion and Energy Recycle

After extraction, the biomass residue (or cake) undergoes a two-stage digestion process where microbes digest the residue and produce methane gas, which is then combusted. In the dry extraction cases, the methane gas is combusted in a furnace to produce heat. In wet extraction cases, methane is combusted in a CHP plant to produce both heat and electricity, which are both recycled back to the facility. In cases where a surplus amount of electricity is produced, the emissions associated with energy-weighted, grid-averaged electricity production is displaced. Table 2.11 and Table 2.12 depict the digestion and biogas performance inputs for various scenarios. In the low cases, it is assumed that the energy load to dry the digester streams come from flue gas feed from the power plant.

Table 2.11: Anaerobic Digester Performance and Power Inputs

| | First stage | Second stage | Notes/Refs. |
|---|---|---|---|
| Digester efficiency (%) | 60 | 10 | |
| $CH_4$ (vol.%) | 65 | 65 | [22,70] |
| $CO_2$ (vol.%) | 35 | 35 | |
| Specific gas production ($m^3/kg_{cake}$) | 1.05 | 1.05 | Adjusted to balance mass across digesters [22] |
| Digester influent solids wt.% | 15 | 7 | [22,70] |
| Nutrient recovery (%) | 60 | | [22,50] |
| Undigested biomass going to supernatant (%) | 10 | | |
| Undigested solids (wt.%) | 80 | | [22,70] |
| Volatile solids (VS) loading ($kg_{VS}/m^3/day$) | 2.5 | | |
| Mixing power per unit volume of digester ($kW/m^3$) | 0.01 | | |

Table 2.12: Biogas Disposition Performance Scenario Inputs

| Scenario | Low | | Baseline | | High | | Notes/Refs. |
|---|---|---|---|---|---|---|---|
| Extraction type | Dry | Wet | Dry | Wet | Dry | Wet | |
| Biogas disposition | CHP | CHP | Biogas Heat | CHP | Biogas Heat | CHP | |
| Electricity generation efficiency (%) | 35 | 35 | N/A | 35 | N/A | 35 | [24,81] |
| Thermal generation efficiency (%)[††] | 50 | 50 | 76 | 50 | 76 | 50 | |
| Biogas heat fraction used in digester (%) | 0 | 0 | 20 | 20 | 20 | 20 | |

2.2.7 Algal Oil Transport to HEFA Facility

Algal oil transportation from the cultivation, harvesting, and extraction facility to the HEFA upgrading facility are assumed to be the same distance and transportation distribution as biodiesel from soy oil in GREET1_2011 [37]. The majority of the oil is transported via truck to a HEFA production plant within 50 miles of the cultivation, harvesting, and extraction facility. The fuels used for the transportation vehicles are diesel for rail and trucks and residual oil for barges. Table 2.13 depicts the assumed algal oil transportation distribution, distances, and energy intensities used in GREET1_2011 for this analysis.

Table 2.13: Transportation Makeup, Distance, and Energy Intensity Inputs

| Transport Type | Percentage of fuel transported by a given mode (%) | Transportation Distance (km) | Energy Intensity (J/kg/km) |
|---|---|---|---|
| Ocean Tanker | - | - | - |
| Barge | 8 | 837 | 291 origin to destination; 222 back-haul |
| Pipeline | - | - | - |
| Rail | 29 | 1287 | 267 origin to destination; 0 back-haul |
| Truck | 63 | 80.4 | 743 origin to destination; 743 back-haul |

[††]In the wet extraction cases, heat from the CHP is not recycled in the LCA due to low system thermal demands.

2.2.8 Algal Oil Processing

HEFA fuels are processed when renewable oils react with hydrogen in the presence of a catalyst. Algal oils in the form of TAGs undergo four chemical transformations: saturation, depropanation, deoxygenation, and rearrangement [33]. First, hydrogen gas in the presence of a catalyst saturates any double bonds. Second, the propane backbone of the triglyceride is removed, leaving three free-fatty acid chains. The fatty acid is deoxygenated in the third step, and can occur either through a hydrodeoxygenation or decarboxylation mechanism. The hydrodeoxygenation step requires nine more moles of hydrogen gas than decarboxylation, and therefore may increase additional capital and operating expenses [82,83]. This analysis assumes the decarboxylation mechanism. Finally, to meet jet fuel specification requirements, the long saturated hydrocarbon chains undergo a chemical rearrangement, known as isomerization to obtain hydrocarbon isomers suitable for blending. Depending on the process inputs and operating conditions, various product slates can be produced [33].

This analysis assumes that the algal oils undergo hydroprocessing and isomerization reactions identical to that of soybean oil HEFA production. Figure 2.8 illustrates carbon chains distributions of conventional plants, microalgae, and cyanobacteria compared to that of n-paraffin carbon chain distributions [9,33,31,84]. The first point to glean from this figure is that – with the exception of palm kernel and certain forms of cyanobacteria – the majority of renewable oils reside in the carbon chain length range of conventional diesel fuel. Additionally, the majority of microalgal oil chain length profiles resemble that of soybean oil with the largest fraction of the chains composed of 18 carbon atoms for multiple green and red algae species.

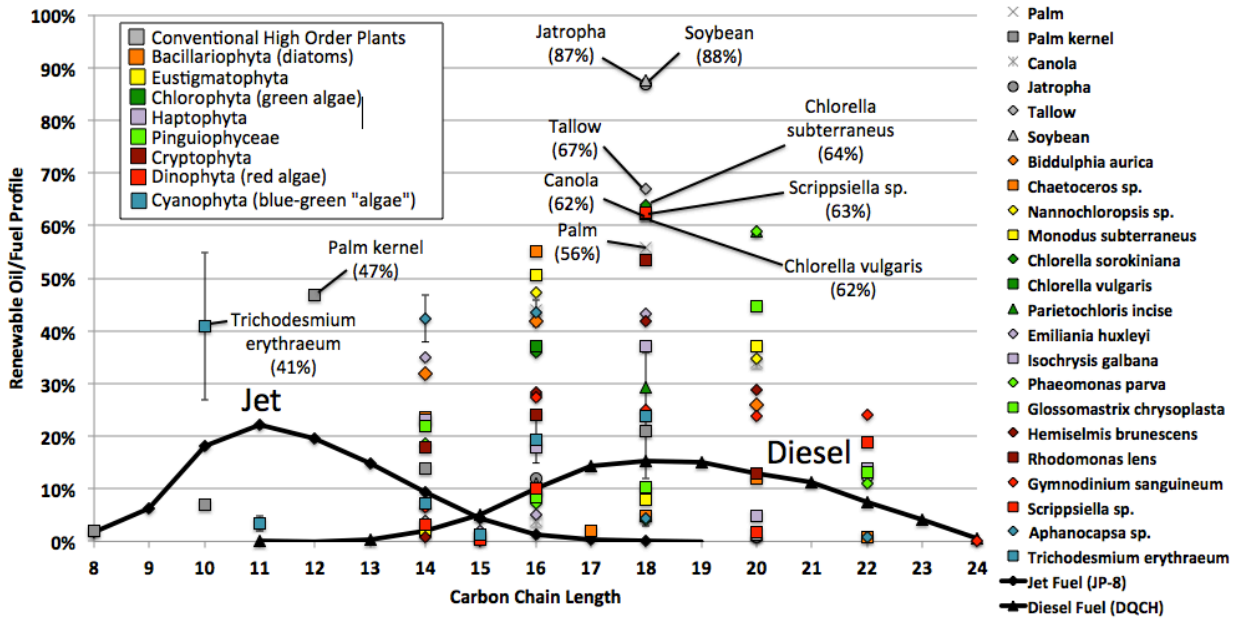


Figure 2.8: Conventional Plant, Microalgal, and Cyanobacteria Renewable Oil Carbon Chain Distributions Compared to Jet and Diesel Fuel n-Paraffin Carbon Chain Distributions

Table 2.14 depicts the hydroprocessing and isomerization process inputs for various product slates and scenarios. The product slate used in this analysis is for maximum distillate fuel. This choice results in lower upgrading environmental and economic costs, but will decrease the potential yield of HEFA jet fuel per amount of algal oil from 49.4% to 12.8%. In future

upgrading analyses, modeling for selectively breed species with lower (or in some cases higher) carbon chain lengths could decrease the predicted upgrading requirements for a maximum HEFA jet fuel product slate.

Table 2.14: Hydrotreating and Isomerization Mass-based Product Yields and Power Inputs by Product Profile from a Soybean Vegetable Oil Feed

| | Low | | Baseline | | High | | Notes/Refs. |
|---|---|---|---|---|---|---|---|
| Units of MJ or kg per 100 $kg_{feed}$ | Max. Distillate | Max. Jet | Max. Distillate | Max. Jet | Max. Distillate | Max. Jet | |
| Power | 14.8 | 14.8 | 19.4 | 19.4 | 24.5 | 24.5 | |
| Natural gas | 0.23 | 0.23 | 0.25 | 0.25 | 0.27 | 0.27 | Assumes algal oils behave similarly to soybean oils when hydrotreated and isomerized; Power and natural gas inputs are from [2,33,85]; Material and product slates are from [33] |
| $H_2$ | 2.7 | 4.0 | 2.7 | 4.0 | 2.7 | 4.0 | |
| Water | 8.7 | 8.7 | 8.7 | 8.7 | 8.7 | 8.7 | |
| Carbon Dioxide | 5.5 | 5.4 | 5.5 | 5.4 | 5.5 | 5.4 | |
| Propane | 5.8 | 10.2 | 5.8 | 10.2 | 5.8 | 10.2 | |
| LPG | 1.6 | 6.0 | 1.6 | 6.0 | 1.6 | 6.0 | |
| Naptha | 1.8 | 7.0 | 1.8 | 7.0 | 1.8 | 7.0 | |
| Diesel | 68.1 | 23.3 | 68.1 | 23.3 | 68.1 | 23.3 | |
| Jet | 12.8 | 49.4 | 12.8 | 49.4 | 12.8 | 49.4 | |

### 2.2.9 HEFA Jet Fuel Transportation and Distribution

The finished HEFA jet fuel product is then transported and distributed following the inputs and assumptions outlined in Table 2.15. The transportation inputs are identical to the oil transportation assumptions. The distribution energy and associated emissions only account for truck transport from the transportation hub to use at airports within a near 50 mile radius. It does not include energy used to monitor and blend the fuels with petroleum-based jet fuel [37].

Table 2.15: HEFA Jet Fuel Transportation and Distribution Inputs and Assumptions

| Vehicle Type | Percentage of fuel transported by a given mode (%) | | Distance (km) | | Energy Intensity (J/kg/km) |
|---|---|---|---|---|---|
| | Transportation | Distribution | Transportation | Distribution | |
| Ocean Tanker | - | - | - | - | - |
| Barge | 8 | - | 837 | - | 291 origin to destination; 222 back-haul |
| Pipeline | - | - | - | - | - |
| Rail | 29 | - | 1290 | - | 267 origin to destination; 0 back-haul |
| Truck | 63 | 100 | 80.4 | 48.3 | 743 origin to destination; 743 back-haul |

### 2.2.10 Fuel Combustion

Fuel combustion scenarios of the HEFA derived jet fuels assumed fuel compositions ranging from 5% to 50% blends with conventional jet fuel. Conventional jet fuel GHG ($CO_2$, $N_2O$, and $CH_4$) and AQ (VOC, CO, $NO_x$, $PM_{10}$, $PM_{2.5}$, and $SO_x$) combustion emissions from the 2009 U.S. origin only fleet of commercial aircraft were estimated for full flight and landing and takeoff (LTO) fuel burn by the John A. Volpe National Transportation Systems Center. Alternative aviation fuel blend combustion emissions are now a part of the GREET1_2011 tool and are classified as Pump-to-Wake (PTW) emissions [37]. Table 2.16 depicts the various blends and

combustion GHG emissions by scenario and by aircraft class. The fuel blend choices are based on the certified maximum allowable blend of 50% SPK and the emissions are linearly interpolated from experimental results with 100% and 50% SPK blends. These studies, as well as AQ emissions from alternative fuel blends, are shown in Appendix E.

Table 2.16: Combustion GHG Emission Scenario Inputs

| Inputs | | Low | Baseline | High | Notes/Refs. |
|---|---|---|---|---|---|
| HEFA jet fuel blend (%) | | 50 | 20 | 5 | Aircraft categories from Aviation Environmental Design Tool (AEDT) [86]; [37] |
| AEDT Aircraft Class | Total Fuel Burn (kg/operation) | GHG PTW Emissions ($g\text{-}CO_2e/MJ$) | | | |
| Single Aisle (SA) | 4,990 | 71.8 | 72.7 | 73.1 | |
| Small Twin Aisle (STA) | 14,600 | 71.8 | 72.7 | 73.1 | |
| Large Twin Aisle (LTA) | 59,500 | 71.8 | 72.6 | 73.0 | |
| Large Quad (LQ) | 91,600 | 71.8 | 72.6 | 73.0 | |
| Regional Jet (RJ) | 1,730 | 71.9 | 72.7 | 73.1 | |
| Business Jet (BJ) | 1,730 | 71.9 | 72.7 | 73.1 | |
| Single Aisle Freight (SA-F) | 3,390 | 71.9 | 72.7 | 73.1 | |
| Small Twin Aisle Freight (STA-F) | 9,800 | 71.9 | 72.7 | 73.1 | |
| Large Twin Aisle Freight (LTA-F) | 31,400 | 71.8 | 72.6 | 73.1 | |
| Large Quad Freight (LQ-F) | 60,800 | 71.8 | 72.6 | 73.1 | |
| Fuel burn weighted average | - | 71.8 | 72.7 | 73.1 | |

# Chapter 3: Algae Photobioreactor Model Development and Optimization

## 3.1 Background

Unlike open ponds, tubular and flat panel microalgae PBR systems require an integrated systems modeling approach using nonlinear, second-order relationships. This approach allows comparison of PBR systems to open pond systems and to understand design factors that influence the various LCA metrics for algae cultivation. For each PBR type, a modeling framework was developed, validated and used within a weighted optimization routine to estimate PBR performance. Local sensitivities of the horizontal tubular model were also produced. All PBRs were considered to be modular and have continuous production rates that can scale to a particular algal oil demand. As depicted in Figure 2.3, PBR scenarios take cultivation and geometric information passed from the optimized PBR models and scale the number of reactors necessary to meet the 137 bpd algal TAG production rate from the baseline open pond pilot facility. The following sections outline the model development, validation and optimization methods for the three PBR types.

## 3.2 Tubular Photobioreactor

### 3.2.1 Model Development

Tubular PBR modeling in this analysis estimates various process metrics given associated assumptions. The tubular models assume: friction losses in degasser are small compared to those in the solar collector and other bubble wake losses in the degasser, constant culture velocity in all pipes (diameters adjust to ensure flow continuity), harvesting and dilution occur at the top of the degasser, dilution rate is held constant while algae concentration varies for a given volumetric productivity during optimization, and all pipes are fully filled. Modeling of the horizontal and vertical tubular PBR systems consisted of the same general and system specific parameters outlined in Table 3.1. The system specific parameters are used to determine the general system parameters. Previous tubular PBR models in the literature were parameterized but did not integrate many of the nonlinear effects of mass transfer and energy balances [53,54,55,57,87]. The PBR models utilized a comprehensive approach from fundamental multiphase fluid dynamics outlined in Table 3.2. This includes a coupled, nonlinear system of equations that encompass a system-wide energy balance, mass transfer in the degasser, the degasser gas holdup (volumetric fraction of gas in the gas-liquid medium), and oxygen equilibrium. The derivation of the coupled, nonlinear system of equations as well as output calculations can be found in Appendix C. The model was designed such that the degasser can have up to four major arms $m$, with each arm supporting a specified number of branched solar collectors $n$. For these analyses, all tubular PBRs were considered to have one arm per degasser and one solar collector per arm. The two major outputs that determine PBR performance are the specific energy ($E_s$) in $MJ/kg_{algae}$ and areal productivity ($P_{areal}$) in $g/m^2/day$, which are determined for a given volumetric productivity (P) in g/L/day.

Table 3.1: General and System Specific Tubular PBR Parameters

| General System Parameters | System Specific Parameters |
|---|---|
| Solar collector: $L_{sc}$, $\Delta h$, $U_L$ | Volumetric productivity: $P$ |
| Degasser: $d_r$, $d_d$, $\theta$, $h_L$ | Solar collector: $d_{sc}$ |
| Non-productive piping: $L_{np}$, $d_{np}$ | Culture solids content: $C_s$ |
| Mass Transfer: $\dot{m}_{air}$, $U_b$ | or |
| Pumping: $\Delta P$ | Dilution rate: $D$ |

Table 3.2: Tubular PBR Model Inputs, Solver, and Outputs

| Static Inputs | Coupled Nonlinear System of Equations | Outputs |
|---|---|---|
| 1. Non-productive tube length and diameter ($L_{np}$, $d_{np}$) | 1. System-wide energy balance | 1. Solar collector tube length ($L_{sc}$) |
| 2. Solar collector diameter ($d_{sc}$) | 2. Degasser mass transfer | 2. Superficial culture circulation velocity ($U_L$) |
| 3. Number of solar collectors per arm (n) | 3. Degasser gas holdup | 3. Mass transfer coefficient in degasser ($k_La$) |
| 4. Number of arms per degasser (m) | 4. Oxygen equilibrium | 4. Gas Holdup in degasser ($\varepsilon_r$) |
| 5. Number of 180 bends in solar collector tube ($N_b$) | | 5. PBR areal footprint ($A_{PBR}$) |
| 6. Degasser height and outer diameter ($h_L$, $d_r$) | | 6. Productive volume ($V_P$) |
| 7. Algae productivity (P) | | 7. Total power input ($P_{in}$) |
| 8. Culture algae and solids density ($C_s$) | | 8. Total algae productivity ($P_{algae}$) |
| 9. Degasser air flow rate ($m_{air}$) | | 9. PBR specific energy ($E_s$) |
| 10. Pump pressure rise ($\Delta P$) | | 10. PBR areal productivity ($P_{areal}$) |
| 11. Physical properties and constants | | |

### 3.2.2 Model Validation

The horizontal tubular model was validated against the experimental setup described in Molina et al and Stephenson et al [53,55]. Figure 3.1 illustrates the original geometry in red and black on the left and the modeling approximation overlaid in green on the right. The original design had overlapping solar collector tubes (red on top) and sixteen U-bends. The model approximating this geometry consists of the same number of U-bends, but each bend is slightly larger and a nonproductive tube returning to the riser has been added. Approximating the design with additional nonproductive tubing did not affect the area and affected the energy balance by 0.25%. The tubular PBRs were modeled in this fashion in order to efficiently facilitate multiple solar collectors and degasser arms as seen in Figure 3.2. The blue and green sections in the figure correspond to the geometric relationship between the solar collector length $L_{sc}$ and the tubular PBR side length $L_2$ shown in Equation (C24). Further geometric tubular model calculations for horizontal and vertical tubular as well as flat panel PBRs can be found in Appendix C. Table 3.3 depicts the parameters for both the Stephenson et al experiment and the results from the model. The model calculated parameters were all within a 10% difference when compared to the experiments. The discrepancies in solar collector length and overall area could be attributed to the model geometry approximations as well as other variations associated with energy and inhibited from biomass buildup along the tube walls.

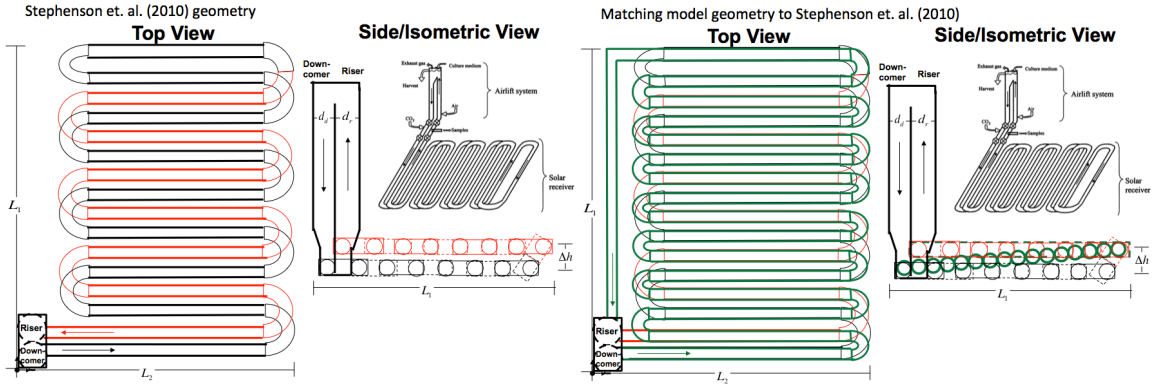


Figure 3.1: Horizontal Tubular PBR Actual (Left) and Modeled (Right) Apparatuses

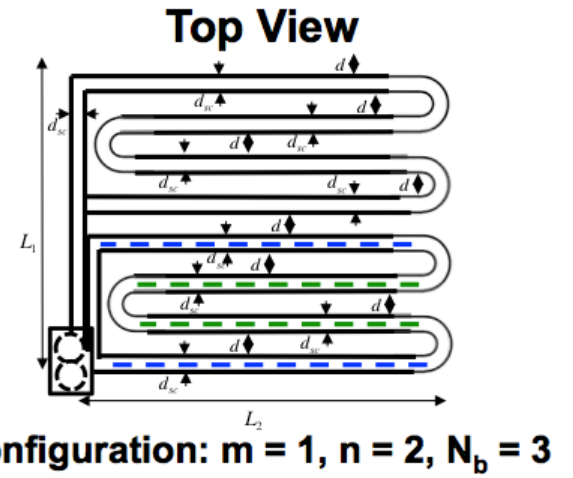


Figure 3.2: Example of a Horizontal Tubular PBR with Multiple Solar Collectors

Table 3.3: Horizontal Tubular Model Validation Parameter Comparisons

| | Corrected Stephenson et al. (2010) [53] | Model | Percent Difference |
|---|---|---|---|
| $[O2]_{in}$ (%) | 146 | 141 | 3.4 |
| $L_{sc}$ (m) | 136 | 123 | 9.6 |
| $A_{PBR}$ ($m^2$) | 19.9 | 19.7 | 1.0 |
| D ($m^3$/day) | 0.06 | 0.055 | 8.3 |
| $k_La$ (1/s) | 0.127 | 0.123 | 3.1 |
| $\varepsilon_r$ (-) | 0.206 | 0.205 | 0.5 |

The vertical tubular PBR model was compared against the experimental in reference [54]. A model matching process, similar to that depicted in Figure 3.1, was undertaken to compare against a limited amount of experimental parameters. The resulting four parameters shown in Table 3.4 had less than a 13% difference when compared to the experimental values. Discrepancies in the model were most likely due to volume estimation and a lack of specific design information for certain experimental parameters. The model governing equations for both horizontal and vertical tubular PBRs can be found in Appendix C.

Table 3.4: Vertical Tubular Model Validation Parameter Comparisons

| | Molina Grima (2009) [54] | Model | Percent Difference |
|---|---|---|---|
| $L_{sc}$ | 280 | 244 | 12.9 |
| $A_{PBR}$ | 20 | 22 | 10.0 |
| $V_P$ | 0.617 | 0.545 | 11.7 |
| D | 0.216 | 0.189 | 12.5 |

3.2.3 Horizontal Serpentine Tubular PBR Sensitivity and Uncertainty Analyses

An extensive sensitivity analysis of the horizontal tubular PBR model was undertaken using Monte Carlo simulations for various parameter ranges. Due to lack of experimental parameter data, pseudorandom triangular distributions for each of the input parameters in Table 3.5 were assumed with minimum, mode, and maximum values with the exception of the discrete inputs. The two output performance parameters investigated were specific energy input to the PBR and the areal productivity. Each performance parameter was evaluated using pseudorandom values for each of the $k$ input parameters out to $N$ iterations. Equation (3.1) and Equation (3.2)

describe three pseudorandom $N \times k$ matrices, which are used as inputs to evaluate the model outputs $y_A$, $y_B$, and $y_{C_i}$. In this algorithm, matrix $C_i$ is formed by all columns of $B$ except the $i^{th}$ column, which is taken from $A$. Equation (3.3) describes how these model outputs are used to evaluate the main $S_i$ and global $S_{T_i}$ index arrays. $S_{T_i} - S_i$ is a "measure of how much each parameter is involved with any other input factor" [88]. $S_{T_i} = 0$ means that the "associated parameter is non-influential and can be fixed anywhere in its distribution without affecting the variance of the output." The sum of all main effects is equal to one for additive models and less than one for nonadditive models. Thus, one minus the sum of all main effects is an indicator of the presence of parameter interactions in the model. Similarly, the sum of the global indices is equal to one for additive models and greater than one for models with multiple parameter interactions [88]. Only local sensitivity analyses were conducted in this thesis.

Table 3.5: Local Sensitivity Parameter Ranges

| Sensitivity Parameter | Symbol | Units | Minimum | Mode | Maximum | Pseudo-Random Distribution Type |
|---|---|---|---|---|---|---|
| Atmospheric pressure | $P_a$ | Pa | $1.00\times10^5$ | $1.01\times10^5$ | $1.03\times10^5$ | Triangular |
| Degasser bubble velocity | $U_b$ | m/s | 0.20 | 0.25 | 0.30 | Triangular |
| Degasser velocity profile | $\lambda$ | - | 0.90 | 0.97 | 1.00 | Triangular |
| Algae specific oxygen production | $\alpha$ | $kg_{O2}/kg_{algae}$ | 3.00 | 3.70 | 5.0 | Triangular |
| Pump efficiency | $\eta_p$ | - | 0.40 | 0.43 | 0.90 | Triangular |
| Compressor efficiency | $\eta_c$ | - | 0.40 | 0.43 | 0.90 | Triangular |
| Degasser diffuser angle | $\theta$ | deg | 15.0 | 20.0 | 30.0 | Triangular |
| Oxygen concentration in culture as a multiple of $C_{sat}$ | $\gamma_i$ | - | 2.50 | 2.60 | 3.00 | Triangular |
| Solar collector tube wall thickness | $t_w$ | m | 0.005 | 0.007 | 0.008 | Triangular |
| Number of solar collectors | $n$ | - | | 1, 2, 3, 4, 5 | | Discrete uniform |
| Number of degasser arms | $m$ | - | | 1, 2, 4 | | Discrete uniform |
| Number of U-bends | $N_b$ | - | | 1, 2, 3, 4, 5 | | Discrete uniform |
| Culture salinity | $S$ | ppt | 0.00 | 10.0 | 35.0 | Triangular |
| Operation temperature | $T_{op}$ | K | 285 | 298 | 305 | Triangular |
| Volumetric productivity | $P$ | $g_{algae}/L/day$ | 0.60 | 1.00 | 1.50 | Triangular |
| Algae culture concentration | $C_s$ | $kg_{algae}/m^3$ | 1.50 | 3.00 | 6.00 | Triangular |
| Solar collector tube diameter | $d_{sc}$ | m | 0.020 | 0.053 | 0.060 | Triangular |
| Degasser riser diameter | $d_r$ | m | 0.100 | 0.150 | 0.200 | Triangular |
| Degasser liquid height | $h_L$ | m | 3.50 | 4.00 | 5.50 | Triangular |
| Degasser air mass flow rate | $\dot{m}_{air}$ | kg/s | $5.00\times10^{-4}$ | $1.00\times10^{-3}$ | $1.50\times10^{-3}$ | Triangular |
| Height between solar collector tubes | $h$ | m | 0.010 | 0.020 | 0.050 | Triangular |
| Distance between solar collector tubes | $d$ | m | 0.070 | 0.090 | 0.010 | Triangular |

$$A = \begin{bmatrix} x_1^{(1)} & x_2^{(1)} & \dots & x_i^{(1)} & \dots & x_k^{(1)} \\ x_1^{(2)} & x_2^{(2)} & \dots & x_i^{(2)} & \dots & x_k^{(2)} \\ \dots & \dots & \dots & \dots & \dots & \dots \\ x_1^{(N-1)} & x_2^{(N-1)} & \dots & x_i^{(N-1)} & \dots & x_k^{(N-1)} \\ x_1^{(N)} & x_2^{(N)} & \dots & x_i^{(N)} & \dots & x_k^{(N)} \end{bmatrix} \quad B = \begin{bmatrix} x_{k+1}^{(1)} & x_{k+2}^{(1)} & \dots & x_{k+i}^{(1)} & \dots & x_{2k}^{(1)} \\ x_{k+1}^{(2)} & x_{k+2}^{(2)} & \dots & x_{k+i}^{(2)} & \dots & x_{2k}^{(2)} \\ \dots & \dots & \dots & \dots & \dots & \dots \\ x_{k+1}^{(N-1)} & x_{k+2}^{(N-1)} & \dots & x_{k+i}^{(N-1)} & \dots & x_{2k}^{(N-1)} \\ x_{k+1}^{(N)} & x_{k+2}^{(N)} & \dots & x_{k+i}^{(N)} & \dots & x_{2k}^{(N)} \end{bmatrix} \tag{3.1}$$

$$C_i = \begin{bmatrix} x_{k+1}^{(1)} & x_{k+2}^{(1)} & \dots & x_i^{(1)} & \dots & x_{2k}^{(1)} \\ x_{k+1}^{(2)} & x_{k+2}^{(2)} & \dots & x_i^{(2)} & \dots & x_{2k}^{(2)} \\ \dots & \dots & \dots & \dots & \dots & \dots \\ x_{k+1}^{(N-1)} & x_{k+2}^{(N-1)} & \dots & x_i^{(N-1)} & \dots & x_{2k}^{(N-1)} \\ x_{k+1}^{(N)} & x_{k+2}^{(N)} & \dots & x_i^{(N)} & \dots & x_{2k}^{(N)} \end{bmatrix} \tag{3.2}$$

$$y_A = f(A) \quad y_B = f(B) \quad y_{C_i} = f(C_i)$$

$$f_0^2 = \left( \frac{1}{N} \sum_{j=1}^{N} y_A^{(j)} \right)^2$$

$$S_i = \frac{V\left[E\left(Y|X_i\right)\right]}{V(Y)} = \frac{y_A \cdot y_{C_i} - f_0^2}{y_A \cdot y_A - f_0^2} = \frac{\frac{1}{N}\sum_{j=1}^{N} y_A^{(j)} y_{C_i}^{(j)} - f_0^2}{\frac{1}{N}\sum_{j=1}^{N} \left(y_A^{(j)}\right)^2 - f_0^2} \tag{3.3}$$

$$S_{T_i} = 1 - \frac{V\left[E\left(Y|X_{\sim i}\right)\right]}{V(Y)} = 1 - \frac{y_B \cdot y_{C_i} - f_0^2}{y_A \cdot y_A - f_0^2} = 1 - \frac{\frac{1}{N}\sum_{j=1}^{N} y_B^{(j)} y_{C_i}^{(j)} - f_0^2}{\frac{1}{N}\sum_{j=1}^{N} \left(y_A^{(j)}\right)^2 - f_0^2}$$

Convergence of the local sensitivities for each output performance parameter is illustrated in Figure 3.3. At 30,000 pseudorandom number iterations, the largest differences from the previous steps were less than 3.0%. The local parameter sensitivities to the specific energy and areal productivity are illustrated in Figure 3.4. In order of decreasing influence on specific energy, the solar collector tube diameter, number of solar collectors per degasser quadrant, number of quadrants per degasser, compressor efficiency, algae specific oxygen production, air mass flow rate, degasser height, and degasser bubble velocity consist of the majority of the main sensitivities. The majority of the dependency on solar collector tube diameter is due to an assumed empirical relationship between solar collector diameter and volumetric productivity shown in Figure 3.11. These results indicate that changing the solar collector tube diameter would have the largest impact on overall photobioreactor performance. Equation (3.9) and Equation (3.10), as well as the nonlinear system of equations for tubular PBRs in Appendix C are referenced for further understanding of various parameter interactions within Section 3.4.3.

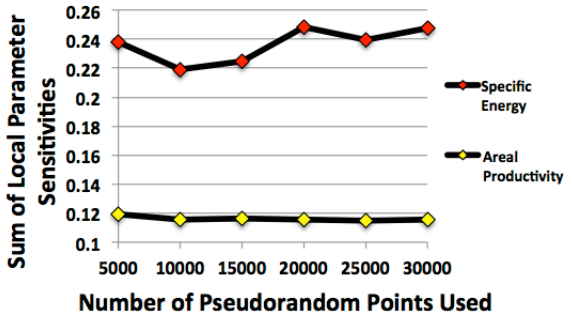


Figure 3.3: Local Sensitivity Parameter Convergence

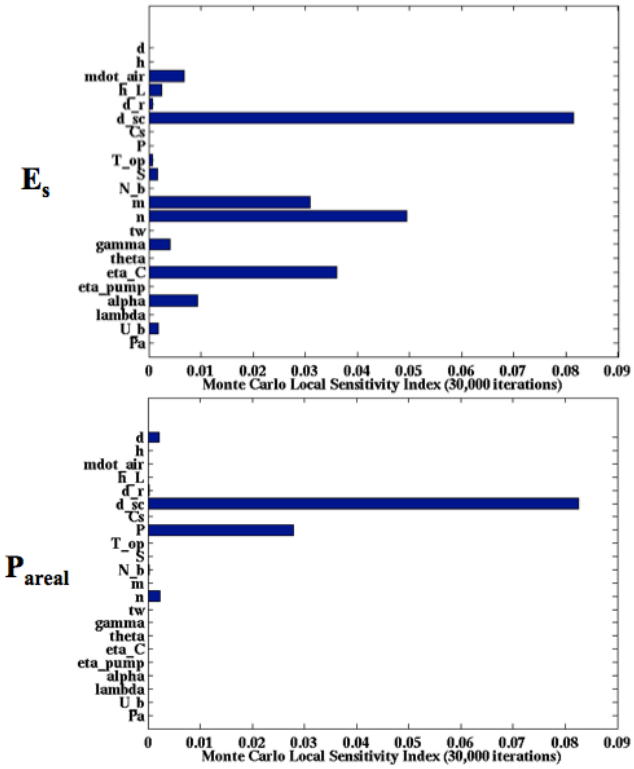


Figure 3.4: Specific Energy (Top) and Areal Productivity (Bottom) Local Sensitivity Indices

## 3.3 Flat Panel Photobioreactor

### 3.3.1 Model Development

The flat panel PBR, in contrast to the tubular systems, incorporates both the solar growth and oxygen degassing in a single system. Two methods were originally developed for modeling the modular flat panel system: one that incorporates both energy and mass transfer influences and one that only predicts mass transfer effects. The two models illustrated in Figure 3.5 provide a view of the various levels of complexity. The model that incorporates energy and mass transfer assumes two large circulating vortices, each surrounding a shear layer. The aerating flow between shear layers (Region 1) is considered twice as large as the upward flow on the outsides of the shear layers (Region 2). Regions 1 and 2 have their own speeds, areas, and gas holdups. The locations of the shear layers (sizes of $A_1$ and $A_2$) were determined by finding the lowest energy state for the system for a given air mass flow rate. The energy balance incorporated

pressure, potential energy, wall friction, top and bottom circulation path, and turbulent countercurrent shear layer losses. For this more complex approach, there were not enough empirical data to estimate the number of unknowns in the turbulent flat panel system. Therefore, a simpler approach assumed a frictionless uniform flow similar to that of the degasser systems in the tubular reactors, which incorporates pressure and potential energy changes as well as mass transfer in an assumed well-mixed, multiphase flow. Appendix C describes the simplified flow model used in these analyses for the flat panel PBR systems.

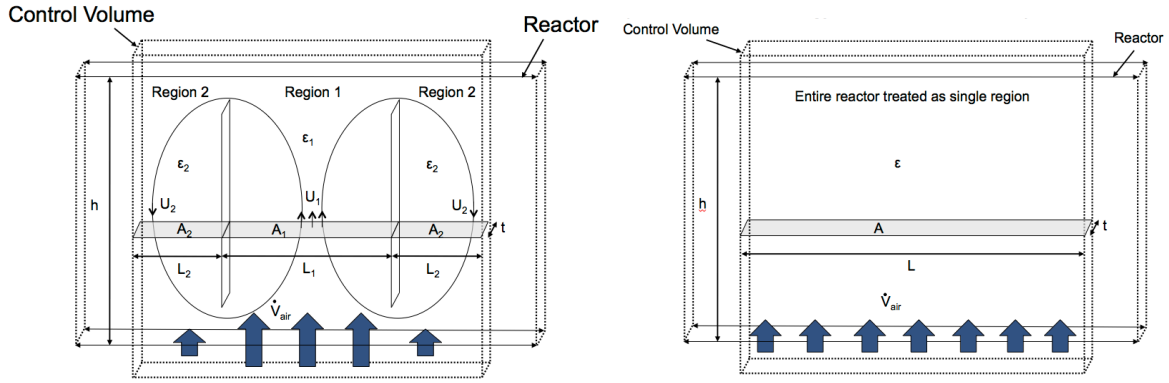


Figure 3.5: Flat Panel Modeling Techniques: Energy + Mass Transfer (Left) and Mass Transfer Only (Right)

3.3.2 Model Validation

Similar to the model validation for the tubular PBRs, the flat panel geometry was approximated to estimate various performance parameters for given growth conditions and volumetric productivities from Sierra et al [56]. Figure 3.6 provides an areal view of a single flat panel with thickness $t$, height $h_L$, length $L$, and spacing parameter $X$. The spacing ratio was determined from the vertical tubular PBR height and distances between PBRs [54]. Given these simplified assumptions and inputs, the various volumetric airflow rates and gas holdups for the model were compared to those in the experimental setup as seen in Figure 3.7. The error in the model ranged from 13% to 18% for low to high flow rates, respectively.

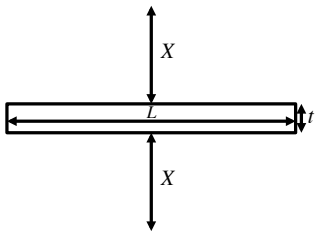


Figure 3.6: Top View of the Flat Panel PBR

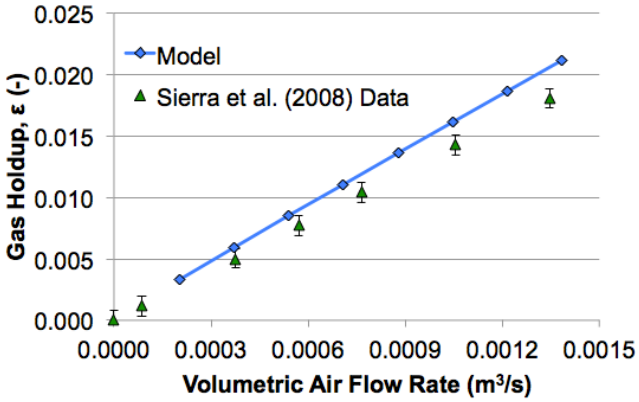


Figure 3.7: Simplified Flat Panel Model Validation of the Experimental Data from Sierra et al. (2008)

## 3.4 Optimization Methods

### 3.4.1 Optimization Process

The PBR optimization methods involve varying PBR design variables, using those variables and other parameters to solve nested models, and then evaluate and minimize objective functions under various constraints. Figure 3.8 illustrates the two-optimization schemes for tubular and flat panel PBRs. The left progression describes the four design variables that can vary for a tubular PBR: degasser height, diameter and air flow rate as well as pump pressure rise. These four design variables and input parameters determine iteration outputs of the coupled, nonlinear system of equations solver. Optimization of the flat panel PBR involved varying the panel height and air mass flow rate, iteratively solving for the average gas holdup in the panel, and then comparing a similar constrained objective function of outputs. The outputs for both kinds of PBRs are weighted in an objective function that is evaluated by the constrained optimization algorithm "fmincon" using the Matrix Laboratory (MATLAB) optimization toolbox computational software. A gradient-based optimization scheme was implemented using sequential quadratic programming (SQP). This nonlinear optimization method solves multiple optimization subsets that each optimizes to the minimum of a quadratic model of the objective function while subject to a linearization of the constraints [89]. This method is relatively inexpensive computationally, but is subject to initial conditions and constraints that might lead to local solutions. The minimized objective function $Y$ in Equation (3.4) involves a weighting scheme of the performance parameters specific energy and areal productivity. These metrics were chosen in order to minimize energy input into the PBR system per unit biomass while maximizing the amount of biomass produced per unit area. The optimization weights $a_1$ and $a_2$ were weighted evenly for this analysis. Figure 3.9 illustrates the effects of other weighting scenarios in the two-dimensional space where each iteration cluster and optimum point color represents a different weighted solution. At certain points in the trade space, any increase in either performance parameter results in a decrease in the other. Assuming equal importance of performance characteristics, the equal weighted optimum (in this case, the yellow triangle) represents one of the better designs for a given scenario and constraints.

$$Y = a_1 E_s + a_2 P_{areal}^{-1} \tag{3.4}$$

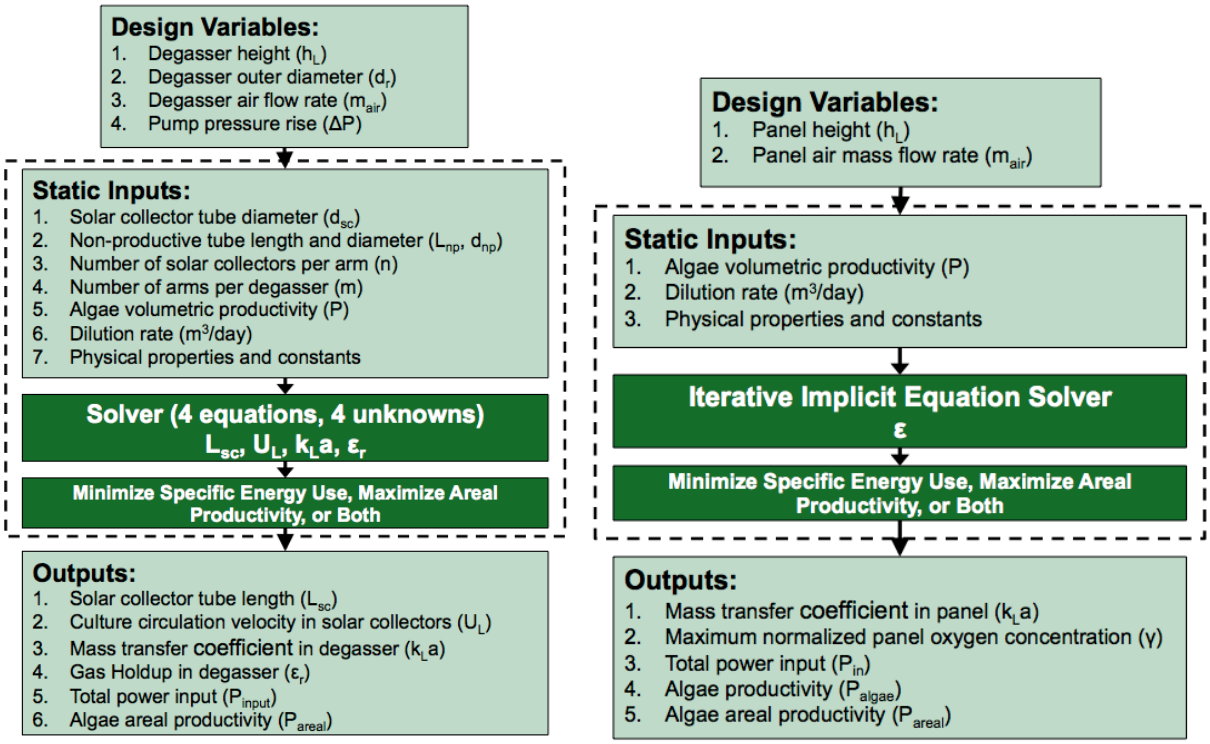


Figure 3.8: Tubular (Left) and Flat Panel (Right) Solver and Optimization Flow Charts

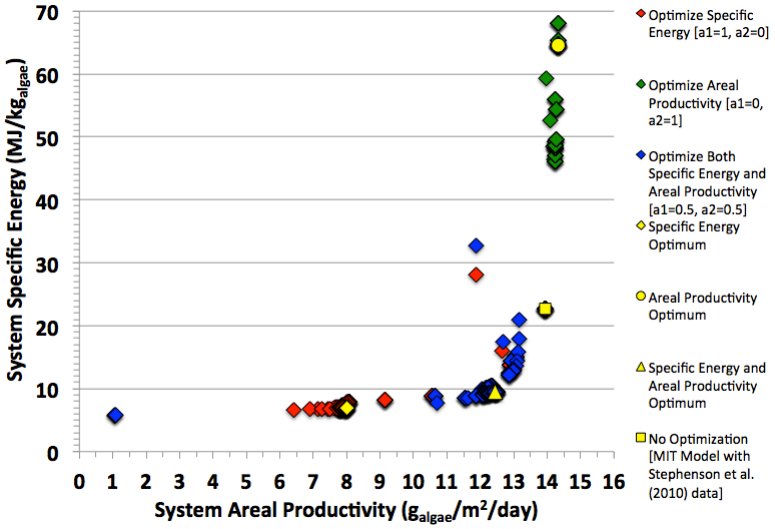


Figure 3.9: Example Performance Parameter Trade Space with Various Parameter Weightings for a Horizontal Tubular PBR with a Volumetric Productivity of 1.0 $g_{algae}$/L/day

### 3.4.2 Constraints

The optimization procedures for both tubular and flat panel PBRs include assumed constraints that greatly affect predicted geometry and end performance. Table 3.6 depicts the solver and optimization parameter constraints used when optimizing the horizontal and vertical tubular PBRs. In initial unconstrained optimizations for minimum specific energy, the degasser increased its diameter to infinity while decreasing its height to zero. This behavior makes sense as the majority of the energy input is due to the air compressor, which is partially a function of

the degasser geometry. To correct for this behavior, a geometric constraint was imposed by relating the degasser height and diameter to a diffuser angle $\theta$ as seen in Figure 3.10 and Equation (3.5). The superficial circulation velocity is constrained at high speeds by excessive turbulence that can damage the algal cells and at low speeds by stagnation in laminar flow, which inhibits algae growth due to the dark interior of the tube culture. Equations (3.6) and (3.7) depict the relationship between flow turbulence and the algal cell using Kolmogoroff's theory of local isotropic turbulence [57]. In this theory, the energy dissipation per unit mass in the pipes $\xi$ is used along with the culture viscosity $\mu_L$ and density $\rho_L$ to estimate the microeddy length $\lambda_m$. Microeddies are represented as swirling of a fluid and reverse current that are present in turbulent flows. $\xi$ is in turn a function of Fanning friction factor $C_f$ (empirically a function of Reynolds number), superficial flow velocity $U_L$, and tube diameter $d_{sc}$. To ensure algal cell integrity, $\lambda_m$ must remain greater than the characteristic dimension of the algal cell, in this case the cell diameter $d_{\text{algae}}$. The lower superficial velocity constraint is governed by the turbulent flow limit as a function of Reynolds number (minimum turbulent value of 3000), culture density, viscosity, and tube diameter as depicted in Equation (3.8). This analysis assumed the diameter of the marine species of Chlorella vulgaris (~4 μm), which under standard day conditions and constraints equates to superficial flow velocities of about 0.05-31.7 m/s [90]. The superficial velocities never increase to such high speeds, but the minimum turbulence constraint can be reached – especially when minimizing specific energy. The solar collector length, normalized pumping pressure, and maximum degasser height all stem from engineering judgment and material stress limitations for high density polyethylene under high wind conditions assuming no side mounted supports. The tubular air mass flow rate ranges were taken from literature.

For the flat panel constraints, the liquid height, air mass flow rate, and normalized maximum oxygen concentration were all determined using either material constraints or ranges from previous designs [56]. The panel thickness and length were assumed fixed for this analysis.

Table 3.6: Tubular PBR Optimization Constraints

| Solver Parameters | Initial | Constraints | Optimization Parameters | Initial | Constraints | Notes |
|---|---|---|---|---|---|---|
| $U_L$ (m/s) | 0.5 | Eqns. (3.7) and (3.8) | $h_L$ (m) | 4.4 | < 7.0; > $h_s$ (vertical only); Figure 3.10 and Eqn. (3.5) | Engineering judgment and material limitations |
| $\varepsilon_r$ (-) | 0.2 | None | $d_r$ (m) | 0.106 | > 0.0; Figure 3.10 and Eqn. (3.5) | |
| $L_{sc}$ (m) | 136 | > 7.0 | $P_r$ (-) | 0.0 | 0.0 – 0.07 | |
| | | | $\dot{m}_{air}$ (kg/s) | 0.001 | 1E-6 – 0.005 | [55] |

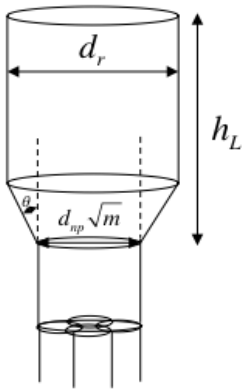


Figure 3.10: Degasser Diameter and Height Constraint Relationship for Tubular Photobioreactors

$$h_L \geq \frac{1}{\tan(\theta)}\left(\frac{d_r - d_{np}\sqrt{m}}{2}\right) \tag{3.5}$$

$$\mathrm{Re} = \frac{\rho_L U_L d_{sc}}{\mu_L}$$

$$C_f = 0.0791\mathrm{Re}^{-\frac{1}{4}} \tag{3.6}$$

$$\xi = \frac{2C_f U_L^3}{d_{sc}}$$

$$\lambda_m = \left(\frac{\mu_L}{\rho_L}\right)^{\frac{3}{4}} \xi^{-\frac{1}{4}} = \left(\frac{\mu_L}{\rho_L}\right)^{\frac{3}{4}} \left[\frac{2}{d_{sc}}\left(0.0791\left(\frac{\rho_L U_L d_{sc}}{\mu_L}\right)^{-\frac{1}{4}}\right) U_L^3\right]^{-\frac{1}{4}} \geq d_{\text{algae}} \tag{3.7}$$

$$U_L \leq 1.96 \frac{\mu_L}{\rho_L} d_{sc}^{\frac{5}{11}} d_{\text{algae}}^{-\frac{16}{11}}$$

$$\mathrm{Re} \geq 3000$$

$$U_L \geq 3000 \frac{\mu_L}{\rho_L d_{sc}} \tag{3.8}$$

Table 3.7: Flat Panel Optimization Constraints

| Optimization Parameters | Initial | Constraints | Notes |
|---|---|---|---|
| $h_L$ (m) | 1.5 | 0.5 – 3.0 | Engineering judgment and material limitations |
| $\dot{m}_{air}$ (kg/s) | 0.001 | 0.0002 – 0.0018 | [56] |
| $\gamma_i$ | N/A | < 3.5 | [56] |

3.4.3 Optimization Scenarios and Photobioreactor Designs

Optimization scenarios were conducted for both tubular and flat panel PBRs initially at a volumetric productivity of 1.0 g/L/day to gain insight into the role of various constraints on

affecting the objective function. All inputs for tubular and flat panel PBR optimizations can be found in Table D1 and Table D2. The optimization parameter variations for both horizontal and tubular PBRs are depicted in Table 3.8. The values highlighted in blue and red represent parameters that have been driven to or near constraints for a specific optimization type. For both kinds of tubular PBRs, the effects of minimizing for specific energy (decreasing $E_s$ by 69.7-89.1%) on the objective function greatly outperform the effects of maximizing for areal productivity (increasing $P_{areal}$ by 1.4-2.8%). As a result, the equally weighted optimization of specific energy and areal productivity yields a greater decrease in specific energy than the decrease in areal productivity for both tubular PBR types. This weighted tradeoff between the two objective parameters can be seen in Figure 3.9.

Equation (3.9) and Equation (3.10) are shown to better understand the influence of various input parameters, design variables and constraints on the objective parameters. When minimizing for specific energy, the optimizer will need to either decrease the energy input to the system $P_{input}$ in W and/or increase the system productivity $P_{\text{algae}}$ in $kg_{algae}/s$. Looking into the expansion of these terms, one notices that decreasing the power input would entail decreasing the degasser height, air flow rate, and circulation flow rate or increasing the gas holdup and compressor and pump efficiencies. Similarly, in order to increase the PBR system productivity for a set algae volumetric productivity and solar collector pipe diameter, one would need to increase the system solar collector length. However, there is a tradeoff between the culture oxygen concentration and the solar collector tube length. This balance [Equation (C15)] relies upon a specified maximum oxygen concentration at the degasser outlet, the culture flow rate, the degasser height and the degasser airflow rate, which all limit solar collector length in the optimizer. The gradient-based optimizer recognizes that decreasing the airflow rate in the degasser has a larger impact on decreasing the PBR specific energy then increasing the solar collector length. Consequently, the degasser height, airflow rate, superficial circulation velocity and solar collector tube length all decrease to near or at their respective minimum constraints.

To maximize areal productivity for a given volumetric productivity, one needs to either increase the productive volume and/or decrease the areal footprint of the system as shown in the first part of Equation (3.10). Expanding the terms, one notices that the areal productivity eventually relies upon an initial solar collector tube diameter, initial volumetric productivity, and solar collector length. Figure 3.11 illustrates the relationship between the solar collector diameter and the volumetric productivity when both are normalized by the initial inputs from Stephenson et al (2010) [53,57]. This normalized relationship was used for modifying the solar collector tube diameter, which accounts for the lower growth rates associated with dark inner sections of the tubes when optimizing the tubular PBRs over varying volumetric productivities. Figure 3.12 portrays the unconstrained relationships between solar collector length and areal productivity for various volumetric productivities and optimization scenarios. For a given solar collector tube length, the areal productivity increases as the volumetric productivity decreases. This occurs because the associated quadratic increase in solar collector tube diameter (and volume) outweighs the combined linear increase and decrease in the PBR footprint and volumetric productivity, respectively. Like the previous optimization, the oxygen concentration balance between the solar collector exit and inlet governs the solar collector length. As a result, the degasser height and airflow rate both increased to their maximum constraint values. However, there are decreasing returns on increases in areal productivity as one increases the solar collector

length. This occurs because the linear increase in PBR volume associated with increasing solar collector tube length is eventually overtaken by the increases in areal footprint. Consequently, the optimization of both areal productivity and specific energy occurs on the lower end of solar collector tube length range (~32 m in Figure 3.12) when compared to the other optimization scenarios.

$$E_s = \frac{P_{input}}{P_{\text{algae}}} = \frac{\dfrac{\Delta P}{\eta_p} A_{sc} U_L + \dot{m}_{air} \dfrac{C_p T_{op}}{\eta_c} \left[ \left( \dfrac{P_a + (1-\varepsilon_r)\rho_L g h_L}{P_a} \right)^{\frac{\gamma-1}{\gamma}} - 1 \right]}{nmA_{sc} L_{sc} P} \tag{3.9}$$

$$P_{areal} = P \frac{V_p}{A_{PBR}} = P \frac{\frac{\pi}{4} d_{sc}^2 L_{sc}}{L_1 L_2} = P \frac{\pi d_{sc}^2 L_{sc}}{4\left[ (nN_b + n)\left((d_{sc} + t_w) + d\right) \left( \frac{1}{N_b + 1} \left( \begin{array}{l} L_{sc} + \frac{1}{2}(d_{sc} + t_w) + N_b d + \\ \frac{5}{2} N_b (d_{sc} + t_w) + \frac{1}{2} n (N_b + 1)(d_{sc} + t_w) \end{array} \right) \right) \right]}$$

$$d = 1.5(d_{sc} + t_w) \tag{3.10}$$

$$d_{sc} = d_{sc_{initial}} d_{sc_{norm}}$$

$$d_{sc_{norm}} = \left(0.37985 P_{norm}^4 - 3.04525 P_{norm}^3 + 9.11265 P_{norm}^2 - 12.3828 P_{norm} + 6.94368\right)$$

$$P_{norm} = \frac{P}{P_{initial}}$$

Table 3.8: Parameter Changes from Models of Experimental Tubular PBR Designs for Various Optimization Types at 1.0 g/L/day: Blue and Red Text Denote Parameters Approaching Minimum and Maximum Constrains, Respectively

| Parameters | PBR Type | Optimization Type | | | |
|---|---|---|---|---|---|
| | | None | Minimum $E_s$ | Minimum $E_s$ and Maximum $P_{areal}$ | Maximum $P_{areal}$ |
| $E_s$ (MJ/kg$_{algae}$) | Horizontal Tubular | 22.6 | 6.85 | 9.4 | 64.5 |
| | Vertical Tubular | 62.5 | 6.80 | 10.3 | 102 |
| $P_{areal}$ (g$_{algae}$/m$^2$/day) | Horizontal Tubular | 13.9 | 8.00 | 12.4 | 14.3 |
| | Vertical Tubular | 12.5 | 7.65 | 11.5 | 12.6 |
| $h_L$ (m) | Horizontal Tubular | 4.40 | **0.999** | 0.712 | **7.00** |
| | Vertical Tubular | 3.25 | **1.27** | 1.27 | **7.00** |
| $d_r$ (m) | Horizontal Tubular | 8.01E-02 | 0.147 | 0.12 | 5.81E-02 |
| | Vertical Tubular | 4.41E-02 | 0.148 | 5.45E-02 | 2.94E-02 |
| $P_r$ (-) | Horizontal Tubular | 0.00 | 0.00 | 0.00 | **0.07** |
| | Vertical Tubular | 0.00 | 7.35E-04 | 0.00 | **0.07** |
| $\dot{m}_{air}$ (kg/s) | Horizontal Tubular | 1.02E-03 | **6.88E-06** | 6.91E-04 | **5.00E-03** |
| | Vertical Tubular | 5.00E-03 | **1.57E-06** | 1.24E-04 | **5.00E-03** |
| $U_L$ (m/s) | Horizontal Tubular | 0.558 | **0.128** | 0.261 | 0.982 |
| | Vertical Tubular | 0.570 | **0.113** | 0.237 | 0.809 |
| $\varepsilon_r$ (-) | Horizontal Tubular | 0.197 | 1.06E-02 | 0.125 | 0.498 |
| | Vertical Tubular | 0.757 | 2.52E-03 | 9.98E-02 | 0.763 |
| $L_{sc}$ (m) | Horizontal Tubular | 104 | **7.00** | 32.7 | 200 |
| | Vertical Tubular | 148 | **7.01** | 32.0 | 196 |
| $[O_2]_{in}$ (-) | Horizontal Tubular | 1.60 | 2.59 | 2.06 | 1.48 |
| | Vertical Tubular | 1.06 | 2.54 | 1.99 | 1.19 |
| $k_L a$ (1/s) | Horizontal Tubular | 9.70E-02 | 4.25E-03 | 0.0565 | 0.393 |
| | Vertical Tubular | 1.23 | 9.99E-04 | 4.39E-02 | 1.28 |
| $A_{PBR}$ (m$^2$) | Horizontal Tubular | 16.4 | 1.72 | 5.61 | 30.8 |
| | Vertical Tubular | 7.86 | 0.512 | 1.81 | 10.4 |
| $C_s$ (kg/m$^3$) | Horizontal Tubular | 3.9 | 0.262 | 1.22 | 7.46 |
| | Vertical Tubular | 1.67 | 7.93E-02 | 0.362 | 2.22 |
| $U_G$ (m/s) | Horizontal Tubular | 0.144 | 3.44E-03 | 5.22E-02 | 1.34 |
| | Vertical Tubular | 2.62 | 7.70E-04 | 4.22E-02 | 5.66 |
| $V_P$ (m$^3$) | Horizontal Tubular | 0.234 | 1.57E-02 | 7.33E-02 | 0.448 |
| | Vertical Tubular | 0.1 | 4.76E-03 | 2.17E-02 | 0.133 |
| $P_{input}$ (W) | Horizontal Tubular | 61.3 | 1.24 | 7.97 | 334 |
| | Vertical Tubular | 72.7 | 0.374 | 2.59 | 158 |
| $P_{algae}$ (kg/s) | Horizontal Tubular | 2.71E-06 | 1.82E-07 | 8.49E-07 | 5.18E-06 |
| | Vertical Tubular | 1.16E-06 | 5.51E-08 | 2.51E-07 | 1.54E-06 |

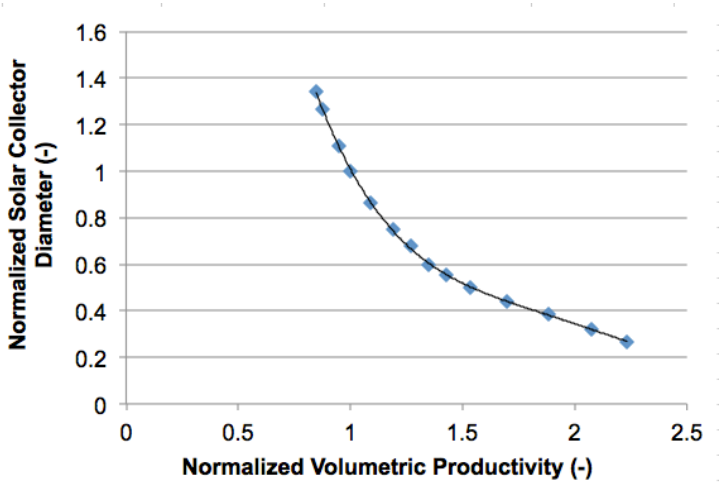


Figure 3.11: Effect of Solar Collector Tube Diameter on Volumetric Productivity Normalized by Stephenson et al. (2010) Initial Parameters [57]

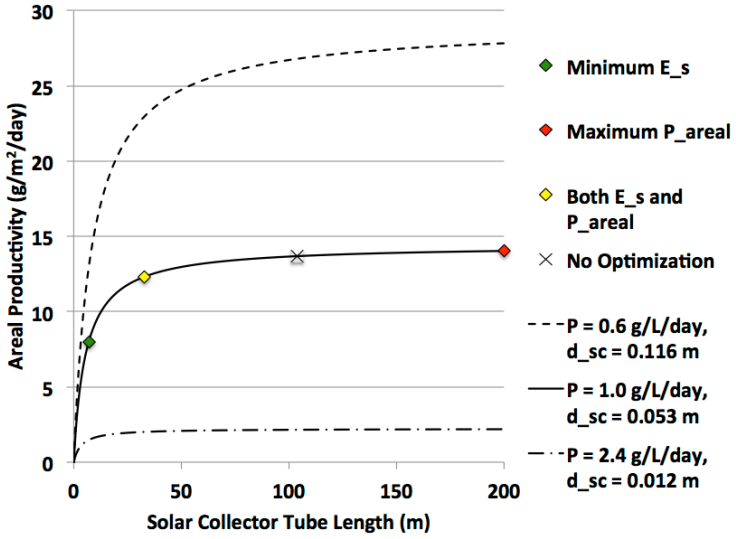


Figure 3.12: Effects of Solar Collector Tube Length and Volumetric Productivity/Solar Collector Tube Diameter on Areal Productivity for a Horizontal Serpentine Tubular PBR

Similarly, the flat panel PBR underwent multiple optimization scenarios to understand various system changes. Equation (3.11), Equation (3.12), and Table 3.9 describe how certain input parameters and constraints influence the objective parameters. When minimizing specific energy, the optimizer decreases the airflow rate and panel height to at or near minimum constraints while reaching the maximum average oxygen concentration in the panel.

Much like the influence of solar collector tube length in the tubular PBRs, the panel height has decreasing returns on areal productivity with increased panel height. The effects of panel height, as well as panel thickness and normalized height-to-spacing ratio are illustrated in Figure 3.13. A 10% increase and decrease in panel thickness yields a ~6-9% increase and decrease in areal productivity over the height range, respectively. A 10% increase and decrease in normalized height-to-spacing ratio produces ~6-20% and ~6-58% areal productivity decreases and increases, respectively. When maximizing areal productivity, the maximum culture concentration and

height both increased to near maximum constraints. Note that the airflow rate did not increase because the average culture oxygen concentration did not reach the maximum value of 250% of saturation concentration. Like the tubular PBRs, the flat panel PBR evenly combined optimization favored PBR characteristics for minimizing specific energy over maximizing areal productivity. However, the effects of minimizing specific energy (decreasing $E_s$ by ~17%) were closer to the effects maximizing areal productivity (increasing $P_{areal}$ by ~1.8%).

$$E_s = \frac{P_{input}}{P_{\text{algae}}} = \frac{\dot{m}_{air}\dfrac{C_p T_{op}}{\eta_c}\left[\left(\dfrac{P_a + (1-\varepsilon)\rho_L g h_L}{P_a}\right)^{\frac{\gamma-1}{\gamma}} - 1\right]}{P \cdot t \cdot L \cdot h_L} = \frac{\dot{m}_{air} C_p T_{op}}{P \cdot t \cdot L \cdot h_L \cdot \eta_c}\left[\left(\frac{P_a + (1-\varepsilon)\rho_L g h_L}{P_a}\right)^{\frac{\gamma-1}{\gamma}} - 1\right] \quad (3.11)$$

$$P_{areal} = P\frac{V_p}{A_{PBR}} = P\frac{L \cdot t \cdot h_L}{L(2X + t)} = \frac{t \cdot h_L}{\left(2h_L \dfrac{1.4}{2.2} + t\right)} = P\frac{11 t h_L}{11 h_L + 14 t} \quad (3.12)$$

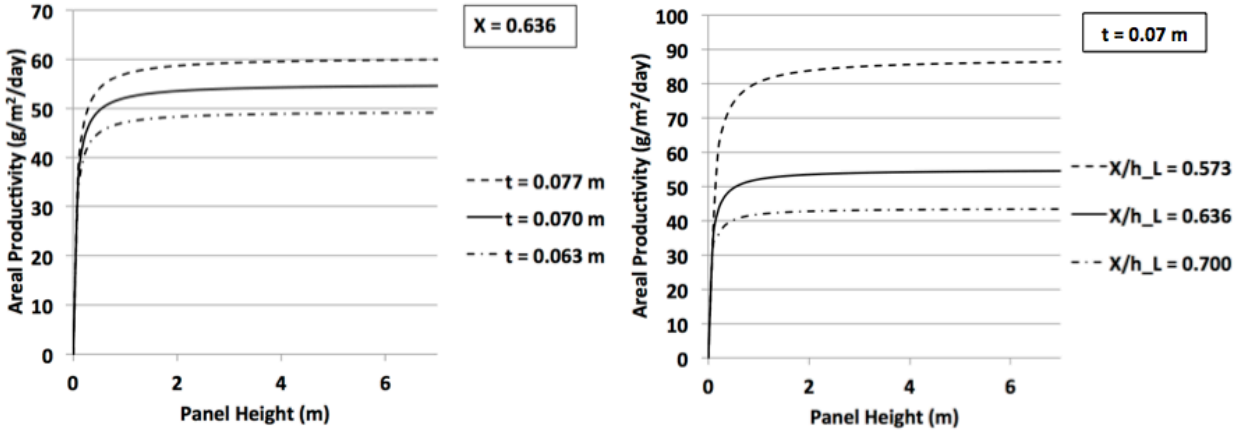


Figure 3.13: Effects of Panel Thickness $t$, Normalized Panel Height-to-Spacing Ratio $X / h_L$, and Panel Height $h_L$ on Areal Productivity for a Volumetric Productivity of 1.0 g/L/day

Table 3.9: Parameter Changes from Models of the Experimental Flat Panel PBR Design for Various Optimization Types at 1.0 g/L/day: Blue and Red Text Denote Parameters Reaching Near Minimum and Maximum Constrains, Respectively

| Parameters | Optimization Type | | | |
|---|---|---|---|---|
| | None | Minimum $E_s$ | Minimum $E_s$ and Maximum $P_{areal}$ | Maximum $P_{areal}$ |
| $E_s$ (MJ/kg$_{algae}$) | 3.37 | 2.78 | 2.80 | 3.22 |
| $P_{areal}$ (g$_{algae}$/m$^2$/day) | 53.1 | 49.5 | 50.8 | 54.0 |
| $h_L$ (m) | 1.50 | **0.5** | 0.672 | **3.00** |
| $\varepsilon$ (-) | 9.23E-03 | 7.76E-03 | 7.80E-03 | 8.67E-03 |
| $\dot{m}_{air}$ (kg/s) | 7.00E-04 | **5.59E-04** | 5.67E-04 | 7.00E-04 |
| $\gamma_i$ (-) | 2.31 | **2.50** | **2.50** | **2.46** |
| $k_L a$ (1/s) | 4.68E-03 | 3.93E-03 | 3.95E-03 | 4.39E-03 |
| $A_{PBR}$ (m$^2$) | 4.95 | 1.77 | 2.31 | 9.72 |
| $C_s$ (kg/m$^3$) | 4.38 | 1.46 | 1.96 | 8.75 |
| $U_G$ (m/s) | 3.15E-03 | 2.63E-03 | 2.65E-03 | 2.95E-03 |
| $P_{input}$ (W) | 10.2 | 2.82 | 3.81 | 19.6 |
| $P_{algae}$ (kg/s) | 3.04E-06 | 1.01E-06 | 1.36E-06 | 6.08E-06 |

After validating and investigating initial optimization scenarios, PBR types were optimized for a variety of volumetric productivities. Each chosen volumetric productivity was optimized for: specific energy, areal productivity, both specific energy and areal productivity, and no optimization. For each optimization scenario, the initial geometric and flow parameters stem from the validated experimental PBR designs. All optimized design points and corresponding performance parameters for various optimization scenarios and PBR types are illustrated in Figure 3.14. As discussed previously, the tubular PBRs decrease performance with increasing volumetric productivity due to the decreasing solar collector tube diameter decreasing the productive volume (and thus, areal productivity) and increasing friction losses (and thus, specific energy). With the flat panel PBRs, performance improves with increasing volumetric productivity because the fixed panel thickness (well-mixed flow not requiring a thickness change with volumetric productivity) and frictionless panel wall assumptions do not adversely affect the performance parameters.

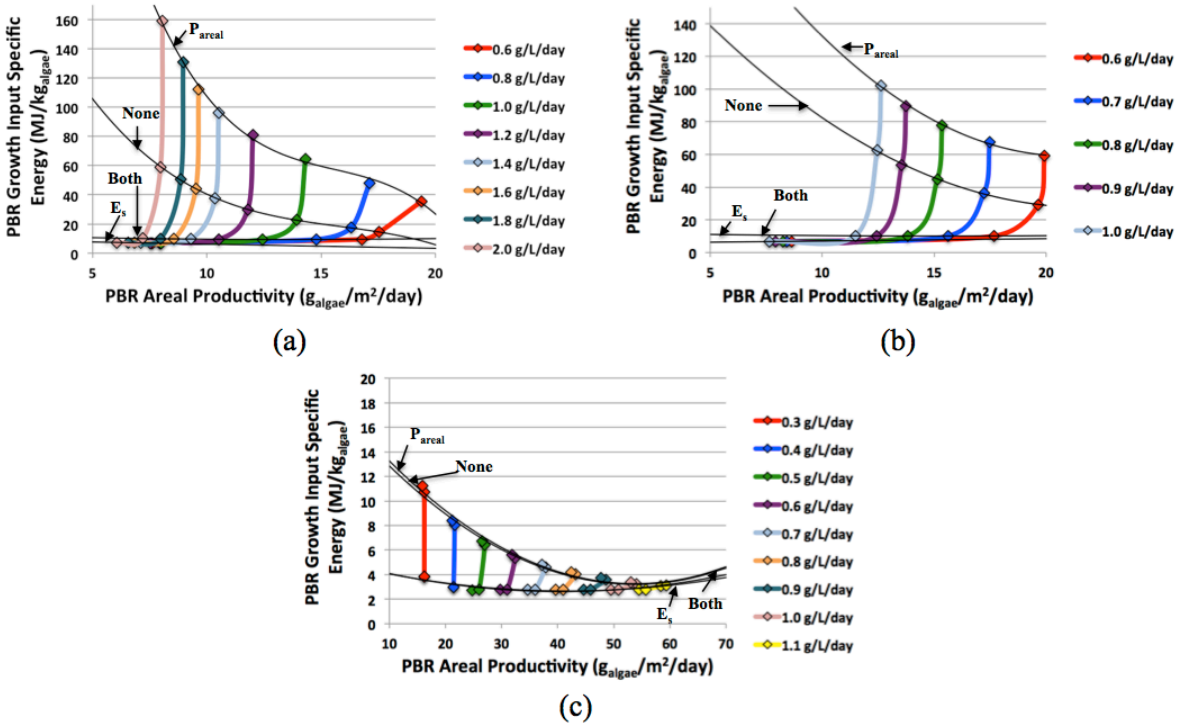


Figure 3.14: Optimization Scenarios for Specific Energy, Areal Productivity, and Volumetric Productivity Carpet Pots of (a) Horizontal Serpentine Tubular, (b) Vertical Serpentine Tubular, and (c) Vertical Flat Panel Photobioreactors

### 3.4.4 Lifecycle Interface

The various optimization scenarios' PBR geometric, flow, and performance parameters at varying volumetric productivities shown in Figure 3.14 were transferred between models as described in Figure 2.3. For each PBR type and optimization scenario, a volumetric productivity range with corresponding output parameters was imported as shown in Figure D1. It is important to note that *every* volumetric productivity in the ranges is an optimized PBR design for a particular optimization scenario. Graphical representations of all PBR types and optimization scenarios' output parameter changes over volumetric productivities are depicted in Figure D2, Figure D3, and Figure D4. The optimized performance parameter variations with optimization scenario and volumetric productivities for each PBR type are illustrated in Figure 3.15. As previously mentioned, increases in volumetric productivity for the tubular PBRs results in lower performance while the opposite is true for flat panel PBRs. This pattern is due to the fixed panel thickness (no variation with volumetric productivity assumes a well-mixed medium with consistent light penetration) and frictionless wall assumptions.

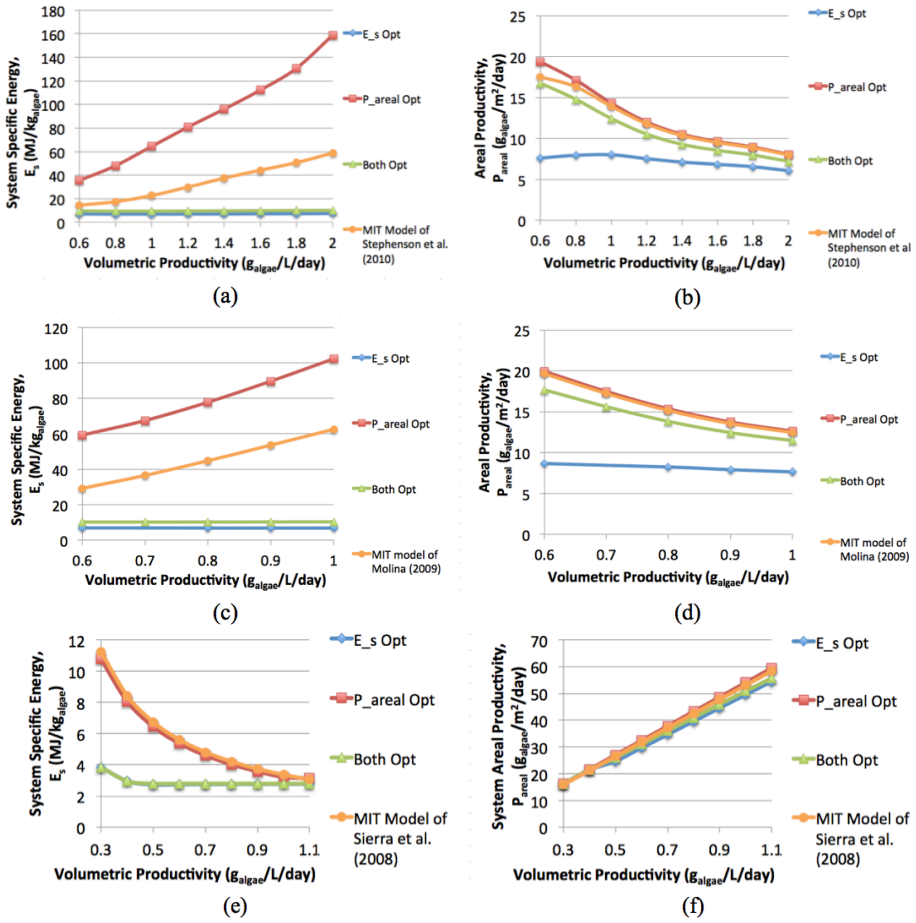


Figure 3.15: Performance Parameters Specific Energy and Areal Productivity for Various Optimization Scenarios and Volumetric Productivities: (a) and (b) Horizontal Tubular Serpentine PBR, (c) and (d) Vertical Tubular Serpentine PBR, (e) and (f) Vertical Flat Panel PBR

*[Page Intentionally Left Blank]*

# Chapter 4: Microalgae Lifecycle Scenario Results

Up to this point, the study described inputs and assumptions associated with a range of technologies for the production of synthetic HEFA-J fuel from microalgae on a lifecycle basis. Variability between cultivation and extraction types were considered, each with their associated uncertainty ranges encompassed by low, baseline, and high emission scenarios. Additionally, modeling, validation, optimization, sensitivity, and uncertainty analyses of enclosed PBRs were conducted to estimate cultivation performance parameters. The following results stem from open ponds cultivation performance inputs defined in Section 2.2.3.1: Open Raceway Pond System and the PBR cultivation performance inputs optimized for specific energy and areal productivity as defined in Section 3.4.3: Optimization Scenarios and Photobioreactor Designs. This chapter is first organized into the following lifecycle metrics: specific energy, greenhouse gas emissions, production cost, and water consumption. Comparisons to other studies, as well as local sensitivity analyses, were also conducted.

## 4.1 Cultivation, Harvesting, Extraction, and Upgrading Energy Balances

As stated in the previous section, the majority of the energy inputs into the algae facility are from cultivation and harvesting for the wet extraction technology set. Figure 4.1 provides a visual of all assessed LCA scenarios on a specific energy basis. For high scenarios, lower oil fractions decrease the total amount of energy available in the algal oil per kilogram of biomass. Note that this decreased oil fraction also accounts for a larger biomass percentage going to the digester, thus increasing the electricity production offsets in the wet extraction technology sets. The high cases also include energy for capturing and distributing highly concentrated $CO_2$ instead of flue gas distribution. For dry extraction, the largest energy debit is associated with drying the biomass with heat from combusted natural gas. No matter the technology set, the energy required for farming the algae in PBRs greatly exceeds that of open pond cultivation systems. The open pond and flat panel PBR cultivation systems using wet extraction techniques provide the most favorable energy balances, while only the low dry extraction scenarios exhibit a favorable energy balance. The specific energies involved in each scenario greatly impact the associated LCA GHG emissions.

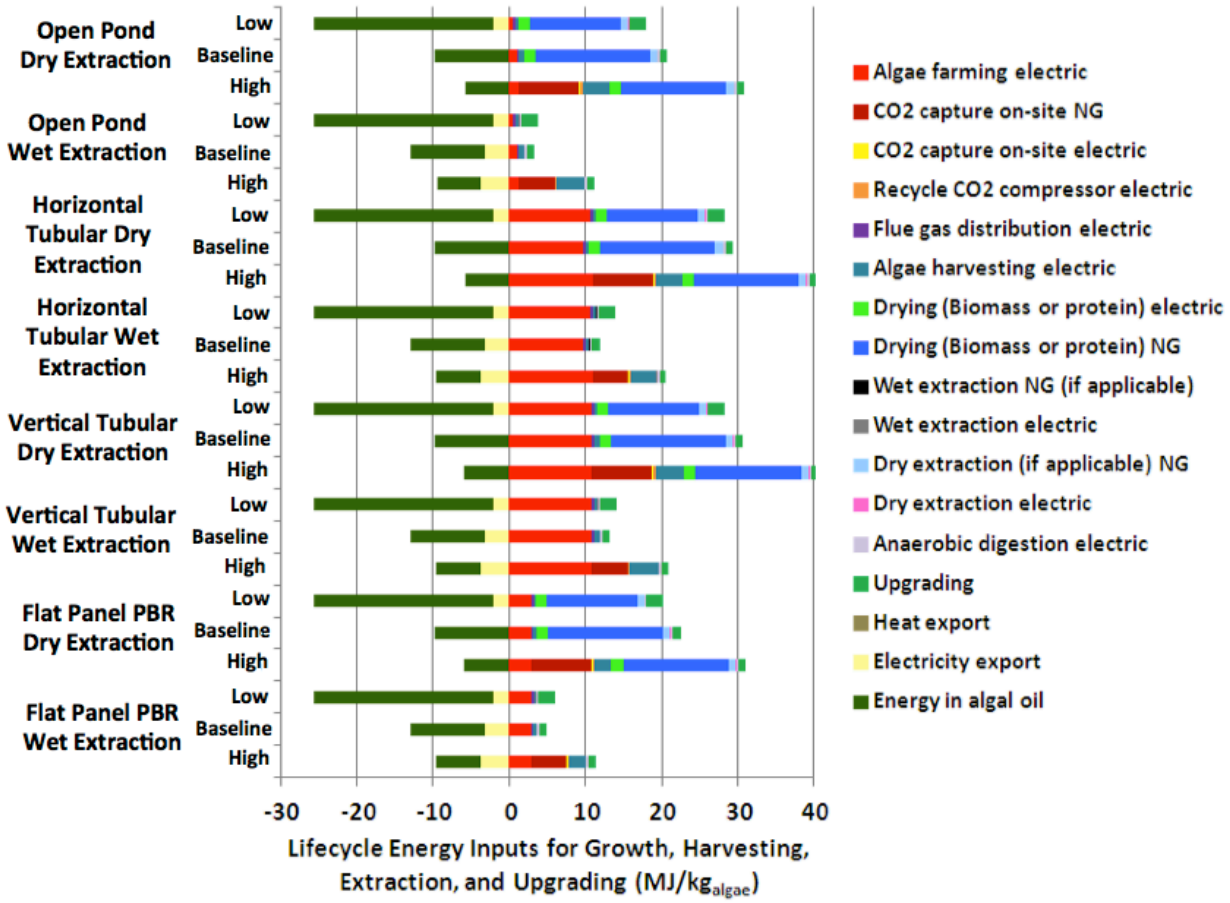


Figure 4.1: Lifecycle Energy Inputs for All Scenarios

## 4.2 Greenhouse Gas Lifecycle Emissions

LCA GHG emissions for all baseline scenarios and variability ranges normalized by baseline conventional jet fuel can be seen in Figure 4.2 and Figure 4.3, respectively. The overall LCA GHG values are based on a 100-year time window for radiative forcing values to determine the overall equivalent carbon dioxide emissions (g-$CO_2$e) from $CO_2$, $CH_4$, and $N_2O$. Direct and indirect land use change, as well as emissions embodied within construction materials are not considered for the algae pathways. Other non-$CO_2$ climate effects (nitrogen oxides, soot, sulfates, contrails, cirrus, water vapor, etc.) were also not considered in this study [2,37,4]. The various algal oil to HEFA-J pathways include flat panel (FP), vertical tubular (VT), horizontal tubular (HT), and open pond (OP) cultivation systems; each with wet extraction (WE) and dry extraction (DE) technology sets. Other feedstock to fuel pathways are shown for comparisons; however, the coproduct allocation methods; cultivation, recovery, biomass residue, and extraction technologies; and jet fuel conversion inputs vary in each scenario [2,53,4]. The majority of LCA GHGs from all scenarios for in this study are comprised of emissions associated with the recovery steps of the lifecycle. When applicable, this step includes emissions associated with algae farming (cultivation and harvesting), drying, $CO_2$ sourcing, nutrient inputs and use, waste water treatment, $CO_2$ losses due to pond outgassing and recycle capture unit, and $CO_2$ debit associated with consumables used in capture and extraction processes, $CO_2$ from

sludge and effluent streams, and blowdown $CO_2$ losses. The other large portion of the LCA GHGs is the biomass credit, which includes displacement credits for $CO_2$ uptake expressed as carbon allocation ratios for algae oil and algae cake as well as in some cases, displacement credits for excess electricity generation from biogas produced onsite. Land use change and infrastructure emissions were not considered in these scenarios. When compared to the baseline open pond algae LCA GHG emissions from Stratton et al., both the recovery and biomass credit emissions from this study are relatively large. The difference in recovery baseline emissions can be attributed to accounting for extensive system recycling and system losses associated with each of the cultivation, harvesting, and dewatering steps. Another source of variation was the use of more energy intensive clarifiers and centrifuges in this study's baseline cases (1.9 $MJ/kg_{algae}$), whereas settling ponds were used in the Stratton et al. report (0.56 $MJ/kg_{algae}$). This study's specific energy inputs for settling ponds and clarifiers estimated 0.45 and 0.64 $MJ/kg_{algae}$, respectively. However, settling ponds were only used in the low cases. The difference in biomass credits can be credited in part to the biogas combustion electricity exports as well as allocating for the carbon displaced within the biomass meal co-product. The last source of overall variation between the studies stems from the coproduct allocation methods. In the baseline case for Stratton et al., energy allocation was used for the excess electricity (from Anaerobic digestion) and the oil coproducts; whereas displacement was used for electricity offsets and energy allocation was used for the algal oil fuel coproducts in this study.

The algal oil to HEFA-J scenario variations normalized by conventional jet fuel (87.5 g-$CO_2$e/MJ) represent a wide range of values that greatly depend on the technology inputs and assumptions. The exceedingly high ranges (upwards of a factor of 11 in some cases) include low productivities and high specific energy inputs that all combine to represent the high emissions scenarios. Thus, most algal baseline scenarios reside closer to the lower end of the variability spectrum as they represent current technology inputs and assumptions. The two algal oil to HEFA-J baseline pathways that fall under 87.5 g-$CO_2$e/MJ are the flat panel and open pond cultivation system wet extraction technology sets, each with values of 53.5 and 31.3 g-$CO_2$e/$MJ_{HEFA\text{-}J}$, respectively. Under the low scenarios, these values decrease to 29.1 and 8.9 g-$CO_2$e/$MJ_{HEFA\text{-}J}$. The less energy intensive cultivation systems and extraction technologies as well as larger algae biomass growth rates and lipid contents account for the majority of these benefits over other scenarios.

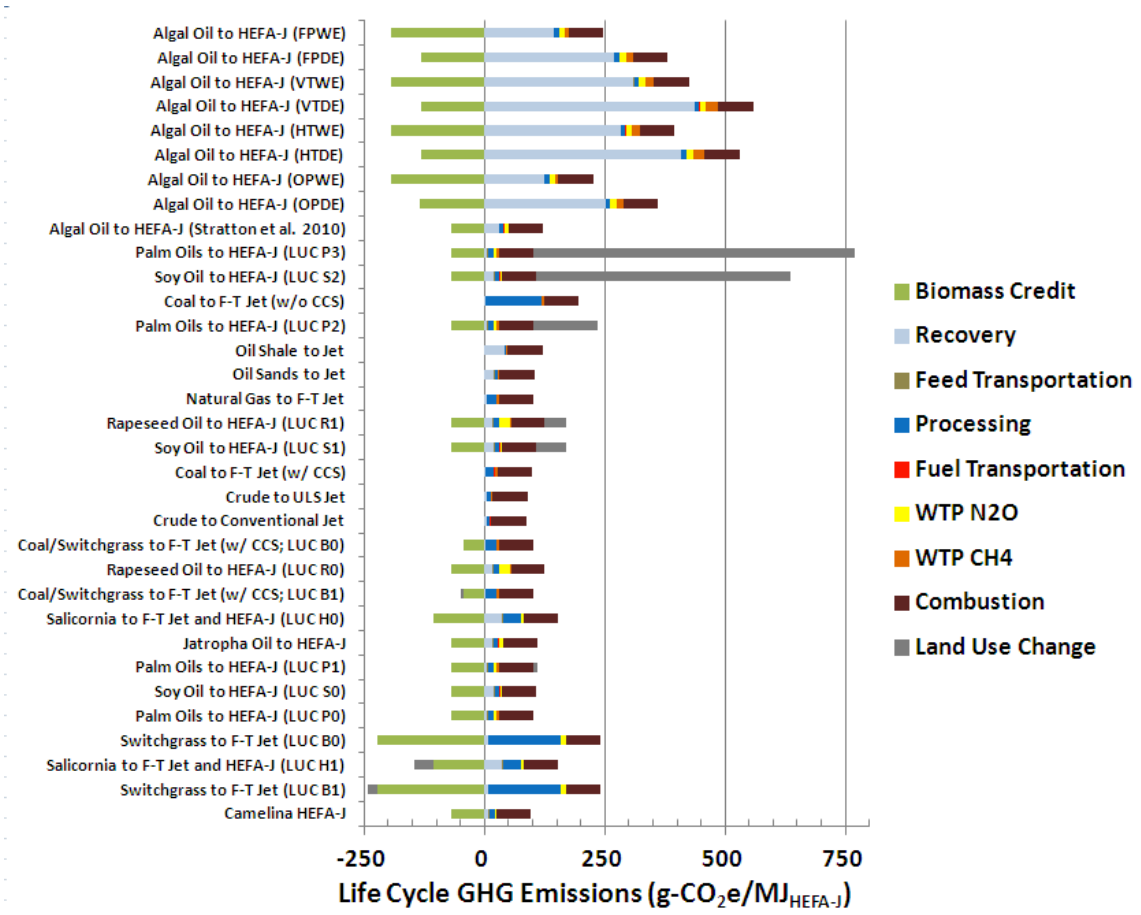


Figure 4.2: Baseline Lifecycle Greenhouse Gas Emissions for Various Jet Fuel Pathways; This Study Conducted Algal Oil to HEFA-J Scenarios for Open Pond Dry Extraction (OPDE), Open Pond Wet Extraction (OPWE), Horizontal/Vertical Tubular PBR Dry Extraction (HTDE/VTDE), Horizontal Tubular PBR Wet Extraction (HTWE/VTWE), Flat Panel PBR Dry Extraction (FPDE), and Flat Panel PBR Wet Extraction (FPWE); Land Use Change (LUC) Scenarios Outlined in [4]

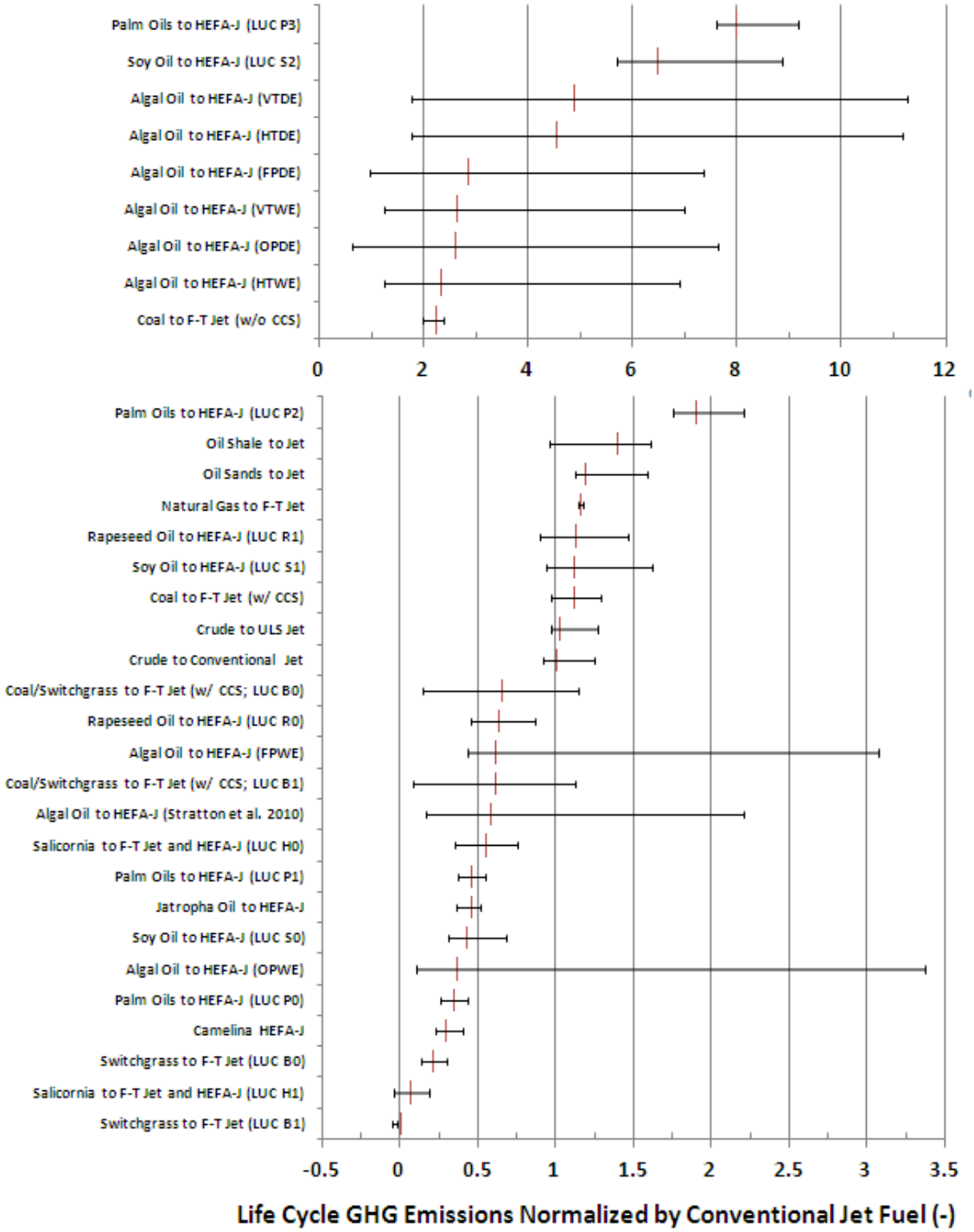


Figure 4.3: Baseline Lifecycle Greenhouse Gas Emissions for Various Jet Fuel Pathways Normalized to Conventional Crude to Jet Fuel; Variability Bars Represent Low and High Scenarios; This Thesis Conducted Algal Oil to HEFA-J Scenarios for Open Pond Dry Extraction (OPDE), Open Pond Wet Extraction (OPWE), Horizontal/Vertical Tubular PBR Dry Extraction (HTDE/VTDE), Horizontal Tubular PBR Wet Extraction (HTWE/VTWE), Flat Panel PBR Dry Extraction (FPDE), and Flat Panel PBR Wet Extraction (FPWE); Land Use Change (LUC) Scenarios Outlined in [4]

## 4.3 Production Cost

An important aspect of the lifecycle analysis is the total financial expense of growing and converting algae into usable fuel. These analyses provide a bottoms-up techno-economic approach to quantifying the various aspects of biofuels production. Up to this point, all metrics were normalized by the energy content of the HEFA jet fuel while allocating for liquid co-products based on energy. For production cost, the total production cost is normalized by the energy content of HEFA-J, but the product slate prices are instead allocated based on five-year market price averages. Table 4.1 provides the mass, energy, and market product slate allocation methods and their associated impact on the HEFA-J fraction for maximum distillate and maximum jet fuel product slates. One notices that the differences between energy and market based allocations are slight for the maximum distillate product slate currently under investigation. However, one could argue that a market-based co-product allocation better reflects the final production price fraction allocated to the jet fuel portion of the chosen product slate. Thus, this market allocation HEFA-J fraction is multiplied by the energy normalized production cost to account for the values of the coproducts.

The overall unallocated production cost is broken down as the sum total of capital, fixed operating, and variable operating expenses as described in Equation (4.1). The total production cost $P_{prod}$ is calculated based on the annualized capital $C_{capex}$, fixed operating $C_{fopex}$, and variable operating $C_{vopex}$ expenses in \$/year for a given algae productivity $P_{\text{algae}}$ in $kg_{algae}$/year and internal rate of return (IRR) $r_i$ while also adding the converted upgrading expenses from reference [33] in \$/$kg_{algae}$. Upgrading expenses for low, baseline, and high scenarios were implemented for 2000, 4000, and 6500 $bpd_{TAG}$ HEFA facilities, respectively. Each of these upgrading expenses had their own similar cost breakdowns not delineated in this thesis. The final production cost is converted to \$/$gal_{TAG}$ (without upgrading expenses), \$/$MJ_{HEFA\text{-}J}$, and \$/$gal_{HEFA\text{-}J}$ based on the process conversion scenario inputs and coproduct allocation fractions. This analysis assumes 15% IRR for a 20 year facility, no loans or interest (100% equity), that costs are before federal taxes and associated depreciation, and that operating cost increases due to inflation are matched by increases in fuel prices over time so as to keep a constant IRR. Note that the upgrading facility estimates also included a 15% IRR, loans (20% equity), depreciation (10 year linear), and inflation (2%) assumptions within its model. Future studies will work towards including similar estimates for the algae growth oil production facility scenarios.

$$R_{prod} = \left[ \frac{C_{capex} + C_{fopex}\left(1+r_i\right) + C_{vopex}\left(1+r_i\right)}{P_{\text{algae}}} + R_{capex_{upgrading}} + R_{fopex_{upgrading}} + R_{vopex_{upgrading}} \right] \frac{\$}{kg_{\text{algae}}} \quad (4.1)$$

Capital costs are broken down by Inside Battery Limits (ISBL), Outside Battery Limits (OSBL), land, special, contingency, and startup costs. ISBL costs consist of engineered equipment expenses including purchasing and installing process units and supporting processes. OSBL costs include storage and basic process utilities. Special costs include siting, project management, offices, laboratory furniture, and other miscellaneous equipment. A cost buildup approach was used for ISBL and land estimates, while the other expenses were based on heuristics of refining facilities [33,91]. Capital cost inputs can be seen in Table B1 for ISBL and Table B2 for land, OSBL, special, contingency, and start up cost estimates. The annual Total Project Investment (TPI) includes all capital costs and is determined based on an assumed internal rate of return and

facility lifetime shown in Table 4.2 and applied in Equation (4.2). The annual capital payments $C_{capex}$ in \$/yr were determined by the total project investment $TPI$, internal rate of return, and facility lifetime $n_{years}$.

Table 4.1: Mass, Energy, and Market Price Coproduct Allocation and Associated Jet Fuel Fractions

| Product Slate | | LHV [37] (MJ/kg) | Gate Price[‡‡] [33] (USD/gal) | Mass [33] (kg/100kg$_{TAG}$) | Energy (MJ/100kg$_{TAG}$) | Market (USD/100kg$_{TAG}$) |
|---|---|---|---|---|---|---|
| HEFA Jet | Maximum Distillate | 44.1 | 2.12 | 12.8 | 564 | 9.47 |
| | Maximum Jet | | | 49.4 | 2180 | 36.54 |
| HEFA Diesel | Maximum Distillate | 44.0 | 2.13 | 68.1 | 2995 | 49.20 |
| | Maximum Jet | | | 23.3 | 1025 | 16.83 |
| HEFA Naphtha | Maximum Distillate | 44.4 | 2.03 | 1.8 | 79.9 | 1.38 |
| | Maximum Jet | | | 7.0 | 311 | 5.36 |
| HEFA Fuel Gas[§§] | Maximum Distillate | 46.9 | 1.77 | 5.8 | 272 | 5.35 |
| | Maximum Jet | | | 10.2 | 478 | 9.40 |
| HEFA-J Fraction | Maximum Distillate | | | 14.5% | 14.4% | 14.5% |
| | Maximum Jet | | | 54.9% | 54.6% | 53.6% |

$$C_{capex} = \frac{TPI \cdot r_i}{\left[1-\left(1+r_i\right)^{-n_{years}}\right]} \tag{4.2}$$

Table 4.2: Capital and Operating Cost Assumptions [22,33,92,93]

| | | |
|---|---|---|
| Internal rate of return (%) | $r_i$ | 15 |
| Facility lifetime (years) | $n_{years}$ | 20 |

The summation of the various capital expenses for each scenario is illustrated in Figure 4.4. The major impact of large ISBL costs for the tubular PBRs impacts the other capital costs based on the heuristic values outlined in Table B2. This effect plays an important role in the sensitivity analyses in Section 4.7, where ISBL expense inputs impact the majority of the final production cost. The extraction technologies made up 0.04-1.5% of the PBR ISBL costs. Looking further into the ISBL expenses in Figure 4.5 and Figure 4.6, one can establish both the component inputs that most affect the ISBL and how each component changes with the various cultivation and extraction scenario inputs.

The majority of the open pond ISBL expenses are fairly evenly distributed (~10-15% of total ISBL) with the exception of the Open Ponds and DAF units in the high scenarios, which consist of ~18-28% and ~34-47% of the total for applicable cases. The DAF as well as the CHP unit prices were based on historical flow capacity and power output curves shown in Figure B1 and Figure B2, respectively. Note that the maximum flow capacity for the DAFs in the scenarios was estimated at 5500 gallons per minute and installed capital cost estimates are based on a linear extrapolation of reference [50]. The ponds (including cement and equipment installation), three-

[‡‡]Based on five year average of market prices for each product
[§§]Consists of propane and liquid petroleum gas (LPG) mix

phase centrifuges, and circulation pumps comprise the majority of the other open pond ISBL expenses. For the tubular and flat panel PBRs, the ISBL consists mainly of the costs associated with purchasing and installing the PBRs, which in some cases exceeded 95% of the total. Over 82% of the PBR equipment costs in some cases were due to the culture solar collector tubing, while the airlift pumps and water cooling and makeup piping hold a large percentage of the small remainder. The cost inputs ($/ft) for the solar collector tubing were priced based on 10 foot lengths, which could be decreased based on a larger volume sale. A 33% decrease in the solar collector tubing costs shows a relatively high sensitivity to overall production costs as seen in Figure 4.18, but does not decrease the overall expenses to the level of either the open raceway pond or flat panel PBRs. The HDPE clear panels for the flat panel PBRs were priced based on manufactured sheets normalized by the sheet area. The manufacturing of these sheets into a panel form was not taken into account and was assumed to be within the range of variability. Replacing these sheets with a double-layered LDPE clear film bags overall production costs by nearly 42%. In the flat panel wet extraction cases, higher biomass harvests yielding more meal coproduct to burn for electricity credits and lower farming electricity requirements (near that of open ponds) both decreased the total power costs. However, for all wet extraction cases, the cost and amount of potassium hydroxide made up 11-42% of the variable operating expenses. In all cases, nitrogen requirements in the form of urea, ammonia, or ammonium nitrate added to these material costs.

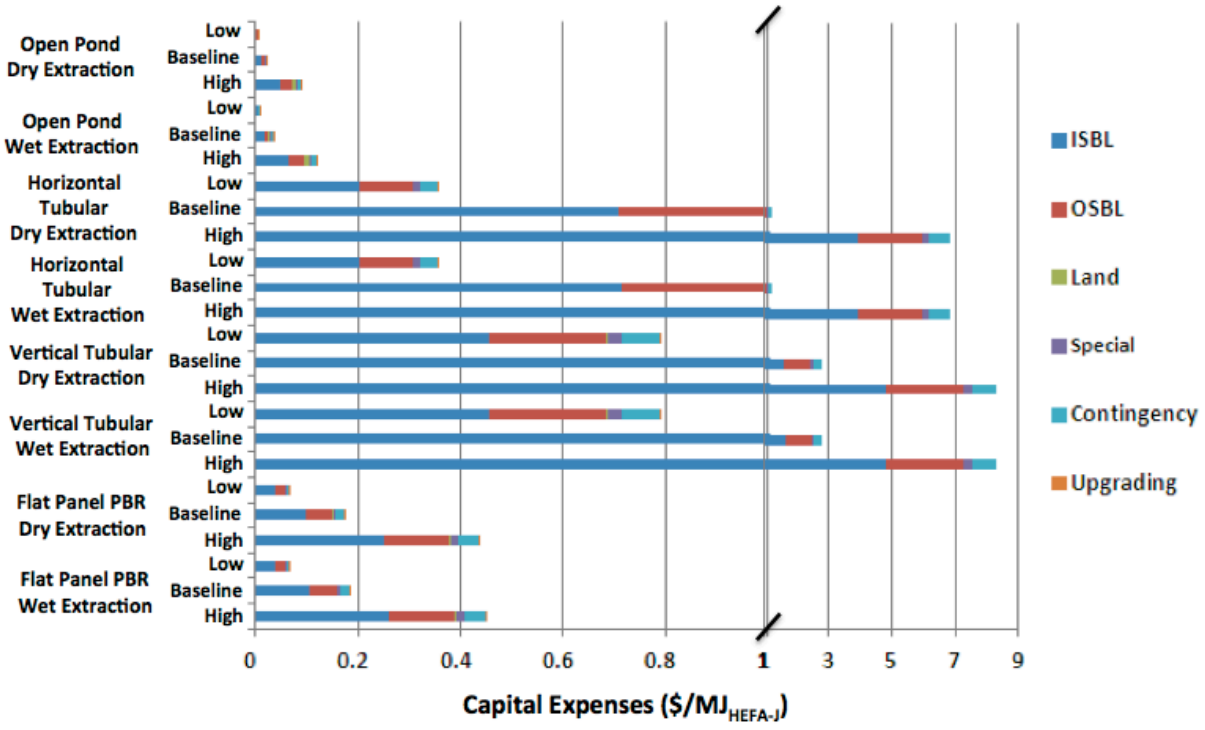


Figure 4.4: Total Capital Expense Scenarios

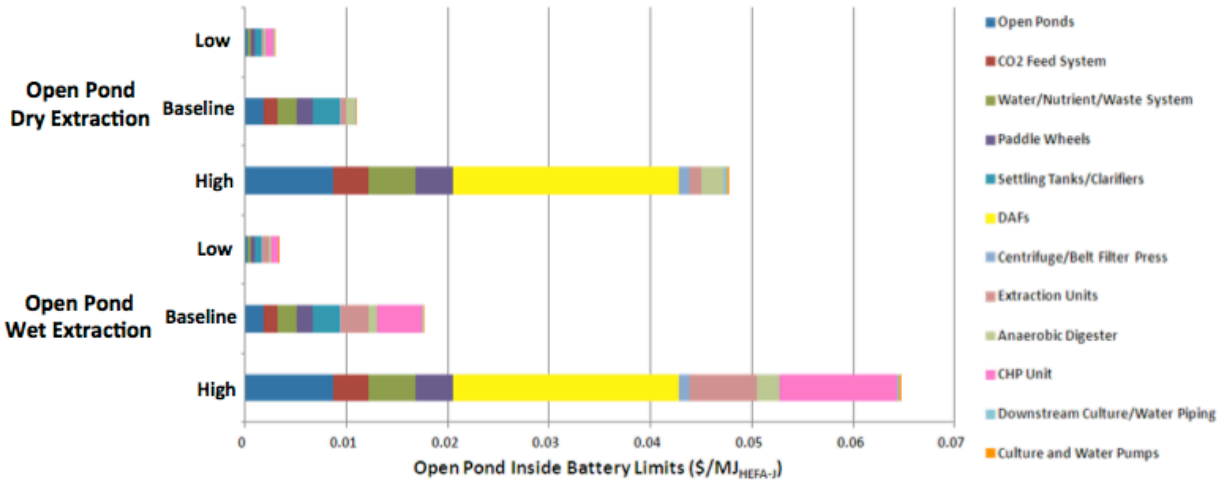


Figure 4.5: Open Pond Inside Battery Limits Capital Expense Scenarios

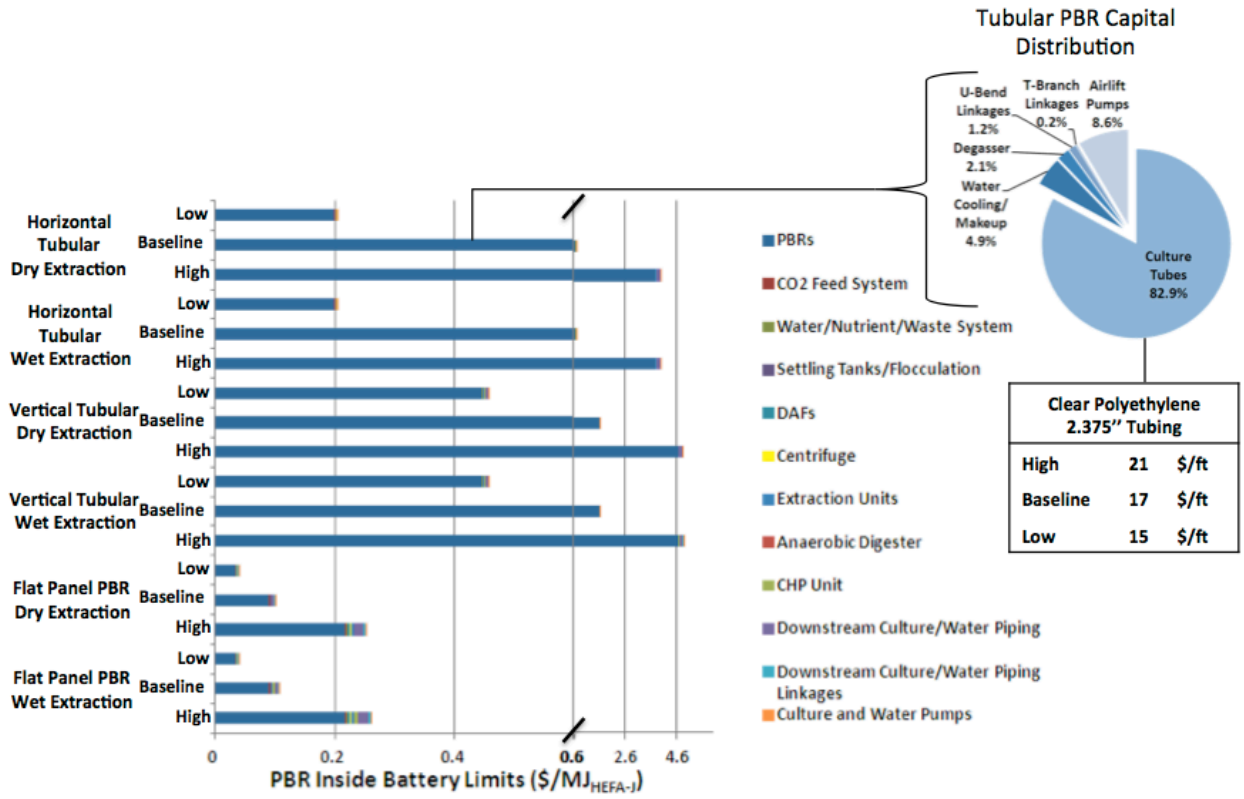


Figure 4.6: PBR Inside Battery Limits Capital Cost Scenarios

Like the other ISBL dependent capital expenses, the fixed operating expenses were subject to the total project investment, heuristics, and employee salaries shown in Table B3 and Table B4. Consequently, the fixed operating expenses follow a similar pattern as that of capital expenses, where the tubular PBRs expenses are exceedingly higher than the other two cultivation systems. All systems and scenarios experience a majority of the expense going towards maintenance

costs, with larger proportions for the PBRs. Like the capital expenses, the fixed operating costs were not greatly affected by the extraction technology sets.

The variable operating expenses were not impacted by capital cost heuristics and therefore, were relatively similar for all cultivation technologies. However, the choice in extraction technology greatly impacted the distribution of the expenses. In the open pond dry extraction cases, the majority of the costs were related to power consumption in the baseline and high cases linked to electricity needs for dry extraction and pure $CO_2$ MEA capture and distribution from the coal power plant. The tubular PBR cases increased these dry extraction power costs further with the power required for cultivation and harvesting. The flat panel scenarios yielded the lowest variable operating expenses due to the higher average weight content of the algae in the culture requiring less power in the dry extraction cases. Additionally, the baseline flat panel wet extraction power values were 87% lower than the baseline dry extraction cases due to the increased biomass productivity yielding more cake to offset electricity requirements and lower cultivation electricity requirements comparable to open ponds.

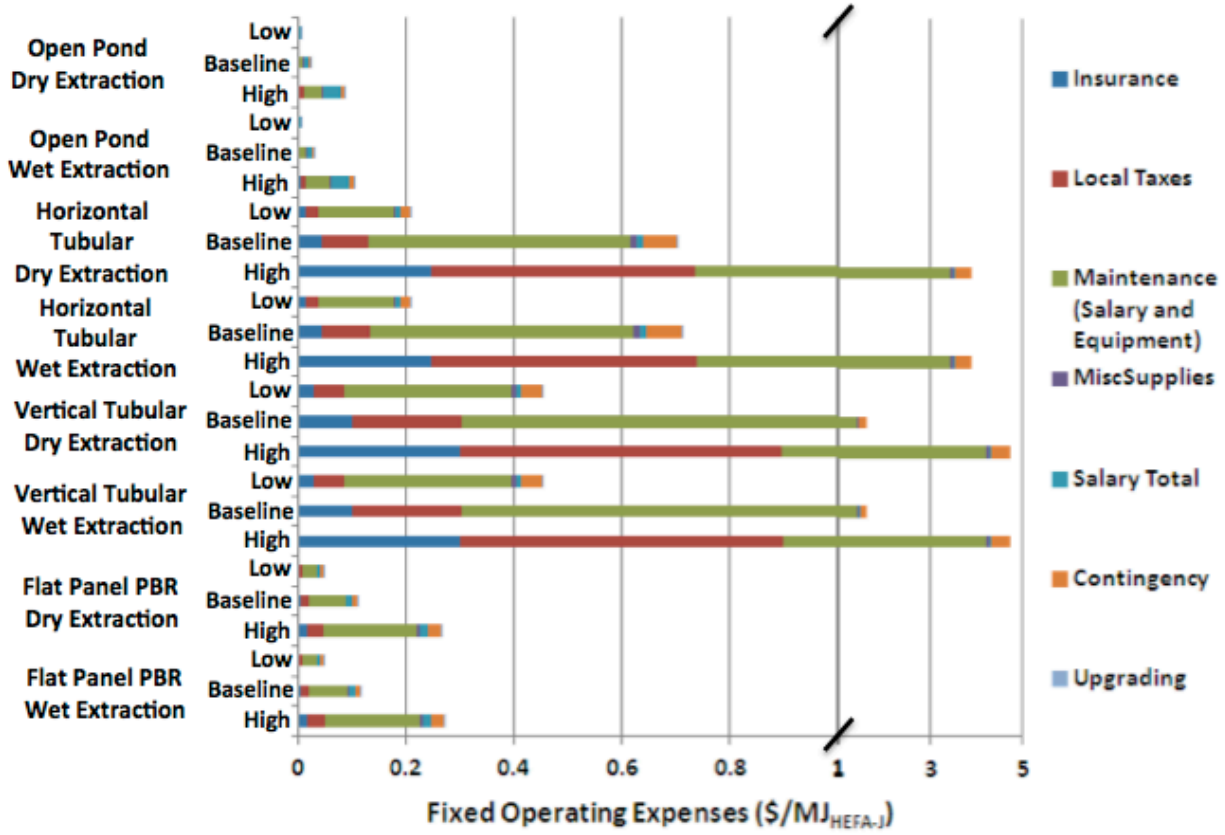


Figure 4.7: Open Pond and PBR Fixed Operating Expense Scenarios

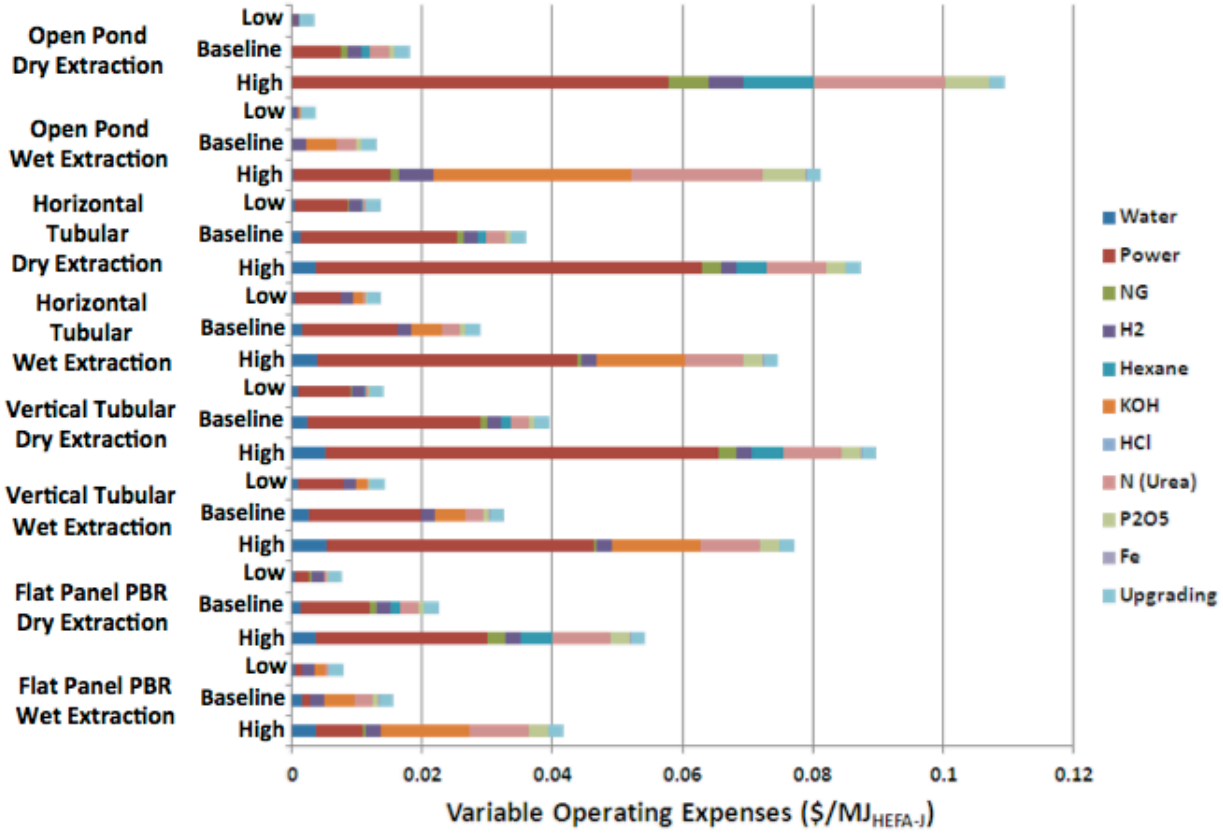


Figure 4.8: Open Pond and PBR Variable Operating Cost Scenarios

The overall production costs for each scenario are depicted in Figure 4.9. As expected, the upstream ISBL cost influences on TPI and ultimately, fixed operating costs, led to a high production costs both types of serpentine tubular PBRs. To get a sense of where these numbers reside on a $/gal$_{HEFA-J}$, one would multiply these values by a factor of ~126 as shown in the concluding chapter. The baseline pilot scale production costs for open ponds dry extraction, open pond wet extraction, flat panel dry extraction, and flat panel wet extraction were 8.3, 9.9, 42.3, and 43.5 $/gal$_{HEFA-J}$, respectively. For the majority of cases, the capital and fixed operating expenses dominated the overall production costs (note the broken step axes for the tubular PBRs). Sensitivity to the heuristic values for fixed operating costs were also undertaken in Figure 4.18 and provided insight as these values were originally applicable for a refinery type environment.

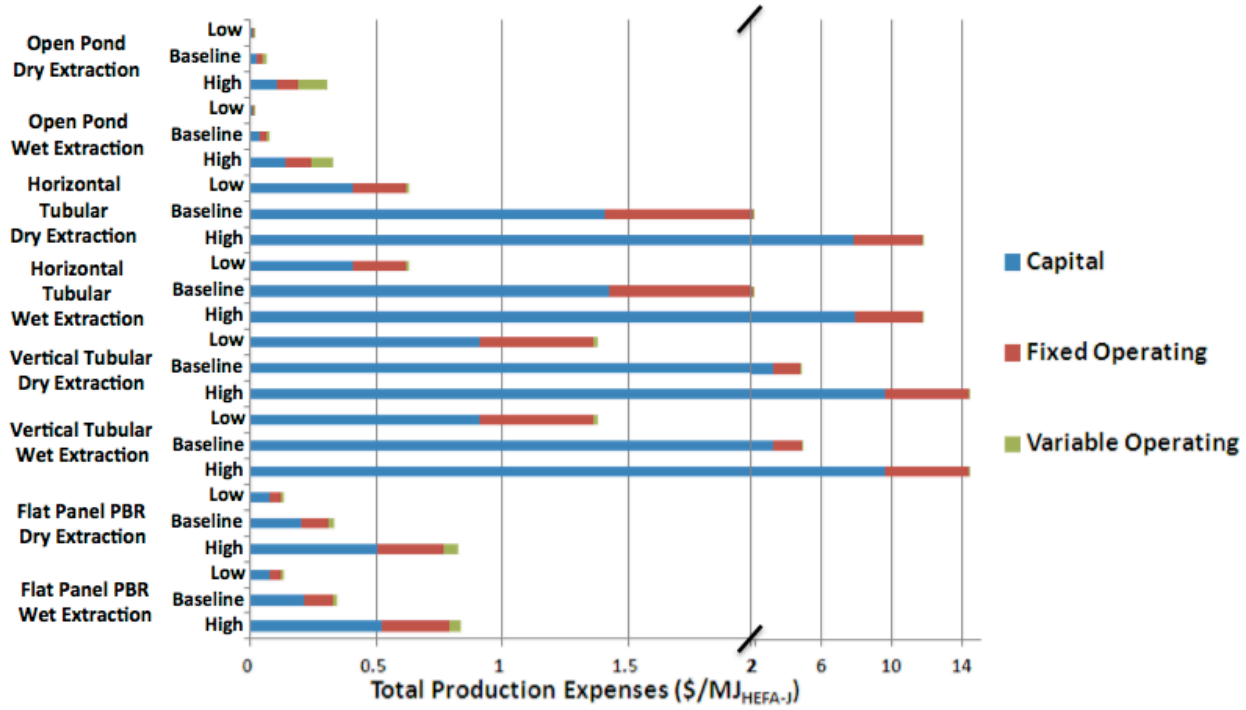


Figure 4.9: Total Algae to HEFA-J Production Expenses for a Maximum Distillate Product Slate

## 4.4 Specific Energy, Greenhouse Gas and Production Cost Comparisons

Comparisons between this thesis and other studies were made for specific energy inputs, lifecycle greenhouse gas emissions, and production costs. Specific energy comparisons were produced for each step in the algae production and upgrading facilities. These steps include energy consumed in cultivation, harvesting, drying, and extraction as well as energy produced from biogas electricity and the energy in the algal oil. Table 4.3 depicts these steps and the net specific energy for various studies, cultivation, extraction, and scenario types. Upgrading specific energies were estimated from Pearlson (2011), which includes heat and electric energy required for hydroprocessing and isomerization where noted [33]. The majority of the literature involved scenarios using open raceway pond cultivation technologies. For both wet and dry extraction open pond net specific energy, this study's low and high results bound the experimental results while the baseline results are fairly close to other study's baseline scenarios. For the horizontal tubular serpentine PBR case, the corrected Stephenson et al. (2010) net specific energy value compared similarly to the baseline wet extraction case. The thesis net specific energy was lower than the literature value because the PBRs were optimized for minimum cultivation specific energy and maximum areal productivity with a less energy intensive extraction technique. Other large variations between the literature and the thesis can be linked to the assumed oil mass fractions for a specific scenario and the harvesting technology electricity inputs (higher is usually DAFs or centrifuge while lower is usually settling ponds or clarifiers).

Lifecycle greenhouse gas emissions in this thesis have similar trends to specific energy when compared with other literature values. Table 4.4 illustrates the lifecycle breakdown of GHG emissions for various studies, cultivation, extraction, and scenario types. The major steps include displacement credits, recovery, feed transportation, processing, fuel transportation, combustion,

WTP $N_2O$, and WTP $CH_4$ GHG emissions. The majority of literature value comparisons are for open raceway pond cultivation. For open raceway pond wet and dry extraction techniques, the low and high total LCA GHG emission for this thesis bound the literature values and the baseline totals are similar to the other studies. The majority of variation from the literature stems from displacement credits associated with algal oil mass fraction and productivity scenario inputs. Other sources of large variation can be linked to emissions during recovery, which includes all consumption specific energy inputs and their variations.

Lastly, algal oil and HEFA-J production cost estimates for various studies were compared to this thesis. The literature techno-economic analyses considered were more numerous than the other two metrics and considered multiple cultivation types. Table 4.5 depicts production cost relative to facility land area and volume of TAG for algae production, harvesting, and oil extraction. Additionally, these previous steps and additional upgrading expenses were estimated in terms of the energy or volume of jet fuel using a market coproduct allocation for a maximum distillate fuel product slate outlined in section 4.3: Production Cost. The comparable cost estimates in the literature for the horizontal serpentine tubular PBRs were all lower for the same extraction and scenario types. This discrepancy is linked to the capital costs; including the assumed solar collector tube prices as well as more detailed downstream piping and pumping estimates and additional recycling, digestion, and electricity/heat production cost estimates not considered in other studies. The open pond thesis production cost estimates compared favorably to other literature values, where the mean and standard deviation of all values were 13.2±11.8 $\$/gal_{TAG}$ and 12.6±11.0 $\$/gal_{HEFA\text{-}J}$ produced for all extraction types (not including the relatively outlier values from [94]). Variation between studies and this thesis stem from multiple sources, including: algae productivity and composition inputs; harvesting, drying, and extraction technologies; fixed operating heuristics; and most importantly, financing assumptions and inputs including loan periods, facility lifetimes, discount rates, taxes, and contingency. Sun et al. (2011) tried to reduce this economic variability by normalizing the input assumptions for many studies and experiments and produced similar results for algal oil production with 10.9-13.3 $\$/gal_{TAG}$ [93].

Table 4.3: Lifecycle Specific Energy Comparisons for Various Studies and Scenarios

| Study | Cultivation Type | Extraction Type | Scenario Type | Consumed (MJ/$kg_{algae}$) | | | | Produced (MJ/$kg_{algae}$) | | Upgrading | Net (Produced - Consumed) |
|---|---|---|---|---|---|---|---|---|---|---|---|
| | | | | Algal Cultivation | Harvesting | Drying | Extraction | Biogas Electricity | Energy in Algal Oil | | |
| Thesis | Horizontal Tubular Serpentine PBR | Dry | Low | 11.0 | 0.3 | 13.4 | 1.1 | 2.0 | 23.5 | 2.2 | -0.4 |
| Thesis | Horizontal Tubular Serpentine PBR | Dry | Baseline | 10.0 | 0.5 | 16.6 | 1.1 | -0.3 | 9.8 | 0.9 | -18.6 |
| Thesis | Horizontal Tubular Serpentine PBR | Dry | High | 19.3 | 3.4 | 15.3 | 1.1 | -0.4 | 5.9 | 0.9 | -33.6 |
| Thesis | Horizontal Tubular Serpentine PBR | Wet | Low | 11.0 | 0.3 | 0.0 | 0.2 | 2.0 | 23.5 | 2.2 | 13.9 |
| [53][***] | Horizontal Tubular Serpentine PBR | Wet | Baseline | 23.4 | 0.2 | 0.0 | 1.2 | 5.9 | 24.2 | 0.9 | 5.1 |
| Thesis | Horizontal Tubular Serpentine PBR | Wet | Baseline | 10.0 | 0.5 | 0.0 | 0.1 | 2.9 | 9.8 | 0.9 | 2.1 |
| Thesis | Horizontal Tubular Serpentine PBR | Wet | High | 15.9 | 3.4 | 0.0 | 0.0 | 3.3 | 5.9 | 0.9 | -10.2 |
| Thesis | Open Raceway Pond | Dry | Low | 0.8 | 0.4 | 13.4 | 1.1 | 2.0 | 23.4 | 2.2 | 9.8 |
| [4][†††] | Open Raceway Pond | Dry | Low | 0.7 | 0.2 | 16.3 | 1.2 | 0.0 | 21.4 | 1.7 | 3.0 |
| [51][‡‡‡] | Open Raceway Pond | Dry | Baseline | 0.6 | 0.6 | 15.2 | 1.5 | 0.0 | 17.5 | 0.9 | -0.4 |
| [4][***] | Open Raceway Pond | Dry | Baseline | 0.7 | 0.2 | 9.4 | 1.2 | 0.0 | 8.9 | 1.1 | -2.6 |
| Thesis | Open Raceway Pond | Dry | Baseline | 1.3 | 0.6 | 16.5 | 1.1 | -0.3 | 9.7 | 0.9 | -10.1 |
| [4][***] | Open Raceway Pond | Dry | High | 15.0 | 0.2 | 7.7 | 1.2 | 0.0 | 5.4 | 0.8 | -18.7 |
| Thesis | Open Raceway Pond | Dry | High | 9.6 | 3.6 | 15.3 | 1.1 | -0.4 | 5.8 | 0.9 | -24.1 |
| Thesis | Open Raceway Pond | Wet | Low | 0.8 | 0.4 | 0.0 | 0.2 | 2.0 | 23.4 | 2.2 | 24.0 |
| [53][§§§] | Open Raceway Pond | Wet | Baseline | 2.6 | 0.9 | 0.0 | 1.3 | 5.7 | 14.2 | 0.9 | 15.1 |
| [51][‡‡‡] | Open Raceway Pond | Wet | Baseline | 0.6 | 0.6 | 0.0 | 3.7 | 0.0 | 17.5 | 0.9 | 12.6 |
| Thesis | Open Raceway Pond | Wet | Baseline | 1.3 | 0.6 | 0.0 | 0.1 | 2.9 | 9.7 | 0.9 | 10.6 |
| [95] | Open Raceway Pond | Wet | Low-A | 1.4 | 0.7 | 0.0 | 2.7 | 2.0 | 11.1 | 1.3 | 8.3 |
| [95] | Open Raceway Pond | Wet | Low-B | 1.3 | 0.7 | 0.0 | 2.0 | 0.7 | 11.1 | 1.8 | 7.9 |
| [95] | Open Raceway Pond | Wet | Baseline | 1.4 | 0.7 | 0.0 | 2.1 | 0.8 | 8.0 | 1.3 | 4.5 |
| Thesis | Open Raceway Pond | Wet | High | 6.3 | 3.6 | 0.0 | 0.0 | 3.3 | 5.8 | 0.9 | -0.8 |
| Thesis | Vertical Flat Panel PBR | Dry | Low | 3.2 | 0.2 | 13.4 | 1.1 | 2.0 | 23.5 | 2.2 | 7.6 |
| Thesis | Vertical Flat Panel PBR | Dry | Baseline | 3.1 | 0.4 | 16.6 | 1.1 | -0.3 | 9.8 | 0.9 | -11.8 |
| Thesis | Vertical Flat Panel PBR | Dry | High | 11.2 | 2.2 | 15.3 | 1.1 | -0.4 | 5.9 | 0.9 | -24.3 |
| Thesis | Vertical Flat Panel PBR | Wet | Low | 3.2 | 0.2 | 0.0 | 0.2 | 2.0 | 23.5 | 2.2 | 21.9 |
| Thesis | Vertical Flat Panel PBR | Wet | Baseline | 3.1 | 0.4 | 0.0 | 0.1 | 2.9 | 9.8 | 0.9 | 9.0 |
| Thesis | Vertical Flat Panel PBR | Wet | High | 7.8 | 2.2 | 0.0 | 0.0 | 3.3 | 5.9 | 0.9 | -0.9 |
| Thesis | Vertical Tubular Serpentine PBR | Dry | Low | 11.1 | 0.4 | 13.4 | 1.1 | 2.0 | 23.5 | 2.2 | -0.5 |
| Thesis | Vertical Tubular Serpentine PBR | Dry | Baseline | 11.1 | 0.8 | 16.6 | 1.1 | -0.3 | 9.8 | 0.9 | -20.0 |
| Thesis | Vertical Tubular Serpentine PBR | Dry | High | 19.2 | 3.8 | 15.3 | 1.1 | -0.4 | 5.9 | 0.9 | -33.9 |
| Thesis | Vertical Tubular Serpentine PBR | Wet | Low | 11.1 | 0.4 | 0.0 | 0.2 | 2.0 | 23.5 | 2.2 | 13.7 |
| Thesis | Vertical Tubular Serpentine PBR | Wet | Baseline | 11.1 | 0.8 | 0.0 | 0.1 | 2.9 | 9.8 | 0.9 | 0.8 |
| Thesis | Vertical Tubular Serpentine PBR | Wet | High | 15.8 | 3.8 | 0.0 | 0.0 | 3.3 | 5.9 | 0.9 | -10.4 |

[***] Original source cultivation value of 34.8 MJ/$kg_{algae}$ included an error in the energy balance that increased the energy required by a factor of 1.49; Non-optimized baseline horizontal serpentine tubular PBR model algae cultivation specific energy was similarly high: ~23 MJ/$kg_{algae}$; Baseline optimized horizontal PBR cultivation specific energy was ~10 MJ/$kg_{algae}$

[†††] Modified for same algal composition inputs as this thesis; Higher digester solids destruction efficiency (70% vs. 60%); Upgrading does not include isomerization steps; No recycling/piping losses

[‡‡‡] No anaerobic digestion; for dry extraction, similar to dry soybean extraction (90 wt.% solids); for wet extraction, assumes heat consumption and hexane loses proportional to total volume of processed material; thesis baseline upgrading specific energy used

[§§§] Nitrogen-deprivation methods; homogenization wet extraction; thesis baseline upgrading specific energy used

Table 4.4: Lifecycle Greenhouse Gas Emission Comparisons for Various Studies and Scenarios

| Study | Cultivation Type | Extraction Type | Scenario Type | Allocation Type | Lifecycle Step ($g\text{-}CO_2e/MJ_{HEFA\text{-}J}$) | | | | | | | | | Normalized to Baseline Conv. Crude to Jet Fuel ($87.5\ g\text{-}CO_2e/MJ_{HEFA\text{-}J}$) [4] |
|---|---|---|---|---|---|---|---|---|---|---|---|---|---|---|
| | | | | | Displacement Credits | Recovery | Feed Transportation | Processing | Fuel Transportation | Combustion | WTP N2O | WTP CH4 | Total | |
| Thesis | Horizontal Serpentine Tubular PBR | Dry | Low | Disp. & Engy. | -109 | 162 | 0.5 | 9.4 | 0.6 | 71.8 | 1.8 | 8.1 | 145 | 1.66 |
| Thesis | Horizontal Serpentine Tubular PBR | Dry | Baseline | Disp. & Engy. | -133 | 409 | 0.5 | 9.9 | 0.6 | 72.1 | 13.9 | 23.8 | 397 | 4.54 |
| Thesis | Horizontal Serpentine Tubular PBR | Dry | High | Disp. & Engy. | -193 | 880 | 0.5 | 10.1 | 0.6 | 73.1 | 180 | 59.0 | 1010 | 11.6 |
| Thesis | Horizontal Serpentine Tubular PBR | Wet | Low | Disp. & Engy. | -109 | 118 | 0.5 | 9.4 | 0.6 | 71.8 | 1.5 | 6.8 | 99.6 | 1.14 |
| Thesis | Horizontal Serpentine Tubular PBR | Wet | Baseline | Disp. & Engy. | -194 | 283 | 0.5 | 9.9 | 0.6 | 72.1 | 13.1 | 16.4 | 202 | 2.31 |
| Thesis | Horizontal Serpentine Tubular PBR | Wet | High | Disp. & Engy. | -309 | 638 | 0.5 | 10.1 | 0.6 | 73.1 | 179 | 45.2 | 637 | 7.28 |
| [53][****] | Horizontal Serpentine Tubular PBR | Wet | Baseline | Disp. & Mkt. | -484 | 2423 | 0.0 | 9.9 | 0.0 | 72.1 | - | - | 2020 | 23.1 |
| Thesis | Open Raceway Pond | Dry | Low | Disp. & Engy. | -109 | 77 | 0.5 | 9.4 | 0.6 | 71.8 | 1.4 | 2.4 | 54 | 0.62 |
| [4][††††] | Open Raceway Pond | Dry | Low | Disp. & Engy. | -74 | 52 | 0.3 | 7.1 | 0.6 | 72.1 | 0.2 | 4.2 | 63 | 0.72 |
| [4][††††] | Open Raceway Pond | Dry | Baseline | Disp. & Engy. | -70 | 75 | 0.3 | 10.3 | 0.6 | 72.1 | 1.3 | 6.0 | 95 | 1.09 |
| Thesis | Open Raceway Pond | Dry | Baseline | Disp. & Engy. | -133 | 251 | 0.5 | 9.9 | 0.6 | 72.1 | 13.3 | 12.9 | 227 | 2.59 |
| [4][††††] | Open Raceway Pond | Dry | High | Disp. & Engy. | -69 | 298 | 3.2 | 13.2 | 0.6 | 72.1 | 15 | 53.7 | 387 | 4.43 |
| Thesis | Open Raceway Pond | Dry | High | Disp. & Engy. | -196 | 595 | 0.5 | 10.1 | 0.6 | 73.1 | 180 | 39.1 | 703 | 8.03 |
| Thesis | Open Raceway Pond | Wet | Low | Disp. & Engy. | -109 | 33 | 0.5 | 9.4 | 0.6 | 71.8 | 1.2 | 1.1 | 8.9 | 0.10 |
| [53][****] | Open Raceway Pond | Wet | Baseline | Disp. & Mkt. | -194 | 125 | 0.5 | 9.9 | 0.6 | 72.1 | 12.5 | 5.5 | 31 | 0.36 |
| [95][††††] | Open Raceway Pond | Wet | Low-B | Disp. & Engy. | -484 | 437 | 0.0 | 9.9 | 0.0 | 72.1 | - | - | 35.3 | 0.40 |
| [95][††††] | Open Raceway Pond | Wet | Baseline | Disp. & Engy. | -117 | 71 | 0.6 | 13.8 | 0.6 | 72.1 | 0.0 | 0.2 | 41 | 0.46 |
| [95][††††] | Open Raceway Pond | Wet | Low-A | Disp. & Engy. | -145 | 103 | 0.6 | 13.8 | 0.6 | 72.1 | 0 | 0.7 | 46 | 0.53 |
| Thesis | Open Raceway Pond | Wet | Baseline | Disp. & Engy. | -114 | 73 | 0.6 | 13.8 | 0.6 | 72.1 | 0.0 | 0.2 | 47 | 0.54 |
| Thesis | Open Raceway Pond | Wet | High | Disp. & Engy. | -311 | 352 | 0.5 | 10.1 | 0.6 | 73.1 | 178 | 25.3 | 329 | 3.76 |
| Thesis | Vertical Flat Panel PBR | Dry | Low | Disp. & Engy. | -109 | 95 | 0.5 | 9.4 | 0.6 | 71.8 | 1.5 | 4.2 | 74.7 | 0.85 |
| Thesis | Vertical Flat Panel PBR | Dry | Baseline | Disp. & Engy. | -133 | 270 | 0.5 | 9.9 | 0.6 | 72.1 | 13 | 15.0 | 249 | 2.84 |
| Thesis | Vertical Flat Panel PBR | Dry | High | Disp. & Engy. | -194 | 568 | 0.5 | 10.1 | 0.6 | 73.1 | 179 | 39.2 | 676 | 7.73 |
| Thesis | Vertical Flat Panel PBR | Wet | Low | Disp. & Engy. | -109 | 51 | 0.5 | 9.4 | 0.6 | 71.8 | 1.3 | 2.9 | 29 | 0.33 |
| Thesis | Vertical Flat Panel PBR | Wet | Baseline | Disp. & Engy. | -194 | 144 | 0.5 | 9.9 | 0.6 | 72.1 | 13 | 7.6 | 54 | 0.61 |
| Thesis | Vertical Flat Panel PBR | Wet | High | Disp. & Engy. | -309 | 325 | 0.5 | 10.1 | 0.6 | 73.1 | 178 | 25.4 | 303 | 3.46 |
| Thesis | Vertical Serpentine Tubular PBR | Dry | Low | Disp. & Engy. | -109 | 163 | 0.5 | 9.4 | 0.6 | 71.8 | 2 | 8.2 | 147 | 1.67 |
| Thesis | Vertical Serpentine Tubular PBR | Dry | Baseline | Disp. & Engy. | -133 | 436 | 0.5 | 9.9 | 0.6 | 72.1 | 14.0 | 25.5 | 426 | 4.87 |
| Thesis | Vertical Serpentine Tubular PBR | Dry | High | Disp. & Engy. | -194 | 889 | 0.5 | 10.1 | 0.6 | 73.1 | 180 | 59.6 | 1020 | 11.7 |
| Thesis | Vertical Serpentine Tubular PBR | Wet | Low | Disp. & Engy. | -109 | 119 | 0.5 | 9.4 | 0.6 | 71.8 | 1.5 | 6.9 | 101 | 1.15 |
| Thesis | Vertical Serpentine Tubular PBR | Wet | Baseline | Disp. & Engy. | -194 | 310 | 0.5 | 9.9 | 0.6 | 72.1 | 13.2 | 18.1 | 231 | 2.64 |
| Thesis | Vertical Serpentine Tubular PBR | Wet | High | Disp. & Engy. | -309 | 646 | 0.5 | 10.1 | 0.6 | 73.1 | 179 | 45.8 | 646 | 7.38 |

[****] LCA metric for Stephenson et al. (2010) originally in units of $g\text{-}CO_2e/mt_{biodiesel}$ and changed to $g\text{-}CO_2e/MJ_{HEFA\text{-}J}$ using biodiesel and baseline HEFA-J conversion and energy inputs [33,53]; $N_2O$ and $CH_4$ WTP emissions are combined in the other LCA steps

[††††] Combustion results taken from low, baseline, and high thesis results for the various scenario SPK blends outlined in Table 2.16; Modified for same algal inputs as this thesis

Table 4.5: Production Cost Comparisons for Various Studies and Scenarios

| Study | Cultivation Type | Extraction Type | Scenario Type | Production, Harvesting, and Extraction | | | | | Production, Harvesting, Extraction, and Upgrading to Jet | | | | |
|---|---|---|---|---|---|---|---|---|---|---|---|---|---|
| | | | | M$/ha | $/ha/yr | | | $/gal$_{TAG}$ | $/MJ$_{HEFA-J}$[‡‡‡‡] | | | | $/gal$_{HEFA-J}$ |
| | | | | Capital | Fixed Operating | Variable Operating | Total | | Capital | Fixed Operating | Variable Operating | Total | |
| Thesis | Flat Bag PBR | Dry | Low | 2.00 | 1.05E+05 | 1.98E+04 | 6.80 | | 0.02 | 0.03 | 0.01 | 0.05 | 6.86 |
| Thesis | Flat Bag PBR | Dry | Baseline | 1.68 | 7.89E+04 | 2.32E+04 | 17.7 | | 0.04 | 0.07 | 0.02 | 0.14 | 17.1 |
| Thesis | Flat Bag PBR | Dry | High | 1.32 | 5.87E+04 | 2.24E+04 | 34.1 | | 0.07 | 0.13 | 0.05 | 0.26 | 32.5 |
| [96] | Flat Bag PBR | Dry | Low | 1.04 | 2.43E+05 | -6.35E+05 | 71.4 | | 0.94 | 0.16 | -0.56 | 0.53 | 67.1 |
| [96] | Flat Bag PBR | Dry | Baseline | 1.03 | 1.65E+05 | -3.33E+05 | 104 | | 0.92 | 0.15 | -0.29 | 0.77 | 97.6 |
| [96] | Flat Bag PBR | Dry | High | 1.05 | 1.76E+05 | -2.18E+05 | 110 | | 0.80 | 0.19 | -0.16 | 0.82 | 103 |
| Thesis | Flat Bag PBR | Wet | Low | 2.00 | 1.05E+05 | 2.20E+04 | 6.88 | | 0.02 | 0.03 | 0.01 | 0.05 | 6.94 |
| Thesis | Flat Bag PBR | Wet | Baseline | 1.84 | 8.52E+04 | 1.62E+04 | 18.1 | | 0.04 | 0.08 | 0.02 | 0.14 | 17.5 |
| Thesis | Flat Bag PBR | Wet | High | 1.41 | 6.19E+04 | 1.69E+04 | 34.1 | | 0.08 | 0.14 | 0.04 | 0.26 | 32.4 |
| Sandia [93] | Horizontal Serpentine Tubular PBR | - | Baseline | - | - | - | 33 | | - | - | - | 0.24 | 30.9 |
| [97] | Horizontal Tubular PBR | - | Low | - | - | - | 41 | | - | - | - | 0.30 | 38 |
| [97] | Double Tubular Bioreactor | - | High | - | - | - | 43 | | - | - | - | 0.32 | 40 |
| Thesis | Horizontal Serpentine Tubular PBR | Dry | Low | 6.14 | 2.49E+05 | 1.50E+04 | 85 | | 0.41 | 0.21 | 0.01 | 0.63 | 79.6 |
| Thesis | Horizontal Serpentine Tubular PBR | Dry | Baseline | 7.89 | 3.12E+05 | 1.52E+04 | 291 | | 1.40 | 0.70 | 0.04 | 2.14 | 271 |
| Thesis | Horizontal Serpentine Tubular PBR | Dry | High | 18.8 | 7.34E+05 | 1.55E+04 | 1602 | | 7.84 | 3.88 | 0.09 | 11.8 | 1492 |
| Thesis | Horizontal Serpentine Tubular PBR | Wet | Low | 6.14 | 2.49E+05 | 1.58E+04 | 84.9 | | 0.41 | 0.21 | 0.01 | 0.63 | 79.6 |
| Thesis | Horizontal Serpentine Tubular PBR | Wet | Baseline | 7.97 | 3.16E+05 | 1.24E+04 | 293 | | 1.42 | 0.71 | 0.03 | 2.16 | 273 |
| Thesis | Horizontal Serpentine Tubular PBR | Wet | High | 18.8 | 7.35E+05 | 1.32E+04 | 1600 | | 7.85 | 3.88 | 0.07 | 11.8 | 1490 |
| Solix - PII [93] | Hybrid | - | Low-B | - | - | - | 0.73 | | - | - | - | 0.01 | 0.69 |
| Solix - PI [93] | Hybrid | - | Low-A | - | - | - | 2.56 | | - | - | - | 0.02 | 2.39 |
| General Atomics [93] | Hybrid | - | Low | - | - | - | 20.0 | | - | - | - | 0.15 | 18.6 |
| Solix [93] | Hybrid | - | High | - | - | - | 31.9 | | - | - | - | 0.23 | 29.7 |
| General Atomics [93] | Hybrid | - | High | - | - | - | 32.8 | | - | - | - | 0.24 | 30.5 |
| [98] | Open Raceway Pond | - | Low | - | - | - | 1.1 | | - | - | - | 0.01 | 1.0 |
| [98] | Open Raceway Pond | - | High | - | - | - | 1.6 | | - | - | - | 0.01 | 1.5 |
| [50] | Open Raceway Pond | Dry | Low | 0.13 | 3.03E+03 | 5.73E+03 | 1.67 | | 0.01 | 0.00 | 0.003 | 0.02 | 1.90 |
| Thesis | Open Raceway Pond | Dry | Low | 0.28 | 1.64E+04 | 3.41E+03 | 1.74 | | 0.01 | 0.01 | 0.00 | 0.02 | 2.15 |
| NREL [93] | Open Raceway Pond | - | Low | - | - | - | 2.4 | | - | - | - | 0.02 | 2.2 |
| [50] | Open Raceway Pond | Dry | Baseline | 0.15 | 3.36E+03 | 8.75E+03 | 2.4 | | 0.02 | 0.001 | 0.003 | 0.02 | 2.59 |
| NREL [93] | Open Raceway Pond | - | Baseline | - | - | - | 3.5 | | - | - | - | 0.03 | 3.2 |
| [99] | Open Raceway Pond | Dry | Low | 0.09 | 1.56E+04 | 4.77E+03 | 3.22 | | 0.02 | 0.003 | 0.004 | 0.03 | 3.53 |
| [99] | Open Raceway Pond | Dry | Baseline | 0.09 | 1.79E+04 | 1.21E+04 | 3.31 | | 0.02 | 0.00 | 0.00 | 0.03 | 3.66 |
| [99] | Open Raceway Pond | Dry | High | 0.09 | 2.03E+04 | 1.95E+04 | 3.33 | | 0.02 | 0.00 | 0.00 | 0.03 | 3.79 |

[‡‡‡‡] All initial $/gal$_{TAG}$ values were converted to $/MJ$_{HEFA-J}$ by adding the low/baseline/high upgrading cost estimates from [33]. Total costs were then converted for HEFA-J using the maximum distillate jet mass fraction and a market coproduct allocation in Table 4.1 as well as a LHV of 44.1 MJ/kg [6].

| | | | | | | | | | | | | | |
|---|---|---|---|---|---|---|---|---|---|---|---|---|---|
| [50] | Open Raceway Pond | Dry | High | 0.16 | 3.88E+03 | 1.13E+04 | 4.8 | 0.03 | 0.002 | 0.004 | 0.04 | 4.6 |
| Thesis | Open Raceway Pond | Dry | Baseline | 0.24 | 1.80E+04 | 1.29E+04 | 8.2 | 0.02 | 0.02 | 0.02 | 0.07 | 8.3 |
| NMSU [93] | Open Raceway Pond | - | Low | - | - | - | 9.52 | - | - | - | 0.07 | 8.9 |
| NREL [93] | Open Raceway Pond | - | High | - | - | - | 10.6 | - | - | - | 0.08 | 9.9 |
| NMSU [93] | Open Raceway Pond | - | Low | - | - | - | 14 | - | - | - | 0.10 | 13 |
| Bayer AG [93] | Open Raceway Pond | - | Baseline | - | - | - | 14.3 | - | - | - | 0.11 | 13.3 |
| Sandia [93] | Open Raceway Pond | - | Baseline | - | - | - | 16 | - | - | - | 0.12 | 15 |
| Cal. Poly. [93] | Open Raceway Pond | - | Baseline | - | - | - | 16.7 | - | - | - | 0.12 | 15.5 |
| [96] | Open Raceway Pond | Dry | Low | 0.05 | 3.29E+04 | 3.99E+03 | 22.3 | 0.08 | 0.05 | 0.037 | 0.17 | 21.3 |
| [96] | Open Raceway Pond | Dry | Baseline | 0.06 | 4.12E+04 | 1.77E+04 | 22.9 | 0.08 | 0.062 | 0.028 | 0.17 | 22.0 |
| Seambiotic [93] | Open Raceway Pond | - | Baseline | - | - | - | 24.9 | - | - | - | 0.18 | 23.2 |
| NMSU [93] | Open Raceway Pond | - | High | - | - | - | 25 | - | - | - | 0.18 | 23 |
| [96] | Open Raceway Pond | Dry | High | 0.06 | 1.24E+05 | 2.37E+04 | 32.2 | 0.08 | 0.16 | 0.01 | 0.24 | 30.7 |
| [92] | Open Raceway Pond | Dry | Baseline | 0.17 | 3.06E+04 | 1.42E+04 | 35.8 | 0.21 | 0.04 | 0.02 | 0.27 | 33.9 |
| NMSU [93] | Open Raceway Pond | - | High | - | - | - | 39 | - | - | - | 0.28 | 36.0 |
| Thesis | Open Raceway Pond | Dry | High | 0.33 | 2.43E+04 | 3.17E+04 | 40.2 | 0.10 | 0.09 | 0.11 | 0.30 | 38.1 |
| [94] | Open Raceway Pond | Dry | Low | 0.36 | 1.05E+05 | 8.10E+04 | 160 | 0.78 | 0.23 | 0.173 | 1.18 | 149 |
| [94] | Open Raceway Pond | Dry | Baseline | 0.46 | 1.05E+05 | 8.10E+04 | 188 | 0.99 | 0.23 | 0.17 | 1.39 | 176 |
| [94] | Open Raceway Pond | Dry | High | 0.56 | 1.05E+05 | 8.10E+04 | 217 | 1.20 | 0.23 | 0.17 | 1.60 | 202 |
| Thesis | Open Raceway Pond | Wet | Low | 0.31 | 1.78E+04 | 3.86E+03 | 2.0 | 0.01 | 0.01 | 0.00 | 0.02 | 2.3 |
| Thesis | Open Raceway Pond | Wet | Baseline | 0.36 | 2.27E+04 | 8.41E+03 | 10.0 | 0.04 | 0.03 | 0.01 | 0.08 | 9.9 |
| Thesis | Open Raceway Pond | Wet | High | 0.47 | 2.96E+04 | 2.32E+04 | 43.2 | 0.14 | 0.10 | 0.08 | 0.32 | 40.9 |
| Thesis | Vertical Flat Panel PBR | Dry | Low | 3.80 | 1.75E+05 | 1.98E+04 | 17.4 | 0.078 | 0.047 | 0.008 | 0.13 | 16.7 |
| Thesis | Vertical Flat Panel PBR | Dry | Baseline | 3.48 | 1.49E+05 | 2.32E+04 | 44.9 | 0.201 | 0.11 | 0.02 | 0.34 | 42.3 |
| Thesis | Vertical Flat Panel PBR | Dry | High | 3.89 | 1.59E+05 | 2.24E+04 | 111 | 0.50 | 0.27 | 0.05 | 0.82 | 104 |
| Thesis | Vertical Flat Panel PBR | Wet | Low | 3.80 | 1.75E+05 | 2.20E+04 | 17.4 | 0.08 | 0.05 | 0.008 | 0.13 | 16.7 |
| Thesis | Vertical Flat Panel PBR | Wet | Baseline | 3.65 | 1.55E+05 | 1.62E+04 | 46.2 | 0.21 | 0.12 | 0.02 | 0.34 | 43.6 |
| Thesis | Vertical Flat Panel PBR | Wet | High | 3.97 | 1.62E+05 | 1.69E+04 | 112 | 0.52 | 0.27 | 0.04 | 0.83 | 105 |
| [54][§§§§] | Vertical Serpentine Tubular PBR | N/A | Baseline | 2.5 | - | - | 128 | - | - | - | - | 120 |
| Thesis | Vertical Serpentine Tubular PBR | Dry | Low | 14.8 | 5.87E+05 | 1.56E+04 | 186 | 0.91 | 0.455 | 0.014 | 1.38 | 174 |
| Thesis | Vertical Serpentine Tubular PBR | Dry | Baseline | 19.0 | 7.44E+05 | 1.79E+04 | 660 | 3.22 | 1.60 | 0.04 | 4.86 | 615 |
| Thesis | Vertical Serpentine Tubular PBR | Dry | High | 29.6 | 1.16E+06 | 2.06E+04 | 1951 | 9.56 | 4.73 | 0.09 | 14.4 | 1820 |
| Thesis | Vertical Serpentine Tubular PBR | Wet | Low | 14.8 | 5.87E+05 | 1.65E+04 | 186 | 0.91 | 0.45 | 0.01 | 1.38 | 174 |
| Thesis | Vertical Serpentine Tubular PBR | Wet | Baseline | 19.1 | 7.48E+05 | 1.50E+04 | 662 | 3.24 | 1.61 | 0.03 | 4.88 | 617 |
| Thesis | Vertical Serpentine Tubular PBR | Wet | High | 29.7 | 1.16E+06 | 1.77E+04 | 1950 | 9.58 | 4.73 | 0.08 | 14.4 | 1820 |

[§§§§]Does not include extraction equipment/operating costs; assumes 25% lipid dry weight fraction and maximum distillate product slate

## 4.5 Freshwater Consumption

As previously stated, water consumption was defined in this study to be any freshwater taken from a source and not directly placed back to the original. This definition includes water quality, i.e., even freshwater withdrawn from a source and placed back to that source without the same water quality (no pretreatment) would be considered consumption. Therefore, any previously freshwater makeup in this study that eventually exits the facility as blowdown is counted as consumptive even when brackish.

Onsite and offsite freshwater consumption was estimated for both freshwater and brackish makeup water in every cultivation and extraction scenario. Onsite freshwater consumption inputs and assumptions are outlined in Table A1 and consist of all water used on the cultivation, recovery and extraction facility as well as the total direct water consumption estimates from upgrading facility. The direct upgrading water consumption includes boiler feed water (BFW) for onsite steam generation and cooling water [33]. Offsite water consumption inputs and assumptions are depicted in Table A2 and Table A3. Offsite nutrient and material manufacture lifecycle energy use and direct water consumption were derived from references [41] and [76]. These inputs include freshwater consumed at offsite facilities for electricity, natural gas, hydrogen, and refined product generation for use onsite and offsite direct material and nutrient manufacture as well as their associated energy and material input freshwater consumption. In applicable scenarios, water consumption for offsite pure $CO_2$ MEA capture was included.

Figure 4.10 and Figure 4.11 depict estimates for onsite and offsite freshwater consumption for a brackish makeup culture. For onsite, the majority of the freshwater consumed for open pond scenarios were for belt drying and BFW steam generation in dry extraction cases and extraction and recovery and biogas electricity generation in wet extraction cases. The biogas electricity generation was assumed to resemble lifecycle water consumption estimates for a Natural Gas Combined Cycle (NGCC) powerplant in units of $L_{water}$/kWh. The vast majority of water consumed from the various PBR scenarios was associated with evaporative spray cooling. This cooling water was assumed to be freshwater due to the issues brought about by solid residues in waste or brackish water inhibiting algae growth within the solar collector tubing or panels. Cooling modeling processes and assumptions are outlined in the first sections of Appendix A. These models include solar irradiance estimations for daily, monthly, and annual average direct radiation on a flat surface at a 25-degree latitude with an average global atmospheric clarity index. These assumptions agree with average annual solar radiation in southeast Texas (~19-20 MJ/$m^2$/day) [100]. An evaporative cooling input was used of 1.5 $kg_{water}$/day for every $m^2$ of exposed solar collector tube piping area. This value was also used for estimating flat panel evaporative losses, where the exposed affected area was assumed to be the sides and top of the tubular PBR.

Offsite freshwater consumption for an onsite brackish makeup mainly consisted of water consumed during energy production processes for the facility. Consequently, PBRs indirectly consumed the majority of freshwater for their high electricity needs. Nutrient and flocculent production (both direct and indirect energy and material) water consumption provided a fairly large percentage of the total offsite freshwater consumption. In specific cases, offsite $CO_2$ capture consumed a fair amount of freshwater as well.

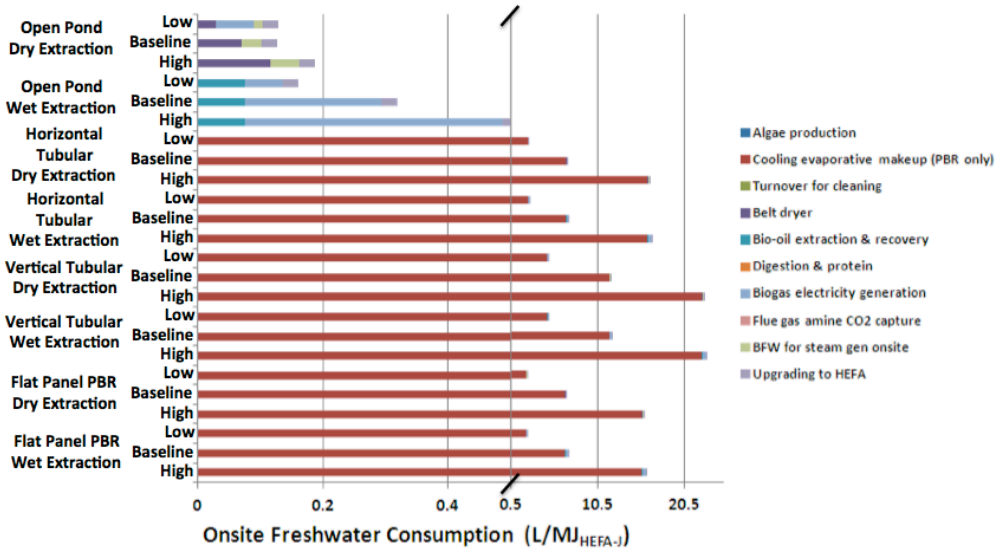


Figure 4.10: Onsite Freshwater Consumption Scenarios for a Brackish Makeup

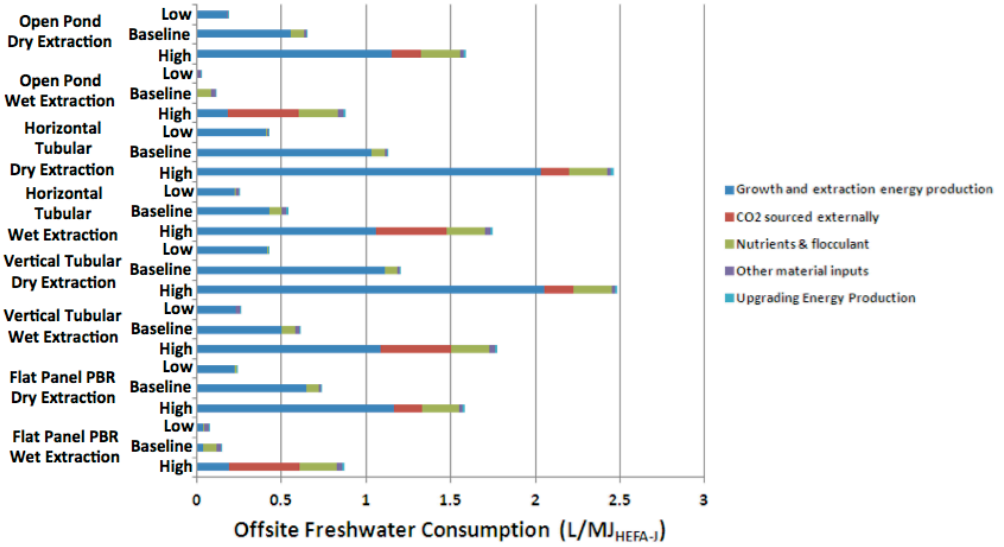


Figure 4.11: Offsite Freshwater Consumption Scenarios for a Brackish Makeup

Onsite freshwater consumption scenarios with a freshwater makeup were largely dominated by open pond evaporation and blowdown losses from algae production as illustrated in Figure 4.12. These values are highly sensitive to the evaporation rate of 0.5 cm/day. Similar trends are found for PBR cultivation systems using freshwater makeup as in brackish water because the water lost in degassing is minor compared to the cooling freshwater evaporation.

The offsite scenarios for an onsite freshwater makeup provided in Figure 4.13 show a slight decrease in freshwater consumption linked to a decrease in offsite energy demand. This is especially evident in the optimistic open pond wet extraction scenario where onsite electricity needs were met and the surplus electricity acted as a displaced freshwater credit for offsite power generation. This is mainly due to decreases in water treatment and pumping energy requirements.

Other than these slight changes, similar trends were noticed between offsite consumption with onsite fresh and brackish water growth makeups.

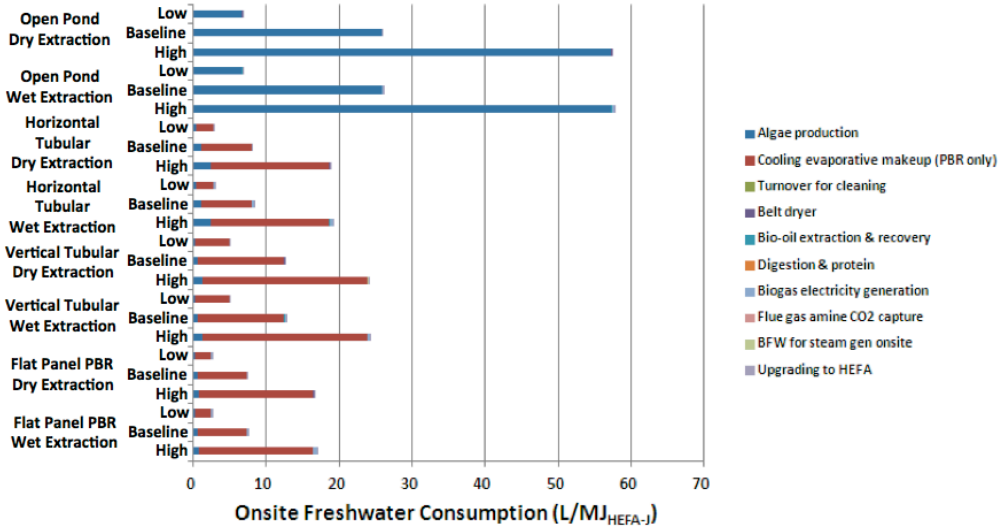


Figure 4.12: Onsite Freshwater Consumption Scenarios for a Freshwater Makeup

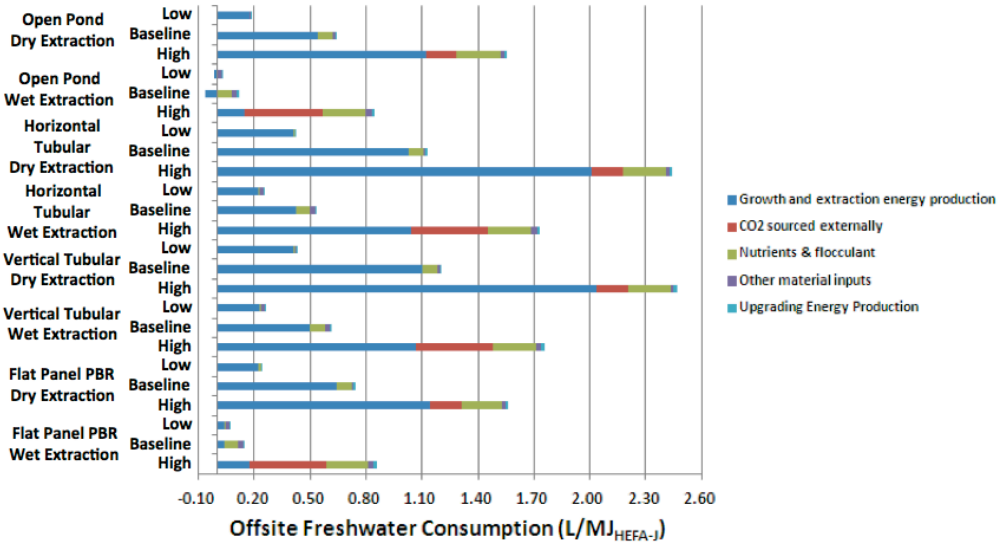


Figure 4.13: Offsite Freshwater Consumption Scenarios for a Freshwater Makeup

## 4.6 Baseline Cultivation, Recovery, and Extraction Water, Carbon, and Nutrient Flows and Total Land Area

One method used to gain perspective into the various magnitudes of the materials involved in biological energy production is the Sankey flow chart. These diagrams help qualitatively and quantitatively navigate the various flow pathways in the microalgae cultivation, recovery, and extraction portions of the lifecycle model. Figure 4.14 and Figure 4.15 provide the water (blue) and carbon (dark red) balances for each baseline cultivation and extraction technology set combination. The system boundaries encompass onsite algae cultivation through algal oil extraction. Nutrient and chemical inputs (magenta), as well as algal oil outputs (green) and PBR cooling water flows (dark blue) are also provided as a reference. Note that all materials were

recycled wherever possible to increase the overall lifecycle efficiency of the facility and that 67-68 $m^3$/day of water is taken out of the system via photosynthesis. For all baseline flow scenarios, brackish makeup water consisting of 20 parts per thousand (ppt) total dissolved solids (TDS) was input on a mass basis. The steady state TDS for the open pond, horizontal tubular, vertical tubular, and flat panel were 40.1, 30.9, 31.9, and 32.3 ppt, respectively.

When comparing between cultivation systems, one first notices that the average water flows associated with growth in open ponds are an order of magnitude larger than that of the PBR systems. This difference is primarily due to the assumed 0.5 cm/day evaporation rates and 4.46 day detention times in the 1.2 million $m^3$, 400 ha ponds. When compared to a 73.3 thousand $m^3$ horizontal tubular PBR systems with a 1.07 day detention time, the open pond water flows appear relatively large. Although the open ponds systems require more circulating water for cultivation, the number of optimized modular tubular PBRs exceeds a million (over two million for vertical tubular PBRs) in all cases. When compared to the 40 ponds, one can already begin to predict the increased maintenance, material and energy costs involved with linking the PBRs in a cultivation field system like the ones illustrated in Figure 2.7. Similarly, the total amount of facility land area for producing the same amount algal oils increases almost threefold for horizontal tubular PBRs over the open pond systems. The facility area specific fuel productivity scenarios are also depicted in Figure 4.16, which also illustrates the larger cultivation to facility area ratio for open raceway ponds (~89%) when compared against the PBR values (~42-63%). This can be attributed to lower areal productivities and the summation of linkage distance assumptions between the various PBR and system rows. The downstream flows are similar between growth systems and are not largely impacted by the upstream recycling processes. However, the number of components in each process increases or decreases as necessary for the PBR cultivation systems to obtain the output of 137 bpd TAG in the form of TAGs.

The differences in extraction technologies are shown between columns for each cultivation system row. The previously stated trends apply between cultivation systems for the wet extraction technology sets. The major differences in flows for extraction technology are the water and carbon flows dealing with pre- and post-processing steps. In dry extraction, an increased amount of carbon in the form of natural gas is needed for drying the algae. The flue gas from the combusted natural gas is recycled and therefore, less powerplant carbon makeup is required for algae growth. Moreover, the algae meal coproduct needs to be diluted to near 15 percent dry weight before entering into the anaerobic digesters. In the wet extraction case, there is an increased need for carbon from the powerplant source because no external heat is needed to dry the algae. Consequently, the separated algae meal culture does not need to be diluted before entering the anaerobic digester and more of the water in the process is recycled to the cultivation system.

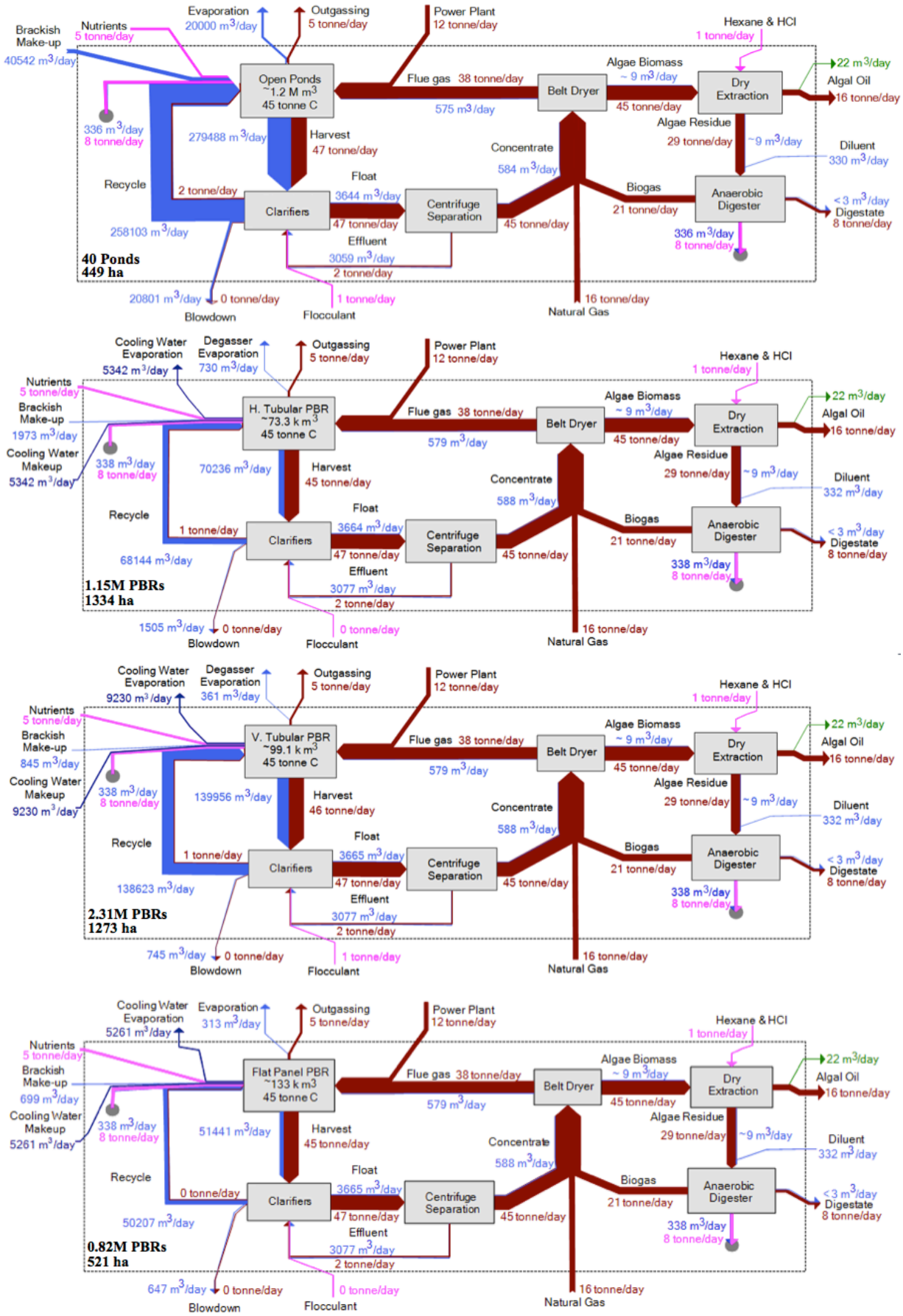


Figure 4.14: Baseline Dry Extraction Carbon (Brown) and Water (Blue) Flows; Nutrients and Chemical (Magenta) Inputs; and Algal Oil (Green) Outputs by Cultivation Type

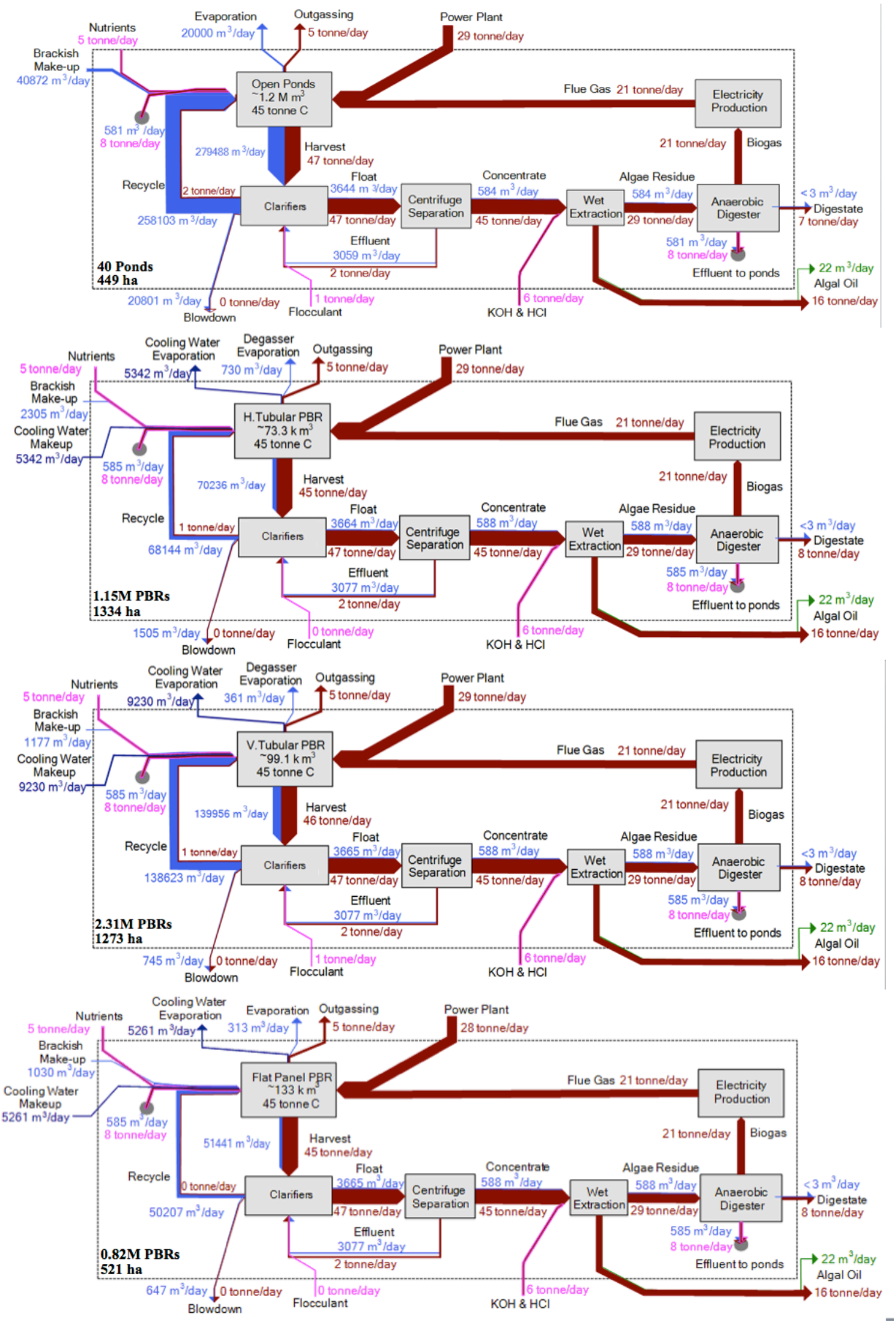


Figure 4.15: Baseline Wet Extraction Carbon (Brown) and Water (Blue) Flows; Nutrients and Chemical (Magenta) Inputs; and Algal Oil (Green) Outputs by Cultivation Type

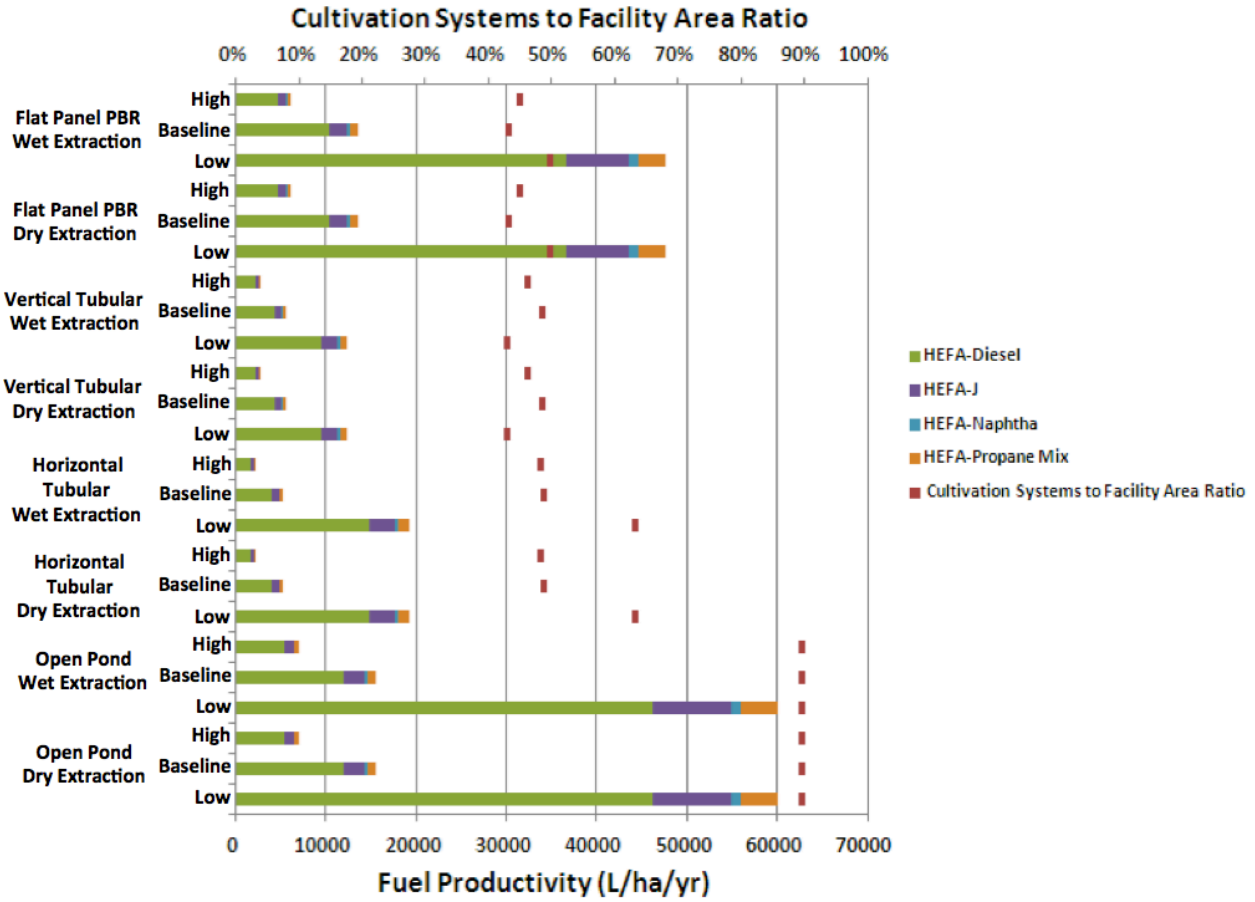


Figure 4.16: Fuel Productivity Scenarios for a Maximum Distillate Product Slate (Area Includes Cultivation, Harvesting, and Extraction Facilities)

## 4.7 Greenhouse Gas and Production Cost Parameter Local Sensitivity Analyses

Main parameter sensitivity analyses were performed to assess the LCA GHG emissions and production costs for various cultivation systems using the baseline wet extraction technology set. Figure 4.17, Figure 4.18, Figure 4.19, and Figure 4.20 depict these metric sensitivities in both absolute and relative terms for open raceway ponds, horizontal serpentine tubular PBRs, vertical serpentine tubular PBRs, and vertical flat panel PBRs, respectively.

For GHG emissions, all cultivation systems are most sensitive to productivity and biogas disposition changes. The higher productivities and oil fractions greatly affect the output product yield for the same amount of energy input into the system. For open ponds, an increase or decrease in areal productivity yields a decrease or increase in GHG emissions, respectively. However, for the PBR cases, the increase or decrease in volumetric productivity has nonlinear effects on cultivation specific energy that result in an increase or decrease in emissions, respectively. These counterintuitive results are mainly due to the solar collector tubing diameter relationship with volumetric productivity adversely affecting friction losses in the optimized PBR design that outweigh gains in algae production (See Chapter 3: Algae Photobioreactor Model Development and Optimization).

The choice to sell biogas impacts the lifecycle, as the associated methane is no longer being burned and recycled along with the $CO_2$ within the system. Additionally, the energy from the biogas is no longer being recycled back into the system, thus increasing the energy demand (and associated emissions) from outside sources. Note that the approximate financial gains from selling the biogas (~1-13%) are overshadowed by the increases in LCA GHGs (~260-2300%). Because the majority of GHG emissions in the tubular PBRs is associated with PBR algae growth, varying the downstream inputs do not affect the overall LCA GHGs as much as the open pond cultivation system. For open ponds, switching the primary harvesting inputs from the clarifiers systems to more energy intensive DAFs or more abundant belt filter presses increases the associated emissions (~100-120% for open ponds). The energy increases associated with providing highly concentrated $CO_2$ to the systems leads to increased emissions. For each cultivation system, emissions (~50% for Open Ponds and ~10-20% for PBRs) can be offset from the baseline by accounting for the carbon and nutrients within sludge from the digester to be used as a fertilizer. For the PBR systems, changing optimization scenarios from the baseline (optimizing for both areal productivity and specific energy) generally leads to increases in the overall GHG emissions. This is again due to the emissions associated with the specific energy inputs in the PBR cultivation systems (see Figure 4.1). The no optimization scenario choice reflects an approximation of the validated PBR experimental designs used in the baseline wet extraction technology sets.

Similar trends are seen with algal productivities and oil contents greatly affecting production costs. The majority of capital costs depend upon the facility land area, which result from areal productivities. In the case of tubular PBRs, areal productivities generally decrease with increasing specific energy and volumetric productivities due to reasons outlined in the previous paragraph. The relative influence of volumetric productivity on production cost is lower than on GHG emissions because the increase in specific energy use affects emissions more than operating costs. When considering siting and engineering, decreasing PBR material costs have significant effects on production costs. This includes sensitivities for decreasing solar collector tube capital costs via assumptions of a 33% decrease in price for large quantity purchases and changing the high density polyethylene (HDPE) panels to low density polyethylene (LDPE) bags. Decreasing the solar collector tube prices by a third and switching the flat panel material would decrease the overall prices by 25% and 42%, respectively. Optimization scenarios are less sensitive on a production cost basis and all result in production cost increases over the baseline for each cultivation type. Overall, both LCA GHGs and production cost are most sensitive to algae productivity and lipid contents for each growth system.

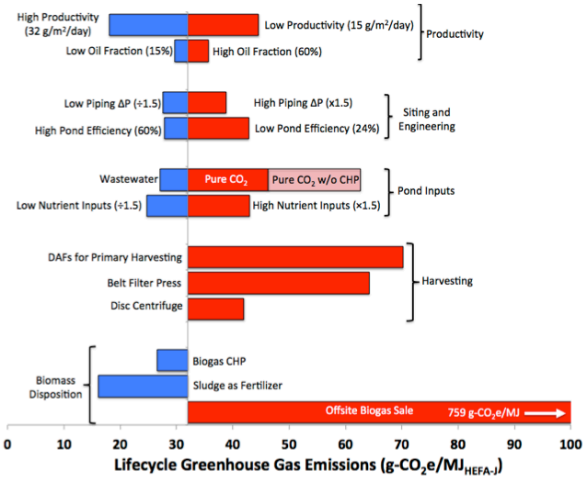


(a)

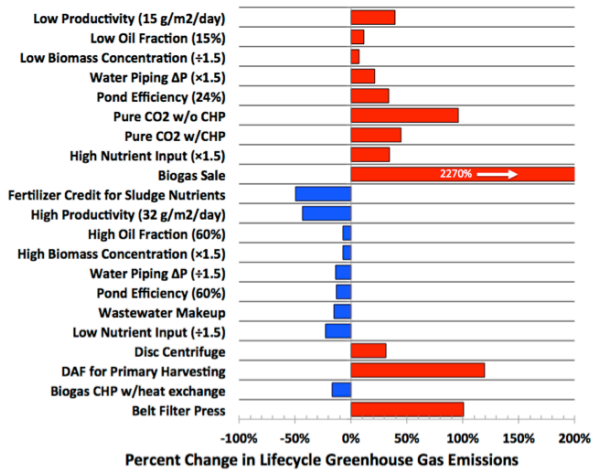


(b)

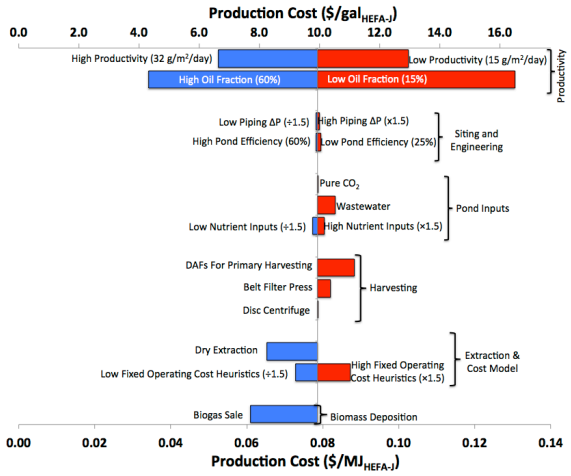


(c)

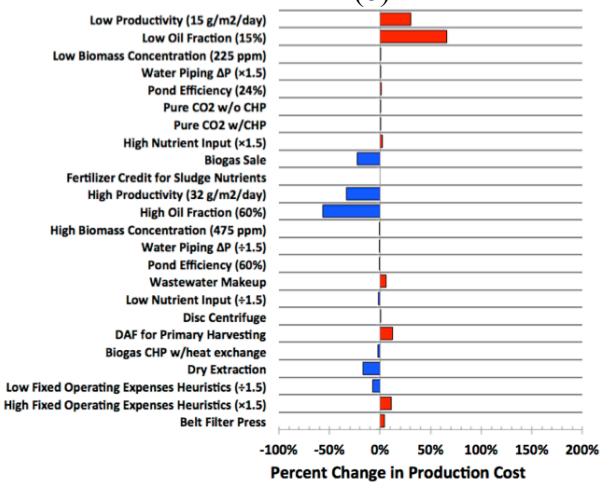


(d)

Figure 4.17: LCA GHG Emissions (a and b) and Production Cost (c and d) Local Sensitivity Analyses for Baseline Wet Extraction Open Raceway Ponds with Absolute and Relative Values

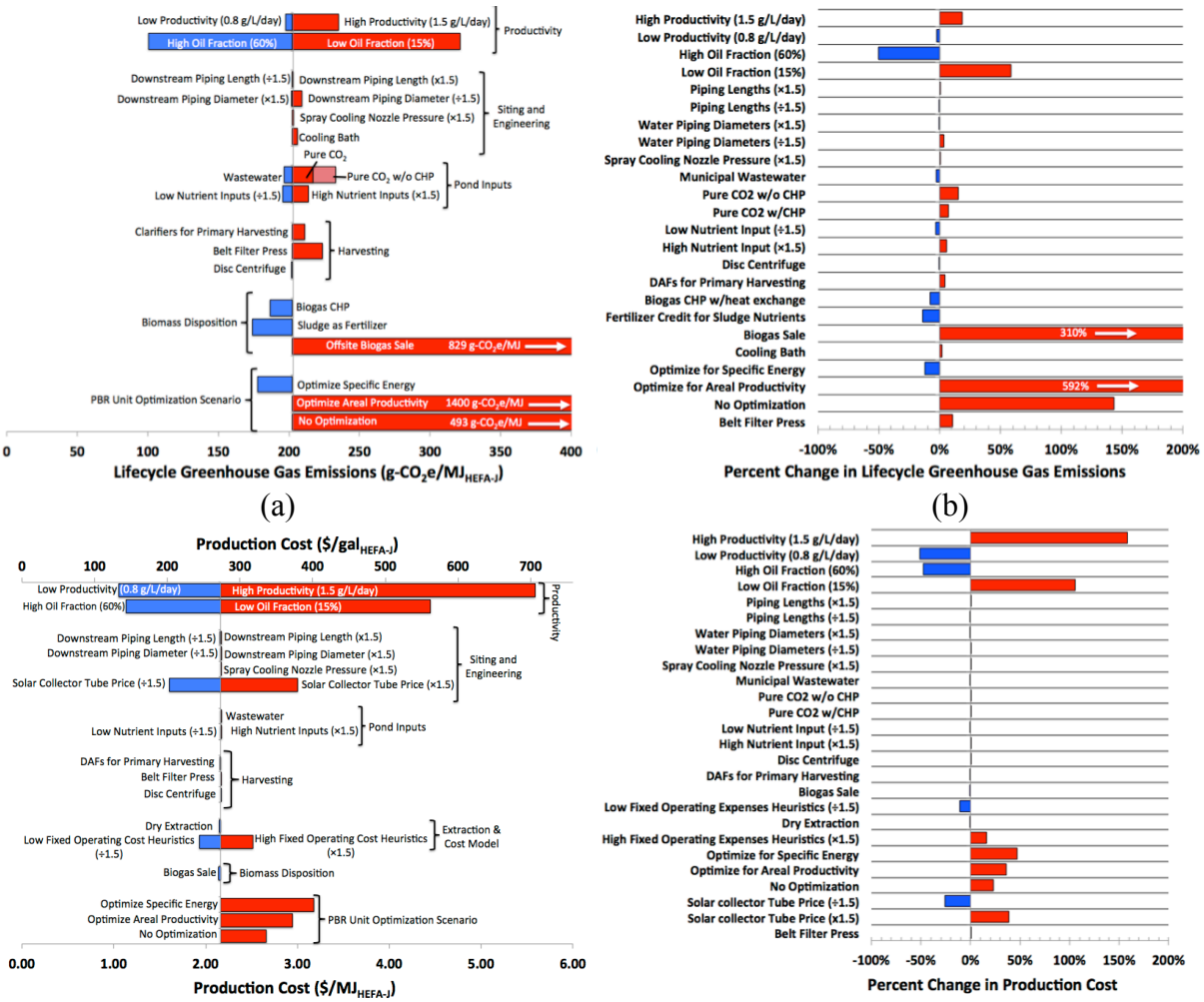


Figure 4.18: LCA GHG Emissions (a and b) and Production Cost (c and d) Local Sensitivity Analyses for Baseline Wet Extraction Horizontal Serpentine Tubular PBRs with Absolute and Relative Values

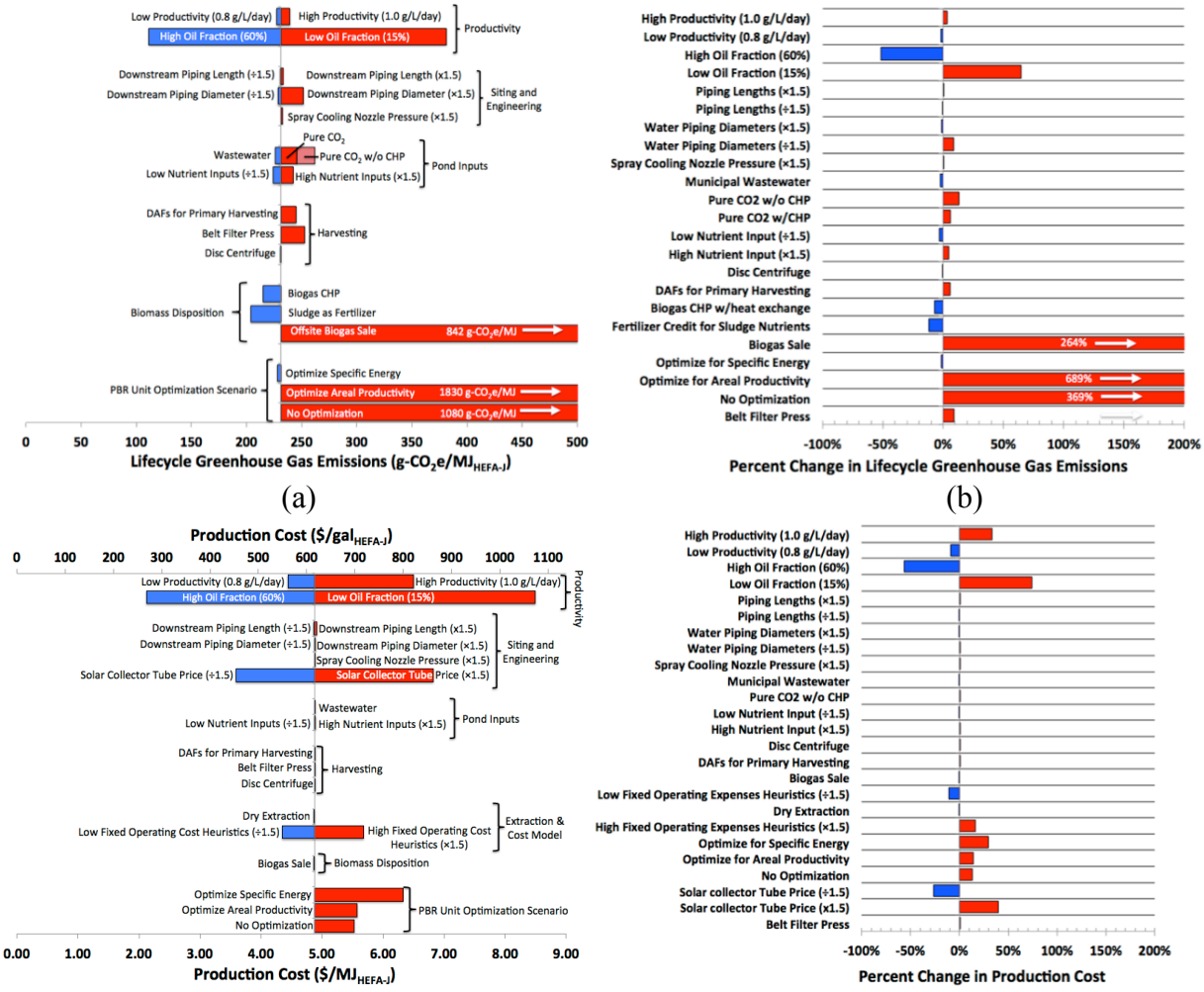


Figure 4.19: LCA GHG Emissions (a and b) and Production Cost (c and d) Local Sensitivity Analyses for Baseline Wet Extraction Vertical Serpentine Tubular PBRs with Absolute and Relative Values

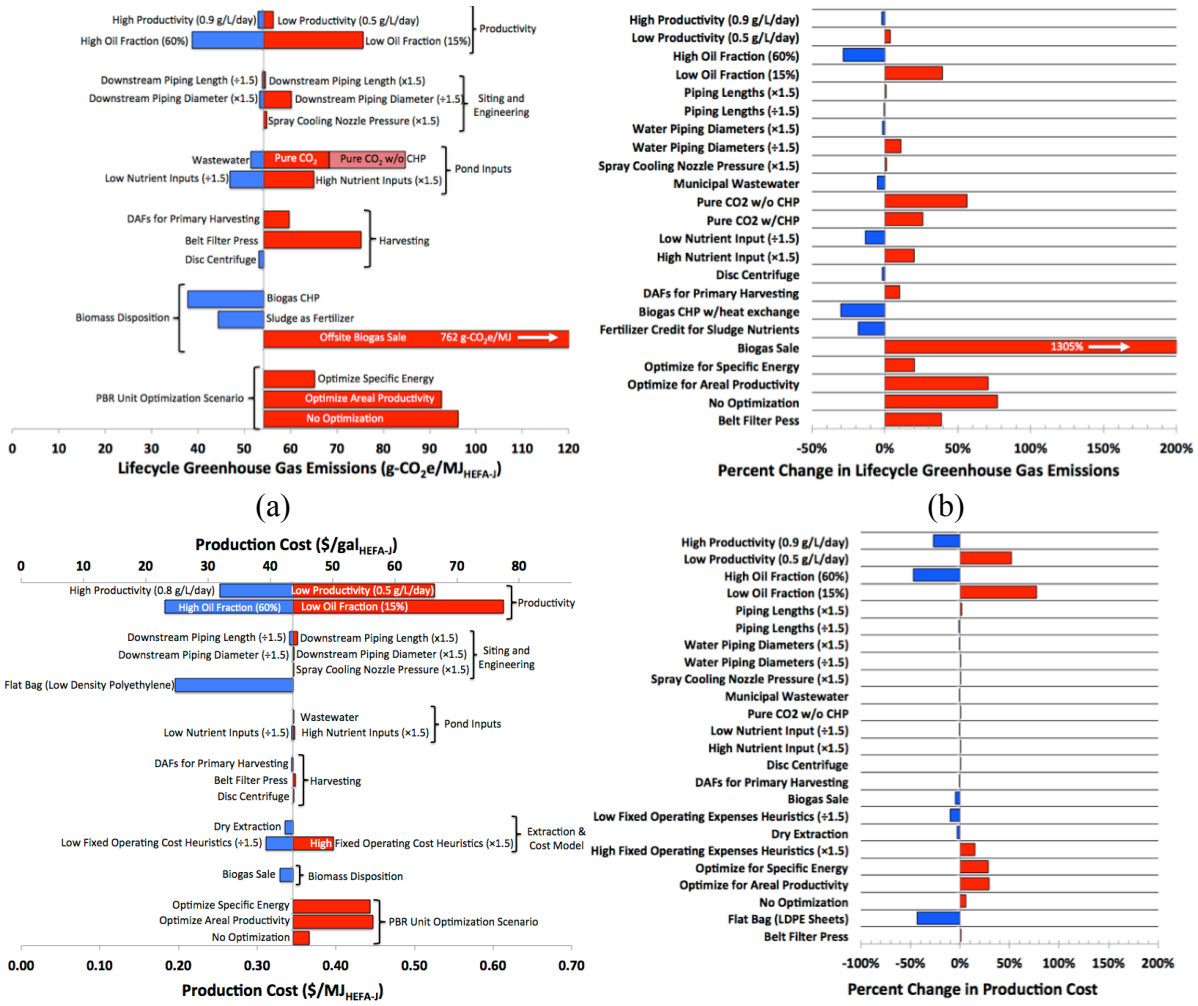


Figure 4.20: LCA GHG Emissions (a and b) and Production Cost (c and d) Local Sensitivity Analyses for Baseline Wet Extraction Vertical Flat Panel PBRs with Absolute and Relative Values

LCA GHG emissions for the baseline dry extraction technology set consisted mainly of the emissions associated with supplying and combusting natural gas for the belt dryer systems. Solar dryers can be used on a small scale without incurring these emissions, but require large land areas and residence times. The difference in emissions as a function of dewatering effluent suspended solids concentration for a solar dryer and natural gas fed belt dryer can be seen in Figure 4.21. Advancements in dewatering technology performance could greatly decrease the amount of energy required to dry downstream. However, such performance increases have decreasing returns. These decreasing returns are also present in the Stratton et al. baseline estimates, but the overall emissions were lower. This discrepancy was due to lower specific energy inputs for algae cultivation and harvesting (combined 0.95 MJ/$kg_{algae}$ for Stratton et al. instead of the 3.2 MJ/$kg_{alage}$ as a baseline in this study) [2,4].

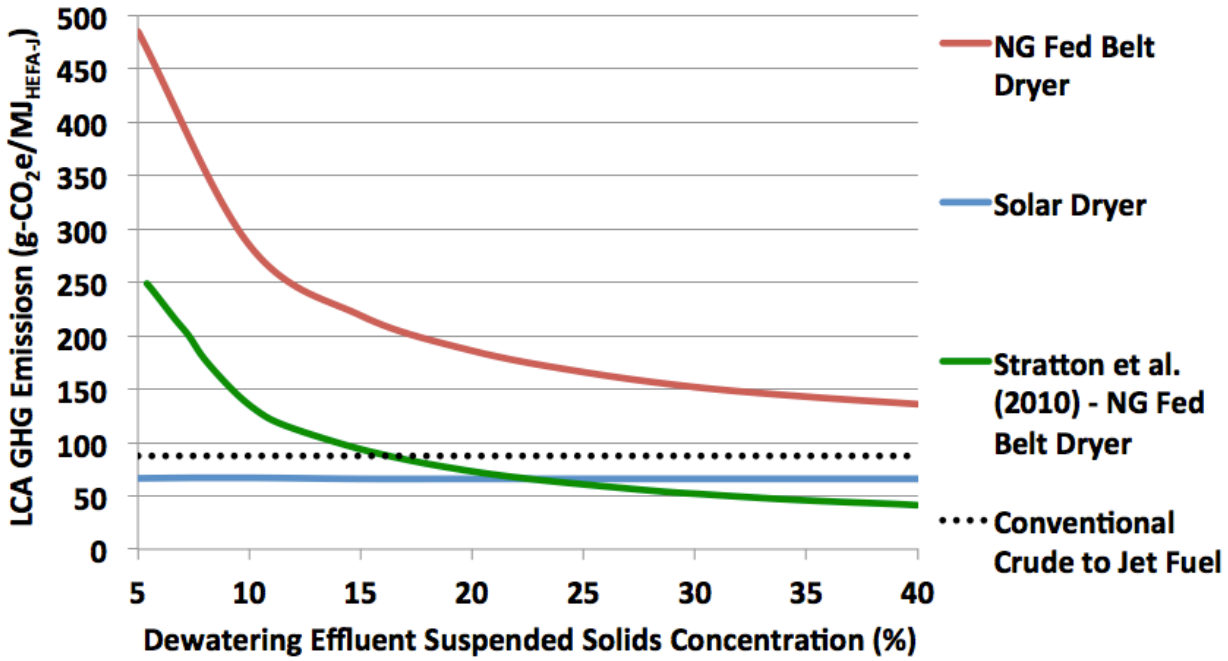


Figure 4.21: Dry Extraction Baseline Open Raceway Pond LCA GHG Emissions as a Function of Dewatering Effluent Suspended Solids Concentration and Drying Technology

Partial and full LCA results for specific energy, GHG emissions, production cost, and water consumption have been provided and discussed for different cultivation and extraction technologies with low, baseline, and high scenarios. Additionally, Sankey diagrams have been used to illustrate the mass flows throughout each baseline system. Lastly, sensitivity studies were conducted on GHG emissions and production costs provide direction on where advancements in certain technology sets within the lifecycle would produce the most environmental and/or economic benefits. Overall conclusions to these results and trends are given in the next chapter.

# Chapter 5: Conclusions and Future Work

## 5.1 Conclusions

Current goals for aviation jet fuel from a renewable feedstocks in the contiguous United States places large economic and environmental challenges at the feet of multiple organizations spanning both military and civil energy production, transportation and distribution, and end use. This thesis attempts a screening-level quantification of environmental impacts and production costs for microalgae to HEFA-J at a pilot scale by modeling current process engineering technologies while utilizing inputs from the ranges of current biotechnology. The future role of microalgae in renewable aviation fuel production will depend heavily on advancements in each area.

At the pilot plant scale, certain scenarios of microalgae can potentially meet environmental and economic goals, specifically production cost and lifecycle greenhouse gases. Figure 5.1 provides both production costs and LCA GHGs for all cultivation and extraction technology scenarios (green) when compared to conventional jet fuel ranges (dashed lines). Under current assumptions and inputs for these scenarios, only a select portion of algae derived jet fuel scenarios fit within the conventional fuel rectangles. However, it is important to note that where the conventional boxes will generally increase (decreasing supply of conventional resources leading toward more energy intensive and environmentally detrimental unconventional sources) and fluctuate greatly over time, the other technologies could decrease or increase with time. An example sensitivity was undertaken to explain such a change in the figure and is depicted in yellow, where the HDPE flat panel PBRs were instead made from LDPE clear film bags (assuming no changes in production dynamics). Finding these more sensitive inputs and exploiting synergies between biology, process engineering, and fiscal policy could ultimately lead to designs that can scale affordably with an environmental impact less than that of conventional crude to jet fuel production.

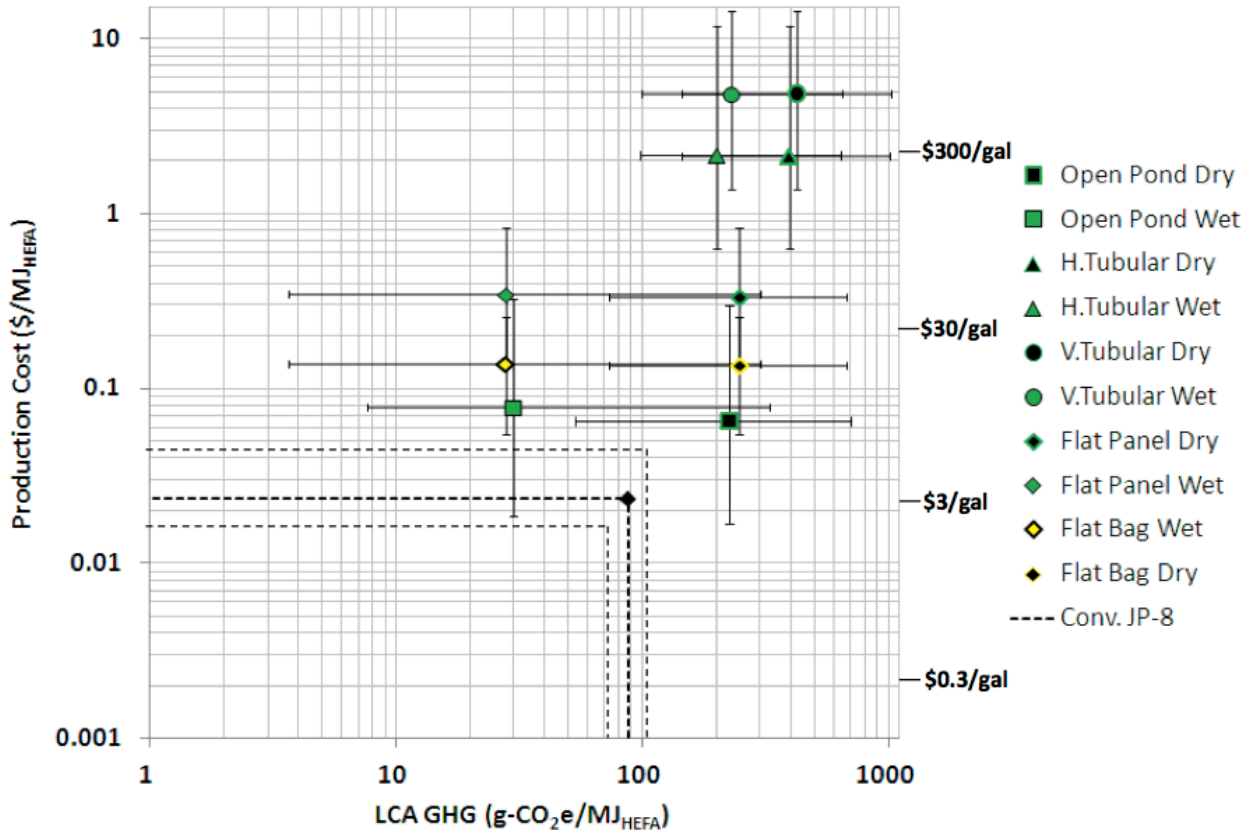


Figure 5.1: Production Cost and Lifecycle Greenhouse Gas Emissions for All Cultivation Systems and Extraction Technology Scenarios for a Microalgae-derived HEFA-J Fuel Compared to Nominal Conventional JP-8 Gate Price Ranges (1.00, 3.00, and 5.00 $/gal) and LCA GHG Emissions (80.7, 87.5, and 109.3 g-$CO_2$/MJ$_{HEFA-J}$) Ranges [4]; Variability Bars Represent Low and High Scenarios

The following list depicts some the major conclusions drawn from these scenarios:

Photobioreactor Modeling and Optimization

- Comprehensive modeling of tubular and flat panel photobioreactors required an integrated systems approach using nonlinear, second order relationships. These relationships involved energy balances, mass transfer, gas holdup, and oxygen balances, each with interrelated parameters for the cultivation system. Validation of these systems suggested less than 15% error for comparable parameters compared to designs in literature for both horizontal and vertical serpentine tubular photobioreactors.
- Local sensitivity analyses of the horizontal serpentine tubular photobioreactor was undertaken to understand input parameter effects on specific energy and areal productivity. One of the more sensitive parameters involved with these output factors were the solar collector tube diameter and associated volumetric productivity.
- Spacing distance and volumetric productivity had a major affect on areal productivities for flat panel photobioreactors.

- Optimization scenarios of specific energy, areal productivity, or both factors yielded higher impact on specific energy than to areal productivity. This is because areal productivity is based on a select few parameters ($L_{sc}$, $h_L$, and $X/h_L$) whereas specific energy includes multiple parameters involved with all coupled system equations.
- Optimization constraints were impacted when solely optimizing for volumetric or areal productivity. However, no constraints were impacted when weight optimizing equally for both specific energy and areal productivity.
- When optimizing for both outputs equally, decreases in specific energy far outweigh the gains in areal productivity.

Lifecycle Trends

- The majority of production cost, specific energy use, lifecycle greenhouse gas emissions, water consumption, and land use for all microalgae to HEFA-J scenarios reside in the direct cultivation, harvesting, dewatering, and (where applicable) drying portions of the lifecycle.
- For a given cultivation technology, greenhouse gas emissions and production costs are most sensitive to microalgae productivity and lipid content inputs, although downstream harvesting technologies are more sensitive for open raceway ponds.
- Near-term dry and wet extraction technologies mainly impact lifecycle greenhouse gas emissions and material inputs. The majority of specific energy inputs and associated GHG emissions for dry extraction occur when drying the dewatered algae.
- For a given extraction technology, optimized serpentine tubular photobioreactors experienced higher specific energies, greenhouse gas emissions, and production costs than open raceway ponds or flat panel photobioreactors. Higher specific energies and greenhouse gas emissions are linked to the higher cultivation specific energy inputs while the higher production costs are mainly due to solar collector tube capital expenses.
- Fixed operating cost refinery heuristic assumptions impact maintenance and total production expenses by nearly 10% for baseline cases. Additionally, potential decreases in capital costs for cultivation systems, i.e., flat bags instead of flat panels or a decreased solar collector tube price, have sizable impacts on total production costs.
- Onsite freshwater consumption for open raceway ponds is highly dependent on makeup water type. The majority of freshwater for photobioreactors in consumed in the spray cooling system water makeup.
- Offsite freshwater consumption is mainly driven by water consumed in offsite electricity generation for most scenarios and onsite makeup water types, although nutrient manufacture and associated energy inputs also play a significant role.
- Water cultivation and recycle flows are greatly reduced from open ponds to photobioreactors, while downstream water and carbon flows are minimally impacted. The downstream flows, including makeup $CO_2$ are impacted more by extraction technologies. Baseline overall land area required nearly triples for some tubular photobioreactors and increases for flat panel photobioreactors. This is mainly a result of photobioreactor field spacing assumptions and areal productivity optimization results.

- For the same pilot scale demand and extraction technology, modular flat panel photobioreactor cultivation systems exhibit the most promise in comparison to other growth systems when quantifying freshwater consumption, specific energy use, and associated greenhouse gas emissions. However, flat panel photobioreactor production expenses and facility land area are estimated to be higher when compared to open pond systems.
- According to these results, there could be a select few current cultivation and extraction technologies reside within the economic and environmental ranges of current conventional petroleum-based jet fuel, even at a pilot scale.

Overall, microalgae have the potential to meet military and civil alternative aviation fuel goals with significantly less land than other fuel feedstocks when accounting for biomass growth rates and oil content. However, algae growth at larger scales will require integrated cultivation systems, high solar irradiance, large supplies of $CO_2$, and energy to manipulate the large water flows involved. Advancements leading to less energy intensive dewatering and oil extraction methods are crucial to sustainably use microalgae as a fuel feedstock. Furthermore, water, nutrient, and energy recycling is critical to minimize specific energy and LCA GHG emissions. These requirements increase overall capital, maintenance, and operating costs when compared to conventional crude derived jet fuels. Nevertheless, choosing less energy intensive and costly cultivation, harvesting, and extraction systems with the correct species of algae could produce jet fuel with environmental impacts and costs similar to that of conventional jet fuel on a pilot scale. If implemented correctly, expansion of these systems in the United States could create a renewable energy base that produces high quality hydrocarbon fuels form $CO_2$, sunlight, and low quality water with options for a multitude of other coproducts. The technology options are not limited to the ones discussed in this study and current advancements in biotechnology and process engineering could revolutionize this field, the United States economy, and geopolitics within the next decade.

## 5.2 Recommendations for Future Studies

*Scaling Effects*

The scenarios in this study focused on comparing various cultivation and extraction technologies for upgrading algal oils to a HEFA product slate. However, the size of this facility modeled a pilot scale operation capable of producing only ~137 barrels per day of algal triglycerides. Benefits and detriments of scaling to larger demand should be studied on a lifecycle basis. Not only could scaling to larger facility sizes affect LCA process economics, but energy and material inputs may also impact environmental lifecycle results in a nonlinear fashion. Additionally, it may not be effective and/or feasible to scale certain technology geometries with demand. In such cases, multiple processing units, each with linkages and inefficiencies of their own, could greatly affect the lifecycle system environmental and economic performance.

*Quantifying Societal Cost of Environmental Impacts: Social Cost of Carbon (SCC) and Air Quality*

This thesis provided scenario estimates for lifecycle emissions ($g\text{-}CO_2e/MJ_{HEFA\text{-}J}$) and production price ($\$/MJ_{HEFA\text{-}J}$) associated with algae to jet fuel production. However, the relationship between these two metrics does not include the externalities associated with environmental costs. Many studies have quantified cost estimates for the impacts of global climate change and air

quality emissions. Global climate change emission economic impacts are usually defined as the social cost of either carbon/carbon dioxide (SCC) or carbon dioxide equivalent (SCCe), while air quality emission costs are usually determined by premature mortality estimates associated with health impacts from population exposure. Theoretically, both the production and societal costs of global climate change and air quality could be taken into account for a more robust cost-benefit comparison of producing alternative fuels [101,102,103]. The total cost of the alternative fuel (including externalities) could then be compared with the total cost of fuels derived from conventional or unconventionally derived petroleum crude.

*Nutrient Supplement and Symbiotic Relationships*

Nutrient recycling and makeup comprise a significant portion of the environmental and economic burdens in the lifecycle of algal fuel production. For example, in the case of the baseline wet extraction open ponds in Figure 4.17, decreasing nutrient inputs by 33% could decrease LCA GHG emissions 13% and production costs by 0.2%. In many cases, the nutrient inputs (especially nitrogen and phosphorous) required for algae cultivation are considered environmental and economic burdens in other systems. Symbiotic relationships between various forms of nutrient-rich waste and algae cultivation systems have the potential to decrease environmental and economic costs for both systems involved. A study involving anaerobically digested dairy manure as a nutrient supply for the cultivation of Chlorella sp. found that the algae removed ammonia, total nitrogen, total phosphorus, and chemical oxygen demand by 100%, 75.7-82.5%, 62.5-74.7%, and 27.4-38.4%, respectively. Additionally, the total dry weight fatty acid content of the algae increased from 9.00% to 13.7% [104]. This oil increase is even more sensitive to the overall environmental and economic metrics in this study. Other relationships can be seen in aquaponic (combining aquaculture with hydroponic) systems where waste from fish grown in aquacultures is use as a supplement for growing oil-rich microalgae for biofuels. The majority of the algae cake byproduct could be anaerobically digested to produce biogas while a smaller portion could be fed back to the fish as a protein supplement (10-15% of dietary protein [105]). An example of aquaponic cultivation methods is being conducted in Boca Raton, Florida by Neptune Industries, which uses fish waste in a patented Aqua-Sphere system to create additional revenue streams through cultivation of algae for biofuels and methane gas [106].

*Role of Biotechnology and Potential Invasiveness*

Phototrophic microalgae to jet fuel pathways have efficiency limitations associated with the number of links in the processing chain. The biology of microalgae governs a tradeoff between biomass production rates and oil contents. Using sugar and starch rich phototrophic microalgae with exceedingly high growth rates as a feed source for genetically engineered microbes that secrete TAGs or free fatty acids via fermentation have the potential to increase hydrocarbon production with less energy and cost inputs. However, as with certain forms of algae, the potential for invasiveness of such organisms could prove more costly on both an environmental and economic basis if not managed correctly. Invasive species studies for biofuels have focused on using weed risk assessment (WRA) tools to predict species invasiveness. Various WRA schemes categorize predictors of invasiveness into the following general categories: reproductive traits, distribution and historical factors, environmental tolerance, growth habit, competition/defense, biotic interactions, pathlogenic factors, genetic factors, and ecosystem diversity. The predictors common to all WRA schemes include drought tolerance, tolerance of marginal soils, rapid growth, and high biomass and/or seed production [107]. In terms of the

Australian WRA, a point system is used based on a list of questions to either accept or reject a plant species into the country. However, these assessment models are mainly meant for conventional crops. Similar invasiveness studies should be conducted using a framework based on plants species that are cultivated in an aquatic culture.

*Spatial Analyses for Facility Siting*

As stated in Section 5.1, phototrophic microalgae need large amounts of sunlight, nutrients, $CO_2$ and low quality water to grow as an energy feedstock. Additionally, a location in the United States with large amounts of frost-free days would be required. Using locations of coal-fired power plants, solar insolation greater than 4 $kWh/m^2/day$, and frost-free days greater than 6 months/year, researchers at PARTNER have found that locations along the golf coast and southwestern United States look most promising [22]. Additionally, studies at PARTNER have located the majority of demand centers for military and civilian jet fuel in Southern California Southeastern Texas, and the eastern United States New York to Washington D.C. [5]. To further these studies, Geographic Information Systems (GIS) could be used in coordination with LCA models to provide a quantified map pinpointing the best locations for sustainable, conventional refinery scale fuel production from microalgae.

## Appendix A – Water Consumption Inputs and Modeling

Photobioreactor Cooling System Modeling

PBR cooling systems included solar irradiance modeling for a site in southeast Texas to provide the energy input required to match via cooling (subtracting photosynthetic conversions). This solar irradiance was also used for evaporative loss calculation estimations as a check to the 0.5 cm/day open pond evaporation loss inputs.

*Solar Irradiance Model*

Solar irradiance model from Duffie and Beckman (1985) includes the daily global extraterrestrial solar radiation $H_0$ and takes into account atmospheric clarity to parse out the diffuse from the direct solar radiation on an assumed flat surface [108,109]. The extraterrestrial solar irradiation is based on the universal solar constant $\xi = 1353\frac{W}{m^2}$, day of the year $N$, geographic latitude $\phi$, declination of the angular position of the Sun at solar noon with respect to the plane of the equator $-23.45^\circ \le \delta \le 23.45^\circ$ (north positive) and hour angle at sunrise $\omega_s$. The atmospheric clarity index א accounts for atmospheric distortions and diffusion on the incoming solar irradiation to produce the total daily direct $H$ and daily diffuse $H_d$ radiation on a horizontal surface. The difference between the daily direct and diffuse radiation equates to the daily direct radiation on a horizontal surface $H_b$. The yearly average direct solar radiation is then calculated as the integrated average of all daily direct solar irradiance averages throughout the year $H_y$.

$$H_o = \left(\frac{24\xi}{\pi}\right)\left(1 + 0.003\cos\left(\frac{360N}{365}\right)\right)\left(\cos\phi\cos\delta\sin\omega_s + \frac{2\pi\omega_s}{360}\sin\phi\sin\delta\right) \quad \text{(A1)}$$

$$H = \text{א}H_0 \quad \text{(A2)}$$

$$H_d = \left(1.390\text{א} - 4.027\text{א}^2 + 5.530\text{א}^3 - 3.108\text{א}^4\right)H_0 \quad \text{(A3)}$$

$$H_b = H - H_d \quad \text{(A4)}$$

$$\omega_s = \cos^{-1}\left(-\tan\delta\tan\phi\right) \quad \text{(A5)}$$

$$\delta = 23.45\sin\left(\frac{360\left(284+N\right)}{365}\right) \quad \text{(A6)}$$

$$H_y = \frac{1}{365}\sum_{N=1}^{365} H_b\left(N\right) \quad \text{(A7)}$$

The average daily and monthly direct radiation model outputs were validated in Figure A1 at multiple locations and times of the year from data accumulated by Liu et al. (1960). The annual averages were validated in Figure A2 at multiple latitudes from National Renewable Energy Laboratory (NREL) satellite observation datasets (1998-2005) [110,100]. Discrepancies in of the model are most likely due to the conservative assumption that the solar radiation is spread along a flat surface. An annual average global clarity index of 0.74 was used, but other locations like

the southwest United States would need a location specific clarity index. These solar irradiance values were not linked to the algae productivity inputs, but multiple strain specific models have been developed [109]. Future studies could link these parameters for performing facility siting spatial analyses. The location for the cooling analyses occurred at a latitude of 25 degrees, which yielded an annual average solar irradiance estimate of 19.8 MJ/m$^2$/day.

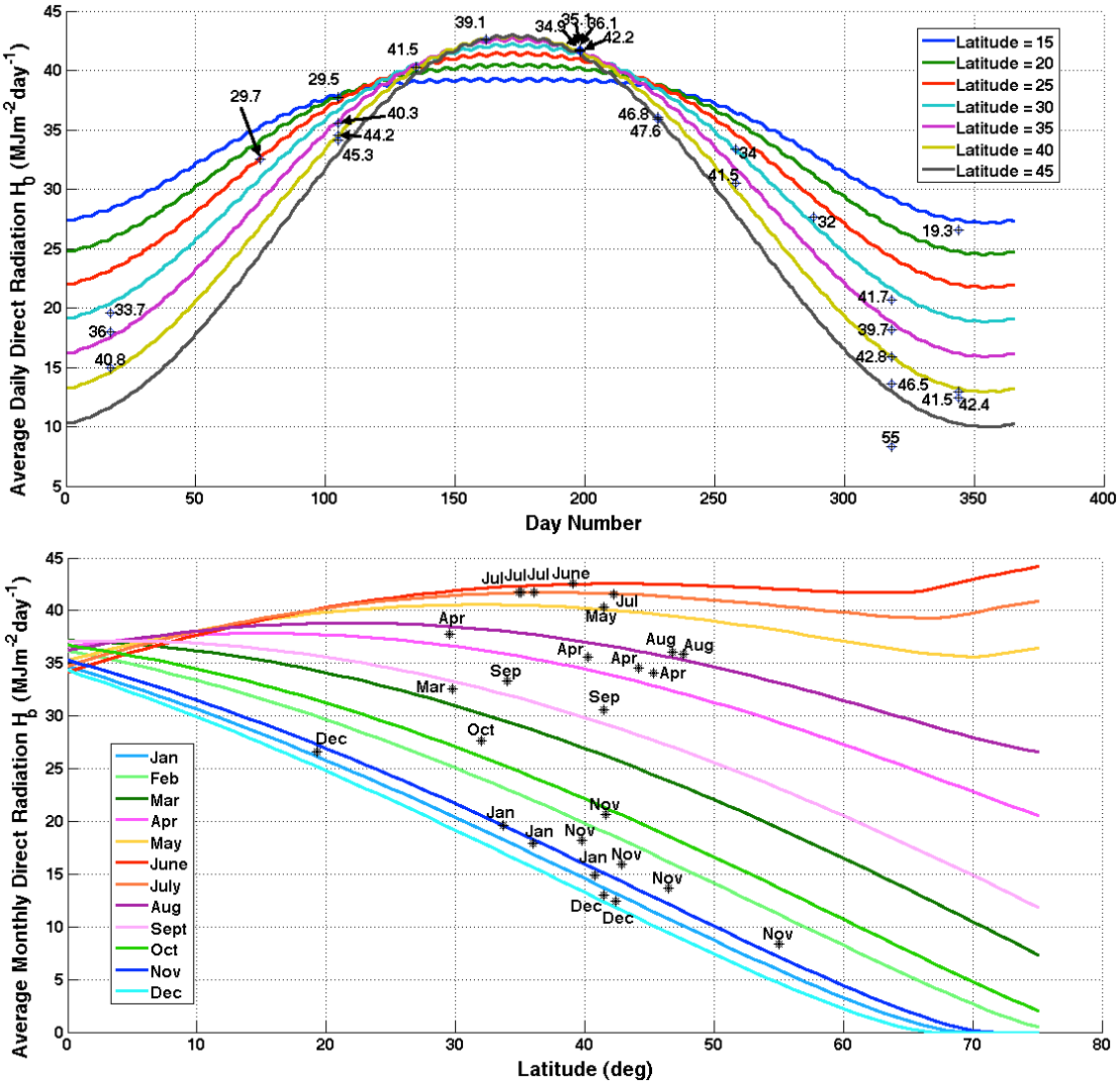


Figure A1: Daily (Top) and Monthly (Bottom) Solar Irradiance Modeling Validation

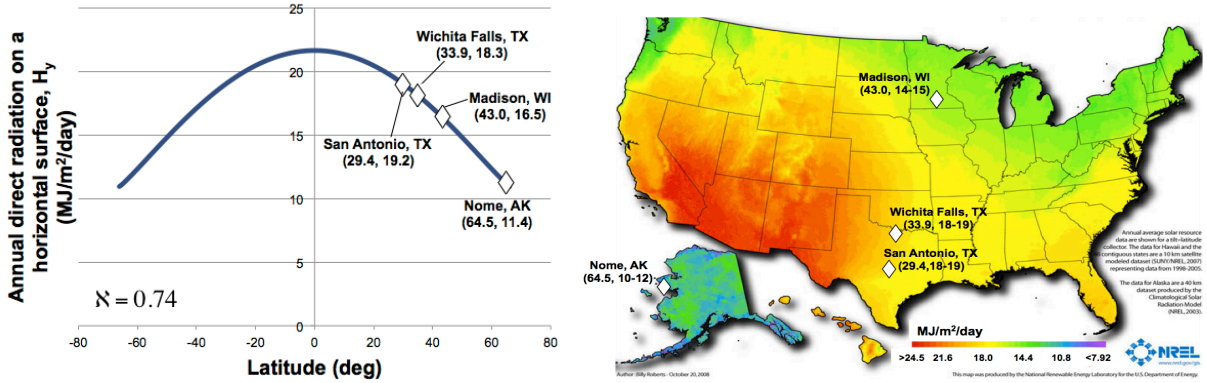


Figure A2: Annual Solar Irradiance Model (Left) and NREL Validation (Right) – (Latitude, Annual Direct Solar Radiation)

*Photobioreactor Cooling System Models*

Once provided with the annual incoming energy from the sun on the PBR systems, one could then calculate the photosynthetic efficiency *PE* of the PBRs, which his based on the areal productivity $P_{areal}$ and energy content of the biomass $E_b$. The specific solar energy input ($MJ/kg_{algae}$) into the system $E_{in}$ not going to photosynthesis can then be calculated based on the PBR surface area, volumetric productivity, and volume. The various cooling systems that can be modeled are shown in Figure A3. The spray cooling models were used for all scenarios; however, a cooling bath could be use for the horizontal tubular case. The spray cooling piping was assumed to cover every solar collector branch as a conservative assumption, while the spray cooling for flat panels were assumed to be over every panel. A spray cooling pressure loss of 0.35 bar was assumed for an ordinary hazard sprinkler with a diameter of 0.021m. The conventional cooling energy losses were calculated according to Equation (2.9). The cooling bath algae evaporation (cm/day) was calculated according to Equation (A10) to check the open pond evaporation input of 0.5 cm/day. The resulting evaporation rate was 0.7 cm/day. Finally, the mass specific ($kg_{water}/kg_{algae}$) and volume specific ($m^3_{water}/kg_{algae}$) are calculated based on cooling type in Equation (A10) and Equation (A11). Additional evaporative losses for spray cooling were derived from Stephenson et al. (2010), which estimated 1-2 $kg_{water}/day/m^2$ of tube area [53]. These values were also used for evaporation off of a flat panel surface. All water not evaporated was assumed to be caught in drains below the PBRs and recycled. Advantages to a spray system are relatively low water loss with low specific energy inputs. However, concerns over water residue caking the solar collector tubes and inhibiting growth have been noticed. Cooling baths have even lower required specific energy, but loses larger amounts of water to evaporation due to the larger surface areas.

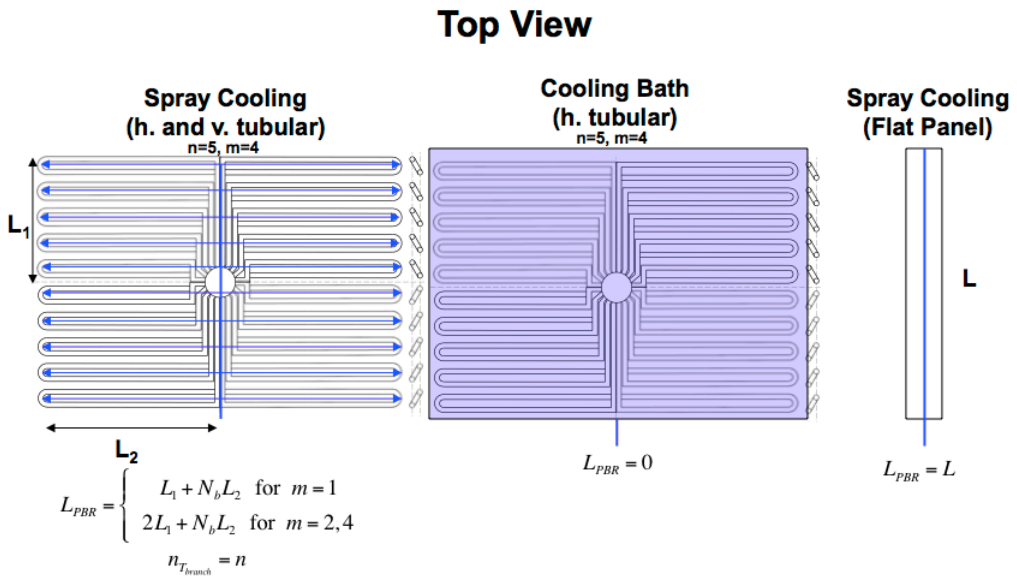


Figure A3: Various PBR Cooling Models

$$PE = \frac{P_{areal} E_b}{H_b} \tag{A8}$$

$$E_{in} = \frac{(1-PE) H_b d_{sc} L_{sc}}{P \frac{\pi}{4} d_{sc}^2 L_{sc}} \text{ (Tubular) or } E_{in} = \frac{(1-PE) H_b (Lt + 2h_L t + 2Lh_L)}{PLh_L t} \tag{A9}$$

(Flat Panel)

$$r_{evap} = \frac{(1-PE) H_b}{\rho_w (\Delta H_{evap} + 75 C_{p_{evap}})} \tag{A10}$$

$$\dot{m}_w = \frac{E_{in}}{\Delta H_{evap} + 75 C_{p_{evap}}} \text{ (spray cooling) or } \dot{m} = \frac{\dot{V}_w}{\rho_w} \text{ (cooling bath)} \tag{A11}$$

$$\dot{V}_w = \frac{\dot{m}_w}{\rho_w} \text{ (spray cooling) or } \dot{m}_w = \frac{r_{evap}}{P_{areal}} \text{ (cooling bath)} \tag{A12}$$

System Water Consumption Inputs and Assumptions

*Onsite Water Consumption*

Table A1: Onsite Water Consumption Inputs and Assumptions

| Component/Process | Input Parameter | Value | Notes/Refs. |
|---|---|---|---|
| PBR degasser water loss | Water saturation at 30°C ($g_{water}/m^3_{air}$) | 31.5 | Assumed constant |
| PBR cultivation evaporation from cooling water | Evaporation Rate ($kg_{water}/m^2/day$) | 1.5 | [53] |
| Open pond cultivation evaporation | Evaporation Rate (cm/day) | 0.5 | [22] |
| | Blowdown ratios | See Table 2.6 | |
| Turnover for cleaning | Pond/PBR Drain Number (#/year) | 3.0 | Assumed brackish; drained directly into the sea after treatment |
| Belt dryer | Cooling water to scrubber ($m^3_{water}$/hr) | 54.0 | Vendor inputs; specific to system design for scaling water consumption based on dry solids production [22,74] |
| | Water evaporated ($m^3_{water}$/hr) | 5.50 | |
| | Total discharge water ($m^3_{water}$/hr) | 59.0 | |
| | Dry solids produced (lb/hr) | 1627 | |
| | Water Lost ($m^3_{water}$/hr) | 0.5 | |
| | Makeup cooling water needed ($m^3_{water}$/hr) | Actual dry solids produced*(0.5/1627) | Scales with amount of biomass being dried |
| | Evaporated water in drying ($m^3_{water}$/hr) | 0.0 | Can be recovered, condensed and recycled; 100% recovery assumed |
| Boiler feed water for steam on-site steam generation | Steam enthalpy (MJ/kg) | 3.40 | [22] |
| | Makeup BFW | 5.0% | |
| | Boiler thermal efficiency | 85% | |
| Dry solvent extraction | Water consumption ($kg_{water}/tonne_{biomass}$) | 3.28 | Based on soy oil hexane extraction [73] |
| Steam lysing wet extraction | Cooling water consumption ($kg_{water}/tonne_{oil}$) | 2.92 | Based on 0.36 gal/$lb_{biodiesel}$ with a 97% biodiesel yield from soybean oil [76] |
| Biogas electricity generation | Water consumption ($L_{water}$/kWh) | 2.36 | Lifecycle water consumption for U.S. NGCC average electricity production; most from cooling tower [111] |
| Flue gas amine $CO_2$ capture | Water use in capture ($L/kg_{CO2}$) | 1.14 | Estimated from [22] |
| Digestion and Protein | Losses in undigested solids assumed to be brackish | | |
| Upgrading | Total water consumption ($m^3$/day) | 19.60 | Includes BFW and cooling makeup with recycle scheme [33] |

*Offsite Water Consumption*

Table A2: Offsite Water Consumption Associated with Energy Inputs

| Component/Process | Input Parameter | Value | Notes/Refs. |
|---|---|---|---|
| Hydrogen production | Total consumptive ($L_{water}$/kg) | 5.60 | Water via steam reforming of natural gas [111] |
| US grid average electricity production | Total consumptive ($L_{water}$/kWh) | 2.05 | Weighted total U.S. average electricity production lifecycle water consumption [111] |
| Natural gas production and transport | Total consumptive ($L_{water}$/kWh) | | Based on 0.08 $gal_{water}$/kWh mining and processing [23] |
| Crude production and refining (to refinery product) | Total consumptive ($L_{water}/L_{refined\ product}$) | 9.88 | Lifecycle crude production (originally in L/km with light-duty vehicle efficiency of 20.5 mpg) [111] |
| IGCC electricity production | Total consumptive ($L_{water}$/kWh) | 2.36 | Lifecycle water consumption for U.S. NGCC average electricity production; most from cooling tower [111] |

Table A3: Water Consumption Associated with $CO_2$ Capture

| $CO_2$ point source electricity generation | Water consumption ($L_{water}$/MWh) | Capture rate ($kg_{CO2}$/MWh) | Water consumption ($L_{water}/kg_{CO2}$) | Notes/Refs. |
|---|---|---|---|---|
| Subcritical pulverized coal | 1770 | 707 | 2.51 | DOE/NETL (reports 402/080108, 2007/1281) |
| Supercritical pulverized coal | 1490 | 669 | 2.22 | |
| IGCC (slurry) | 541 | 593 | 0.91 | |
| IGCC (dry fed) | 681 | 573 | 1.19 | |
| NGCC | 553 | 317 | 1.74 | |

# Appendix B – Production Cost Inputs

Capital Expenses

Table B1: Inside Battery Limit (ISBL) Capital Cost Scenario Ranges for Various Algal Cultivation, Harvesting, Extraction, and Upgrading Technology Sets (±10% Variability from Baseline Unless Referenced)

| Category | Component | Low | Baseline | High | Notes/Refs. |
|---|---|---|---|---|---|
| | | ISBL Expenses ($/ha unless otherwise noted) | | | |
| Open Pond Cultivation | Open ponds | 3,950 | 8,300 | 17,400 | Low - [94], Baseline - [92] |
| | $CO_2$ feed system | 260 | 5,900 | 6,900 | Low - [50], Baseline - [92], High - [99] |
| | Water/nutrient/waste system | 6,040 | 8,500 | 9,350 | Low - [50], Baseline - [92] |
| | Paddle wheel | 6,210 | 6,900 | 7,410 | Baseline - [92], High - [94] |
| Harvesting | Settling tanks/flocculation | 11,400 | 12,000 | 13,200 | Low - [50], Baseline - [92] |
| | One DAF unit | See Figure B2 | | | [50,112,113] |
| | Belt filter press | | | | [114] |
| | Three-phase centrifuge | | | | [115] |
| Extraction/ Digestion | Wet extraction unit | 10,800 | 12,000 | 13,200 | Assumed near capital cost of settling tanks |
| | Dry extraction unit | 1,890 | 2,100 | 2,300 | Scrubber/dryer (200 cfm); Baseline - [94] |
| | Anaerobic digester | 3,600 | 4,000 | 4,400 | Baseline - [94,92] |
| | CHP unit | See Figure B1 | | | [92,116,117] |
| Downstream Pumps | All components ($) | See Equation (B1) | | | "a" value determined from [50] Equation from [118]; Volumetric flow rate Q($m^3$/s), and head h(m) used for each step to determine installed cost C($) |
| Upgrading | Total upgrading plant investment (cents/$gal_{TAG}$) | 13 | 15 | 21 | Includes hydrotreater, isomerizer, saturated gas plant, storage, cooling water system, offsites, special, contingency, and escalation costs for 2000, 4000, and 6500 bpd TAG facilities [33]***** |
| | | ISBL Expenses ($/ft unless otherwise noted) | | | |
| PBR Cultivation††††† | Solar collector tubes (Tubular only) | 15.4 | 17.1 | 20.9 | 2.375" dia. clear polyethylene [119] |
| | Degasser tubes (Tubular only) | 11.9 | 19.5 | 64.6 | 8" dia. PVC [119] |
| | Panel surface (Flat panel only) ($/$ft^2$) | 5.43 | 5.56 | 5.87 | 0.25" thick UV resistant HDPE clear sheets |
| | Panel Surface (Flat panel only) ($/$ft^2$) | 0.15 | 0.16 | 0.18 | 1/100" thick double-layered clear LDPE sheets |
| | Water cooling/makeup Tubes | 0.79 | 0.88 | 0.97 | 0.8" dia. PVC [119] |

***** Add 1.0 cents/$gal_{TAG}$ feed for maximum jet product slate

††††† All PVC tubes are schedule 80 thick-walled dark gray unthreaded unless otherwise noted

| | | | | | |
|---|---|---|---|---|---|
| | Piping U-Bend Linkages ($/unit) | 1.51 | 1.68 | 1.85 | 5/8-1.0" dia. PVC [119] |
| | T-Branch Linkages ($/unit) | 4.88 | 5.42 | 5.96 | 1-1.25" dia. PVC [119] |
| | Airlift Pumps ($/unit) | 170 | 190 | 210 | Similar PBR size as in [119] |
| | Circulation Pumps ($/unit) | 540 | 600 | 660 | |
| Open Pond Downstream Tubes†††† | Source to manifold | 6 | 9 | 15 | 10-20" dia. PVC [50] |
| | Manifold to growth ponds | 4.15 | 4.61 | 5.07 | 3" dia. PVC 10’ lengths [119] |
| | Ponds to primary harvesting | 0.57 | 0.64 | 0.70 | 0.6" dia. PVC 10’ lengths [119] |
| | Primary harvesting to source (blowdown) | 0.41 | 0.46 | 0.51 | 0.25" PVC dia. 8’ lengths [119] |
| | Primary harvesting to secondary harvesting | 1.04 | 1.16 | 1.27 | 1.2" PVC dia. 10’ lengths [119] |
| | Primary harvesting to ponds (recycle) | 0.00 | 0.01 | 0.00 | 0.3" PVC dia. 10’ lengths [119] |
| | Secondary harvesting to primary harvesting (recycle) | 0.57 | 0.64 | 0.70 | 0.6" PVC dia. 10’ lengths [119] |
| | Secondary harvesting to extraction | 4.15 | 4.61 | 5.07 | 6" PVC dia. 8’ lengths [119] |
| | Extraction to digester | 4.15 | 4.61 | 5.07 | 3" PVC dia. 8’ lengths [119] |
| PBR Downstream Tubes††††† | PBR exit to skid row algae | 1.71 | 1.90 | 2.09 | 2" PVC dia. 10’ lengths [119] |
| | PBR exit to skid row water | 1.71 | 1.90 | 2.09 | 2" PVC dia. 10’ lengths [119] |
| | Skid row to cluster artery algae | 1.30 | 1.45 | 1.59 | 4" PVC dia. 10’ lengths; sewer pipe [119] |
| | Skid row to cluster artery water | 1.32 | 1.46 | 1.61 | 4" PVC dia. 10’ lengths; sewer pipe [119] |
| | Cluster artery to system algae | 3.38 | 3.75 | 4.13 | 8" PVC dia. 10’ lengths [119] |
| | Cluster artery to system water | 3.38 | 3.75 | 4.13 | 8" PVC dia. 10’ lengths [119] |
| | System to DAF algae | 22 | 25 | 30 | 12" PVC dia. Vendor Input |
| | System to cluster central arteries water | 22 | 25 | 30 | 12" PVC dia. Vendor Input |
| | DAFs to boundary (blowdown water) | 22 | 25 | 30 | 12" PVC dia. Vendor input |
| | DAFs to centrifuges | 0.75 | 0.83 | 0.91 | 1.6" PVC dia. 10’ lengths [119] |
| | DAFs to cluster artery (recycled water) | 22 | 25 | 30 | 12" PVC dia. Vendor input |
| | Centrifuge to DAF (recycled water) | 1.32 | 1.47 | 1.61 | 1.6" PVC dia. 10’ lengths [119] |
| | Centrifuge to extraction | 1.32 | 1.47 | 1.61 | 1.6" PVC dia. 10’ lengths [119] |
| | Extraction to digester | 4.15 | 4.61 | 5.07 | 3" PVC dia. 10’ lengths [119] |

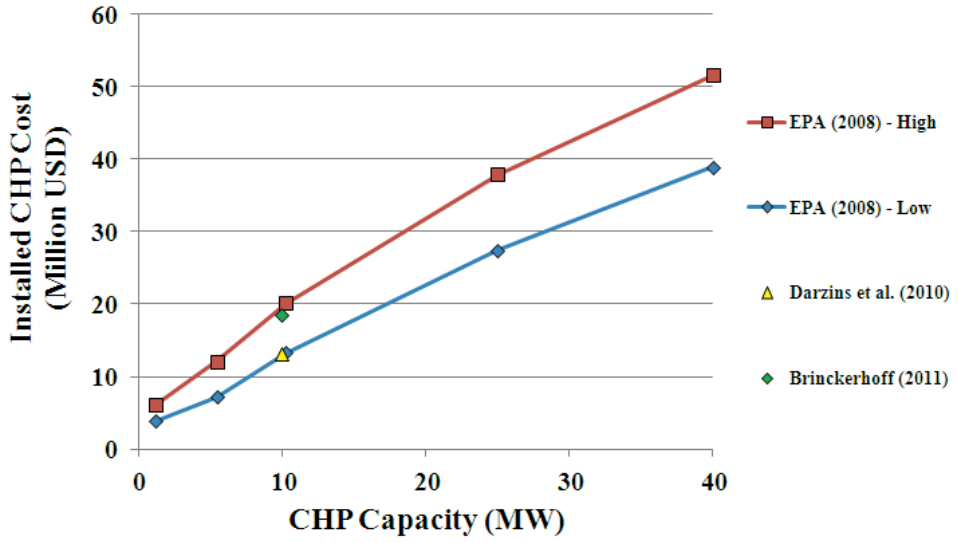


Figure B1: Combined Heat and Power Unit Installed Capital Cost Based on Energy Generation Capacity (~3.0 MW for 400 ha Open Pond Facility) [92,116,117]

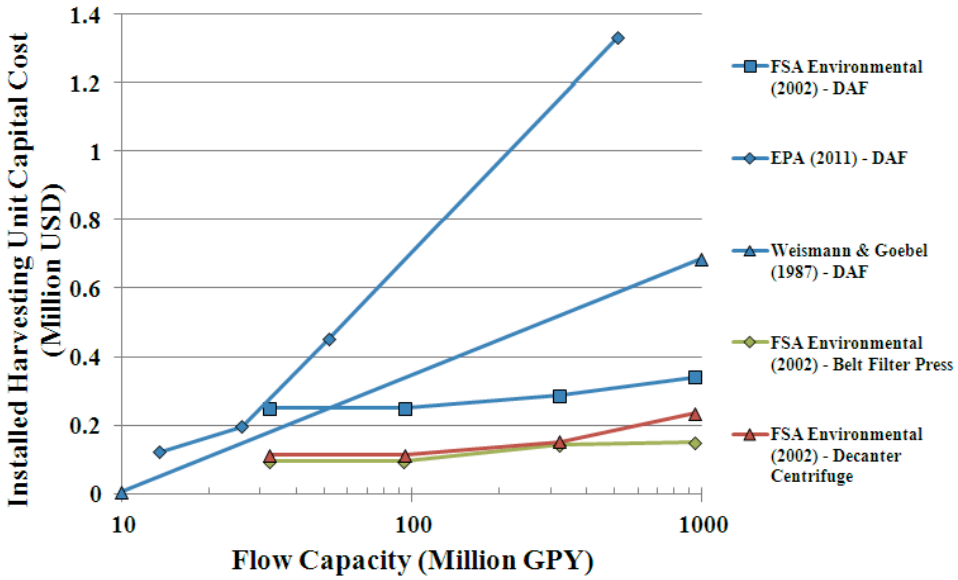


Figure B2: Dissolved Air Flotation, Belt Filter Press, Disc Centrifuge, and Decanter Centrifuge Installed Capital Cost Based on Flow Capacity (2890, 32.8, 210, and 526 Million GPY, respectively) [50,112,113,114,115]

$$C(\$) = aQ^b h^c$$
$$a = 2.58$$
$$b = 0.7 \qquad \text{(B1)}$$
$$c = 0.4$$

Table B2: Other Capital Expenses and Total Project Investment (TPI) Buildup

| Other Capital Expenses ($/ha) | Low | Baseline | High | Notes/Refs. |
|---|---|---|---|---|
| Land | 11,250 | 12,500 | 13,750 | Baseline - [117] |
| Outside Battery Limits (OSBL) | 50%×ISBL | | | Includes storage, basic process utilities, roads, and fences; based on upgrading plant heuristics for a greenfield facility [91] |
| Special | 4.0%×(ISBL+OSBL+Land) | | | Includes land, project management, and office and lab furniture [91] |
| Contingency | 15%×(ISBL+Special) | | | [91] |
| Installed Capital Cost (ICC) | Land+ISBL+OSBL+Special+Contingency | | | [91] |
| Total Project Investment (TPI) | 115%×ICC | | | Includes startup of 15% ICC [91] |

## Fixed Operating Expenses

Table B3: Algae Cultivation, Harvesting, and Extraction Facility Staff and Salaries

| Facility staff | Low | Baseline | High | Notes/Refs. |
|---|---|---|---|---|
| Facility manager | 1 | 1 | 1 | Salary – 90k $/yr |
| Operations manager | 1 | 1 | 1 | Salary – 90k $/yr |
| Maintenance manager | 1 | 1 | 1 | Salary – 75k $/yr |
| Engineers | 3 | 3 | 3 | Salary – 80k $/yr |
| Operators | 32 | 32 | 32 | Salary – 50k $/yr; Enough operators to inspect facility in 8 hour shifts for a 400 ha facility |
| Laboratory personnel | 2 | 2 | 2 | Salary – 60k $/yr |
| Technicians | 2 | 2 | 2 | Salary – 55k $/yr |
| Clerical personnel | 4 | 4 | 4 | Salary – 50k $/yr |
| Total | 46 | 46 | 46 | |
| Average staff salary ($) | 35,000 | 55,000 | 72,000 | |
| Salary overhead | 1.25 | 1.25 | 1.25 | |

Table B4: Fixed Operating Cost Variability Scenario Inputs

| Fixed Operating Costs (Million $/yr) | Low | Baseline | High | Notes/Refs. |
|---|---|---|---|---|
| Land lease | | 0 | | |
| Royalties | | 0 | | |
| Insurance | | 0.5%×TPI | | |
| Local taxes | | 1.0%×TPI | | |
| Maintenance (Salaries and equipment) | | 5.5%×TPI | | [33,91] |
| Miscellaneous supplies | | 0.15%×TPI | | |
| Salary total | 2.01 | 3.16 | 4.14 | |
| Contingency | 10%×(Land Lease+Royalties+Insurance+Local taxes+Maintenance+Miscellaneous supplies+Salary) | | | |
| Upgrading (cents/gal$_{TAG}$) | 13 | 17 | 23 | Includes similar breakdown of costs for upgrading facility [33] |

Variable Operating Expenses

Table B5: Variable Operating Cost Variability Scenario Inputs

| Variable Operating Costs | Low | Baseline | High | Notes/Refs. |
|---|---|---|---|---|
| Water ($/gal) | 0.001 | 0.001 | 0.001 | Baseline - [92] |
| Power ($/kWh) | 0.06 | 0.07 | 0.07 | Baseline - [92] |
| Natural gas ($/scf) | 0.007 | 0.008 | 0.009 | Baseline - [33] |
| Hydrogen ($/scf) | 0.005 | 0.006 | 0.007 | Baseline - [33] |
| Hexane ($/kg) | 1.00 | 1.50 | 2.00 | Low/Baseline/High – 10 ton minimum [120] |
| Potassium hydroxide ($/kg) | 0.42 | 1.18 | 3.44 | Baseline - [121] |
| Nitrogen (urea) ($/kg) | 0.42 | 0.46 | 0.51 | Low - [122], Baseline - [123], High - [124] |
| Hydrochloric acid ($/kg) | 0.13 | 0.15 | 0.17 | Low/High - [125] |
| Potassium pentoxide ($/kg) | 1.00 | 1.20 | 1.40 | Low/High - [126] |
| Ferric Iron ($/kg) | 0.04 | 0.04 | 0.05 | Baseline - [94] |
| Upgrading (¢/$gal_{TAG}$) | 13 | 17 | 23 | Includes similar breakdown of costs for upgrading facility [33] |

*[Page Intentionally Left Blank]*

# Appendix C – Photobioreactor Model Development

## Horizontal and Vertical Tubular Model Derivations

### System-wide energy balance derivation

$$\dot{E}_{pump} = nmP_r P_a U_L A_{sc} \tag{C1}$$

$$\dot{E}_{airlift} = nm\rho_L g h_L \varepsilon_r U_L A_{sc} \tag{C2}$$

Haaland friction coefficient approximation of moody chart (plastic roughness) in fully filled, turbulent pipe flow

$$\varepsilon_m = 0.0000025m \text{ (for glass, plastic, and perspex)}$$

$$k_B = \left(-1.8\log\left[\left(\frac{\varepsilon_m / d_{sc}}{3.7}\right)^{1.1} + \frac{6.9}{\mathrm{Re}}\right]\right)^{-2} \frac{L}{d} \tag{C3}$$

$$k_{B_{sc}} = \left(-1.8\log\left[\left(\frac{\varepsilon_m / d_{sc}}{3.7}\right)^{1.1} + \frac{\mu_L 6.9}{\rho_L U_L d_{sc}}\right]\right)^{-2} \frac{L_{sc}}{d_{sc}} \quad and$$

$$k_{B_{np}} = \left(-1.8\log\left[\left(\frac{\varepsilon_m / d_{np}}{3.7}\right)^{1.1} + \frac{\mu_L 6.9}{\rho_L U_{L_{np}} d_{np}}\right]\right)^{-2} \frac{L_{np}}{d_{sc}} \tag{C4}$$

$$\dot{E}_{friction} = mn\frac{1}{2}\rho_L U_L^3 k_{B_{sc}} A_{sc} + m\frac{1}{2}\rho_L U_{L_{np}}^3 k_{B_{np}} A_{np}$$

$$\dot{E}_{friction} = \left[\begin{array}{l} mn\frac{1}{2}\rho_L U_L^3\left(-1.8\log\left[\left(\frac{\varepsilon_m / d_{sc}}{3.7}\right)^{1.1} + \frac{\mu_L 6.9}{\rho_L U_L d_{sc}}\right]\right)^{-2} \frac{L_{sc}}{d_{sc}} A_{sc} + \\ \frac{1}{2}\rho_L U_{L_{np}}^3\left(-1.8\log\left[\left(\frac{\varepsilon_m / d_{np}}{3.7}\right)^{1.1} + \frac{\mu_L 6.9}{\rho_L U_{L_{np}} d_{np}}\right]\right)^{-2} \frac{L_{np}}{d_{sc}} A_{np} \end{array}\right] \tag{C5}$$

$$\dot{E}_{friction} = \left[\begin{array}{l} mn\frac{1}{2}\rho_L U_L^3\left(-1.8\log\left[\left(\frac{\varepsilon_m / d_{sc}}{3.7}\right)^{1.1} + \frac{\mu_L 6.9}{\rho_L U_L d_{sc}}\right]\right)^{-2} \frac{L_{sc}}{d_{sc}} A_{sc} + \\ m\frac{1}{2}\rho_L U_L^3\left(\frac{A_{sc}}{A_{np}}\right)^3\left(-1.8\log\left[\left(\frac{\varepsilon_m / d_{np}}{3.7}\right)^{1.1} + \frac{\mu_L 6.9}{\rho_L U_L\left(\frac{A_{sc}}{A_{np}}\right) d_{np}}\right]\right)^{-2} \frac{L_{np}}{d_{np}} A_{np} \end{array}\right]$$

$$\dot{E}_{head} = \frac{1}{2} nm\rho_L h_{sc} A_{sc} U_L^3 + \frac{1}{2} m\rho_L h_{np} A_{np} U_{L_{np}}^3$$

$$\dot{E}_{head} = \frac{1}{2} nm\rho_L h_{sc} A_{sc} U_L^3 + \frac{1}{2} m\rho_L h_{np} A_{np} U_L^3 \left(\frac{A_{sc}}{A_{np}}\right)^3 \tag{C6}$$

$$\dot{E}_{head} = \frac{1}{2} \rho_L U_L^3 \left[ nmh_{sc} A_{sc} + mh_{np} A_{np} \left(\frac{A_{sc}}{A_{np}}\right)^3 \right]$$

$$\dot{E}_{potential} = nm\rho_L g \Delta h A_{sc} U_L \tag{C7}$$

Assume all solar collector tubes share a single nonproductive tubing line to the degasser per quadrant (m)

$$\dot{E}_{pump} + \dot{E}_{airlift} = \dot{E}_{friction} + \dot{E}_{potential} + \dot{E}_{head}$$

$$nmP_r P_a U_L A_{sc} + nm\rho_L g h_L \varepsilon_r U_L A_{sc} = \left\{ \begin{array}{l} mn \frac{1}{2} \rho_L U_L^3 \left( -1.8 \log \left[ \left( \frac{\varepsilon / d_{sc}}{3.7} \right)^{1.1} + \frac{\mu_L 6.9}{\rho_L U_L d_{sc}} \right] \right)^{-2} \frac{L_{sc}}{d_{sc}} A_{sc} + \\ m \frac{1}{2} \rho_L U_L^3 \left( \frac{A_{sc}}{A_{np}} \right)^3 \left( -1.8 \log \left[ \left( \frac{\varepsilon / d_{np}}{3.7} \right)^{1.1} + \frac{\mu_L 6.9}{\rho_L U_L \left( \frac{A_{sc}}{A_{np}} \right) d_{np}} \right] \right)^{-2} \frac{L_{np}}{d_{np}} A_{np} + \\ nm\rho_L g \Delta h A_{sc} U_L + \frac{1}{2} \rho_L U_L^3 \left[ nmh_{sc} A_{sc} + mh_{np} A_{np} \left( \frac{A_{sc}}{A_{np}} \right)^3 \right] \end{array} \right\} \tag{C8}$$

$$P_r P_a + \rho_L g h_L \varepsilon_r = \left\{ \begin{array}{l} \frac{1}{2} \rho_L U_L^2 \left( -1.8 \log \left[ \left( \frac{\varepsilon / d_{sc}}{3.7} \right)^{1.1} + \frac{\mu_L 6.9}{\rho_L U_L d_{sc}} \right] \right)^{-2} \frac{L_{sc}}{d_{sc}} A_{sc} + \\ \frac{1}{2n} \rho_L U_L^2 \left( \frac{A_{sc}}{A_{np}} \right)^2 \left( -1.8 \log \left[ \left( \frac{\varepsilon / d_{np}}{3.7} \right)^{1.1} + \frac{\mu_L 6.9}{\rho_L U_L \left( \frac{A_{sc}}{A_{np}} \right) d_{np}} \right] \right)^{-2} \frac{L_{np}}{d_{np}} + \\ \rho_L g \Delta h + \frac{1}{2} \rho_L U_L^2 \left[ h_{sc} + \frac{h_{np}}{n} \left( \frac{A_{sc}}{A_{np}} \right)^2 \right] \end{array} \right\}$$

**Oxygen balance derivation**

Oxygen balance options include an uncoupled $C_L$ and $C_{sat}$ oxygen balance without pressure effects (C9), an uncoupled $C_L$ and $C_{sat}$ oxygen balance with pressure effects (C10), and a coupled $C_L$ and $C_{sat}$ oxygen balance with pressure effects (C11). Accuracy increased compared to experimental results with increasing balance complexity, however, the coupled equation solutions are unstable for certain model inputs due to machine precision limitations. Therefore, (C10) was used as an oxygen balance in this study. The full derivation of this oxygen balance is shown in (C12). All oxygen balance relations are from the fundamental relation in [87].

$$\frac{dC_L}{dh} = \frac{(1-\varepsilon_r)k_L a}{U_L}\left(C_{sat} - C_L\right) \text{ and } C_L(0) = \gamma C_{sat} \tag{C9}$$

$$\frac{dC_L}{dh} = \frac{(1-\varepsilon_r)k_L a}{U_L}\left[C_{sat}\left(1+\frac{\rho_L g(h_L-h)}{P_a}\right) - C_L\right] \text{ and } C_L(0) = \gamma C_{sat} \tag{C10}$$

$$\frac{dC_L}{dh} = \frac{(1-\varepsilon_r)k_L a}{U_L}\left[C_{sat}\left(1+\frac{\rho_L g(h_L-h)}{P_a}\right) - C_L\right] \text{ and } C_L(0) = \gamma C_{sat}$$

$$\frac{dC_{sat}}{dh} = -\frac{M_{air}c_{water}k_L a(1-\varepsilon_r)}{\rho_{air}\left(\frac{U_L}{1-\varepsilon_r}+U_b\right)\varepsilon_r}\left[C_{sat}\left(1+\frac{\rho_L g(h_L-h)}{P_a}\right) - C_L\right] \text{ and } C_{sat}(0) = C_{sat} \tag{C11}$$

$$\frac{dC_L}{dt} = k_L a\left(C_{sat} - C_L\right) = k_L a(1-\varepsilon_r)\left(C_{sat}\frac{P(h)}{P_a} - C_L\right)$$

$$\frac{dC_L}{dh} = \frac{k_L a(1-\varepsilon_r)}{U_L}\left(C_{sat}\frac{P(h)}{P_a} - C_L\right) \tag{C12}$$

$$\frac{dC_L}{dh} = \frac{(1-\varepsilon_r)k_L a}{U_L}\left[C_{sat}\left(1+\frac{\rho_L g(h_L-h)}{P_a}\right) - C_L\right] \text{ and } C_L(0) = \gamma C_{sat}$$

Solve ODE in (C12) assuming constant $C_{sat}$ for some height $h$ in the degasser

$$C_L(h)=\left[\begin{array}{l} e^{-k_L a\frac{(1-\varepsilon_r)}{U_L}h}\left(\gamma C_{sat}-C_{sat}\left(1+\frac{\rho_L g h_L}{P_a}\right)-C_{sat}\frac{U_L\rho g}{k_L a(1-\varepsilon_r)P_a}\right)+ \\ C_{sat}\left(1+\frac{\rho_L g h_L}{P_a}+\frac{\rho_L g}{P_a}\frac{U_L}{(1-\varepsilon_r)k_L a}-\frac{\rho_L g h}{P_a}\right)\end{array}\right]$$

$$C_L(h)=C_{sat}\left[\begin{array}{l} e^{-k_L a\frac{(1-\varepsilon_r)}{U_L}h}\left(\gamma-1+\frac{(1-\varepsilon_r)\rho_L g h_L}{P_a}-\frac{U_L\rho_L g}{k_L a(1-\varepsilon_r)P_a}\right)+1+\frac{(1-\varepsilon_r)\rho_L g h_L}{P_a}+ \\ \frac{U_L\rho_L g(1-\varepsilon_r)}{k_L a(1-\varepsilon_r)P_a}-\frac{(1-\varepsilon_r)\rho_L g h}{P_a}\end{array}\right] \quad \text{(C13)}$$

$$C_L(h_L)=C_{sat}\left[\begin{array}{l} e^{-k_L a\frac{(1-\varepsilon_r)}{U_L}h_L}\left(\gamma-1+\frac{(1-\varepsilon_r)\rho_L g h_L}{P_a}-\frac{U_L(1-\varepsilon_r)\rho_L g}{k_L a(1-\varepsilon_r)P_a}\right)+1+\frac{(1-\varepsilon_r)\rho_L g h_L}{P_a}+ \\ \frac{U_L(1-\varepsilon_r)\rho_L g}{k_L a(1-\varepsilon_r)P_a}-\frac{(1-\varepsilon_r)\rho_L g h_L}{P_a}\end{array}\right]$$

$$A=k_L a\frac{(1-\varepsilon_r)}{U_L} \quad E=1+\frac{\rho_L g h_L(1-\varepsilon_r)}{P_a} \quad F=\frac{\rho_L g(1-\varepsilon_r)}{P_a}$$

$$C_L(h_L)=C_{sat}\left[e^{-Ah_L}\left(\gamma-E-\frac{F}{A}\right)+E+\frac{F}{A}-Fh_L\right]$$

Oxygen concentration at the solar collector inlet is assumed to be a weighted average of the dilution and makeup volumetric flows.

$$[O_2]_{in}=C_{sat}\left[\left(e^{-Ah_L}\left(\gamma-\frac{A\cdot E+F}{A}\right)+\frac{A\cdot E+F-A\cdot F\cdot h_L}{A}\right)\left(1-\frac{D}{A_{sc}U_L}\right)+\frac{D}{A_{sc}U_L}\right] \quad \text{(C14)}$$

Solar collector length relation in (C15) from [55]

$$L_{sc}=\frac{U_L\left([O_2]_{out}-[O_2]_{in}\right)}{R_{O_2}}=\frac{U_L\left(C_{sat}\gamma-[O_2]_{in}\right)}{R_{O_2}}$$

$$L_{sc}=\frac{U_L C_{sat}}{\alpha\cdot P}\left[\gamma-\left(\left(e^{-Ah_L}\left(\gamma-\frac{A\cdot E+F}{A}\right)+\frac{A\cdot E+F-A\cdot F\cdot h_L}{A}\right)\left(1-\frac{D}{A_{sc}U_L}\right)+\frac{D}{A_{sc}U_L}\right)\right] \text{ or} \quad \text{(C15)}$$

$$L_{sc}=\frac{U_L C_{sat}}{\alpha\cdot P}\left[\gamma-\left(\left(e^{-Ah_L}\left(\gamma-\frac{A\cdot E+F}{A}\right)+\frac{A\cdot E+F-A\cdot F\cdot h_L}{A}\right)\left(1-\frac{P\cdot L_{sc}}{C_s\cdot U_L}\right)+\frac{P\cdot L_{sc}}{C_s\cdot U_L}\right)\right]$$

**Mass transfer and gas holdup**

Semi-empirical relationships in (C16) and (C17) from [55]

$$k_L a = \frac{6\varepsilon_r}{1-\varepsilon_r}\left[5.63\cdot 10^{-5}\left(\frac{gD_L\rho_L^2\sigma_L}{\mu_L^3}\right)^{0.5} e^{-0.131C_s^2}\right] \text{ or}$$

$$k_L a = \frac{6\varepsilon_r}{1-\varepsilon_r}\left[5.63\cdot 10^{-5}\left(\frac{gD_L\rho_L^2\sigma_L}{\mu_L^3}\right)^{0.5} e^{-0.131\left(\frac{P\cdot A_{sc}\cdot L_{sc}}{D}\right)^2}\right] \quad \text{(C16)}$$

$U_G$ derived assuming steady, 1-D flow and that air density scales with pressure as an ideal gas

$$U_G = \frac{\dot{m}_{air}}{\rho_{air}\cdot A_r}\left(\frac{P_a}{P_a+\frac{1}{2}\rho_L g h_L}\right) = \frac{\dot{m}_{air}}{\rho_{air}A_r\left(1+\frac{1}{2}\frac{\rho_L g h_L}{P_a}\right)} = \frac{\dot{m}_{air}}{\rho_{air}A_r\left(1+\frac{\rho_L g h_L}{P_a}-\frac{\rho_L g h_L}{2P_a}\right)}$$

$$U_G = \frac{\dot{m}_{air}}{\rho_{air}A_r\left(E-\frac{1}{2}Fh_L\right)}$$

$$\varepsilon_r = \frac{\beta}{\lambda+\frac{U_b}{U_G+U_L}} \qquad \beta = \frac{U_G}{U_G+U_L} \quad \text{(C17)}$$

$$\varepsilon_r = \frac{\frac{U_G}{U_G+U_{L_r}}}{\lambda+\frac{U_b}{U_G+U_L}} = \frac{U_G}{\left(U_G+nmU_L\frac{A_{sc}}{A_r}\right)\lambda+U_b}$$

**Output derivations**

Assume calorically perfect gas; isentropic air compression

$$P_{input} = P_{pump} + P_{airlift}$$

$$P_{input} = \frac{P_r P_a}{\eta_p} A_{sc} U_L + \frac{\dot{m}_{air} C_p}{\eta_c} \left(T_b - T_a\right)$$

$$P_{input} = \frac{P_r P_a}{\eta_p} A_{sc} U_L + \frac{\dot{m}_{air} C_p T_a}{\eta_c} \left(\frac{T_b}{T_a} - 1\right) = \frac{P_r P_a}{\eta_p} A_{sc} U_L + \frac{\dot{m}_{air} C_p T_a}{\eta_c} \left[\left(\frac{P_b}{P_a}\right)^{\gamma - 1/\gamma} - 1\right] \tag{C18}$$

$$P_{input} = \frac{P_r P_a}{\eta_p} A_{sc} U_L + \frac{\dot{m}_{air} C_p T_a}{\eta_c} \left[\left(1 + \frac{\rho_L g h_L}{P_a}\right)^{\gamma - 1/\gamma} - 1\right]$$

$$P_{\text{algae}} = nmA_{sc} L_{sc} P \tag{C19}$$

$$E_s = \frac{P_{input}}{P_{\text{algae}}} \tag{C20}$$

$$P_{areal} = P \frac{V_p}{A_{PBR}} \tag{C21}$$

**Geometric and Head Loss Calculations**

Geometry notes: assumed average solar collector length if there is more than one solar collector; reference Figure C1 for a specific areal configuration of both horizontal and vertical serpentine tubular PBRs; U-bend caps are assumed to be nonproductive tubes that do not allow light through to the culture [54]

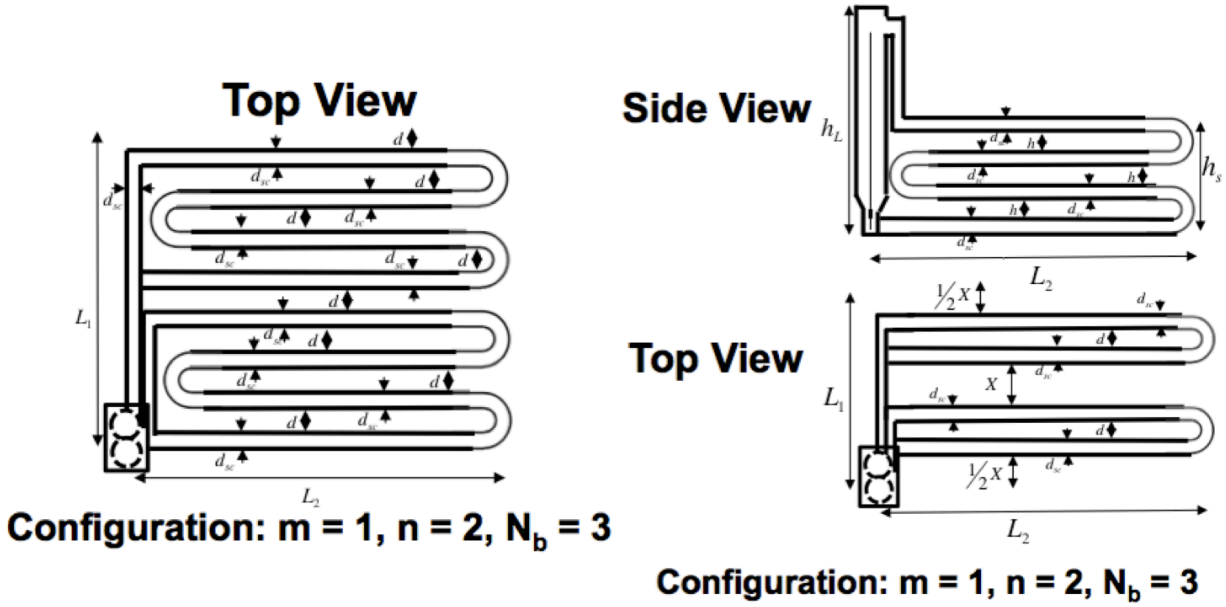


Figure C1: Reference Figure for Geometric Calculations: (a) Horizontal and (b) Vertical Serpentine Tubular PBRs

$$L_1 = \left(nN_b + n\right)\left(d_{sc} + d\right) \text{ for horizontal}$$
$$L_1 = nX + 2nd_{sc} + nd \text{ for vertical} \tag{C22}$$

$$h_s = d_{sc}\left(N_b + 1\right) + hN_b \text{ for vertical only} \tag{C23}$$

$$L_{sc} = \frac{1}{n}\sum_{i=1}^{n}\begin{Bmatrix} 2\left[L_2 - id_{sc} - \frac{1}{2}d - d_{sc}\right] + \\ \left(N_b - 1\right)\left[L_2 - id_{sc} - d - 2d_{sc}\right] \end{Bmatrix} = \left(N_b + 1\right)L_2 - \frac{d_{sc}}{2} + N_b d - \frac{5}{2}N_b d_{sc} + \frac{1}{2}n\left(N_b + 1\right)d_{sc} \tag{C24}$$

$$L_2 = \frac{1}{\left(N_b + 1\right)}\left[L_{sc} + \frac{1}{2}d_{sc} + N_b d + \frac{5}{2}N_b d_{sc} + \frac{1}{2}n\left(N_b + 1\right)d_{sc}\right]$$

$$L_{np} = \frac{1}{n}\sum_{i=1}^{n}\left[N_b i\left(d + d_{sc}\right) + d\left(i - 1\right)\right] = \frac{1}{2}\left[N_b\left(d + d_{sc}\right) + n\left(d + N_b d + N_b d_{sc}\right) - d\right] \text{ for horizontal}$$
$$L_{np} = \frac{1}{n}\sum_{i=1}^{n}\left[\left(2d_{sc} + d\right)i + X\left(i - 1\right)\right] + \left(h_L - h_s\right) = \frac{1}{2}\left[d - X + n\left(X + d + 2d_{sc}\right)\right] + d_{sc} + \left(h_L - h_s\right) \text{ for vertical} \tag{C25}$$

$$A_{PBR} = \begin{Bmatrix} L_1 L_2 + \frac{d_r}{2}L_1 + \frac{d_d}{2}L_2 \text{ for } m = 1 \\ mL_1 L_2 \text{ for } m = 2,4 \end{Bmatrix} \tag{C26}$$

Head losses

$$h_{v_{sc}} = mnN_b 0.2$$
$$h_{v_{np}} = mn0.3 + m\left(n - 1\right)0.2 + m1.0 \tag{C27}$$

## Flat Panel

Assume mass transfer only; well mixed with only pressure and potential energy losses

**Oxygen balance**

Oxygen balance plus oxygen production term in panel, assume average steady state concentration at a given height [87]

**Mass transfer and gas holdup**

From [55] for Equations (C28) and (C29); includes oxygen accumulation term $\alpha$ in flat panel

$$\frac{dC_L}{dt} = k_L a\left[C_{out} - C_L(h)\right]$$

$$\frac{dC_L}{dt} = k_L a\left[C_{sat}\left(1 + \frac{P_L(1-\varepsilon)\rho_L g h_L}{2P_a} - \gamma_i C_{sat}\right)\right] + P\cdot\alpha \tag{C28}$$

$$\gamma_i = \frac{P\cdot\alpha}{C_{sat}k_L a} + 1 + \frac{(1-\varepsilon)\rho_L g h_L}{2P_a}$$

$$k_L a = \frac{6\varepsilon}{1-\varepsilon}\left[5.63\cdot 10^{-5}\left(\frac{g D_L \rho_L^2 \sigma}{\mu_L^3}\right) e^{-0.131 C_S^2}\right] \tag{C29}$$

Relate pressure differences in the panel at various heights to the air mass flow rate

$$P_a = \rho_{air} RT$$

$$P_{airh} = P_a + (1-\varepsilon)\rho_L g h = \rho_{air} RT$$

$$\frac{P_{airh}}{P_a} = \frac{P_a + (1-\varepsilon)\rho_L g h}{P_a} = \frac{\rho_{airh} RT}{\rho_{air} RT} \tag{C30}$$

$$\rho_{airh} = \rho_{air}\frac{P_a + (1-\varepsilon)\rho_L g h}{P_a}$$

$$\dot{m}_{air} = \rho_{airh} L t U_G = \rho_{air}\frac{P_a + (1-\varepsilon)\rho_L g h}{P_a} L t U_G$$

Assume an average gas velocity $U_G$ taken at half of the panel height; Related volume specific power consumption to gas flow rate from [87] for (C32)

$$U_G(h) = \frac{\dot{m}_{air}}{\rho_{air} Lt\left(\frac{P_a + (1-\varepsilon)\rho_L g h}{P_a}\right)}$$
$$U_G\left(\frac{h}{2}\right) = \frac{\dot{m}_{air}}{\rho_{air} Lt\left(\frac{P_a + (1-\varepsilon)\rho_L g h}{2P_a}\right)} \tag{C31}$$

$$\frac{P_G}{V_L} = \frac{\rho_L g h}{V_L}\left(\frac{\dot{m}_{air}}{\rho_{air}}\right) = \frac{\rho_L g}{A}\dot{V}_{air} = \rho_L g U_G$$
$$\varepsilon = 3.32 \cdot 10^{-4}\left(\frac{P_G}{V_L}\right)^{0.97} = 3.32 \cdot 10^{-4}\left(\rho_L g U_G\right)^{0.97} \tag{C32}$$

$$\varepsilon = 3.32 \cdot 10^{-4}\left(\frac{\rho_L g \dot{m}_{air}}{\rho_{air}\left(1 + \frac{(1-\varepsilon)\rho_L g h_L}{2P_a}\right) Lt}\right)^{0.97} \tag{C33}$$

**Output derivations**

Assume calorically perfect gas; isentropic air compression; average aeration height

$$P_{in} = \frac{\dot{m}_{air} C_p T_{op}}{\eta_c}\left[\left(1 + \frac{(1-\varepsilon)\rho_L g h_L}{2P_a}\right)^{\frac{2}{7}} - 1\right] \tag{C34}$$

$$P_{\text{algae}} = Lth_L P \tag{C35}$$

$$E_s = \frac{P_{in}}{P_{\text{algae}}} \tag{C36}$$

$$P_{areal} = P\frac{V_p}{A_{PBR}} \tag{C37}$$

**Geometric Calculations**

Spacing ratio $X$ for flat panels based on [54]

$$X = h_L\left(\frac{1.4}{2.2}\right) \tag{C38}$$

$$A_{PBR} = L(2X + t) \tag{C39}$$

*[Page Intentionally Left Blank]*

# Appendix D – Photobioreactor Optimization Inputs and Results

Table D1: Tubular PBR Optimization Inputs

| Parameter | Symbol | Value | Units | Notes/Refs. |
|---|---|---|---|---|
| Atmospheric pressure | $P_a$ | 101,325 | Pa | - |
| Bubble velocity | $U_b$ | 0.3 | m/s | [55] |
| Radial flow velocity profile characteristic parameter | $\lambda$ | 1.1 | - | Usually 1.0-1.3 going from turbulent to laminar flow [55] |
| Acceleration due to gravity | g | 9.81 | $m/s^2$ | - |
| Oxygen production during photosynthesis | $\alpha$ | 4.66 | $kg_{O2}/kg_{algae}$ | 4.66 [53]<br>3.316 [55] |
| Heat capacity of air | $C_p$ | 1005 | J/kg/K | Assuming calorically perfect gas (CAP) for airlift energy relationship |
| Pump and air compressor efficiencies | $\eta_p$ and $\eta_c$ | 0.43 and 0.43 | - | 0.8 and 0.8 efficiencies for [54] |
| Diffuser angle in riser column | $\theta$ | 25 | degrees | Determines constrained relationship between $d_r$ and $h_L$ |
| Maximum concentration of $O_2$ at the degasser inlet normalized by the $O_2$ saturation concentration of water at standard pressure ($C_{sat}$) | $\gamma$ | 3.0 | - | Maximum value of 300% $C_{sat}$ [55] |
| Molar mass of $O_2$ | $O_{2\,mm}$ | 32 | g/mol | [68] |
| Mole fraction of $O_2$ in air | $O_{2\,mf}$ | 0.21 | - | [68] |
| Thickness of tubing wall | $t_w$ | 0.007 | m | [68] |
| Algae diameter | $d_{algae}$ | 5.0E-6 | m | Chlorella vulgaris |
| Salinity of culture medium | S | 0 | ppt | Range: 0-35 ppt |
| Operating temperature | $T_{op}$ | 293 | K | 273K – 323K |
| Air density | $\rho_{air}$ | Spline interpolated from database | $kg/m^3$ | [68] |
| Fluid density | $\rho_L$ | Spline interpolated from database | $kg/m^3$ | [68]<br>990 for [53] |
| Fluid viscosity | $\mu_L$ | Spline interpolated from database | kg/m/s | [68]<br>9E-4 for [53] |
| Medium interfacial tension (surface tension) | $\sigma$ | Spline interpolated from database | $J/m^2$ | [68]<br>0.073 for [53] |

| | | | | |
|---|---|---|---|---|
| Saturation concentration of O2 in water at ambient pressure | $C_{sat}$ | Spline interpolated from database | $kg/m^3$ | [68]<br>0.0081 for [53] |
| Diffusivity of O2 in water | $D_L$ | Spline interpolated from database | $m^2/s$ | [68]<br>2.06E-9 for [53] |
| Volumetric productivity | P | 0.6–1.5 (horizontal)<br>0.6–1.0 (vertical) | g/L/day | Table 2.6 |
| Dilution rate | D | 0.06 | m3/day | [53] |
| Number of arms per solar collector | m | 1.0 | - | Both for [53] and [55] |
| Number of solar collectors per arm | n | 1.0 | - | Both for [53] and [55] |
| Number of U-bends per solar collector | $N_b$ | 15 (horizontal); 17 (vertical) | - | 16 from [53]<br>17 from [55] |

Table D2: Flat Panel Optimization Inputs

| Parameter | Symbol | Value | Units | Notes |
|---|---|---|---|---|
| Atmospheric pressure | $P_a$ | 101,325 | Pa | - |
| Acceleration due to gravity | g | 9.81 | $m/s^2$ | - |
| Oxygen production during photosynthesis | α | 3.316 | $kg_{O2}/kg_{algae}$ | 4.66 [53]<br>3.316 [55] |
| Heat capacity of air | $C_p$ | 1005 | J/kg/K | Assuming calorically perfect gas for airlift energy relationship |
| Air compressor efficiency | $\eta_c$ | 0.43 | - | [53] |
| Salinity of culture medium | S | 0 | ppt | Range: 0-35 ppt |
| Operating temperature | $T_{op}$ | 293 | K | 273K – 323K |
| Air density | $\rho_{air}$ | Spline interpolated from database | $kg/m^3$ | [68] |
| Fluid density | $\rho_L$ | Spline interpolated from database | $kg/m^3$ | [68]<br>990 for [53] |
| Fluid viscosity | $\mu_L$ | Spline interpolated from database | kg/m/s | [68]<br>9E-4 for [53] |
| Medium interfacial tension (surface tension) | σ | Spline interpolated from database | $J/m^2$ | [68]<br>0.073 for [53] |
| Saturation concentration of O2 in water at ambient pressure | $C_{sat}$ | Spline interpolated from database | $kg/m^3$ | [68]<br>0.0081 for [53] |
| Diffusivity of O2 in water | $D_L$ | Spline interpolated from database | $m^2/s$ | [68]<br>2.06E-9 for [53] |
| Volumetric productivity | P | 0.6–2.4 | g/L/day | See Table 2.6 |
| Dilution rate | D | 0.06 | m3/day | [53] |
| Panel thickness | t | 0.07 | m | [56] |
| Panel length | L | 2.5 | m | [56] |
| Distance between PBRs | X | $h_L$*(1.4/2.2) | m | [55] |

| Optimize Specific Energy | | | | | | | | | | | | |
|---|---|---|---|---|---|---|---|---|---|---|---|---|
| | Flat Panel | | | | | | | | | | | |
| C | Polynomial Coefficients | | | | | | | | | | | |
| 1 | -190.43 | 18.8714 | 18.4063 | 0.00828 | 0.00071 | -5.9548 | 0.00419 | 58.5656 | -0.01832 | 0.002836 | 33.381279 | -1.27206E-08 |
| 2 | 427.076 | -57.252 | -73.164 | -0.0151 | -0.0017 | 9.2392 | -0.0077 | -232.79 | -79.2731 | -0.00519 | -145.5381 | -5.50508E-05 |
| 3 | -344.79 | 68.0325 | 82.3487 | 0.00969 | 0.00138 | -4.4543 | 0.00491 | 262.019 | 121.9124 | 0.003334 | 169.10304 | 8.46614E-05 |
| 4 | 172.184 | -39.244 | -35.17 | -0.0026 | -0.0005 | 3.50351 | -0.0013 | -111.91 | -50.3135 | -0.00089 | -73.35554 | -3.49399E-05 |
| 5 | -14.445 | 10.8985 | 8.00372 | 0.00343 | 0.00031 | 1.15827 | 0.00173 | 25.6414 | 8.972441 | 0.001136 | 17.562318 | 6.23086E-06 |
| $R^2$ | 0.99994 | 0.99989 | 0.96254 | 0.99175 | 0.9697 | 0.99865 | 0.99176 | 0.96254 | 0.939527 | 0.991803 | 0.9649072 | 0.939526938 |

| Opt_Type | Productivity, P (g/L/day) | Areal Productivity, P_areal (g/m$^2$/day) | Specific Energy, E_s (MJ/kg-algae) | Panel height, h_L (m) | Panel gas holdup, ε (-) | Panel air mass flow rate, mdot_air (kg/s) | Max O2 concentration multiple of saturation at degasser inlet, gamma (-) | Volumetric gas-liquid mass transfer coefficient, kLa (1/s) | Panel surface area, A (m2) | Biomass concentration, Cs (kg/m3) | Superficial gas velocity in riser, U_G (m/s) | Total algae production, P_system (kg/s) | Total algae production, P_system (kg/s) |
|---|---|---|---|---|---|---|---|---|---|---|---|---|---|
| 1 | 0.3 | 16.2029 | 3.85853 | 3 | 0.00319 | 0.00025 | 2.00637 | 0.00161 | 9.72045 | 2.625 | 0.001054 | 7.0337706 | 1.82E-06 |
| 1 | 0.4 | 21.6039 | 2.89389 | 3 | 0.00319 | 0.00025 | 2.29371 | 0.00161 | 9.72045 | 3.5 | 0.001054 | 7.0337706 | 2.43E-06 |
| 1 | 0.5 | 27.0049 | 2.31512 | 3 | 0.00319 | 0.00025 | 2.58105 | 0.00161 | 9.72045 | 4.375 | 0.001054 | 7.0337706 | 3.04E-06 |
| 1 | 0.6 | 32.4059 | 1.92926 | 3 | 0.00319 | 0.00025 | 2.8684 | 0.00161 | 9.72045 | 5.25 | 0.001054 | 7.0337706 | 3.65E-06 |
| 1 | 0.7 | 37.8069 | 1.65365 | 3 | 0.00319 | 0.00025 | 3.15574 | 0.00161 | 9.72045 | 6.125 | 0.001054 | 7.0337706 | 4.25E-06 |
| 1 | 0.8 | 43.2079 | 1.44695 | 3 | 0.00319 | 0.00025 | 3.44309 | 0.00161 | 9.72045 | 7 | 0.001054 | 7.0337706 | 4.86E-06 |
| 1 | 0.9 | 47.7541 | 1.34384 | 1.50433 | 0.0034 | 0.00025 | 3.5 | 0.00171 | 4.96151 | 3.948867 | 0.001124 | 3.6851707 | 2.74E-06 |
| 1 | 1 | 49.5495 | 1.30195 | 0.5 | 0.0037 | 0.00026 | 3.5 | 0.00187 | 1.76591 | 1.458333 | 0.001228 | 1.3185227 | 1.01E-06 |

Figure D1: A Screenshot Example of Optimized PBR Model Output Ranges; Each Volumetric Productivity Row is a Different Optimized PBR Design; Each Dependent Output Parameter Column is Fit With Corresponding Polynomial Coefficients to be Used in Scenarios Throughout the Lifecycle Model

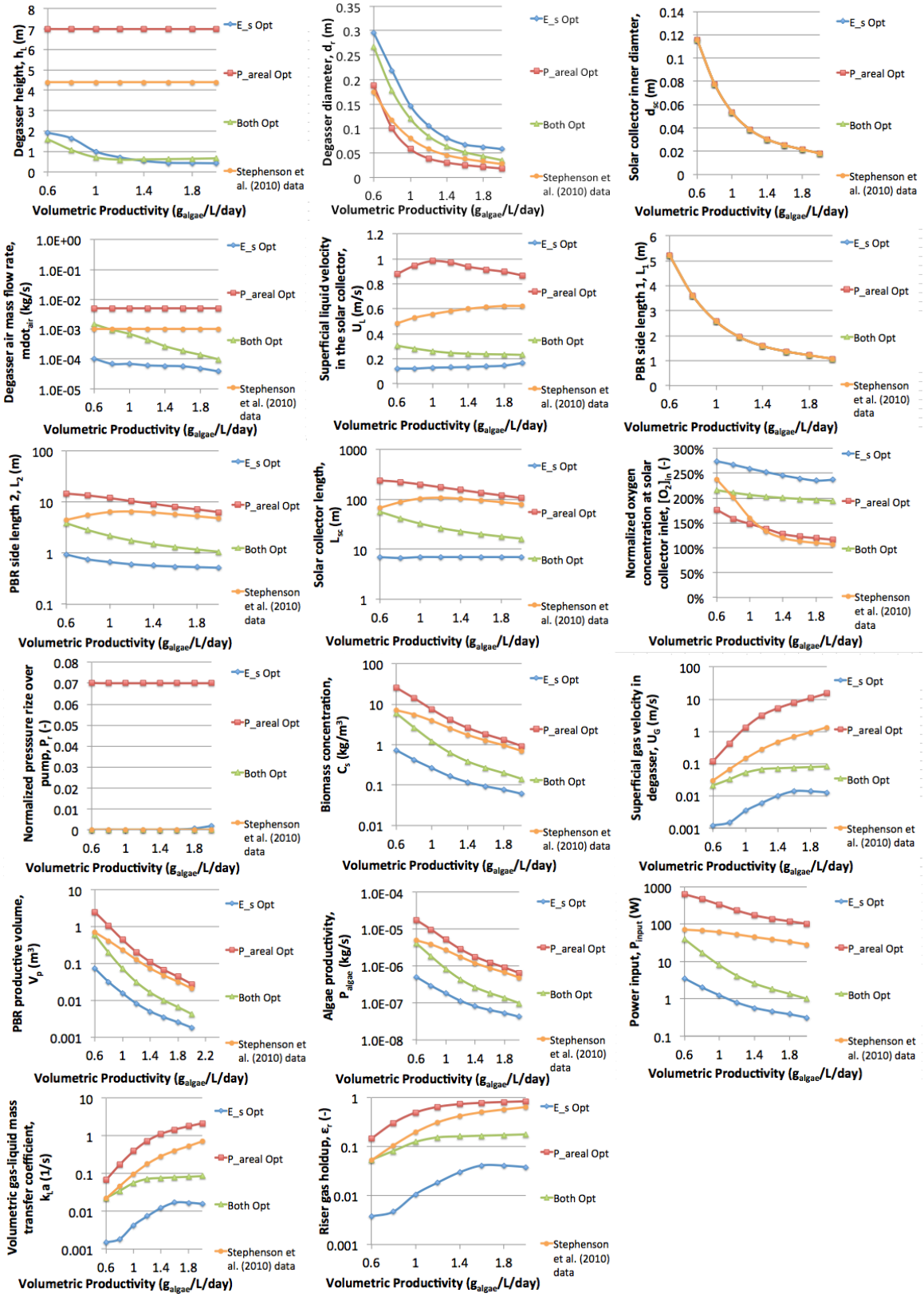


Figure D2: Horizontal Tubular Serpentine PBR Optimization Output Parameters for Various Volumetric Productivities

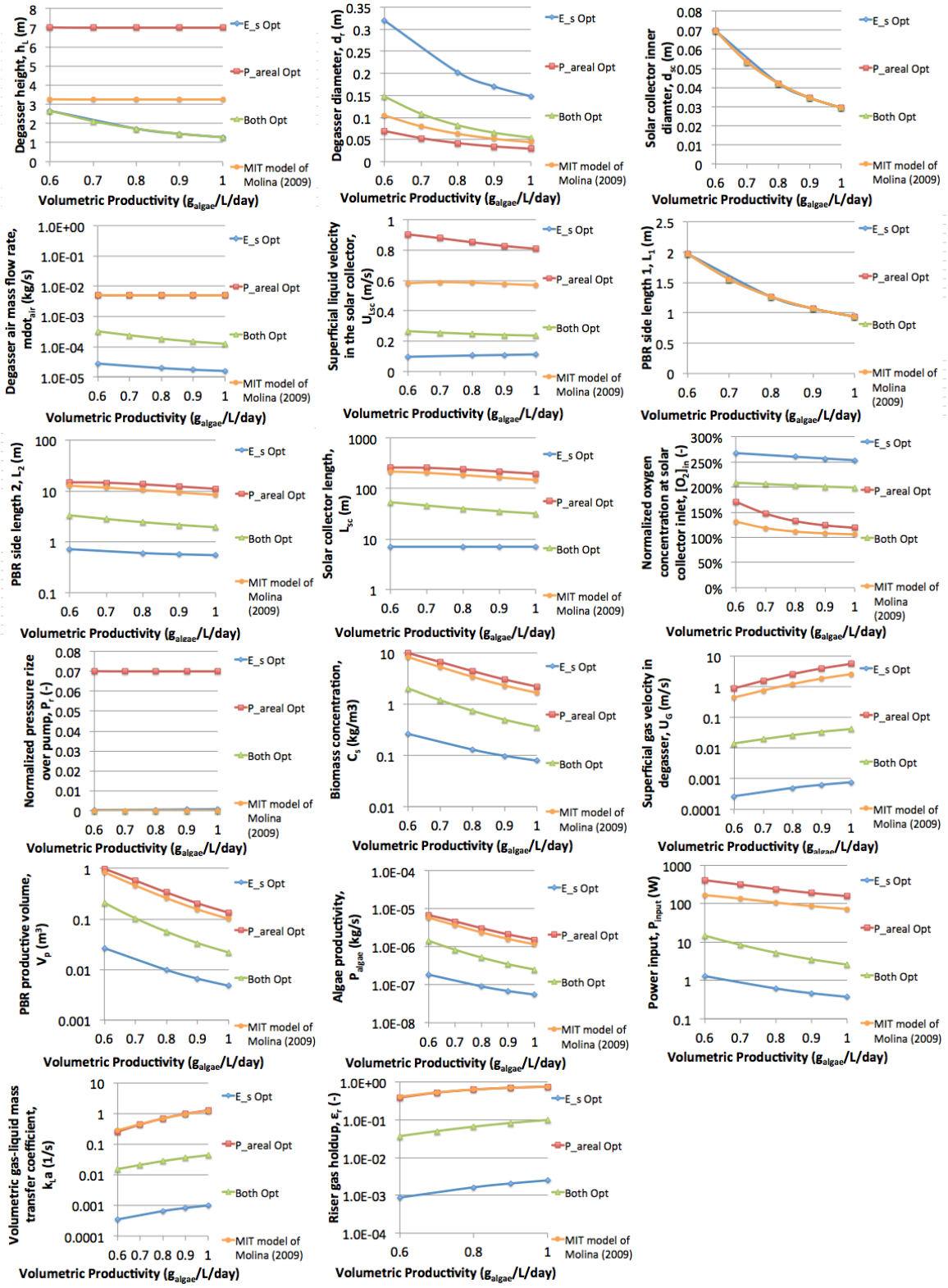


Figure D3: Vertical Tubular Serpentine PBR Optimization Output Parameters for Various Volumetric Productivities

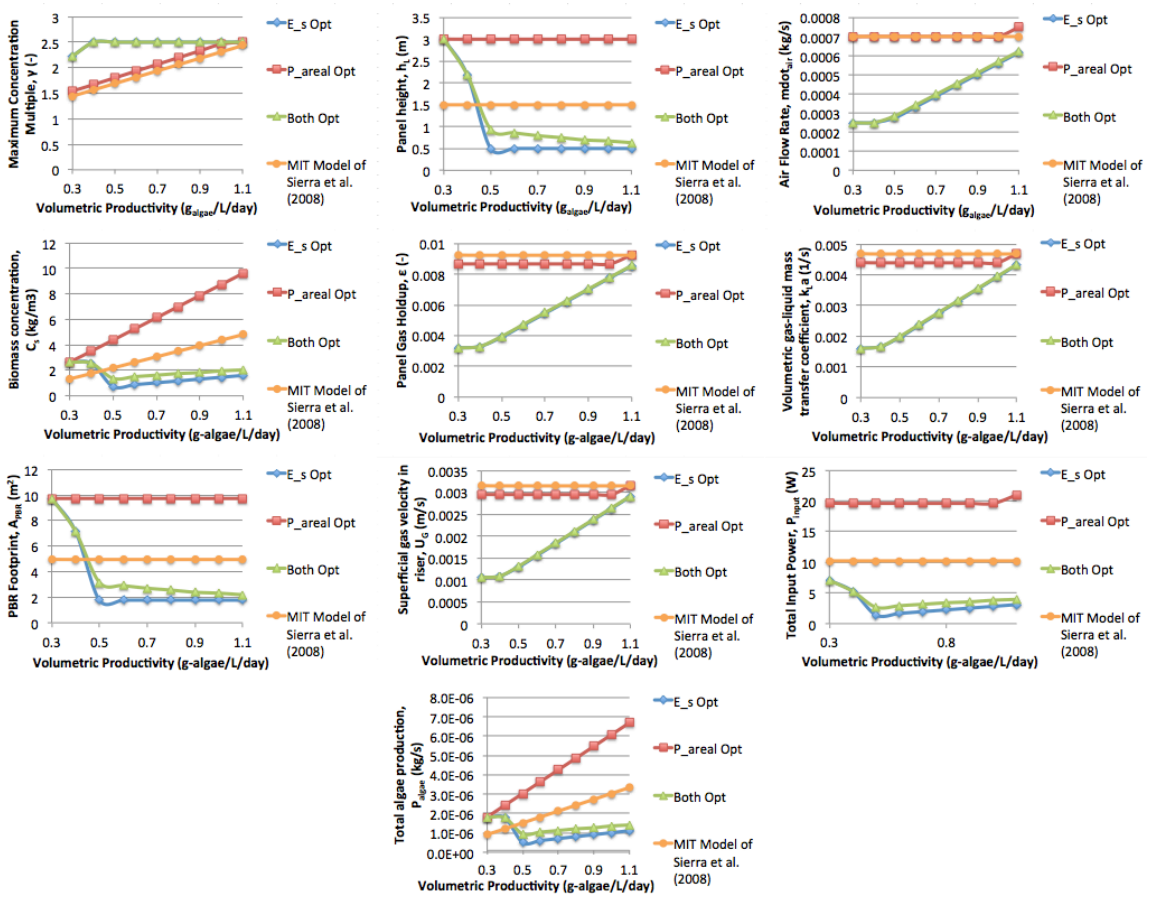


Figure D4: Flat Panel PBR Optimization Output Parameters for Various Volumetric Productivities

*[Page Intentionally Left Blank]*

## Appendix E – Air Quality Emissions from Conventional and Synthetic Jet Fuels

Air quality emissions from aircraft combustion are primarily functions of atmospheric conditions, fuel composition and gas turbine engine parameters. As seen in Figure 1.1, the majority of conventional jet fuel is comprised of normal, iso-, and cyclo- paraffins with up to a quarter of the fuel consisting of aromatics and naphthalenes. ~700 ppm sulfur is also present in conventional jet fuels [127,128]. As described previously, SPK fuels lack aromatics and sulfur that leads to a decrease in surface air quality emissions. These emissions are loosely defined as particles under 3,000 feet and are associated with direct or indirect impacts on plant life and human health through acid rain, ozone, and other forms of air pollution. There are two types of standards surrounding air quality: those directed at engine emissions and those aimed at regional ambient pollutant concentrations. Engine emissions of smoke, unburned hydrocarbons, carbon monoxide and nitrogen oxides from the commercial fleet must meet the internationally agreed upon ICAO Annex 16 Volume II standards [129]. Regional ambient air pollutant concentrations in the United States must meet the EPA National Ambient Air Quality Standards (NAAQS) standards, which are defined in Table E1, as set forth under the Clean Air Act of 1990 [130]. Both civil and military airports within the United States must comply with NAAQS, and regions that do not meet the NAAQS are said to be in nonattainment. Although the United States military does not have specific engine standards, they must complete an Environmental Impact Statement (EIS) whenever new aircraft are deployed. The EIS includes an evaluation of ambient air quality impacts.

Table E1: National Ambient Air Quality Standards (NAAQS)

| Pollutant | Primary Standards | |
|---|---|---|
| | Level | Averaging Time |
| Carbon Monoxide (CO) | 9 ppm (10 mg/m$^3$) | 8- hour |
| | 35 ppm (40 mg/m$^3$) | 1-hour |
| Lead | 0.15 μg/m$^3$ | Rolling 3-Month average |
| Nitrogen Dioxide ($NO_2$) | 53 ppb | Annual (Arithmetic Average) |
| | 100 ppb | 1-hour |
| Particulate Matter ($PM_{10}$) | 150 μg/m$^3$ | 24-hour |
| Particulate Matter ($PM_{2.5}$) | 15.0 μg/m$^3$ | Annual (Arithmetic Average) |
| | 35 μg/m$^3$ | 24-hour |
| Ozone ($O_3$) | 0.075 ppm (2008 std) | 8-hour |
| | 0.08 ppm | 8-hour |
| | 0.12 ppm | 1-hour |
| Sulfur Dioxide ($SO_2$) | 0.03 ppm | Annual (Arithmetic Average) |
| | 0.14 ppm | 24-hour |
| | 75 ppb | 1-hour |

The primary emissions of concern to aviation are nitrogen oxides ($NO_X$ consisting of NO and $NO_2$), sulfur oxides ($SO_X$ consisting of $SO_2$ and $SO_3$), and particulate matter [131]. Particulate matter are regulated in the NAAQS by average particle; the notation $PM_{10}$ and $PM_{2.5}$ are used to describe particles with diameters of 10 and 2.5 micrometers or less, respectively. It is important to note the difference between primary and secondary particulate matter as the NAAQS regulate the combination of primary particular matter from sources such as aircraft engines as well as secondary particulate matter that forms from the chemical reaction and transport of emissions

such as $NO_X$ and $SO_X$ in the atmosphere. Primary particulate matter consists of both volatile and nonvolatile ($PM_{NV}$) components. The later is also known as black carbon or soot emissions. An additional class of species of interest is volatile organic compounds (VOCs) that consist of unburned hydrocarbons (UHCs) and various aldehydes. Emissions affecting surface air quality are usually assessed over a standard landing-takeoff (LTO) cycle with an assumed combination of power settings and times in mode, as seen in Table E2.

Table E2: ICAO LTO Modes, Power Settings and Times in Mode

| ICAO Stage | Power Setting (%) | Time in Mode (min) | Time Weighting (%) |
|---|---|---|---|
| Takeoff | 100 | 0.7 | 2 |
| Climb Out | 85 | 2.2 | 7 |
| Approach | 30 | 4.0 | 12 |
| Taxi/Idle | 7 | 26 | 79 |

To understand how SPK fuel use changes air quality emissions, documented $NO_X$, $SO_2$, $PM_{NV}$, CO, and UHC emissions from multiple engine types operating on conventional jet fuel, 50% and 100% SPK fuels were organized and compared at various power settings. Table E3 lists the compiled engine combustion tests using fuel blends up to 100% SPK. Although a 50% blend of SPK has been approved, additional testing and analysis is needed for approval of higher blend percentages. Figure E1 stratifies the test engines by bypass ratio on an energy normalized fuel flow versus percent thrust chart where blue, red, and green correspond to turboshaft, low bypass turbofan, and high bypass turbofan engines, respectively. The engine types span a wide spectrum of engine technologies for both civil and military fleets. The mass-based emissions indices ($EI_m$) are in units of grams of pollutant per kilogram of fuel. Each EI was energy normalized by the fuel specific energy using the lower heating value provided in each test document. In cases where raw data were obtained, EI were humidity corrected and temperature normalized between fuel types. Data uncertainties were calculated using a stochastic process assuming a normal distribution range for each test fuel.

Table E3: Experimental SPK Emissions Tests

| Engine | Representative Military Aircraft | Representative Civil Aircraft | Notes/Refs. |
|---|---|---|---|
| CFM56-2C1 | Boeing KC-135R | Douglas DC-8-70 | [132,133] |
| CFM56-7B | Boeing C-40 | Boeing 737-600 to 900 | [134] |
| F117-PW-100 (PW2000 series) | Boeing C-17 | Boeing 757 | [8] |
| PW308 | Hawker C-29A | Hawker 4000 | [135] |
| RR-Allison T63-A-700 | Sikorsky S-75 | Bell 206, MD 500, MBB Bo 105 | [9,136] |
| T700-GE-701<br>T700-GE-701C | Boeing AH-64, Sikorsky UH60/SH60 | Saab 340 | [137]<br>[138] |
| TF33 P-103 (JT3D) | B-52H Stratofortress<br>Boeing KC/NKC/RC/OC/RE-135E/U/N/V/X | Boeing 707 | [10] |

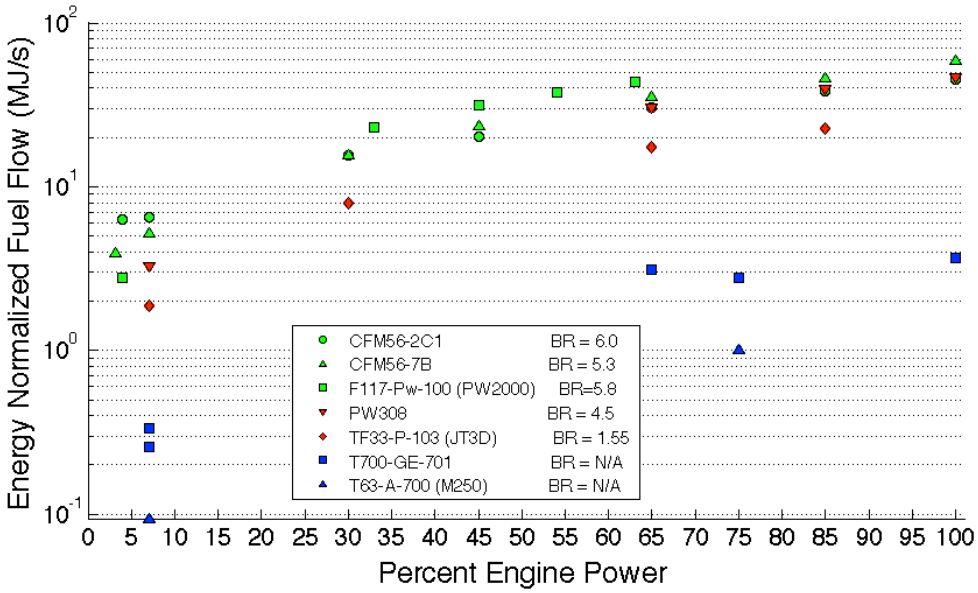

Figure E1: Fuel Flow Ranges for SPK Engine Tests

The assembled energy normalized SPK emissions changes from conventional jet fuel are quantified in Figure E2. The 100% SPK $PM_{NV}$ $EI_m$ experience reductions between 80% and 98% at midrange power settings and between 32% and 92% at higher power settings depending on the engine type. This decreased reduction at higher power settings could be due to a thermal mechanism of $PM_{NV}$ overshadowing the reduction seen from the scarce aromatics in SPK fuels. The 50% SPK $PM_{NV}$ reductions vary between 0%-50%, 31-60%, and 36-96% for low bypass turbofan, turboshaft, and high bypass turbofan engines depending on power setting, respectively. The variation of the reductions based on engine type is statistically significant. Therefore, it appears that at 50% SPK blends, the effect of technology levels on $PM_{NV}$ emissions formation is more apparent than at 100% SPK. UHC and CO reductions are both most pronounced at near idle power settings with values of 13-40%, 4-27%, 5-25%, and 0-40% for UHC 100% SPK, UHC 50% SPK, CO 100% SPK, and CO 50% SPK, respectively. High uncertainties are present particularly for the change in UHC with 50% SPK use at low power settings. Neat SPK $NO_X$ reductions varied most at lower power settings but were nearly constant at higher power settings with reductions between 2-11%. It is important to note that the reductions are within instrument noise for some of the data and will need further testing to confirm any potential environmental benefits.

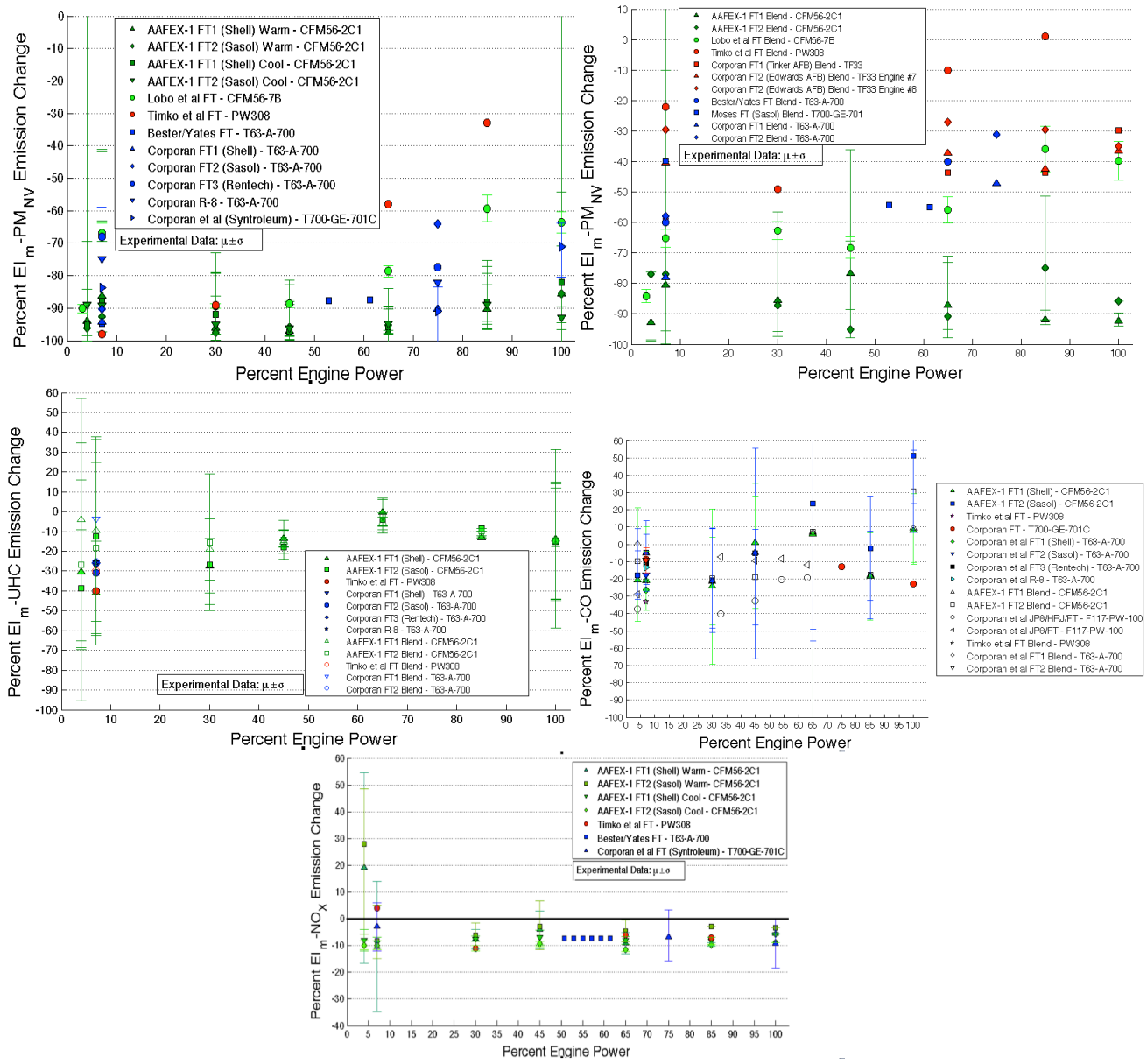


Figure E2: Energy Normalized Percent Change in 50% and 100% SPK $PM_{NV}$, UHC, CO, and $NO_X$ Emissions

The ICAO time and fuel weighted averages from Table E4 were used to calculate the 50% and 100% SPK jet fuel LTO $NO_X$, $PM_{NV}$, CO, and UHC conventional jet fuel normalized emissions in Table E5. The normalized emissions do not change significantly between ICAO time or fuel burn weighted averages. These emissions reductions with the use of 50% or 100% SPK could potentially provide military and civil aviation planners with more options in terms of locating aircraft in nonattainment areas within the CONUS. For some emissions, the introduction of SPK fuels could provide for additional aircraft for the same environmental impact or decrease the overall AQ footprint for an existing location.

Table E4: Assumed Times and Fuel Flows for Each ICAO Mode and Engine Type Considered in Table E3

| ICAO Mode | ICAO Time in Mode (min) | Fuel Flow (kg/s) [139] | | | | |
|---|---|---|---|---|---|---|
| | | CFM56-2B (CFM56-2C1) | CFM56-7 (CFM56-7B) | F117-PW-100 | TFE731-2-2B (PW308) | TF33-P-103 |
| Taxi/Idle | 26 | 1,070 | 847 | 1,210 | 209 | 986 |
| Approach | 4 | 2,600 | 2,100 | 4,360 | 542 | 3,880 |
| Climb Out | 2.2 | 6,730 | 5,740 | 11,060 | 1,390 | 6,320 |
| Takeoff | 0.7 | 8,030 | 6,840 | 14,110 | 1,640 | 7,510 |

Table E5: Turbofan 50% and 100% Average SPK LTO Emissions Normalized to Conventional Jet Fuel

| | | Experiment | Bulzan et al. (2010) | Lobo, Hagen, Whitefield (2011) | Corporan and Dewitt (2010) | Timko et al (2008) | Corporan et al. (2007) |
|---|---|---|---|---|---|---|---|
| | | Test Engine | CFM56-2C1 | CFM56-7B | F117-PW-100 | PW308 | TF33-P-103 |
| $NO_X$ | 100% SPK | Taxi/Idle | 0.91 | | | 1.04 | |
| | | Approach | 0.92 | | | 0.89 | |
| | | Climb Out | 0.92 | | | 0.93 | |
| | | Takeoff | 0.94 | | | 0.93 | |
| | | **ICAO time wt. avg.** | **0.91** | | | **1.01** | |
| | | **ICAO fuel wt. avg.** | **0.92** | | | **0.97** | |
| $PM_{NV}$ | 50% SPK | Taxi/Idle | 0.28 | 0.35 | | 0.78 | 0.57 |
| | | Approach | 0.22 | 0.37 | | 0.51 | 0.64 |
| | | Climb Out | 0.18 | 0.64 | | 0.64 | 0.61 |
| | | Takeoff | 0.20 | 0.60 | | 1.01 | 0.66 |
| | | **ICAO time wt. avg.** | **0.27** | **0.38** | | **0.74** | **0.58** |
| | | **ICAO fuel wt. avg.** | **0.24** | **0.46** | | **0.72** | **0.61** |
| | 100% SPK | Taxi/Idle | 0.09 | 0.33 | | 0.02 | |
| | | Approach | 0.05 | 0.11 | | 0.11 | |
| | | Climb Out | 0.11 | 0.41 | | 0.42 | |
| | | Takeoff | 0.13 | 0.36 | | 0.67 | |
| | | **ICAO time wt. avg.** | **0.09** | **0.31** | | **0.07** | |
| | | **ICAO fuel wt. avg.** | **0.09** | **0.31** | | **0.72** | |
| CO | 50% SPK | Taxi/Idle | 0.92 | | 0.67 | 0.79 | |
| | | Approach | 0.80 | | 0.76 | 1.00 | |
| | | Climb Out | 0.82 | | 1.00 | 1.00 | |
| | | Takeoff | 1.20 | | 1.00 | 1.00 | |
| | | **ICAO time wt. avg.** | **0.91** | | **0.71** | **0.83** | |
| | | **ICAO fuel wt. avg.** | **0.90** | | **0.82** | **0.90** | |
| | 100% SPK | Taxi/Idle | 0.87 | | | 0.67 | |
| | | Approach | 0.77 | | | 1.00 | |
| | | Climb Out | 0.90 | | | 1.00 | |
| | | Takeoff | 1.30 | | | 1.00 | |
| | | **ICAO time wt. avg.** | **0.87** | | | **0.74** | |
| | | **ICAO fuel wt. avg.** | **0.90** | | | **0.85** | |
| UHC | 50% SPK | Taxi/Idle | 0.86 | | | 0.70 | |
| | | Approach | 0.83 | | | 1.00 | |
| | | Climb Out | 0.89 | | | 1.00 | |
| | | Takeoff | 0.85 | | | 1.00 | |
| | | **ICAO time wt. avg.** | **0.86** | | | **0.76** | |
| | | **ICAO fuel wt. avg.** | **0.86** | | | **0.86** | |
| | 100% SPK | Taxi/Idle | 0.73 | | | 0.60 | |
| | | Approach | 0.73 | | | 1.00 | |
| | | Climb Out | 0.89 | | | 1.00 | |
| | | Takeoff | 0.85 | | | 1.00 | |
| | | **ICAO time wt. avg.** | **0.75** | | | **0.68** | |
| | | **ICAO fuel wt. avg.** | **0.78** | | | **0.82** | |

## Works Cited


[1] P.D. Donohoo, "Scaling Air Quality Effects from Alternatife Jet Fuel in Aircraft and Ground Support Equipment," Engineering Systems Division, Massachusetts Institute of Technology, SM Thesis 2010.

[2] R.W. Stratton, "Life Cycle Assessment of Greenhouse Gas Emissions and Non-CO2 Combustion Effects from Alternative Jet Fuels," Department of Aeronautics and Astronautics, Massachusetts institue of Technology, SM Thesis 2010.

[3] J.I. Hileman et al., "Near-term Feasibility of Alternative Jet Fuels," Department of Aeronautics and Astronautics, Massachusetts Institute of Technology and RAND Corporation, Technical Report 2009.

[4] R.W. Stratton, H.M. Wong, and J.I. Hileman, "Life Cycle Greenhouse Gas Emissions from Alternative Jet Fuels," Partnership for AiR Transportation Noise and Emissions Reduction, Report NO. PARTNER-COE-2010-001 2010.

[5] N.A. Carter, R.W. Stratton, M.K. Bredehoeft, and J.I. Hileman, "Energy and Environmental Viability of Select Alternative Jet Fuel Pathways," *American Institute of Aeronautics and Astronautics*, no. 5968, 2011.

[6] J.I. Hileman, R.W. Stratton, and P.E. Donohoo, "Energy Content and Alternative Jet Fuel Viability," *Journal of Propulsion and Power*, vol. 26, no. 6, pp. 1184-1196, 2010.

[7] J.L. Graham et al., "Impact of Alternative Jet Fuel and Fuel Blends on Non-Metallic Materials Used in Commerical Aircraft Fuel Systems," Federal Aviation Administration and The Boeing Company, Technical Report DTFAWA-10-C-0030, 2011.

[8] E. Corporan, M.J. DeWitt, C.D. Klingshirn, and D. Anneken, "Alternative Fuels Tests on a C-17 Aircraft: Emissions Characteristics," Air Force Research Laboratory Propulsion Directorate, Wright-Patterson AFB, AFRL-RZ-WP-TR 2010.

[9] E. Corporan et al., "Chemical, Thermal Stability, Seal Swell and Emissions Characteristics of Jet Fuels from Alternative Sources," in *IASH 2009, the 11th International Conference on Stability, Handling and Use of Liquid Fuels*, Prague, 2009, pp. 1-19.

[10] E. Corporan, M.J. DeWitt, C.D. Klingshirn, and R.C. Striebich, "DOD Assured Fuels Initiative: B-52 Aircraft Emissions Burning A Fischer-Tropsch/JP-8 Fuel Blend," in *IASH 2007, the 10th International Conference on Stability, Handling and Use of Liquid Fuels*, Tucson, 2007, pp. 1-14.

[11] Department of Defense, "Detail Specification: Turbine Fuel, Aviation, Grades JP-4 and JP-5," MIL-DTL-5624U 2004.

[12] Department of Defense, "Detail Specification: Turbine Fuel, Aviation, Kerosene Type, JP-8 (Nato F-34), NATO F-35, and JP-8+100 (NATO F-37)," MIL-DTL-83133H 2011.

[13] ASTM International, Std., "Standard Specification for Aviation Turbine Fuels," West Conshohocken, PA, ASTM D1655-11b DOI: 10.1520/D1655-11B, 2010.

[14] ASTM International, Std., "Standard Specification for Aviation Turbine Fuel Containing Synthesized Hydrocarbons," West Conshohocken, PA, ASTM D7566-11a DOI: 10.1520/D7566-11A, 2011.

[15] Air Transport Association. (2008) US Jet Fuel Use by Airport Location. Database Query.

[16] Defense Logistics Agency. (2011) Total Fuel Sales from April 2010 through March 2011.

Database Query.

[17] U.S. Energy Information Administration. (2011, December) Refinery Yield. Electronic Database.

[18] Airlines for America. (2012, Feb) A4A. [Online]. http://www.airlines.org/Pages/Environmentally-Friendly-Alternative-Fuels.aspx

[19] Feneral Aviation Administration. (2011) Destination 2025. [Online]. http://www.faa.gov/about/plans_reports/

[20] United States Air Force, "Air Force Energy Plan 2010," 2010.

[21] United States Navy, "A Navy Energy Vision for the 21st Century," 2010.

[22] V. Vasudevan et al., "The Environmental Performance of Algal Biofuel Technology Options," *Environmental Science and Technology*, vol. 46, pp. 2451-2459, February 2012.

[23] C.W. King and M.E. Weber, "The Water Intensity of the Plugged-in Automotive Economy," *Environmental Science and Technology*, vol. 42, pp. 4305-4311, 2008.

[24] C.W. King and M.E. Webber, "Water Intensity of Transportation," *Environmental Science and Technology*, vol. 42, pp. 7866-7872, 2008.

[25] P.G. Falkowki and Raven J.A., *Aquatic Photosynthesis*. London: Blackwater Science, 1997.

[26] R.E. Lee, *Phycology*. New York: Cambridge University Press, 1980.

[27] S.A. Khan, Rashmi, Hussain M.Z., S. Prasad, and U.C. Banerjee, "Prospects of Biodiesel Production from Microalgae in India," *Renewable and Sustainable Energy Reviews*, vol. 13, no. 9, pp. 2361-72, 209.

[28] C.Y. Chen, K.L. Yeh, Aisyah R., D.J. Lee, and J.S. Chang, "Cultivation, Photobioreactor Design and Harvesting of Microalgae for Biodiesel Production: A Critical Review," *Bioresource Technology*, no. 102, pp. 71-81, 2011.

[29] L. Brennan and P. Owende, "Biofuels from Microalgae- A Review of Technologies for Production, Processing, and Extractions of Biofuels and Co-products," *Renewable and Sustainable Energy Reviews*, no. 14, pp. 557-577, 2010.

[30] T.M. Mata, A.A. Martins, and N.S. Caetano, "Microalgae for Biodiesel Production and Other Applications: a Review," *Renewable and Sustainable Energy Reviews*, no. 14, pp. 217-232, 2010.

[31] Q. Hu et al., "Microalgal Triacylglycerols as Feedstocks for Biofuel Production: Perspectives and Advances," *The Plant Journal*, vol. 54, pp. 621-639, 2008.

[32] Y. Chisti, "Biodiesel from Microalgae," *Biotechnology Advances*, no. 25, pp. 294-306, 2007.

[33] M.N. Pearlson, "A Techno-Economic and Environmental Assessment of Hydroprocessed Renewable Distillate Fuels," Engineering Systems Division, Massachusetts Institute of Technology, Cambridge, MS Thesis 2011.

[34] C.Y. Chen et al., "Reduction of CO2 by a High-Density Culture of Chlorella sp. in a Semicontinuous Photobioreactor," *Bioresource Technology*, no. 99, pp. 3389-3396, 2008.

[35] S.Y. Chiu, M.T. Kao, S.C. Ong, C.H. Chen, and C.S. Lin, "Lipid Accumulation and CO2 Utilization of Nannochloropsis Oculata in Response to CO2 Aeration," *Bioresource Technology*, no. 100, pp. 833-838, 2009.

[36] A. Richmond and Z. Cheng-Wu, "Optimization of a Flat Plate Glass Reactor for Mass Production of Nannochloropsis sp. Outdoors," *Journal of Biotechnology*, vol. 85, pp. 259-269, 2001.

[37] U.S. Department of Energy. (2011, Oct) Greet Model: The Greenhouse Gasses, Regulated Emissions, and Energy Use in Transportation Model. [Online]. http://greet.es.anl.gov/

[38] J. Koornneef, T. van Kuelen, A. Faaij, and W. Turkenburg, "Life Cycle Assessment of a Pulverized Coal Power Plant with Post-Combustion Capture, Transport and Storage of CO2," *International Journal of Greenhouse Gas Control*, no. 2, pp. 448-467, 2008.

[39] K. Kadam, "Microalgae Production from Power Plant Flue Gas: Environmental Implications on a Life Cycle Basis," National Renewable Energy Laboratory, Golden Colorado, NREL/TP-510-29417 2001.

[40] H. Herzog, D. Golomb, and S. Zemba, "Feasibility, Modeling and Economics of Sequestering Power Plant CO2 Emissions in the Deep Ocean.," *Environmental Progress*, vol. 10, no. 1, pp. 64-74, 1991.

[41] EcoInvent Center. (2012) Ecoinvent Life Cycle Inventory Data. Database.

[42] Product Ecology Consultants. (2011) SimaPro Version 7.3.3. [Online]. http://www.pre-sustainability.com/

[43] J. Black, "Cost and Performance Baseline for Fossile Energy Plants. Volume 1: Bituminous Coal and Natural Gas to Electricity," Department of Energy, National Energy Technology Laboratory, DOE/NETL-2010/1397 2010.

[44] M.E. Huntley and D.G. Redalje, "CO2 Mitigation and Renewable Oil from Photosynthetic Microbes: A New Appraisal," *Mitigation and Adaptation Strategies for Global Change*, no. 12, pp. 573-608, 2007.

[45] E.W. Becker, "Micro-algae as a Source of Protein," *Biotechnology Advances*, no. 25, pp. 207-210, 2007.

[46] E.W. Becker, *Microalgae: Biotechnology and Microbiology*. Cambridge, U.K.: Cambridge University Press, 1994.

[47] D. Feinberg and M. Karpuk, "CO2 Sources for Microalgae Based Liquid Fuel Production," Solar Energy Research Institute, Golden, CO, Technical Report 1990.

[48] D. Feinberg, "Fuel Optiosn from Microalgae with Representative Chemical Compositions," Solar Energy REsearch Institute, Golden, CO, Technical Report 1984.

[49] J.S. Burlew, *Algae Culture: From Laboratory to Pilot Plant*. Washington, D.C.: Carnegie Institute of Washington, 1976.

[50] J.C. Weissman and R.P. Goebel, "Design and Analysis of Microalgal Open Pond Systems for the Purpose of Producing Fuels," Solar Energy Research Institute, Golden, CO, Technical Report 1987.

[51] L., Helias, A. Lardon, B. Sialve, L.P. Steyer, and O. Bernard, "Life-Cycle Assessment of Biodiesel Production from Microalgae," *Environmental Science & Technology*, vol. 43, no. 17, pp. 6475-6481, June 2009.

[52] L.B. Brentner, M.J. Eckelman, and J.B. Zimmerman, "Combinatorial Life Cycle Assessment to Inform Process Design of Industrial Production of Algal Biodiesel," *Environmental Science & Technology*, vol. 10, no. 10, pp. 1-24, July 2011.

[53] A.L. Stephenson et al., "Life-Cycle Assessment of Potential Algal Biodiesel Production in

the United Kingdom: A Comparison of Raeways and Air-Lift Tubular Bioreactors," *Energy & Fuels*, no. 24, pp. 4062-4077, 2010.

[54] E. Molina Grima, "Challenges in Microalgae Biofuels," in *Energy Manufacturing Workshop, National Science Foundation*, Arlington, VA, 2009, pp. 1-34.

[55] E. Molina, J. Fernandez, G. Acien Fernandez, and Y. Chisti, "Tubular Photobioreactor Design for Algal Culture," *Journal of Biotechnology*, no. 92, pp. 113-131, October 2001.

[56] E. Sierra, J.M. Acien, J.L. Garcia, C. Gonzalez, and E. Molina, "Characterization of a Flat Plate Photobioreactor for the Production of Microalgae," *Chemical Engineering Journal*, no. 138, pp. 136-147, 2008.

[57] F.G.A. Fernandez, J.M.F. Sevilla, J.A.S. Perez, E.M. Grima, and Y. Chisti, "Airlift-driven External-loop Tubular Photobioreactors for Outdoor Production of Microalgae: Assessment of Design and Performance," *Chemical Engineering Science*, no. 56, pp. 2721-2732, 2001.

[58] F. Camacho Rubio, F.G. Acien Fernandez, J.A. Sanchez Perez, F. Garcia Camacho, and E. Molina Grima, "Prediction of Dissolved Oxygen and Carbon Dioxide Concentration Profiles in Tubular Photobioreactors for Microalgal Culture," *Biotechnology and Bioengineering*, vol. 62, no. 1, pp. 71-86, 1999.

[59] C., Garcia-Malea Lopez, M.C. Brindley Alias, F.G. Acien Fernandez, J.M. Fernandez Sevilla, J.L. Garcia Sanchez, and E. Molina Grima, "Influence of Power Supply in the Feasibility of Phaeodactylum Tricornutum Cultures," *Biotechnology and Bioengineering*, vol. 87, no. 6, pp. 723-733, September 2004.

[60] P. Trotta, "A Simple and Inexpensive System for Continuous Monoxenic Mass Culture of Marine Microalgae," *Aquaculture*, vol. 22, pp. 383-387, 1981.

[61] C.N. Dasgupta et al., "Recent Trends on the Development of Photobiological Processes and Photobioreactors for hte Improvement of Hydrogen Production," *International Journal of Hydrogen Energy*, vol. 102, pp. 10218-10238, 2010.

[62] M.J. Barbosa, Hadiyanto, and R.H. Wijffels, "Overcoming Shear Stress of Microalgae Culture in Sparged Photobioreactors," *Biotechnology and Bioengineering*, vol. 85, pp. 78-85, 2004.

[63] L. Rodolfi et al., "Microalgae for Oil: Strain Selection, Induction of Lipid Synthesis and Outdoor Mass Cultivation in a Low-Cost Photobioreactor," *Biotechnology and Bioengineering*, vol. 102, pp. 100-112, 2008.

[64] K. Zhang, S. Miyachi, and Kurano N., "Evaluation of Vertical Flat-Plate Photobioreactor for Outdoor Biomass Production and Carbon Dioxide Bio-fixation: Effects of Reactor Dimensions, Irradiation and Cell Concentration on the Biomass Productivity and Irradiation Utilization Efficiency," *Applied Microbiology and Biotechnology*, vol. 55, pp. 428-433, 2001.

[65] M. Morita, Y. Watanable, and H. Saiki, "Investigation of Photobioreactor Design for Enhancing the Photosynthetic Productivity of Microalgae," *Biotechnology and Bioengineering*, vol. 74, pp. 135-144, 2001.

[66] A.P. Carvalho, L.A. Meireles, and F.X. Malcata, "Microalgal Reactors: A Review of Enclosed System Designs and Performances," *Biotechnology Progress*, vol. 22, pp. 1490-1506, 2006.

[67] "Study on Inproving the Energy Efficiency of Pumps," European Commission, Technical Report AEAT-6559/v 5.1, 2001.

[68] (2011, September) The Engineering Toolbox. [Online]. http://www.engineeringtoolbox.com

[69] L. Rieger, G. Langergraber, M. Thomann, N. Fleischmann, and H. Siegrist, "Spectral in-situ of NO2, NO3, COD, DOC, and TSS in the Effluent of a WWTP," Swiss Federal Institute for Environmental Science and Technology, Duebendorf, Switzerland, Technical Report 2004.

[70] P.A. Vesilind, *Wastewater Treatment Plant Design*. VA: IWA Publishing, 2003.

[71] T.J. Lundquist, I.C. Woertz, N.W.T. Quinn, and J.R. Benemann, "A Realistic Technology and Engineering Assessment of Algae Biofuel Production," Energy Biosciences Institute, Berkeley, CA, Technical Report 2010.

[72] L.K. Wang, N.K. Shammas, and Y.T. Hung, Eds., *Biosolids Treatment Processes*. Totowa, NJ: Humana Press, 2007.

[73] J. Sheehan, V. Camobreco, J. Duffield, M. Graboski, and H. Shapouri, "Life Cycle Inventory of Biodiesel and Petroleum Diesel for Use in an Urban Bus," Department of Energy, National Renewable Energy Laboratory, Golden, CO, NREL-SR-580-24089 1998.

[74] (2011) Water Technologies: Belt Dryers. [Online]. http://www.water.siemens.com/en/products/sludge_biosolids_processing/sludge_dryers/Pages/drying_beltdryer.aspx

[75] C.M. Ruecker, A.P. Adu-peasah, B.S. Engelhardt, and G.T. Veeder, "Solventless Extraction Process," 7,351,558 B2, 2008.

[76] S. Vaswani, "Biodiesel from Algae," SRI Consulting, Melo Park, CA, Process Economics Program Review 2009.

[77] T.J. Czartoski, R. Perkins, J.L. Villaneuva, and G. Richards, "Algae Biomass Fractionation," 0233761, 2010.

[78] E.N. D'Addario, F. Capuano, E. D'Angeli, and R. Medici, "Process for the Extraction of Fatty Acids from Algal Biomass," 00416 A1, 2010.

[79] Product Ecology Consultants. (2012) Sima Pro UK. [Online]. http://www.simapro.co.uk/

[80] Heger M. (2009) Technology Review. [Online]. http://www.technologyreview.com/energy/22572/

[81] J.D. Murphy and E. McKeogh, "Technical, Economic and Environmental Analysis of Energy Production from Municipal Solid Waste," *Renewable Energy*, vol. 29, pp. 1043-1057, 2004.

[82] D. Kubicka and L. Kaluza, "Deoxygenation of Vegetable Oils Over Sulfided Ni, Mo and NiMo Catalysts," *Applied Catalysis A: General*, vol. 372, no. 2, pp. 199-208, 2010.

[83] UOP, "Opportunities for Biorenewables in Oil Refineries," http://www.osti.gov/bridge/servlets/purl/861458-Wv5uum/861458.pdf, Des Plains, Illinois, Technical Report 2005.

[84] Y. Lu, F. Quyang, S. Wang, and H. Weng, "Carbon Distribution of n-Paraffins in Diesel and the Effects on the Sensitivity of Flow Improvers," *Petroleum Science and Technology*, vol. 24, pp. 1205-1214, 2006.

[85] H.M. Wong, "Life-cycle Assessment of Greenhouse Gas Emissions from Alternative Jet Fuels," Department of Aeronautics and Astronautics, Massachusetts Institute of Technology, Cambridge, MA, MS Thesis 2008.

[86] Federal Aviation Administration. (2011, February) Aviation Environmental Design Tool (AEDT). [Online]. http://www.faa.gov/about/office_org/headquarters_offices/apl/research/models/aedt/

[87] M.Y. Chisti, *Airlift Bioreactors*. New York: Elsevier Applied Science, Ltd., 1989.

[88] A. Saltelli et al., *Global Sensitivity Analysis: The Primer*. West Sussex, England: John Wiley & Sons, Ltd., 2008.

[89] MathWorks. (2011a) MathWorks: Accelarating the Pace of Engineering and Science. [Online]. http://www.mathworks.com/products/matlab/

[90] B.G. Grooth, T.H. Geerken, and J. Greve. (2010, May) B10NUMB3RS: A Database of Useful Biological Numbers. [Online]. http://bionumbers.hms.harvard.edu//bionumber.aspx?id=101481&ver=7

[91] J.H. Gary, G.E. Handwerk, and M.J. Kaiser, *Petroleum Refining Technology and Economics, 5th Ed.* Boca Raton: CRC Press, 2007.

[92] A. Darzins, P. Pienkos, and L. Edye, "Current Status and Potential for Algal Biofuels Production," Department of Energy, National Renewable Energy Laboratory, T39-T2 2010.

[93] A. Sun et al., "Comparative Cost Analysis of Algal Oil Production for Biofuels," *Energy*, vol. 36, pp. 5169-5179, 2011.

[94] R Putt, "Algae as a Biodiesel Feestock: A Feasibility Assessment," Department of Chemical Engineering, Auburn University, Technical Report 2008.

[95] E.D. Frank, J. Han, I. Palou-Rivera, A. Elgowainy, and M.Q. Wang, "Life-Cycle Analysis of Algal Lipid Fuels with the GREET Model," Unted States Department of Energy, Argonne National Laboratory - Energy Systems Division, Argonne, Illinois, Technical Report: ANL/ESD/11-5 2011.

[96] L. Amer, B. Adhikari, and J. Pellegrino, "Technoeconomic Analysis of Five Microalgae-to-biofuels Processes of Varying Complexity," *Bioresource Technology*, vol. 102, pp. 9350-9359, 2011.

[97] P. Tapie and A. Bernard, "Microalgae Production: Technocal and Economic Evaluations," *Biotechnology and Bioengineering*, vol. 32, pp. 873-885, 1988.

[98] J. Benneman and W. Oswald, "Systems and Economic Analysis of Microalgae Ponds for Conversion of CO2 to Biomass," Pittsburg Energy Technology Center, Pittsburg, PA, Technical Report DE-FG22-93PC93204, 1996.

[99] V. Kovacevic and J. Wesseler, "Cost-effectiveness Analysis of Algae Energy Production in the EU," *Energy Policy*, vol. 38, pp. 5749-5757, 2010.

[100] National Renewable Energy Laboratory. (2012) Dynamic Maps, GIS Data, & Analysis Tools. [Online]. http://www.nrel.gov/gis/solar.html

[101] R.S.J. Tol, "The Social Cost of Carbon: Trends, Outliers and Catastrophes," *Economics: The Open-Access, Open-Assessment E-Journal*, vol. 2, no. 25, pp. 1-22, August 2008.

[102] R.S.J. Tol, "The Marginal Damage Costs of Carbon Dioxide Emissions: an Assessment of the Uncertainties," *Energy Policy*, vol. 33, pp. 2064-2074, 2005.

[103] S.R.H. Barrett et al., "Public Health, Climate and Economic Impacts of Desulfurizing Jet Fuel," *Environmental Science and Technology*, vol. 46, no. 8, pp. 4275-4282, 2012.

[104] L. Wang et al., "Anaerobic Digested Diary Manure as a Nutrient Supplement for Cultivation of Oil-Rich Green Microalgae Chlorella sp.," *Bioresource Technology*, vol. 101, no. 8, pp. 2623-2628, April 2010.

[105] M.R. Hasan and R. Chakrabarti, "Use of Algae and Aquatic Macrophytes as Feed in Small-scale Aquaculture: A Review," FAO Fisheries and Aquaculture, Rome, Italy, Technical Report ISSN 2070-7010, 2010.

[106] J. Singh and S. Gu, "Commercialization Potential of Microalgae for Biofuels Production," *Renewable and Sustainable Energy Reviews*, vol. 14, no. 9, pp. 2596-2610, December 2010.

[107] K.C. Lewis and R.D. Porter, "Biofuels and Invasive Species Risks: Assessing and Managing Risks Through Feedstock Selection and Cultivation Strategies," U.S. Department of Transportation, John A. Volpe National Transportation Systems Center, Cambridge, MA, Technical Report DOT-VNTSC-FAA-12-02,.

[108] J.A. Duffie and W.A. Beckman, *Solar Engineering of Thermal Processes*. New York: John Wiley & Sons, Inc., 1985.

[109] E. Molina Grima, F.G.A. Fernandez, F.G. Camacho, and Y. Chisti, "Photobioreactors: Light Regime, Mass Transfer, and Scaleup," *Journal of Biotechnology*, vol. 70, pp. 231-247, 1999.

[110] B.Y.H. Liu and Jordan R.C., "The Interrelationship and Characteristic Distribution of Direct, Diffuse and Total Solar Radiation," Department of Mechanical Engineering, University of Minnesota, PhD Thesis 1960.

[111] C.D. Scown, A. Horvath, and T.E. McKone, "Water Footpring of U.S. Trnasportation Fuels," *Environmental Science and Technology*, vol. 45, pp. 2541-2553, 2011.

[112] FSA Environmental, "Case Study 11 - Dissolved Air Flotation," Solid Separation Systems for the Pig Industry, Technical Report 2002.

[113] Office of Research and Development National Risk Managment Research Laboratory - Land Remediation and Pollution Control Division, "Principles of Design and Operations of Wastewater Treatment Pond Systems for Plant Operators, Engineers, and Managers," Environmental Protection Agency, Cincinnati, Ohio, Technical Report EPA/600/R-11/088, 2011.

[114] FSA Environmental, "Case Study 8 - Belt Press," Solid Separation Systems for the Pig Industry, Technical Report 2002.

[115] FSA Environmental, "Case Study 10 - Centrifuge Decanter," Solid Separation Systems for the Pig Industry, Technical Report 2002.

[116] Energy and Environmental Analysis, "Technology Characterization: Gas Turbines," Environmental Protection Agency, Technical Report 2008.

[117] P. Brinckerhoff, "Electricity Generation Cost Model," Department for Energy and Climate Change, Parsons Brinckerhoff, Technical Report 2011.

[118] T.M. Walski, "Planning-Level Capital Cost Estimates for Pumping," *Journal of Water Resources Planning and Management*, vol. 10, May 2011.

[119] (2012) McMaster-Carr: Over 490,000 Products. [Online]. http://www.mcmaster.com/

[120] (2012) [Online]. http://yfhexane.en.alibaba.com/product/456131521-212582159/Normal_Hexane_110_54_3.html

[121] (2012) Biodiesel Supply Store & Chemicals. [Online]. http://www.amazon.com/Potassium-Hydroxide-Caustic-Potash-Flakes/dp/B003TA7F10/ref=sr_1_sc_10?s=industrial&ie=UTF8&qid=1328130840&sr=1-10-spell

[122] Amazon.com. (2012, March) 2000 lb of Potassium Hydroxide Caustic Potash Flakes 90+%. [Online]. http://www.amazon.com/Potassium-Hydroxide-Caustic-Potash-Flakes/dp/B003TA7F10/ref=sr_1_sc_10?s=industrial&ie=UTF8&qid=1328130840&sr=1-10-spell

[123] (2012, August) Caustic Soda Flake 99%. [Online]. http://www.made-in-china.com/showroom/catherinesong86/offer-detailkonEemJYmIrV/Sell-Caustic-Soda-Flake-99-400-USD-MT-430-USD-MT-.html

[124] (2012) [Online]. http://www.amazon.com/Urea-NH2-46-0-0-Fertilzer-Pounds/dp/B0054PD4QI/ref=sr_1_5?ie=UTF8&qid=1328212953&sr=8-5

[125] ICIS. (2011, September) ICIS Pricing: Hydrochloric Acid. [Online]. http://www.icispricing.com/il_shared/Samples/SubPage110.asp

[126] (2012) [Online]. http://www.alibaba.com/product-gs/226804316/Phosphorus_pentoxide.html

[127] J.I. Hileman and R.W. Stratton, "Alternative Jet Fuel Feasibility," *Accepted to Transport Policy*, 2010.

[128] L.M. Shafer, R.C. Striebich, J. Gomach, and T. Edwards, "Chemical Class Composition of Commercial Jet Fuels and Other Specialty Kerosene Fuels," in *14th AIAA/AHI Space Planes and Hypersonic Systems and Technologies Conference*, vol. AIAA 2006-7972, 2006.

[129] International Civil Aviation Organization, "International Standards and Recommended Practices: Environmental Protection - Aircraft Engine Emissions," ICAO Annex 16: Vol. II, Technical Report 1993.

[130] Environmental Protection Agency. (1990) National Ambient Air Quality Standards. [Online]. http://www.epa.gov/air/criteria.html

[131] G. Ratliff et al., "Aircraft Impacts on Local and Regional Air Quality in the United States," Partnership for Air Transportation Noise and Emissions Reduction, Cambridge, MA, Technical Report 2009.

[132] D. Bulzan et al., "Gaseous and Particulate Emissions of the NASA Alternative Aviation Fuel Experiment (AAFEX)," in *ASME Turbo Expo 2010: Power for Land, Sea and Air*, Glasgow, UK, 2010, pp. 1-13.

[133] B.E. Anderson et al., "Alternative Aviation Fuel Experiment (AAFEX)," National Aeronautics and Space Administration, Palmdale, CA, Technical Report 2011.

[134] P. Lobo, D.E. Hagen, and P.D. Whitefield, "Comparison of PM Emissions from a Commercial Jet Engine Burning Conventional, Biomass, and Fischer-Tropsch Fuels," *Environmental Science & Technology*, vol. 45, pp. 10744-10749, November 2011.

[135] M.T. Timko et al., "Particulate Emissions of Gas Turbine Engine Combustion of a Fischer-Tropsch Synthetic Fuel," *Energy & Fuels*, vol. 24, pp. 5883-5896, October 2010.

[136] N. Bester and A. Yates, "Assessment of the Operational Performance of Fischer-Tropsch Synthetic-Paraffinic Kerosene in a T63 Gas Turbine Compared to Conventional Jet A-1 Fuel," in *ASME Turbo Expo 2009: Power for Land, Sea and Air*, Orlando, FL, 2009, pp. 1-15.

[137] C.A. Moses, G. Wilson, and P. Roets, "Evaluation of Sasol Synthetic Kerosene for Suitability as Jet Fuel," Sowthwester Research Institute and Sasoil Oil R&D, San Antonio and Sasolburg, Technical Report: 08-04438 2003.

[138] E. Corporan and M.-D. Cheng, "Emissions Characteristics of Military Helicopter Engines with JP-8 and Fischer–Tropsch Fuels," *Journal of Propulsion and Power*, vol. 26, no. 2, pp. 317-324, March 2010.

[139] United States Air Force. (2011) Air Quality Analysis/Air Conformity Applicability Model (ACAM). [Online]. http://www.afcee.lackland.af.mil/air/acam/acam.asp

[140] One Hundred Tenth Congress of the United States of America, "Energy Independence and Security Act," One Hundred Tenth Congress of the United States of America, Congressional Act 2007.

[141] Origin Oil. (2012) Origin Oil: Converting Algae to Renewable Crude Oil. [Online]. http://www.originoil.com/technology/single-step-extraction.html